UNIVERSITÀ DEGLI STUDI ROMA TRE
DEPARTMENT OF MATHEMATICS AND PHYSICS
PH.D. PROGRAM IN PHYSICS
XXXII CYCLE

ISOSPIN BREAKING CORRECTIONS TO MASSES AND HADRONIC PROCESSES ON THE LATTICE

A dissertation submitted in partial fulfillment of
the requirements for the degree of
Doctor of Philosophy

Author
Dr. Davide Giusti

Advisors
Prof. Vittorio Lubicz
Prof. Silvano Simula

Coordinator of the Doctoral Program
Prof. Giuseppe Degrassi

October 2019

CONTENTS

Introduction

The Standard Model (SM) of particle physics is a description of nature in terms of elementary particles and their interactions, except gravity.
So far, the SM has been proven to be very successful in reproducing the experimental data. In the last forty years, many experiments have tested it obtaining excellent agreement with theoretical predictions. Despite its success in describing with high precision a large set of experimental results, there are several reasons to believe that the SM is not a complete theory of particle interactions, but just a low-energy approximation to a more fundamental theory. The fact that the SM does not provide a description for the gravitational interaction is perhaps its most evident limit. Other problems which affect the model are also: the instability of the Higgs mass to radiative corrections, the lack of a mechanism that explains baryogenesis and the masses of the neutrinos, the absence of a candidate for dark matter, and the failure to truly unify all the fundamental forces.

In addition, several issues related to the flavor structure of the SM remain still unanswered. In particular, the fact that the model parametrizes the observed hierarchy of particles masses and mixing angles through free parameters (for quark sector we have: 6 masses, 3 angles and 1 complex phase) without explaining it. Moreover, the mixing among different flavors of quarks represents the only source of CP violation in the Standard Model, an effect which has been proven to be too small, however, to explain the observed dominance of matter over anti-matter in the Universe. This observation provides therefore a strong hint for the existence of new sources of CP violation beyond the SM.

All these questions could find an answer in a more fundamental theory that manifests itself at some higher scale. The search for this new physics can be carried out in a direct way by using very high energy particle accelerators. In addition, research activities in flavor physics aims at clarifying the open questions by testing the SM itself with increasing accuracy and by searching new physics effects through indirect searches, i.e. by looking at processes that are sensitive to virtual (loop) contributions of new physics particles. In the last years a new era of exploration has started with the coming into operation of the Large Hadron Collider at CERN.

In the direction of highlighting and quantifying the effects of new physics testing the predictions of the Standard Model, a dominant role is played by flavor physics which, because of its highly non-trivial structure, is particularly sensitive to higher scales. In the hadronic sector, flavor physics involves the elements of the Cabibbo-Kobayashi-Maskawa (CKM) ma-

trix [1, 2]. Their accurate determination, obtained by combining experimental inputs with theoretical calculations, represents the strictest test of the Standard Model.

In the SM, the CKM matrix describing the quark flavor mixing phenomenon occurring in weak interactions, is a 3×3 unitary matrix of the form

$$V_{\text{CKM}} = \begin{pmatrix} V_{ud} & V_{us} & V_{ub} \\ V_{cd} & V_{cs} & V_{cb} \\ V_{td} & V_{ts} & V_{tb} \end{pmatrix} . \tag{0.1}$$

Unitarity (i.e. $V^{-1} = V^\dagger$) enforces several restrictions. In particular, the sum of the squared entries of each row (or column) should equal 1. By measuring independently the different entries of the CKM matrix, it is possible to test the SM by verifying if these conditions are experimentally satisfied.

A possible way to measure CKM matrix elements is from the study of leptonic decays of pseudoscalar mesons $P \to \ell\nu_\ell$, whose branching ratio is given by [3]

$$\Gamma(P \to \ell\nu_\ell) = \frac{G_F^2 |V_{ij}|^2}{8\pi} f_P^2 \, M_P \, m_\ell^2 \left(1 - \frac{m_\ell^2}{M_P^2}\right) . \tag{0.2}$$

We see that this experimental quantity is expressed in terms of some SM known parameters, a CKM matrix element and some non-perturbative quantity, such as the *decay constant f_P*. The dominant uncertainty in the theoretical prediction of flavor observables comes from the hadronic parameters that include the non perturbative contributions [4]. The calculation of the ratio between the kaon and pion decay constants, namely f_K and f_π, enables one to extract $|V_{us}/V_{ud}|$ from the decays $K \to \mu\nu_\mu$ and $\pi \to \mu\nu_\mu$. Most of the mixing angles $|V_{ij}|$ can also be determined from the study of semileptonic decays. For example, $|V_{cd}|$ and $|V_{cs}|$ can be extracted from the branching ratios of $D \to \pi\ell\nu_\ell$ and $D \to K\ell\nu_\ell$, if one knows the values of the form factors at $q^2 = 0$, $f_+^{D\pi}(0)$ and $f_+^{DK}(0)$. Furthermore, the determination of the $K \to \pi$ vector form factor, $f_+^{K\pi}(0)$, provides the most precise determination of the matrix element $|V_{us}|$ through the analysis of the semileptonic decay $K \to \pi\ell\nu_\ell$, also known as $K_{\ell 3}$ decay.

From the theoretical point of view, the calculations are challenging due to the effects of the strong interactions, which in the SM are described by Quantum Chromodynamic (QCD). At high energies (or equivalently at short distances) the theory is weakly interactive, so that it is possible to study the theory with perturbative techniques. On the contrary, the interaction increases with the decrease of the energy (or with the increase of the distance), and at energies lower than ~ 1 GeV the theory is non-perturbative. For this reason, every calculation of low energy hadronic states needs a non-perturbative treatment. The only available technique that permits to calculate observables non-perturbatively from first principles is Lattice QCD (LQCD), which is the tool used in this thesis. It consists in the simulation of QCD by formulating the Lagrangian on a discrete and finite Euclidean space-time, that allows for the numerical computation of path integrals via Monte Carlo methods.

One advantage of LQCD is that by the introduction of a finite 4-dimensional volume $V = L^3 \times T$ and a lattice spacing a, the theory is both IR and UV regularized. Furthermore,

the LQCD degrees of freedom are finite. So we can use the path-integral formalism, which provides by itself a non-perturbative approach. By discretizing the gauge and fermion fields, we can elaborate a lattice gauge field theory with some freedom, as long as in the continuum limit we recover the target QCD theory. By choosing properly the lattice action we can minimize discretization effects, leaving $O(a^2)$ as the leading contributions.

In the Euclidean space-time the path-integral has the form of a partition function and it can be calculated using numerical simulations. Given the large number of lattice points, Monte Carlo methods are employed with the *importance sampling* technique, by weighting the contributions to the integral using the Boltzmann factor. The finite volume effects, the introduction of the lattice and in many cases the simulated values of the light quark masses which are larger than the physical ones introduce systematic uncertainties which have to be precisely controlled and accounted for.

Thanks to the increased computational power as well as to the algorithm and action improvements of the last decade, LQCD simulations have made significant progresses reaching a remarkable level of precision. In particular, this is due to the so-called un-quenched calculations, where the contributions of loops of dynamical sea quarks is properly taken into account.

Most of the theoretical predictions on phenomenologically relevant hadronic observables have been derived assuming the exact validity of the isospin symmetry and completely neglecting the effects of electromagnetic interactions. In an isospin symmetric world, the up and down quarks would be identical particles. It is known that in Nature the isospin symmetry is explicitly broken by the non-zero mass and electric charge differences between the u and d quarks. The mass difference $\widehat{m}_d - \widehat{m}_u$[1] represents one percent or less of any typical QCD energy scale. Similarly, the typical relative size of the electromagnetic (e.m.) breaking of the isospin symmetry is given by the fine structure constant and it is small on hadronic observables because in the low energy regime $\widehat{\alpha}_{em} \ll 1$. In particular, we have

$$\frac{\widehat{m}_d - \widehat{m}_u}{\Lambda_{\text{QCD}}} \simeq 0.01 \quad \text{and} \quad \widehat{\alpha}_{em} = \frac{\widehat{e}^2}{4\pi} \simeq \frac{1}{137.036} \ . \tag{0.3}$$

For these reasons we can reasonably state that, for observables with a non-vanishing isospin symmetric part the, isospin symmetry is a good approximation of reality with an $O(1\%)$ relative error. However, these small isospin breaking corrections are crucial to describe the structure of atomic matter in the Universe [5]. One of the most important consequences of the difference between the u and d quarks is that proton and neutron have different masses and charges. The sign of that mass splitting makes the proton, and thus the hydrogen atom, a stable particle. In addition, its value plays a crucial role in the determination of the initial conditions of the Big Bang Nucleosynthesis.

Even if the hadronic isospin mass splittings are well known quantities, predicting it from first principles is still a challenging problem because of the complex non-perturbative interactions of quarks inside the hadrons. Furthermore, an important part of the structure of atomic matter, as we know it, relies on a subtle cancellation between the small EM and strong

---

[1] We indicate the quantities renormalized in the QCD+QED theory with an "hat".

breaking effects of the isospin symmetry, e.g. in the kaon and nucleon systems. Therefore, it is fundamental to have a theoretical understanding of the hadronic mass splittings.

Is also interesting to understand how to deduce the individual $\widehat{m}_u$ and $\widehat{m}_d$ quark masses and their difference. For example, it is important to know if $\widehat{m}_u = 0$ could be a realistic solution to the strong CP problem. One way to do this is to consider that the kaon is a pseudo-Goldstone boson of chiral symmetry breaking and so the mass splitting $\Delta M_K^2 = M_{K^+}^2 - M_{K^0}^2$ is particularly sensitive to the strong isospin breaking. In order to calculate this effect, we have to find a way to evaluate the QED isospin breaking contributions. One well known result in this direction is the Dashen's theorem [6] that states that in the $SU(3)$ chiral limit the electromagnetic kaon mass splitting is equal to the pion one. Since ΔM_π^2 is known a pure QED effect with good accuracy (the strong IB corrections being quadratic in $\widehat{m}_d - \widehat{m}_u$), we conclude that $(\Delta M_K^2)_{em} = (\Delta M_\pi^2)_{em} + O(\alpha_{em} m_s)$.

Starting from the relevant two-points correlation functions calculated on the lattice, we have computed the isospin breaking corrections to pseudoscalar (P) meson masses [7]. In particular, we here provide results for the pion, kaon and charmed-meson mass splittings, for the various ε parameters describing the violations of the Dashen's theorem. Furthermore, we have calculated the $\widehat{m}_u$ and $\widehat{m}_d$ quark masses and their difference.

The method we have adopted in this work to calculate leading isospin breaking effects on the lattice by including those associated with QED interactions has been developed in [8, 9]. These effects are tiny because very small couplings, namely $(\widehat{m}_d - \widehat{m}_u)/\Lambda_{\text{QCD}}$ and $\widehat{\alpha}_{em}$, multiply sizable matrix elements of hadronic operators. The approach is based on a perturbative expansion of the lattice path-integral in powers of $(\widehat{m}_d - \widehat{m}_u)/\Lambda_{\text{QCD}}$ and $\widehat{\alpha}_{em}$, considering the two expansion parameters of the same size and neglecting higher orders. In this sense we talk of *leading isospin breaking* (LIB) effects.

A great advantage of our method is that, by working at a fixed order in the perturbative expansion, we are able to factorize the small coefficients and to get relatively large numerical signals. For the same reason, we do not need to perform simulations at unphysical values of the electric charge, thus avoiding extrapolations of the lattice data with respect to $\widehat{\alpha}_{em}$.

The expansion of the lattice path-integral in powers of $\widehat{\alpha}_{em}$ leads to correlators containing the integral over the whole space-time of insertions of the quark electromagnetic currents, multiplied by the lattice photon propagator. These correlators have both infrared (zero modes), and ultraviolet divergences, that must be removed by providing an infrared safe finite volume definition of the lattice photon propagator and by imposing suitable renormalization conditions.

At first order of the expansion, the pion mass difference is generated only by QED corrections. Furthermore, α_{em} does not need to be renormalized at this order. For this reason the pion mass splitting is a particularly clean theoretical prediction. Our result has been obtained by neglecting a quark disconnected contribution to M_{π^0} which is, however, of order $O(\alpha_{em} m_{ud})$, with m_{ud} the average u and d quark mass. This contribution is expected to be numerically of the same order of the neglected second-order contributions to the expansion.

The kaon and D-meson mass splittings are determined by both electromagnetic and strong isospin breaking (SIB) effects. We implemented a renormalization prescription in

order to separate these effects (see Section 1.10 later on). Using that prescription, we have calculated $[M_{K^+} - M_{K^0}]^{QED}$, $[M_{K^+} - M_{K^0}]^{SIB}$, $M_{D^+} - M_{D^0}$, together with the Dashen's theorem breaking parameters ε_{π^0}, ε_γ, ε_{K^0} (defined in Eqs. (2.51), (2.56) and (2.80) respectively) and the u and d quark mass difference. Those results have been obtained using the so-called electro-quenched approximation, i.e. by considering dynamical sea quarks as neutral with respect to electromagnetism. For the present study we have used lattice gauge field configurations generated by European Twisted Mass (ETM) Collaboration with $N_f = 2 + 1 + 1$ sea quark flavors. We here anticipate our findings

$$M_{\pi^+} - M_{\pi^0} \;=\; 4.21\,(26)\text{ MeV }\; [4.5936\,(5)\text{ MeV}]_{exp}\,, \qquad (0.4)$$

$$[M_{K^+} - M_{K^0}]^{QED}\,(\overline{MS}, 2\text{ GeV}) \;=\; 2.07\,(15)\text{ MeV}\,, \qquad (0.5)$$

$$[M_{K^+} - M_{K^0}]^{SIB}\,(\overline{MS}, 2\text{ GeV}) \;=\; -6.00\,(15)\text{ MeV}\,, \qquad (0.6)$$

$$(\widehat{m}_d - \widehat{m}_u)(\overline{MS}, 2\text{ GeV}) \;=\; 2.38\,(18)\text{ MeV}\,, \qquad (0.7)$$

$$\frac{\widehat{m}_u}{\widehat{m}_d}(\overline{MS}, 2\text{ GeV}) \;=\; 0.513\,(30)\,, \qquad (0.8)$$

$$\widehat{m}_u(\overline{MS}, 2\text{ GeV}) \;=\; 2.50\,(17)\text{ MeV}\,, \qquad (0.9)$$

$$\widehat{m}_d(\overline{MS}, 2\text{ GeV}) \;=\; 4.88\,(20)\text{ MeV}\,, \qquad (0.10)$$

$$\varepsilon_{\pi^0} \;=\; 0.01\,(4)\,, \qquad (0.11)$$

$$\varepsilon_\gamma(\overline{MS}, 2\text{ GeV}) \;=\; 0.80\,(11)\,, \qquad (0.12)$$

$$\varepsilon_{K^0}(\overline{MS}, 2\text{ GeV}) \;=\; 0.01\,(2)\,, \qquad (0.13)$$

$$[M_{D^+} - M_{D^0}]^{QED}\,(\overline{MS}, 2\text{ GeV}) \;=\; 2.42\,(51)\text{ MeV}\,, \qquad (0.14)$$

$$[M_{D^+} - M_{D^0}]^{SIB}\,(\overline{MS}, 2\text{ GeV}) \;=\; 3.06\,(27)\text{ MeV}\,, \qquad (0.15)$$

$$M_{D^+} - M_{D^0} \;=\; 5.47\,(53)\text{ MeV }\; [4.75\,(8)\text{ MeV}]_{exp}\,, \qquad (0.16)$$

$$\delta M_{D_s^+} \;=\; 2.3\,(4)\text{ MeV}\,, \qquad (0.17)$$

where the errors include an estimate of the effects of the QED quenching. In Eqs. (0.4) and (0.16) the experimental values from PDG [3] are given in squared brackets for comparison. Instead the experimental value of the kaon mass splitting $M_{K^+} - M_{K^0} = -3.934(20)$ MeV [3] is used as the input to determine the quark mass difference $(\widehat{m}_d - \widehat{m}_u)$ given in Eq. (0.7). Moreover, in Eq. (0.17) we provide an estimate of the electromagnetic corrections to the D_s^+-meson mass.

Apart from the hadronic spectrum, for many physical quantities relevant to studies of flavor physics, the recent improvements in lattice computations have led to such a precision

that electromagnetic effects and isospin breaking contributions cannot be neglected anymore. An example is provided by the leptonic decay constants f_K and f_π, relevant for $K_{\ell 2}$ and $\pi_{\ell 2}$ decays, and the form factor $f^+(0)$ appearing in semileptonic $K_{\ell 3}$ decays. These quantities are used to extract the CKM entries $|V_{us}|$ and $|V_{us}|/|V_{ud}|$ from the experimental decay rates, and they have been computed on the lattice with a precision at the sub-percent level [4]

$$f_\pi = 130.2\,(1.4) \text{ MeV} \qquad f_K = 155.6\,(4) \text{ MeV}$$
$$f_K/f_\pi = 1.193\,(3) \qquad f^+(0) = 0.9704\,(32) \ . \tag{0.18}$$

The quoted QCD errors are of the same order of the uncertainties due to the explicit breaking of isospin symmetry and to electromagnetic corrections to the leptonic and semileptonic decay rates. For this reason, if one wants to improve the precision of theoretical calculations, these corrections have to be taken into account.

Recently a method has been proposed to compute electromagnetic effects in hadronic processes, like decay rates, using lattice simulations [10]. The computations of this quantities is made much more complicated with respect to the computation of the hadronic spectrum by the presence of infrared divergences in the intermediate stages of the calculation. Infrared divergences can be removed by considering diagrams containing different numbers of real and virtual photons [11]. Let us consider the leptonic decays of charged P mesons, $P^+ \to \ell^+ \nu_\ell$. As we mentioned, in the absence of electromagnetism the non-perturbative QCD effects are contained in the decay constant f_P, defined by

$$\langle 0|\bar{q}_1 \gamma^\mu \gamma^5 q_2|P^+(p)\rangle = ip^\mu f_P \tag{0.19}$$

where P^+ is composed of the valence quarks $\bar{q}_1$ and q_2, and the axial current in (0.19) is composed of the corresponding quark fields. When we include electromagnetism, the constant f_P has not any more a physical definition, because of the contribution of diagrams in which a photon is exchanged between a quark into the hadron and the charged lepton. Thus the physical width is not just given in terms of the matrix element of the axial current and can only be obtained by a full calculation of the electromagnetic corrections at a given order.

The first step in the calculation of the weak decay width is to remove the IR divergence contained in $\Gamma_0 = \Gamma(P^+ \to \ell^+ \nu_\ell)$ by including the contributions from real photons. Defining $\Gamma_1(\Delta E)$ the partial width for the decay $P^+ \to \ell^+ \nu_\ell \gamma$, with ΔE the maximum value of the energy of the photon in the centre-of-mass of P^+, we have that the sum $\Gamma_0 + \Gamma_1(\Delta E)$ is free from IR divergences.

Let us consider $P^+ = \pi^+$. At lowest order in electromagnetic perturbation theory the process $u\bar{d} \to \ell^+ \nu_\ell$ proceeds by a W exchange in the s channel. Since the momentum transfers in this kind of processes are much smaller than M_W, we can rewrite the amplitude in terms of a four-fermions local interaction

$$\mathcal{L}_W = -\frac{G_F}{\sqrt{2}} V_{ud}^* [\bar{d}\gamma_\mu(1-\gamma_5)u][\bar{\nu}_\ell \gamma^\mu(1-\gamma_5)\ell] \ , \tag{0.20}$$

where G_F is the Fermi constant.

In lattice calculations this replacement is necessary since the lattice spacing is much greater than $1/M_W$ (typically $a^{-1} \simeq 2-4$ GeV). When including the $O(\alpha_{em})$ corrections, the ultraviolet contributions to the matrix element of the local operator (0.20) are different from those in the SM. However all divergences can be reabsorbed into the definition of G_F. Indeed, according to Sirlin [12], the evaluation of the amplitude for the process $\pi^+ \to \ell^+ \nu_\ell$ up to $O(\alpha_{em})$ can be performed in the effective theory with the effective Hamiltonian

$$H_{eff} = \frac{G_F}{\sqrt{2}} V_{ud}^* \left(1 + \frac{\alpha_{em}}{\pi} \log \frac{M_Z}{M_W} \right) [\bar{d}\gamma_\mu (1-\gamma_5)u][\bar{\nu}_\ell \gamma^\mu (1-\gamma_5)\ell] \qquad (0.21)$$

and the photon propagator in this effective theory defined (in the Feynman gauge) in the so-called *W-regularization*, namely

$$\frac{1}{k^2} \to \frac{M_W^2}{M_W^2 - k^2} \frac{1}{k^2} \, . \qquad (0.22)$$

The UV divergent contribution of the photon propagator, namely $(k^2 - M_W^2)^{-1}$, is absorbed in the re-definition of the Fermi constant G_F.

Up to now we are not still able to implement the W-regularization on the lattice, due to the heavy mass of W bosons. Thus, the matching between the operator in (0.21) defined on the lattice and in W regularization has to be exploited. The renormalization of the weak Hamiltonian is performed in two steps [13]. First of all, the lattice operators are renormalized non-perturbatively in the RI'-MOM scheme [14] at $O(\alpha_{em})$ and to all orders in the strong coupling α_s. Because of the breaking of chiral symmetry in the twisted mass formulation we have adopted in our study, this renormalization includes the mixing with other four-fermion operators of different chirality. In the second step we perform the matching from the RI'-MOM scheme to the W-regularization scheme perturbatively. By calculating and including the two-loop anomalous dimension at $O(\alpha_{em}\alpha_s)$, the residual truncation error of this matching is of $O(\alpha_{em}\alpha_s(M_W))$.

It is clear that the problem of calculating Γ_0 is the evaluation on the lattice of correlation functions involving the effective Hamiltonian (0.21). The diagrams contributing at $O(\alpha_{em})$ to the amplitude for the decay $\pi^+ \to \ell^+ \nu_\ell$ are those reported in Fig. 0.0.1.

This thesis constitutes a step forward in the context of non-perturbative calculations of isospin breaking effects in hadronic processes, since the leading electromagnetic and strong isospin breaking corrections to the $\pi^+ \to \mu^+ \nu_\mu(\gamma)$ and $K^+ \to \mu^+ \nu_\mu(\gamma)$ leptonic decay rates have been evaluated for the first time on the lattice. This study demonstrates that such calculations are within reach of present lattice technology. The successful implementation of the proposed method in the case of leptonic decays of hadrons can be also extended to the *ab initio* calculation of radiative QED corrections to semileptonic decays.

The main results of our calculation are presented in Chapter 4 together with a detailed discussion of their implications. Here, we anticipate some key results: After extrapolation of the data to the physical pion mass, and to the continuum and infinite-volume limits, the
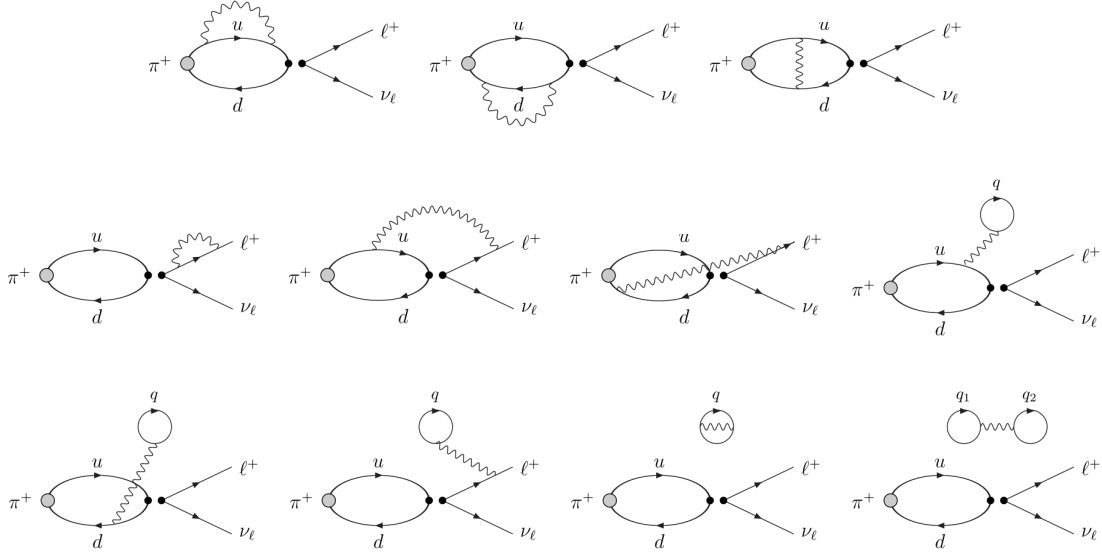
Figure 0.0.1: Connected and disconnected diagrams contributing at $O(\widehat{\alpha}_{em})$ contribution to the amplitude for the decay $\pi^+ \to \ell^+ \nu_\ell$.

isospin-breaking corrections to the leptonic decay rates can be written in the form [13]:

$$\Gamma(\pi^\pm \to \mu^\pm \nu_\mu[\gamma]) = (1.0153 \pm 0.0019)\, \Gamma^{(0)}(\pi^\pm \to \mu^\pm \nu_\mu), \tag{0.23}$$

$$\Gamma(K^\pm \to \mu^\pm \nu_\mu[\gamma]) = (1.0024 \pm 0.0010)\Gamma^{(0)}(K^\pm \to \mu^\pm \nu_\mu), \tag{0.24}$$

where $\Gamma^{(0)}$ is the leptonic decay rate at tree level. The corrections are about 1.6% for the pion decays and 0.3% for the kaon decay, in line with the generic $O(1\%)$ naive expectations.

Taking the experimental value of the rate for the $K_{\mu 2}$ decay, Eq. (0.24) together with $\Gamma^{(0)}(K^\pm \to \mu^\pm \nu_\mu)$ obtained using the lattice determination of the kaon decay constant we obtain $|V_{us}| = 0.22567(42)$, in agreement with the latest estimate $|V_{us}| = 0.2253(7)$, recently updated by the PDG [3] but with better precision. Alternatively, by taking the ratio of $K_{\mu 2}$ and $\pi_{\mu 2}$ decay rates and the updated value $|V_{ud}| = 0.97420\,(21)$ from super-allowed nuclear beta decays [15], we find [16]

$$|V_{us}| = 0.22538\,(46)\,. \tag{0.25}$$

The unitarity of the first row of the CKM matrix is satisfied at the per-mille level; e.g. taking the value of V_{us} from the ratio of decay rates and $|V_{ub}| = 0.00413(49)$ [3], we get

$$|V_{ud}|^2 + |V_{us}|^2 + |V_{ub}|^2 = 0.99988\,(46)\,. \tag{0.26}$$

The work described in this thesis has been undertaken between November 2016 and October 2019 while I was a Ph.D. student at the Mathematics and Physics Department of Università degli Studi Roma Tre and it has been carried out under the supervision of Prof. Vittorio Lubicz and Prof. Silvano Simula. Parts of this thesis have appeared in the following papers:

- D. Giusti, V. Lubicz, G. Martinelli, F. Sanfilippo, S. Simula, N. Tantalo and C. Tarantino
  Leading isospin-breaking corrections to pion, kaon and charmed-meson masses with Twisted-Mass fermions
  Phys. Rev. D 95 (2017) 114504 [arXiv:1704.06561 [hep-lat]] [7].

- D. Giusti, V. Lubicz, G. Martinelli, C. T. Sachrajda, F. Sanfilippo, S. Simula, N. Tantalo and C. Tarantino
  First lattice calculation of the QED corrections to leptonic decay rates
  Phys. Rev. Lett. 120 (2018) 072001 [arXiv:1711.06537 [hep-lat]] [16].

- M. Di Carlo, D. Giusti, V. Lubicz, G. Martinelli, C. T. Sachrajda, F. Sanfilippo, S. Simula and N. Tantalo
  Light-meson leptonic decay rates in Lattice QCD+QED
  Phys. Rev. D 100 (2019) 034514 (Editor's suggestion) [arXiv:1904.08731 [hep-lat]] [13].

This work is organized as follows[2]

- In Chapter 1 we explain the method used in the calculation of the isospin breaking effects, that is basically a combined expansion in $(\widehat{m}_d - \widehat{m}_u)/\Lambda_{\mathrm{QCD}}$ and $\widehat{\alpha}_{em}$ of the two-points correlation functions [8, 9]. We explain how QED is introduced in our simulation using the non-compact formulation, i.e. by using as dynamical variable on the lattice the electromagnetic field A_μ. When including QED on the lattice, we have to deal with the fact that it is a long-ranged interaction, so we have to take into account finite volume effects (FVEs) [17] that are not exponentially suppressed, as is often the case of QCD, but decrease only as inverse powers of the lattice size. We also discuss in some detail how one might define the QCD contribution from the full (QCD+QED) theory. Although such a separate definition of QCD is not required in order to obtain results computed in the full theory, it is convenient if one wishes to talk about radiative (and strong IB) corrections to results obtained in QCD. For this we need to specify what we mean by QCD. Finally, the renormalization of the quark field, bilinear and four-fermion operators in the combined QCD+QED theory is discussed.

- In Chapter 2 we describe the lattice computation of the isospin breaking corrections to pseudoscalar meson masses. Using the strategy described in Chapter 1 we obtain results for the pion, kaon and charmed-meson mass splittings, for the ε parameters related to the violations of the Dashen's theorem and for the light quark mass difference [7].

- Chapter 3 contains a thorough illustration of the method proposed in [10] to compute electromagnetic effects in hadronic processes using lattice simulations. We discuss the framework for including radiative QED corrections in leptonic decays of hadrons, including the treatment of infrared divergences in intermediate stages of the calculation.

---

[2]In this thesis the basic ingredients of the lattice QCD regularization are assumed to be known. In particular we do not discuss how to discretize the fermion and the gauge fields and how to perform the renormalization on the lattice.

In order to compute the physical widths, diagrams with virtual photons must be combined with those corresponding to the emission of real photons. Only in this way do the infrared divergences cancel as first understood by Bloch and Nordsieck in 1937. We also discuss the effective weak Hamiltonian and its renormalisation in the presence of electromagnetism. Finally, we address the additional theoretical issues which arise when including electromagnetic corrections to semileptonic decays, such as $K_{\ell 3}$ decays.

- In Chapter 4 we present the first lattice determination of the radiative corrections to the light meson leptonic decay rates. By adopting the method described in Chapter 3 we provide results for the leading electromagnetic and strong isospin breaking corrections to the $\pi^+ \to \mu^+ \nu_\mu(\gamma)$ and $K^+ \to \mu^+ \nu_\mu(\gamma)$ leptonic decay rates [13, 16]. For these channels the real soft-photon contributions and the structure dependent (SD) corrections are estimated, by relying on the quoted chiral perturbation theory results, to be negligible. On the other hand SD corrections might be relevant in the case of heavy flavors and for the decays of pions and kaons into electrons when the energy of the photon becomes larger than about 20 MeV. Therefore, at the end of the chapter, we also present a preliminary non-perturbative calculation of the form factors which contribute to the amplitudes for the radiative decays $P \to \ell \nu_\ell \gamma$ for P mesons ranging from the pion to the D_s meson. Together with the non-perturbative determination of the virtual photon corrections to the processes $P \to \ell \nu_\ell$, this will allow accurate predictions to be made at $O(\alpha_{em})$ for leptonic decay rates for pseudoscalar mesons, leading to significantly improved precision in the determination of the corresponding CKM matrix elements. Precise predictions for the emission of a hard photon are also very interesting, especially for the decays of heavy D and B mesons for which currently only model-dependent predictions are available to compare with existing experimental data.

Appendix A contains an expanded discussion of the renormalisation of the effective weak Hamiltonian, including electromagnetic corrections, along with some important aspects peculiar to the twisted mass fermions used in the numerical calculation. Finally, we end this thesis with some conclusions where we summarize the main results and indicate some future perspectives.

1 Isospin Breaking Effects on the Lattice

1.1 Introduction

Isospin symmetry $SU(2)_V$, is an almost exact property of strong interactions as described by the QCD Lagrangian. This happens because the difference between the up and down quark masses is much smaller than the QCD scale, $(\widehat{m}_d - \widehat{m}_u)/\Lambda_{QCD} \ll 1$, and it remains true also when electromagnetic interactions are switched on, because isospin breaking effects due to the different quark electric charges ($e_u \neq e_d$) are suppressed by the electromagnetic coupling constant, $\widehat{\alpha}_{em} \simeq 1/137.036$. For these reasons most of theoretical predictions of several physical quantities assume isospin symmetry, i.e. the masses of the up and down quarks are taken equal and electromagnetic effects are neglected.

One of the primary goals of lattice QCD is to calculate non-perturbatively hadronic observables at the level of accuracy required for phenomenological applications. In the flavor physics sector, for instance, the combined efforts of the lattice QCD community resulted in calculations of quantities such as the $K_{\ell2}$ and $K_{\ell3}$ decay rates with relative overall uncertainties at the few per mille level [4, 18].These results have been obtained, in most of the cases, within the isosymmetric theory.

Nowadays, with the increasing precision of the experimental determinations of many physical quantities, and in some cases with the improvement of the theoretical predictions, the control over isospin breaking effects is becoming phenomenologically relevant. For example, by neglecting the pion mass difference (3%) and the kaon mass difference (1%) a systematic error is unavoidably introduced on the corresponding determination of the $K_{\ell3}$ decay rate or on any dimensional quantity if these masses are used to calibrate the lattice. Isospin breaking effects are important also for hadron spectroscopy, for the meson decay constants, for the π-π scattering length, for the quark condensate and for many other quantities.

In the past, isospin breaking effects due to the light quark mass difference (in the following referred to as SIB effects for *strong isospin breaking effects*) have been accommodated within the chiral perturbation theory (ChPT) framework or relying on model-dependent approximations (see [19–22] for a largely incomplete list of references on the subject), while several attempts to compute electromagnetic effects for the hadron spectroscopy in lattice

QCD have been presented [23–26]. It is very difficult to take into account in numerical simulations SIB effects (see [27–31] for a selection of previous lattice works on the subject) because the effect is in general rather small and comparable with the errors in the determination of, say, the hadron masses or decay constants. Furthermore, in order to perform unitary dynamical simulations of two light quarks of different mass the single quark determinant must be positive and this happens only in the case of lattice discretizations of the fermion action that are very expensive from the numerical point of view.

In this chapter we will first discuss how to compute hadron masses in LQCD and then the method that we used to evaluate leading isospin breaking effects (LIB) on the lattice by including those associated with QED interactions [8, 9]. These are tiny corrections because very small factors, $(\widehat{m}_d - \widehat{m}_u)/\Lambda_{QCD}$ and $\widehat{\alpha}_{em}$, multiply sizable matrix elements of hadronic operators.

Our approach, known as the *RM123* approach, consists in a perturbative combined expansion of euclidean correlation functions in powers of the electric charge $\widehat{e}$ and the mass difference $\widehat{m}_d - \widehat{m}_u$ of the light quark masses. We consider the two expansion parameters of the same order of magnitude, $(\widehat{m}_d - \widehat{m}_u)/\Lambda_{QCD} \sim \widehat{\alpha}_{em} \sim \varepsilon$, and neglect in this work terms of $O(\varepsilon^2)$. In this sense we talk of "leading isospin breaking" (LIB) effects. Next-to-leading SIB corrections, i.e. second or higher orders in the $\widehat{m}_d - \widehat{m}_u$ expansion, have not been calculated in the present work. The associated effects are estimated to be negligible at the current level of (both theoretical and experimental) precision on flavor physics observables. Indeed, on the basis of dimensional arguments, higher orders corrections are expected to be suppressed by additional powers of the small expansion parameter $(\widehat{m}_d - \widehat{m}_u)/\Lambda_{QCD}$. Clearly, we cannot exclude the existence of specific observable for which higher order SIB effects may be larger than expected. Nevertheless if necessary, the method suggested can be extended to evaluate higher order contributions (for example, for the π^+-π^0 mass splitting [8]).

A great advantage of our method with respect to other approaches (see for example [23, 25, 32–34]) is that, by working at fixed order in a perturbative expansion, we are able to factorize the small coefficients and to get relatively large numerical signals. For the same reason, we do not need to perform simulations at unphysical values of the electric charge, thus avoiding extrapolations of the lattice data with respect to $\widehat{\alpha}_{em}$.

In order to better understand our strategy we will start by describing how to calculate isospin breaking effects due to the u and d mass difference (see Sec. 1.3). We will then include the electromagnetic effects and explain how we included electromagnetism in our numerical simulations using a non-compact formulation of QED, i.e. by using as dynamical variable on the lattice the electromagnetic field A_μ. The expansion of the lattice path-integral in powers of $\widehat{\alpha}_{em}$ leads to correlators containing the integral over the whole space-time lattice volume of two insertions of the quark electromagnetic currents multiplied by the lattice photon propagator. These quantities have both infrared and ultraviolet divergences that must be removed by providing an infrared safe finite volume definition of the lattice photon propagator and by imposing suitable renormalization conditions. These issues will be discussed in detail in Sec. 1.4.

In Sec. 1.5 we will also give some details about the lattice fermion action, in particular

of the mixed-action setup used in this work.

In Secs. 1.6 and 1.7 we then describe our method explaining how we perform the expansions of the physical observables in $\widehat{m}_d - \widehat{m}_u$ and $\widehat{\alpha}_{em}$ and how to calculate corrections to the lattice path-integral. For illustrative purposes we will focus on two-point correlation functions, from which we evaluated isospin breaking corrections to hadron masses.

The method is applicable in principle to any hadronic observable which can be computed on the lattice and it was tested, applying it to the computation of leading isospin breaking effects for several physical quantities of interest: the pseudoscalar meson masses [7], the neutron-proton mass splitting [9, 35], the light meson decay constants [13, 16, 36], the form factors of semileptonic $K_{\ell 3}$ decays [8] and the hadronic vacuum polarization contribution to the lepton anomalous magnetic moments [37, 38].

Our results have been obtained within the electro-quenched approximation, i.e. by considering dynamical sea quarks as neutral with respect to electromagnetism.

Working on the lattice in finite volume, and being electromagnetism a long range interaction, we need to correct for QED finite volume effects which are by far not negligible. In Sec. 1.9 we will discuss how they have been evaluated in our calculations.

Moreover, a discussion of the relation between the "full" QCD+QED theory, including electromagnetic and SIB effects, and isospin-symmetric QCD without electromagnetism will be given in Sec. 1.10.

Finally, in Sec. 1.11 we will present a non-perturbative renormalization procedure for quark bilinear and four fermion operators in the combined QCD+QED theory.

1.2 HADRON MASSES ON THE LATTICE

Before discussing LIB effects on the lattice, we want to briefly sketch the strategy used to study the spectroscopy in LQCD.

Hadron masses are a crucial ingredient for any lattice calculation and are the simplest quantities that can be computed on the lattice. They are usually determined from the asymptotic behavior of the two point Euclidean-time correlation functions.

1.2.1 CORRELATION FUNCTIONS

The two-point correlator function in its general form is written as the vacuum expectation value of the T-product of two interpolating operators $O_j^\dagger(y)$ and $O_i(x)$, i.e., any local interpolators that create in y ad annihilate in x the state of interest from the vacuum

$$C_{ij}(x,y) = \langle \Omega | T(O_i(x)O_j^\dagger(y)) | \Omega \rangle. \tag{1.1}$$

For this reason we refer to $O_j^\dagger(y)$ and $O_i(x)$ as *source* and *sink interpolators* respectively. In fact, the first step of a spettroscopy calculation is the identification of the suitable hadron interpolators O_i and $O_j^\dagger$. For hadron spettroscopy one studies interpolators constructed out of quarks and gluons, namely functionals of lattice fields with the quantum numbers of the

state one is interested in. There is a huge number of these interpolators to choose from. In practice, any operator which have the same quantum numbers of the state of interest is suitable for the purpose.

We can rewrite the general correlator in eq.(1.1) in an operative form following two steps. Firstly, we can insert a complete set of energy eigenstates $|\tilde{E}_n\rangle = \sqrt{2E_n}|E_n\rangle$, which are covariantly normalized

$$\langle \tilde{E}_m | \tilde{E}_n \rangle = 2E_n \delta_{n,m} \tag{1.2}$$

and so satisfy the completeness relation in the form

$$\sum_n \frac{1}{2E_n} |\tilde{E}_n\rangle\langle\tilde{E}_n| + |\Omega\rangle\langle\Omega| = \mathbb{1}. \tag{1.3}$$

Secondly, due to the spatial and temporal traslational symmetry, $O_i(x)$ has a simple dependence from x, which allows us to replace

$$O_i(x) = e^{ipx} O_i(0) e^{-ipx}, \tag{1.4}$$

where $e^{-ipx} = e^{-i(Ht - \vec{p}\cdot\vec{x})}$ is the space-time evolution operator. Introducing these expressions into eq.(1.1) and assuming that O_i and O_j do not have the quantum numbers of the vacuum, the correlation function analytically continued to Euclidean times τ through the Wick's rotation $it \to \tau$ takes the following expression

$$
\begin{aligned}
C_{ij}(x,y) &= \sum_n \frac{1}{2E_n} \langle\Omega|e^{ipx}O_i(0)e^{-ipx}|\tilde{E}_n\rangle\langle\tilde{E}_n|e^{ipy}O_j^\dagger(0)e^{-ipy}|\Omega\rangle = \\
&= \sum_n \frac{1}{2E_n} \langle\Omega|O_i(0)|\tilde{E}_n\rangle\langle\tilde{E}_n|O_j^\dagger(0)|\Omega\rangle e^{-E_n(\tau_x - \tau_y) + i\vec{p}_n\cdot(\vec{x}-\vec{y})},
\end{aligned}
\tag{1.5}
$$

and we consider the case E_n satisfies the relativistic dispersion relation

$$E_n = \sqrt{M_n^2 + \vec{p}_n^2}. \tag{1.6}$$

There is no loss in generality in setting $y = 0$. Applying the Fourier Transform in the space component we can write

$$
\begin{aligned}
C_{ij}(\tau, \vec{p}) &= \frac{1}{L^3} \sum_{\vec{x}} C_{ij}(x) e^{-i\vec{p}\cdot\vec{x}} = \\
&= \sum_n \sum_{\vec{x}} \frac{1}{L^3 2E_n(\vec{p}_n)} \langle\Omega|O_i(0)|\tilde{E}_n\rangle\langle\tilde{E}_n|O_j^\dagger(0)|\Omega\rangle e^{-E_n\tau} e^{i(\vec{p}_n - \vec{p})\cdot\vec{x}} = \\
&= \sum_n \frac{1}{2E_n(\vec{p}_n)} \langle\Omega|O_i(0)|\tilde{E}_n\rangle\langle\tilde{E}_n|O_j^\dagger(0)|\Omega\rangle e^{-E_n\tau} \delta(\vec{p}_n - \vec{p}) = \\
&= \sum_n \frac{1}{2E_n(\vec{p})} \langle\Omega|O_i(0)|\tilde{E}_n\rangle\langle\tilde{E}_n|O_j^\dagger(0)|\Omega\rangle e^{-E_n\tau}.
\end{aligned}
\tag{1.7}
$$

Then, the correlation function at zero momentum $\vec{p} = 0$ is simply given by

$$C_{ij}(\tau) = \sum_{\vec{x}} C_{ij}(x) = \sum_n \frac{1}{2M_n} \mathcal{Z}_i^n \mathcal{Z}_j^{n\dagger} \mathrm{e}^{-M_n \tau}, \qquad (1.8)$$

where we have called the matrix element

$$\langle 0|O_i(0)|\tilde{E}_n\rangle = \mathcal{Z}_i^n. \qquad (1.9)$$

We finally write the Eulidean-time correlation function as

$$C_{ij}(\tau) = \frac{1}{2M_0} \mathcal{Z}_i^0 \mathcal{Z}_j^{0\dagger} \mathrm{e}^{-M_0 \tau} \left(1 + \sum_{n>0} C_n \mathrm{e}^{-(M_n - M_0)\tau} \right), \qquad (1.10)$$

$$C_n = \frac{M_0}{M_n} \frac{\mathcal{Z}_i^n \mathcal{Z}_j^{n\dagger}}{\mathcal{Z}_i^0 \mathcal{Z}_j^{0\dagger}} \qquad (1.11)$$

where we have taken out of the summation the *fundamental state*, i.e., the lightest state excited from the vacuum by the operators O_i and O_j. All other states in the sum with $M_n > M$ are *excited states*. The elements $\mathcal{Z}_i^n \mathcal{Z}_j^{n\dagger}$ quantify the overlap between the interpolators chosen for the calculation of the Euclidean two-point correlation function and the n-th one-particle state.

1.2.2 EFFECTIVE MASSES

We have seen that the correlation function can be written as a superposition of single (and multiple) particle states weighted by a decreasing exponential factor depending on the mass M_n of the state. At large time distances heavier states will be suppressed, so that we can assume that only the fundamental state will survive:

$$C_{ij}(\tau) \xrightarrow[t\gg0]{} \frac{1}{2M_0} \mathcal{Z}_i^0 \mathcal{Z}_j^{0\dagger} \mathrm{e}^{-M_0 \tau}. \qquad (1.12)$$

This condition allows us to extract M_0, the mass of the hadron we are interested in, from an *effective mass* formula:

$$m_{\mathrm{eff}}(\tau) = \log \frac{C_{ij}(\tau)}{C_{ij}(\tau + 1)} \xrightarrow[\tau\gg0]{} M_0, \qquad (1.13)$$

which approaches M_0 for large enough τ. Indeed, eq.(1.13) could becomes slightly more complicated on the lattice. As simulations can be performed on a $V = L^3 \times T$ finite space-time lattice, there will be a reflected wave coming from the boundaries and traveling in opposite direction with respect to the signal. Time reversal symmetry implies that, for mesons, propagation in τ and $(T - \tau)$ is identical up to a possible relative minus sign and,

when only the ground state is considered, the correlator shows a cosh- or sinh-dependence on τ.

At large times, from a certain time $\tau_{\min}$ in lattice units, the effective mass curve exhibits a *plateau*. In this region, i.e. for $\tau \geq \tau_{\min}$, we can consider negligible the effect of the excited states. The main advantage of using an effective mass formula is that it makes it possible to extract the fundamental hadron mass directly from a *constant fit* in this interval, i.e. simply a weighted average over the points in the plateau interval $[\tau_{\min}, t_{\text{MAX}}]$. A proper choice of the fit interval $[\tau_{\min}, \tau_{\text{MAX}}]$ is a crucial step in our analysis:

- The choice of the $\tau_{\min}$ time should be done very carefully. The signal to noise ratio becomes weaker with the increasing of time and taking a small $\tau_{\min}$ will reduce the statistical uncertainty on M_0. On the other hand, by taking it too small, may not cut the contribution of the exited states properly. The last circumstance will introduce a systematic error by increasing the estimate of the effective mass.

- The choice of τ_{MAX}, for its part, is not equally delicate but requires a bit of attention as well. The signal to noise ratio gets weaker in the proximity of the boundary T. The final points are strongly fluctuating. We see in eq.(1.13) that the effective mass is written in terms of a $\log(x)$ function and strong fluctuations of the argument make m_{eff} not defined for all the points in the time interval. In such cases we are forced to choose a smaller τ_{MAX}.

1.3   LEADING ISOSPIN BREAKING EFFECTS ON THE LATTICE

In order to illustrate the strategy, we first describe the calculation of LIB induced by the small mass difference between the up and down quarks [8]. The introduction of QED isospin breaking effects is somewhat less straightforward and could be better understood if the basic ideas of the strategy are clear.

In this section we present the basic ingredients of the method, which is based on a perturbative expansion in the small parameter $(m_d - m_u)/\Lambda_{QCD}$. In this way one expresses isospin breaking corrections as a sum of amplitudes calculated in the isospin symmetric theory and multiplied by the small parameter.

Let us start by considering a generic euclidean correlation function $\langle \mathcal{O} \rangle$ used to extract information about physical quantities such as masses, decay constants, form factors etc.,

$$\langle \mathcal{O} \rangle = \frac{\int D\phi \, \mathcal{O} \, e^{-S}}{\int D\phi \, e^{-S}} \, , \tag{1.14}$$

where $D\phi$ represents schematically the full functional integration measure of the theory. By neglecting electromagnetic corrections we can write the Lagrangian density as a term which

is $SU(2)_V$ symmetric plus a term which violates the isospin symmetry,

$$
\begin{aligned}
\mathcal{L} &= \mathcal{L}_{kin} + \mathcal{L}_m = \\[2mm]
&= \mathcal{L}_{kin} + \frac{m_u + m_d}{2}(\bar{u}u + \bar{d}d) - \frac{m_d - m_u}{2}(\bar{u}u - \bar{d}d) = \\[2mm]
&= \mathcal{L}_{kin} + m_{ud}\,\bar{q}q - \Delta m_{ud}\,\bar{q}\tau^3 q = \\[2mm]
&= \mathcal{L}_0 - \Delta m_{ud}\,\tilde{\mathcal{L}}\,,
\end{aligned}
\tag{1.15}
$$

where $q^T = (u,d)$, $m_{ud} = (m_d + m_u)/2$ and $\Delta m_{ud} = (m_d - m_u)/2$. By expanding at first order the exponential of the action, $S = \sum_x \mathcal{L}(x)$, with respect to Δm_{ud} we obtain

$$
\begin{aligned}
\langle \mathcal{O} \rangle &\simeq \frac{\int D\phi\,\mathcal{O}\,(1 + \Delta m_{ud}\,\tilde{S})\,e^{-S_0}}{\int D\phi\,(1 + \Delta m_{ud}\,\tilde{S})\,e^{-S_0}} = \frac{\langle \mathcal{O} \rangle_0 + \Delta m_{ud}\,\langle \mathcal{O}\tilde{S} \rangle_0}{1 + \Delta m_{ud}\,\langle \tilde{S} \rangle_0} = \\[2mm]
&= \langle \mathcal{O} \rangle_0 + \Delta m_{ud}\,\langle \mathcal{O}\tilde{S} \rangle_0\,,
\end{aligned}
\tag{1.16}
$$

where $\langle \cdot \rangle_0$ represent the vacuum expectation value in the isospin symmetric theory and $\tilde{S}$ is the isospin breaking term,

$$
\tilde{S} = \sum_x [\bar{q}\tau^3 q](x) = \sum_x [\bar{u}u - \bar{d}d](x)\,.
\tag{1.17}
$$

The correction in the denominator of eq. (1.16) vanishes, $\langle \tilde{S} \rangle_0 = 0$, because of isospin symmetry.

We can apply eq. (1.16) to the calculation of the u and d propagators

$$
\begin{aligned}
S_u(x_1, x_2) &= S_\ell(x_1, x_2) + \Delta m_{ud} \sum_y S_\ell(x_1, y)\,S_\ell(y, x_2) + \cdots\,, \\[2mm]
S_d(x_1, x_2) &= S_\ell(x_1, x_2) - \Delta m_{ud} \sum_y S_\ell(x_1, y)\,S_\ell(y, x_2) + \cdots\,;
\end{aligned}
\tag{1.18}
$$

that can be diagrammatically represented as[1]

$$
\tag{1.19}
$$

---

[1]Here and in the following the up quark line in the full theory is drawn in light blue color while the down quark line in green. The black lines refer to S_ℓ, the propagator with the symmetric mass m_{ud} in the isospin symmetric theory.

where the insertion of the scalar density is represented by a cross and

$$y \longrightarrow x \; = \; S_\ell(x-y) = \langle \ell(x)\bar{\ell}(y)\rangle \,,$$

$$\otimes \; = \; \sum_z \bar{\ell}(z)\mathbb{1}\ell(z), \qquad\qquad (1.20)$$

with ℓ either u or d[2]. Using the expansion (1.16) we have written the u and d propagators as a sum of isospin symmetric propagators with a scalar insertion. The same procedure can be applied to all correlation functions in order to extract the leading isospin breaking corrections to physical observables.

In this work we have applied the method discussed above by using the so called Twisted Mass lattice discretization of the QCD action. This choice has advantages and drawbacks. The main advantage is the automatic $O(a)$ improvement. A drawback is the breaking of isospin symmetry at finite lattice spacing, even with $\Delta m_{ud} = 0$. The associated $O(a^2)$ cutoff effects are eliminated by performing continuum extrapolations. Our method is general and can be applied with any lattice regularization of the quark action (e.g. Wilson, Overlap, etc.).

1.3.1   CORRELATION FUNCTIONS AT FIRST ORDER

We shall consider the following two point correlation functions in order to give a description of how the method works:

$$C_{\pi^+\pi^-}(t,\vec{p}) = \sum_{\vec{x}} e^{-i\vec{p}\cdot\vec{x}} \langle\, \bar{u}\gamma_5 d(x)\; \bar{d}\gamma_5 u(0)\,\rangle \,,$$

$$C_{\pi^0\pi^0}(t,\vec{p}) = \frac{1}{2}\sum_{\vec{x}} e^{-i\vec{p}\cdot\vec{x}} \langle\, (\bar{u}\gamma_5 u - \bar{d}\gamma_5 d)(x)\; (\bar{u}\gamma_5 u - \bar{d}\gamma_5 d)(0)\,\rangle \,,$$

$$C_{K^+K^-}(t,\vec{p}) = \sum_{\vec{x}} e^{-i\vec{p}\cdot\vec{x}} \langle\, \bar{u}\gamma_5 s(x)\; \bar{s}\gamma_5 u(0)\,\rangle \,,$$

$$C_{K^0K^0}(t,\vec{p}) = \sum_{\vec{x}} e^{-i\vec{p}\cdot\vec{x}} \langle\, \bar{d}\gamma_5 s(x)\; \bar{s}\gamma_5 d(0)\,\rangle \,,$$

$$(1.21)$$

Using eq. (1.18) to expand the u and d propagator, we can calculate isospin breaking corrections. The first order corrections to pion masses do vanish, as can be shown by

---

[2]$\Delta\widehat{m}_{ud} = Z_{\Delta m}\Delta m_{ud}$, where $Z_{\Delta m}$ is scale and scheme dependent while the combination $\Delta m_{ud}\sum_z \bar{\ell}(z)\ell(z)$ is renormalization group invariant.

considering the diagrammatic expansion of the correlation functions of the charged pion,

$$C_{\pi^+\pi^-}(t) \quad = \quad -\overset{u}{\underset{d}{\bigcirc}} = -\bigcirc - \Delta m_{ud}\,\bigotimes + \Delta m_{ud}\,\bigcirc + \cdots =$$

$$= \quad -\bigcirc + O(\Delta m_{ud})^2\,, \tag{1.22}$$

and of the connected diagrams entering neutral pion two point function $C_{\pi^0\pi^0}(t)$,

$$\overset{u}{\underset{u}{\bigcirc}} = \bigcirc + \Delta m_{ud}\,\bigotimes + \Delta m_{ud}\,\bigcirc + \cdots =$$

$$= \bigcirc + 2\Delta m_{ud}\,\bigotimes + O(\Delta m_{ud})^2\,,$$

$$\overset{d}{\underset{d}{\bigcirc}} = \bigcirc - \Delta m_{ud}\,\bigotimes - \Delta m_{ud}\,\bigcirc + \cdots =$$

$$= \bigcirc - 2\Delta m_{ud}\,\bigotimes + O(\Delta m_{ud})^2\,,$$

$$C_{\pi^0\pi^0}(t) = -\frac{1}{2}\left[\overset{u}{\underset{u}{\bigcirc}} + \overset{d}{\underset{d}{\bigcirc}}\right] = -\bigcirc + O(\Delta m_{ud})^2\,. \tag{1.23}$$

The first order corrections cancel also for the disconnected diagrams contributing to $C_{\pi^0\pi^0}(t)$.

For kaon mesons first order corrections to masses and decay constants are instead different from zero. The strong IB correction to the two point correlation functions of the strange mesons are

$$C_{K^+K^-}(t) \quad = \quad -\overset{s}{\underset{u}{\bigcirc}} = -\bigcirc - \Delta m_{ud}\,\bigcirc + O(\Delta m_{ud})^2\,,$$

$$C_{K^0K^0}(t) \quad = \quad -\overset{s}{\underset{d}{\bigcirc}} = -\bigcirc + \Delta m_{ud}\,\bigcirc + O(\Delta m_{ud})^2\,. \tag{1.24}$$

In the diagrams above and in the following the strange quark line is red.

In the following sections (we will strictly follow the description of [9]) we are going to discuss the inclusion of QED isospin breaking effects, by performing an expansion in both $\widehat{m}_d - \widehat{m}_u$ and $\widehat{\alpha}_{em}$. As we have seen from eq. (1.22) and (1.23) the pion does not receive isospin breaking corrections at first order from the u and d mass difference and the leading correction comes from QED. On the contrary, kaons have both types of corrections at the leading order. In this case we will define a convention to separate QED and QCD effects.

1.4 NON-COMPACT QED ON THE LATTICE AT $O(\alpha_{em})$

In this section we describe how QED is regularized on the lattice and we discuss the issues associated with the expansion of the quark action with respect to the electric charge. In particular we present a safe prescription for the definition of the IR regularized finite volume lattice photon propagator, i.e. a way to eliminate the infrared divergence associated with the zero momentum mode, that can be conveniently used in numerical calculations by working directly in coordinate space.

We adopted the non–compact formulation of lattice QED, that consists in treating the electromagnetic gauge potential $A_\mu(x)$ in a fixed (Feynman) gauge as a dynamical variable. The field $A_\mu(x)$ is introduced as a free field with the Maxwell action

$$
\begin{aligned}
S_{gauge}[A] &= \frac{1}{2} \sum_{x,\mu,\nu} A_\mu(x) \left[-\bar{\nabla}_\nu^- \bar{\nabla}_\nu^+ \right] A_\mu(x) = \\
&= \frac{1}{2} \sum_{k,\mu,\nu} \tilde{A}_\mu^\star(k) \left[2\sin(k_\nu/2) \right]^2 \tilde{A}_\mu(k) ,
\end{aligned}
\tag{1.25}
$$

which is gaussian distributed in momentum space. $A_\mu(x)$ is a real field, while $\tilde{A}_\mu(k)$ denotes its Fourier transform that is a complex field satisfying the condition $\tilde{A}_\mu^\star(k) = \tilde{A}_\mu(-k)$.

Non-compact lattice QED has been used also in [23], where the effects of electromagnetism have been computed non-perturbatively on the lattice for the first time, and in most of the other lattice simulations subsequently performed ([25, 32–34] for recent works on the subject).

The electromagnetic interaction of quarks is written in terms of the quarks discrete covariant derivatives, by introducing the QED link variables through exponentiation[3],

$$
A_\mu(x) \longrightarrow E_\mu(x) = e^{-ieA_\mu(x)} ,
\tag{1.26}
$$

and multiplying the QCD links by the appropriate $U(1)_{em}$ factors. The covariant derivatives are thus defined as:

$$
\mathcal{D}_\mu^+[U,A]\, \psi_f(x) = [E_\mu(x)]^{e_f}\, U_\mu(x)\psi_f(x+\mu) - \psi_f(x) ,
$$

$$
\mathcal{D}_\mu^-[U,A]\, \psi_f(x) = \psi_f(x) - [E_\mu(x)]^{e_f}\, U_\mu(x)\psi_f(x-\mu) .
\tag{1.27}
$$

In the previous expressions e_f is the fractional electric charge of the quark of flavor f, i.e. e_f is 2/3 for up–type quarks and $-1/3$ for down–type quarks. Given our conventions, exact gauge invariance is obtained if the fields are transformed as follows

$$
\psi_f(x) \longrightarrow e^{ie_f e\lambda(x)}\psi_f(x) , \quad \bar{\psi}_f(x) \longrightarrow \bar{\psi}_f(x)e^{-ie_f e\lambda(x)} , \quad A_\mu(x) \longrightarrow A_\mu(x) + \bar{\nabla}_\mu^+\lambda(x) ,
\tag{1.28}
$$

---

[3]In the following $a = 1$.

where we define

$$\bar{\nabla}^+_\mu f(x) = f(x + \widehat{\mu}) - f(x) , \qquad \bar{\nabla}^-_\mu f(x) = f(x) - f(x - \widehat{\mu}) , \qquad \bar{\nabla}_\mu = \frac{\bar{\nabla}^+_\mu + \bar{\nabla}^-_\mu}{2} .$$
(1.29)

In order to calculate isospin breaking corrections we will perform a combined perturbative expansion in $\widehat{\alpha}_{em}$ and $\widehat{m}_d - \widehat{m}_u$ We want to treat electromagnetism at fixed order with respect to $\widehat{\alpha}_{em}$ and, to this end, we need to expand the quarks action in powers of e. This procedure is performed by starting from the explicit expression of the lattice Dirac operator $D_f[U, A; \vec{g}]$ to be used in numerical simulations and expanding up to order e^2

$$\sum_x \bar{\psi}_f(x) \Big\{ D_f[U, A; \vec{g}] - D_f[U, 0; \vec{g}] \Big\} \psi_f(x) =$$

$$= \sum_{x,\mu} \left\{ (e_f e) A^\mu(x) V^\mu_f(x) + \frac{(e_f e)^2}{2} A^\mu(x) A^\mu(x) T^\mu_f(x) + \dots \right\} ,$$
(1.30)

where $V^\mu_f(x)$ is the conserved vector current corresponding to the quark f while $T^\mu_f(x)$ is the "tadpole" vertex. Both the conserved vector current and the tadpole vertex depend upon the particular choice made for the discretization of the fermion action and we shall provide the explicit expressions for V^μ_f and T^μ_f corresponding to the regularization used in this work in the following sections, see eqs. (1.39). Note that tadpole insertions, a characteristic feature of lattice discretization, cannot be neglected because these play a crucial role in order to preserve gauge invariance at order e^2. The electromagnetic current and the tadpole vertex to be inserted in correlators are the sums over all the quarks of V^μ_f and T^μ_f with the corresponding charge factors,

$$J^\mu(x) = \sum_f e_f e\, V^\mu_f(x) = \sum_f e_f e\, \bar{\psi}_f \Gamma^\mu_V[U]\, \psi_f(x) ,$$

$$T^\mu(x) = \sum_f (e_f e)^2\, T^\mu_f(x) = \sum_f (e_f e)^2\, \bar{\psi}_f \Gamma^\mu_T[U]\, \psi_f(x) .$$
(1.31)

Furthermore, at the $O(\widehat{\alpha}_{em})$ at which we are working, there is no need to renormalize the electric charge, a problem that has to be faced instead at higher orders.

Once the fermion action has been expanded, the leading QED corrections to a given lattice correlator are obtained by considering the time ordered product of the original operators with two integrated insertions of the combination $A_\mu(x) J_\mu(x)$ or with a single integrated insertion of $\sum_\mu A_\mu(x) A_\mu(x) T_\mu(x)$.

By having introduced non–compact QED on the lattice, we have to give a prescription for treating the zero mode of the photon propagator.

The lattice action of the QED gauge field in Feynman gauge defined in eq. (1.25) is explicitly shown in momentum space to highlight a well known problem with the definition of the lattice

photon propagator, i.e. the infrared divergence associated with the zero momentum mode. The A_μ propagator is defined as the inverse of the kinetic term and, in order to define the inverse of the lattice Laplace operator $-\bar{\nabla}_\nu^- \bar{\nabla}_\nu^+$, one has to provide a prescription to cope with its kernel.

One possibility, widely used in the literature after the original proposal made in [23], is to make the zero momentum mode to vanish identically. There are alternative possible ways to regularize the zero momentum mode of the photon propagator, resulting into different finite volume behaviors (for a recent review we refer the reader to [39]). In our calculations we have adopted the so called QED_L prescription, which amounts to setting $\tilde{A}^\mu(k_0, \vec{0}) = 0$, for all μ and k_0.

We define the infrared regularized photon propagator in terms of expectation value of the time-orderd product of photon fields:

$$G_{\mu\nu}(y_1, y_2) = \langle A_\mu(y_1) A_\nu(y_2) \rangle,$$

where the photon field $A_\mu(y)$ must be generated from the distribution of probability:

$$P(A)\, dA \propto \exp\left[-A_\mu(y_1) G_{\mu\nu}^{-1}(y_1, y_2) A_\nu(y_2)\right].$$

This can be readily obtained drawing each mode of the photon field in momentum space in which the probability distribution is local in k, as was first noted in Ref. [23]:

$$P\left(\tilde{A}\right) d\tilde{A} \propto \exp\left[-\tilde{A}_\mu(k) \tilde{G}_{\mu\nu}^{-1}(k) \tilde{A}_\nu(k)\right].$$

After the local change of variable $\tilde{B}_\rho(k) = \sqrt{G_{\rho\nu}^{-1}(k)} \tilde{A}_\nu(k)$ each component of $\tilde{B}$ can be drawn independently:

$$P\left(\tilde{B}\right) d\tilde{B} \propto \exp\left[-\tilde{B}_\mu^2(k)\right],$$

and the value of $\tilde{A}_\mu(k)$ can be constructed via

$$\tilde{A}_\nu(k) = \sqrt{\tilde{G}_{\rho\nu}(k)} \tilde{B}_\rho(k).$$

The matrix $\sqrt{\tilde{G}_{\rho\nu}(k)}$ can be easily computed, and for the Wilson action in the Feynman gauge it amounts simply to

$$\sqrt{\tilde{G}_{\rho\nu}(k)} = \delta_{\rho\nu} \sqrt{\frac{1}{\widehat{k}^2}}.$$

1.5 QUARK LATTICE ACTION

In this section we enter into the details of the quark lattice action used in this work, namely the maximally twisted Wilson action [40, 41]. We will also give the explicit expression of the conserved vector current $V_f^\mu(x)$ and of the tadpole vertex $T_f^\mu(x)$.

In order to minimize cutoff effects we have been working within a mixed–action approach [42, 43]. In particular, the results described in the following sections have been obtained with the action $S = S_{sea} + S_{val}$.

The sea quark action S_{sea} is the Wilson twisted mass action at maximal twist with $N_f = 2 + 1 + 1$ sea quarks and with the introduction of the electromagnetic field A_μ. The expression of the action is

$$S_{sea} = S_{tm}^\ell + S_{tm}^h \tag{1.32}$$

where S_{tm}^ℓ and S_{tm}^h tm are the up/down and strange/charm actions respectively.

Up and down sea quarks are arranged in mass–degenerate doublet and the action at maximal twist is of the form [40]:

$$S_{tm}^\ell = a^4 \sum_x \overline{\psi}(x) \left\{ \frac{1}{2} \gamma_\mu (\mathcal{D}_\mu^+ + \mathcal{D}_\mu^-) - i\gamma_5 \tau^3 \left[m_{cr} - \frac{a\,r}{2} \mathcal{D}_\mu^+ \mathcal{D}_\mu^- \right] + \mu_\ell \right\} \psi(x), \tag{1.33}$$

with the covariant derivate $\mathcal{D}_\mu^\pm$ defined in eq. (1.27).

For the strange and charm doublet we have [44]

$$S_{tm}^h = a^4 \sum_x \overline{\psi}(x) \left\{ \frac{1}{2} \gamma_\mu (\mathcal{D}_\mu^+ + \mathcal{D}_\mu^-) - i\gamma_5 \tau^1 \left[m_{cr} - \frac{a\,r}{2} \mathcal{D}_\mu^+ \mathcal{D}_\mu^- \right] + \mu_\sigma + \mu_\delta \tau^3 \right\} \psi(x), \tag{1.34}$$

where the twisted masses μ_σ and μ_δ are related to the strange and charm masses by the relation

$$\widehat{m}_{sea}^{c,s} = \frac{1}{Z_P} \left(\mu_\sigma \pm \frac{Z_P}{Z_S} \mu_\delta \right), \tag{1.35}$$

with Z_P and Z_S the pseudo–scalar and scalar quark density operator respectively. In eq. (1.35) the term proportional to τ^3 is used to split the masses of the members of the doublet; consequently the Wilson term was twisted with the flavor matrix τ^1. The twisted-mass action (1.32) leads to a mixing in the strange and charm sectors [44, 45], but the non–unitary mixed set up guarantees that K and D mesons do not mix.

Concerning the content of the valence sector, we have considered a doublet of fermionic fields for each flavor, $\psi_f^T = (\psi_f^+, \psi_f^-)$, and a corresponding doublet of bosonic fields (pseudo-quarks), $\phi_f^T = (\phi_f^+, \phi_f^-)$. The ghost doublets are never considered in the calculation of physical observables, but they have the only purpose of canceling the valence quark determinant. The fields within the same doublet have the same mass m_f, the same electric charge e_f but opposite chirally rotated Wilson terms. In lattice units the valence action reads as

$$S_{val} = \sum_{f,x} \left\{ \bar{\psi}_f D_f[U, A] \psi_f + \bar{\phi}_f D_f[U, A] \phi_f \right\}, \tag{1.36}$$

23

where the lattice Dirac operator is

$$D_f[U, A] = \frac{1 + \tau^3}{2} D_f^+[U, A] + \frac{1 - \tau^3}{2} D_f^-[U, A] \,, \tag{1.37}$$

with

$$D_f^\pm[U, A]\, \psi(x) = m_f \psi(x) \quad \pm \quad i\gamma_5(m_f^{crit} + 4)\psi(x) - \sum_\mu \frac{\pm i\gamma_5 - \gamma_\mu}{2} U_\mu(x)[E_\mu(x)]^{e_f}\psi(x + \mu) +$$

$$- \quad \sum_\mu \frac{\pm i\gamma_5 + \gamma_\mu}{2} U_\mu^\dagger(x - \mu)[E_\mu^\dagger(x - \mu)]^{e_f}\psi(x - \mu) \,. \tag{1.38}$$

The symbol $\pm$ distinguish between the sign of the Wilson parameter r.

As far as the mass splittings of pseudoscalar mesons are concerned, the mixed action setup used in this work allows to compute observables with $O(a^2)$ cutoff effects at the price of introducing unitarity violations that disappear when the continuum limit is performed (at matched sea and valence renormalized quark masses the resulting continuum theory is unitary). For each correlator, by possibly replicating some of the valence matter fields, the choice made for the action allows to consider only the fermionic Wick contractions that would arise in the continuum theory, thus avoiding the introduction of isospin breaking lattice artifacts at finite lattice spacing. The resulting diagrams are then discretized by using for each quark propagator a convenient choice of the sign of the twisted Wilson term.

Using the Dirac operator in eq. (1.38) and expanding the lattice quark action according to eq. (1.30), we can calculate the conserved vector current and the tadpole vertex

$$V_\mu^f(x) \;=\; i\left[\bar{\psi}_f(x)\frac{i\tau^3\gamma_5 - \gamma_\mu}{2} U_\mu(x)\psi_f(x + \mu) - \bar{\psi}_f(x + \mu)\frac{i\tau^3\gamma_5 + \gamma_\mu}{2} U_\mu^\dagger(x)\psi_f(x)\right] \,,$$

$$T_\mu^f(x) \;=\; \bar{\psi}_f(x)\frac{i\tau^3\gamma_5 - \gamma_\mu}{2} U_\mu(x)\psi_f(x + \mu) + \bar{\psi}_f(x + \mu)\frac{i\tau^3\gamma_5 + \gamma_\mu}{2} U_\mu^\dagger(x)\psi_f(x) \,. \tag{1.39}$$

1.6 ELECTROMAGNETIC CORRECTIONS TO HADRONIC OBSERVABLES

Generalizing the strategy described in Sec. 1.3, we are going to introduce QED in our calculation of isospin breaking effects on the lattice [9] by performing a combined perturbative expansion of the full theory lattice path-integral in the small parameters:

$$\frac{\widehat{m}_d - \widehat{m}_u}{\Lambda_{QCD}} \quad \sim \quad \widehat{\alpha}_{em} \quad \sim \quad O(\varepsilon) \,, \tag{1.40}$$

neglecting contributions of order $O(\varepsilon^2)$.

In order to calculate $O(\widehat{\alpha}_{em})$ corrections to a given physical quantity we have to cope with correlators containing two insertions of the electromagnetic current or one insertion of the tadpole vertex, multiplied by the IR regularized photon propagator and integrated over the space-time volume. More precisely, in the first case the correction to a given correlator is proportional to

$$T\langle\mathcal{O}(x_i)\rangle \quad \longrightarrow \quad T \int d^4y d^4z \; D_{\mu\nu}(y-z) \; \langle\mathcal{O}(x_i)J_\mu(y)J_\nu(z)\rangle \;, \qquad (1.41)$$

where $T\langle\mathcal{O}(x_i)\rangle$ is the T–product of a certain number of local operators, $D_{\mu\nu}(y-z)$ is the photon propagator in a fixed QED gauge and $J_\mu(x)$ is the sum of the electromagnetic currents of all the flavors. In sec. 1.4 we have already given a proper definition of the finite volume infrared regularized photon propagator so that eq. (1.41) is infrared regularized. On the other hand, because of the contact interactions of the electromagnetic currents, eq. (1.31) is ultraviolet divergent and need to be regularized. The introduction of the electromagnetism induce a (divergent) shift of the quark masses, of the strong coupling of QCD and, because we are working with Wilson twisted mass fermions, also of the critical masses.

By neglecting for now the critical mass term and the tadpole vertex contribution, consider the short distance expansion of the product of electromagnetic currents, which reads

$$J^\mu(x)J^\mu(0) \quad \sim \quad c_1(x)\mathbf{1} + \sum_f c_m^f(x)m_f\bar{\psi}_f\psi_f + c_{g_s}(x)G^{\mu\nu}G^{\mu\nu} + \cdots \;. \qquad (1.42)$$

The "counter–term" coefficients c_1, c_m^f and c_{g_s} are divergent quantities that must be fixed by specifying appropriate renormalization prescriptions. In particular, the terms proportional to c_m^f can be reabsorbed by a redefinition of each quark mass m_f in the full theory with respect to isosymmetric QCD, the term proportional to c_{g_s} can be reabsorbed by a redefinition of the strong coupling constant (i.e. of the lattice spacing) while the term proportional to c_1 corresponds to the vacuum polarization and the associated divergence cancels by taking the fully connected part of the right hand side of eq. (1.41).

Let us consider a generic "physical" observable $\mathcal{O}$ in the full theory,

$$\mathcal{O}(\vec{g}) \;=\; \mathcal{O}(e^2, g_s^2, m_u, m_d, m_s, m_c, \dots) \;=\; \langle\mathcal{O}\rangle^{\vec{g}} \;, \qquad (1.43)$$

where we have used the following compact vector notation for the bare parameters of the theory

$$\vec{g} = \left(e^2, g_s^2, m_u, m_d, m_s, m_c, \dots\right) \qquad (1.44)$$

and where the notation $\langle\cdot\rangle^{\vec{g}}$ means that the path-integral average is performed in the full theory. In the previous expressions we listed the bare mass parameters of the four lightest quarks, but the discussion can be easily generalized to include heavier quarks as indicated by the dots.

Our method consists in expanding any observable $\mathcal{O}(\vec{g})$ with respect to the isosymmetric QCD result $\mathcal{O}(\vec{g}^0)$ according to

$$
\begin{aligned}
\mathcal{O}(\vec{g}) &= \mathcal{O}(\vec{g}^0) + \left\{ e^2 \frac{\partial}{\partial e^2} + [g_s^2 - (g_s^0)^2] \frac{\partial}{\partial g_s^2} + [m_f - m_f^0] \frac{\partial}{\partial m_f} \right\} \mathcal{O}(\vec{g}) \Bigg|_{\vec{g}=\vec{g}^0} \\
&= \langle \mathcal{O} \rangle^{\vec{g}^0} + \delta\mathcal{O} \,,
\end{aligned}
\tag{1.45}
$$

where

$$
\vec{g}^0 = \left(0, (g_s^0)^2, m_{ud}^0, m_{ud}^0, m_s^0, m_c^0, \dots \right) \,.
\tag{1.46}
$$

The notation $\langle \cdot \rangle^{\vec{g}^0}$ means that the path–integral average is performed in the isosymmetric theory.

The bare parameters $\vec{g}^0$ of the isosymmetric theory can be fixed by matching the renormalized couplings of the two theories at a given scale $\mu^\star$ [46]. More precisely, once the renormalized parameters $\widehat{g}_i(\mu) = Z_i(\mu)g_i$ have been fixed by using an hadronic prescription, the renormalized couplings of the isosymmetric theory $\widehat{g}_i^0(\mu) = Z_i^0(\mu)g_i^0$ at the scale $\mu^\star$ are fixed by imposing the following matching conditions

$$
\widehat{g}_s^0(\mu^\star) = \widehat{g}_s(\mu^\star) \,,
$$

$$
\widehat{m}_{ud}^0(\mu^\star) = \widehat{m}_{ud}(\mu^\star) = \frac{\widehat{m}_d(\mu^\star) + \widehat{m}_u(\mu^\star)}{2} \,,
$$

$$
\widehat{m}_s^0(\mu^\star) = \widehat{m}_s(\mu^\star) \,.
\tag{1.47}
$$

This prescription is known as the Gasser-Rusetsky-Scimemi (GRS) one [46] and in this work we rely on it by matching the couplings renormalized in the $\overline{\text{MS}}$ scheme at $\mu^\star = 2$ GeV. We refer the reader to Sec. 1.10 for a detailed discussion on possible alternative prescriptions.

By using the property that a physical observable is a Renormalization Group Invariant (RGI) quantity, i.e.

$$
\mathcal{O}(g_i) = \mathcal{O}(\widehat{g}_i) \,, \qquad\qquad \mathcal{O}(g_i^0) = \mathcal{O}(\widehat{g}_i^0) \,.
\tag{1.48}
$$

the perturbative expansion of eq. (1.45) can be expressed in terms of the renormalized couplings according to

$$
\mathcal{O}(\widehat{g}_i) = \mathcal{O}\left(\widehat{g}_i^0\right) + \left\{ \widehat{e}^2 \frac{\partial}{\partial \widehat{e}^2} + \left[\widehat{g}_s^2 - \left(\frac{Z_{g_s}}{Z_{g_s}^0} \widehat{g}_s^0 \right)^2 \right] \frac{\partial}{\partial \widehat{g}_s^2} + \left[\widehat{m}_f - \frac{Z_{m_f}}{Z_{m_f}^0} \widehat{m}_f^0 \right] \frac{\partial}{\partial \widehat{m}_f} \right\} \mathcal{O}(\widehat{g}_i) \Bigg|_{\widehat{g}_i = \frac{Z_i}{Z_i^0} \widehat{g}_i^0} \,.
\tag{1.49}
$$

From the comparison of the previous equation with eq. (1.42) we find in the differential operator language the divergent terms proportional to $Z_{m_f}/Z_{m_f}^0$ and $Z_{g_s}/Z_{g_s}^0$ that correspond

to the short distance expansion counter–terms c_m^f and c_{g_s} respectively. In practice, these counter–terms do appear because the renormalization constants (the bare parameters) of the full theory are different from the corresponding quantities of isosymmetric QCD, the theory in which we perform the numerical simulations. Once the counter–terms have been properly tuned, our procedure can be interpreted as the expansion of the full theory in the renormalized parameters $\widehat{\alpha}_{em}$ and $\widehat{m}_d - \widehat{m}_u$.

In eq. (1.42) we didn't take into account the shift of the critical mass induced by electromagnetism in the presence of a Wilson term in the fermionic action. To do this we re–write eq. (1.42) modifying both the left–hand side, to take into account the presence of the tadpole vertices of the different quarks, and the right–hand side, because of the appearance of additional divergent contributions that have to be reabsorbed by a redefinition of the critical masses

$$
\begin{aligned}
J^\mu(x)J^\mu(0) \;\; + \;\; & \sum_\mu T^\mu(x) \\
\sim \;\; & c_1(x)\mathbb{1} \;\; + \;\; \sum_f c_k^f(x)\bar{\psi}_f i\gamma_5\tau^3\psi_f \;\; + \;\; \sum_f c_m^f(x)m_f\bar{\psi}_f\psi_f \;\; + \;\; c_{g_s}(x)G^{\mu\nu}G^{\mu\nu} \;\; + \;\; \cdots ,
\end{aligned}
$$
(1.50)

where $c_k^f(x)$ are the critical mass counter-term coefficients

In order to determine the counter–term associated with the electromagnetic shift of the critical mass, [9] adopted a method commonly used to implement the maximal twist condition in simulations of isosymmetric QCD.

By starting from the explicit expression of the lattice Dirac operator for a given valence flavor doublet, eqs. (1.37) and (1.38), one can separately tune the critical mass of each valence quark by imposing the following vector Wilson Twisted Identity (WTI)

$$
W_f(\vec{g}) = \bar{\nabla}^\mu \langle \, \left[\bar{\psi}_f \gamma^\mu \tau^1 \psi_f \right](x) \, \left[\bar{\psi}_f \gamma^5 \tau^2 \psi_f \right](0) \, \rangle^{\vec{g}} = 0 \,. \qquad f = \{u, d, s\} \,.
$$
(1.51)

The explicit formulae corresponding to its expansion in powers of e can be obtained generalizing the operator δ of eq. (1.45). To do this let us consider the general expression of eq. (1.45) taking into account also the critical mass shift. Given a general observable in the full theory, we have

$$
\mathcal{O}(\vec{g}) \;\; = \;\; \mathcal{O}(e^2, g_s^2, m_u, m_d, m_s, m_c, m_u^{crit}, m_d^{crit}, m_s^{crit}, m_c^{crit}, \dots) \,,
$$
(1.52)

where we have enlarged the parameter space of the theory

$$
\vec{g} = \left(e^2, g_s^2, m_u, m_d, m_s, m_c, m_u^{crit}, m_d^{crit}, m_s^{crit}, m_c^{crit}, \dots \right) \,.
$$
(1.53)

By calling m_0^{crit} the single critical mass parameter of the symmetric theory, we see that isosymmetric QCD simulations correspond to

$$
\vec{g}^0 = \left(0, (g_s^0)^2, m_{ud}^0, m_{ud}^0, m_s^0, m_c^0, m_0^{crit}, m_0^{crit}, m_0^{crit}, m_0^{crit}, \dots \right) \,.
$$
(1.54)

27

The value of m_0^{crit} has been precisely determined in [47] in the isosymmetric theory by requiring the validity of the vector Ward–Takahashi identity of eq. (1.51) with $m_f^0 = m_{ud}^0$,

$$W_{ud}(\vec{g}^0) = 0 \qquad \longrightarrow \qquad m_0^{crit} \ . \tag{1.55}$$

Our gauge ensembles have been generated at this well defined value of critical mass for each $\beta^0 = 6/(g_s^0)^2$. The LIB corrections to any observable can be obtained by making an expansion, at fixed lattice spacing, with respect to the differences $m_f^{crit} - m_0^{crit}$ which represents a regularization specific isospin breaking effect induced by the electromagnetic interactions. The generalization of eq. (1.45) to be used on the lattice with Wilson fermions is

$$\delta \mathcal{O} = \left\{ e^2 \frac{\partial}{\partial e^2} + \left[g_s^2 - (g_s^0)^2 \right] \frac{\partial}{\partial g_s^2} + [m_f - m_f^0] \frac{\partial}{\partial m_f} + [m_f^{crit} - m_0^{crit}] \frac{\partial}{\partial m_f^{crit}} \right\} \mathcal{O}O(\vec{g}) \Bigg|_{\vec{g}=\vec{g}^0} \ . \tag{1.56}$$

1.7 EXPANSION OF THE LATTICE PATH-INTEGRAL

In this section, by following the strategy outlined in the previous sections, we discuss the details concerning the derivation of the formulae necessary to calculate the LIB corrections to specific observables. The starting point is the path–integral representation of the observable in the full theory,

$$\mathcal{O}(\vec{g}) = \langle \mathcal{O} \rangle^{\vec{g}} = \frac{\int dA e^{-S_{gauge}[A]} \, dU \, e^{-\beta S_{gauge}[U]} \prod_{f=1}^{n_f} \det \left(D_f^{\pm}[U, A; \vec{g}] \right) \, \mathcal{O}[U, A; \vec{g}]}{\int dA e^{-S_{gauge}[A]} \, dU \, e^{-\beta S_{gauge}[U]} \prod_{f=1}^{n_f} \det \left(D_f^{\pm}[U, A; \vec{g}] \right)} \ , \tag{1.57}$$

where $S_{gauge}[A]$ has been given in eq. (1.25) and is a functional of the gauge potential A_μ, $S_{gauge}[U]$ is the QCD gauge action ($\beta = 6/g_s^2$) and is a functional of the link variables $U_\mu(x)$, $D_f^{\pm}[U, A; \vec{g}]$ are the Dirac operators defined in eq. (1.38). We want to express the observable $\mathcal{O}(\vec{g})$ in terms of the path-integral average in the isosymmetric theory, i.e.

$$\mathcal{O}(\vec{g}^0) = \langle \mathcal{O} \rangle^{\vec{g}^0} = \frac{\int dU \, e^{-\beta^0 S_{gauge}[U]} \prod_{f=1}^{n_f} \det \left(D_f^{\pm}[U; \vec{g}^0] \right) \, \mathcal{O}[U]}{\int dU \, e^{-\beta^0 S_{gauge}[U]} \prod_{f=1}^{n_f} \det \left(D_f^{\pm}[U; \vec{g}^0] \right)} \ . \tag{1.58}$$

This can be done by introducing the appropriate reweighting factor and the functional average $\langle \cdot \rangle^A$ with respect to the free photon field,

$$R[U, A; \vec{g}] = e^{-(\beta - \beta^0) S_{gauge}[U]} \; r[U, A; \vec{g}] \; ,$$

$$r[U, A; \vec{g}] = \prod_{f=1}^{n_f} r_f[U, A; \vec{g}] \; = \; \prod_{f=1}^{n_f} \frac{\det\left(D_f^{\pm}[U, A; \vec{g}]\right)}{\det\left(D_f^{\pm}[U; \vec{g}^0]\right)} \; ,$$

$$\langle \mathcal{O} \rangle^A = \frac{\int dA \; e^{-S_{gauge}[A]} \; \mathcal{O}[A]}{\int dA \; e^{-S_{gauge}[A]}} \; . \tag{1.59}$$

Eq. (1.57) can be conveniently rewritten as follows

$$\langle \mathcal{O} \rangle^{\vec{g}} \;=\; \frac{\langle R\mathcal{O} \rangle^{A,\vec{g}^0}}{\langle R \rangle^{A,\vec{g}^0}} \;=\; \frac{\left\langle \left\langle \; R[U, A; \vec{g}] \; O[U, A; \vec{g}] \; \right\rangle^A \right\rangle^{\vec{g}^0}}{\left\langle \left\langle \; R[U, A; \vec{g}] \; \right\rangle^A \right\rangle^{\vec{g}^0}} \; , \tag{1.60}$$

and leading order isospin breaking corrections can now be obtained by applying the differential operator δ defined in eq. (1.56) to the observable $\mathcal{O}$ defined in eq. (1.60). More precisely,

$$\delta\mathcal{O} \;=\; \langle \delta(R\mathcal{O}) \rangle^{A,\vec{g}^0} - \langle \delta R \rangle^{A,\vec{g}^0} \langle \mathcal{O} \rangle^{\vec{g}^0} = \langle \delta\mathcal{O}[U, A; \vec{g}]\big|_{\vec{g}=\vec{g}^0} \rangle^{A,\vec{g}^0} +$$

$$+ \; \left\{ \langle \delta\left(R\mathcal{O} - \mathcal{O}\right)[U, A; \vec{g}]\big|_{\vec{g}=\vec{g}^0} \rangle^{A,\vec{g}^0} - \langle \delta R[U, A; \vec{g}]\big|_{\vec{g}=\vec{g}^0} \rangle^{A,\vec{g}^0} \langle \mathcal{O}[U; \vec{g}^0] \rangle^{\vec{g}^0} \right\} \; . $$

$$\tag{1.61}$$

In the previous expression we have separated the term $\langle \delta\mathcal{O} \rangle^{A,\vec{g}^0}$, representing the correction to the given observable, from the contributions in curly brackets coming from the corrections to the reweighting factor and, consequently, to the sea quark determinants. In the following we shall call these contributions "vacuum polarization terms" or "disconnected terms".

In order to apply the differential operator δ, it is useful to observe that

$$\frac{\partial \langle \mathcal{O} \rangle^A (e^2)}{\partial(e^2)}\bigg|_{e^2=0} \;=\; \left\langle \frac{1}{2} \frac{\partial^2 \mathcal{O}[A; e]}{\partial e^2}\bigg|_{e=0} \right\rangle^A \; , \tag{1.62}$$

and to consider the following expressions and related graphical representations of the derivates

in eq. (1.56) applied to the quark propagator and to the Dirac operator.

$$\frac{1}{2}\frac{\partial^2 S_f}{\partial e^2} = S_f \frac{\partial D_f}{\partial e} S_f \frac{\partial D_f}{\partial e} S_f - \frac{1}{2} S_f \frac{\partial^2 D_f}{\partial e^2} S_f \quad = \quad e_f^2 \; \rightsquigarrow \quad + \; e_f^2 \; \star \quad ,$$

$$\frac{\partial S_f}{\partial m_f} = -S_f \frac{\partial D_f}{\partial m_f} S_f \quad = \quad - \; \otimes \quad ,$$

$$\frac{\partial S_f^{\pm}}{\partial m_f^{crit}} = -S_f^{\pm} \frac{\partial D_f^{\pm}}{\partial m_f^{crit}} S_f^{\pm} \quad = \quad \mp \; \otimes \quad . \tag{1.63}$$

In writing eqs. (1.63) we assumed that the derivatives have been evaluated at $\vec{g} = \vec{g}^0$ and that the functional integral $\langle \cdot \rangle^A$ with respect to the photon field has already been performed. The compact notation S_f indicates the isosymmetric QCD lattice quark propagator $S_f[U; \vec{g}^0]$ obtained by inverting the Dirac operator $D_f[U] = D_f[U, \vec{g}^0]$.

The diagram $\otimes$ represents the propagator of a quark with flavor f with the insertion of the local scalar operator $\sum_y \overline{\psi}_f(y)\psi_f(y)$, while $\otimes$ of the local pseudoscalar operator $i \sum_y \overline{\psi}_f(y)\gamma_5 \psi_f(y)$.

The graphical representation given in the last of the previous formulae (1.63), corresponding to the derivative of the quark propagator with respect to the critical mass, is specific to the lattice Dirac operators used in this work and the $\mp$ signs of the Wilson parameters correspond respectively to $D_f^{\pm}$ defined into eq. (1.38). In the case of standard Wilson fermions red and grey "blobs" would coincide.

When deriving the Dirac operator with respect to e we have to calculate

$$\frac{\partial (E_\mu(x))^{e_f}}{\partial e} = \frac{\partial}{\partial e} e^{-ie\,e_f A_\mu(x)} = (-ie_f)A_\mu(x)(E_\mu(x))^{e_f},$$

$$\frac{\partial^2 (E_\mu(x))^{e_f}}{\partial e^2} = (-ie_f)^2 A_\mu(x)A_\mu(x)(E_\mu(x))^{e_f}. \tag{1.64}$$

Using the previous equations, we can see that the first graphical representation of the first expression in eqs. (1.63) is obtained through the insertion of two derivatives $\dfrac{\partial D_f}{\partial e}$ calculated in two different space–time points $\left(\text{in} \; \rightsquigarrow \; \text{the electromagnetic vector current operator} \right.$ $\sum_{y,z} V_f^\mu(y)V_f^\nu(z)D^{\mu\nu}(y,z)$ is inserted $\bigg)$; from $\dfrac{\partial^2 D_f}{\partial e^2}$ it originates the insertion of the tadpole vertex operator $\dfrac{1}{2}\sum_y T_f^\mu(y)D^{\mu\mu}(y,y)$.

Here we remark again that the lattice photon propagator $D^{\mu\nu}$ has to be IR regularized as discussed in sec. 1.4 and that, having performed the path-integral average over the gauge potential A_μ, the diagrams involving the numerical calculation of $D^{\perp}_{\mu\nu}$ can be computed following the steps outlined in sec. 1.4 through the average over a specific stochastic distribution. The computation of correlators in which, for example, a photon is exchanged between two quark lines is then reduced to the calculation of sequential propagators, solving the following systems

$$
\begin{aligned}
\left\{ D_f[U]\, \Psi_B^f \right\}(x) &= \sum_\mu B^\mu(x)\Gamma_V^\mu S_f[U;x]\,, \\
\left\{ D_f[U]\, \Psi_C^f \right\}(x) &= \sum_\mu C^\mu[B;x]\Gamma_V^\mu S_f[U;x]\,,
\end{aligned}
\tag{1.65}
$$

for different values of the $B_\mu(x)$ and $C_\mu[B;x]$ fields.

All the disconnected contributions coming from the reweighting factor can be readily obtained by using eqs. (1.63). For example,

$$
\frac{\partial R}{\partial g_s^2} = \frac{6}{(g_s^0)^4} S_{gauge}[U] = \boxed{G_{\mu\nu}G^{\mu\nu}}\,,
$$

$$
\begin{aligned}
\frac{1}{2}\frac{\partial^2 r_f}{\partial e^2} &= \frac{1}{2}\mathrm{Tr}\left(S_f \frac{\partial^2 D_f}{\partial e^2}\right) - \frac{1}{2}\mathrm{Tr}\left(S_f \frac{\partial D_f}{\partial e} S_f \frac{\partial D_f}{\partial e}\right) + \frac{1}{2}\mathrm{Tr}\left(S_f \frac{\partial D_f}{\partial e}\right)\mathrm{Tr}\left(S_f \frac{\partial D_f}{\partial e}\right) \\
&= -e_f^2\ \text{⬡} - e_f^2\ \text{◯✳} + e_f^2\ \text{◯⌇◯}\,.
\end{aligned}
\tag{1.66}
$$

We have to note however that, in order to apply the operator δ to the product $(R[U,A;\vec{g}]\,\mathcal{O}[U,A;\vec{g}])$ (see eqs. (1.61) and (1.62) above), at fixed QED gauge background one also needs the following expressions for the first order derivatives of the quark propagators and of the quark determinants with respect to e

$$
\frac{\partial S_f}{\partial e} = -S_f \frac{\partial D_f}{\partial e} S_f = e_f\ \text{↗⌇────}\,,
$$

$$
\frac{\partial r_f}{\partial e} = \mathrm{Tr}\left(S_f \frac{\partial D_f}{\partial e}\right) = -e_f\ \text{◯⌇}\,.
\tag{1.67}
$$

A concrete example of application of the formulae given in eqs. (1.63) and (1.66) is

represented by the correction to the $S_f^\pm$ quark propagators worked out below

$$\delta \longrightarrow^\pm =$$

$$= (e_f e)^2 \ \longrightarrow + (e_f e)^2 \ \longrightarrow - [m_f - m_f^0] \ \longrightarrow\!\otimes\!\longrightarrow \ \mp [m_f^{crit} - m_0^{crit}] \ \longrightarrow\!\otimes\!\longrightarrow \ +$$

$$- e^2 e_f \sum_{f_1} e_{f_1} \ \longrightarrow - e^2 \sum_{f_1} e_{f_1}^2 \ \longrightarrow - e^2 \sum_{f_1} e_{f_1}^2 \ \longrightarrow + e^2 \sum_{f_1 f_2} e_{f_1} e_{f_2} \ \longrightarrow \ +$$

$$+ \sum_{f_1} \pm [m_{f_1}^{crit} - m_0^{crit}] \ \longrightarrow + \sum_{f_1} [m_{f_1} - m_{f_1}^0] \ \longrightarrow + [g_s^2 - (g_s^0)^2] \ \longrightarrow \ . \tag{1.68}$$

Here quark propagators of different flavors have been drawn with different colors and different lines. Quark disconnected diagrams are noisy and difficult to calculate and for this reason in this work we used the so called electro– quenched approximation. This approximation consists of forcing the sea quarks to be neutral with respect to electromagnetic interactions, corresponding to the action $S_{sea}^{e=0}$ for the sea quarks, setting $g_s = g_s^0$ and

$$r_f[U, A, \vec{g}_0] = 1 \ . \tag{1.69}$$

In the electro-quenched approximation all quark disconnected contributions are absent. It follows that in this theory eq. (1.68) simply becomes

$$\delta \longrightarrow^\pm = (e_f e)^2 \left[\ \longrightarrow + \ \longrightarrow \ \right] - [m_f - m_f^0] \ \longrightarrow\!\otimes\!\longrightarrow \ \mp [m_f^{crit} - m_0^{crit}] \ \longrightarrow\!\otimes\!\longrightarrow \ . \tag{1.70}$$

1.7.1 LEADING ISOSPIN BREAKING CORRECTIONS TO HADRON CORRELATORS

In order to extract the mass of a given hadron H, by including electromagnetic interactions and QCD isospin breaking corrections, we start by considering in the full theory the two-point correlator of an interpolating operator $O_H(t, \vec{p} = 0)$ having the appropriate quantum numbers,

$$C_{HH}(t; \vec{g}) = \langle O_H(t) \overline{O}_H(0) \rangle^{\vec{g}} = Z_H e^{-t M_H} + \cdots ,$$

$$e^{M_H} = \frac{C_{HH}(t-1; \vec{g})}{C_{HH}(t; \vec{g})} + \cdots , \tag{1.71}$$

where the dots represent non leading exponential contributions to the correlator and Z_H is proportional to the residue of the pole corresponding to the hadron H It is important to stress that, if H is an electrically charged particle, the correlator $C_{HH}(t; \vec{g})$ is *not* invariant under $U(1)_{em}$ gauge transformations (see also [48] concerning this point). On the other hand, the mass of the hadron M_H is gauge invariant and *finite* in the continuum limit, provided the parameters $\vec{g}$ of the action have been properly tuned. It follows that, at large times and at any given order in a perturbative expansion in any of the parameters of the action, the ratio $C_{HH}(t-1; \vec{g})/C_{HH}(t; \vec{g})$ is both gauge and renormalization group invariant (up to discretization effects and exponentially suppressed contributions). From eqs. (1.71) it follows

$$C_{HH}(t; \vec{g}) = C_{HH}(t; \vec{g}^0) \left[1 + \frac{\delta C_{HH}(t)}{C_{HH}(t; \vec{g}^0)} + \dots \right] \,,$$

$$\delta M_H = M_H - M_H^0 = -\partial_t \frac{\delta C_{HH}(t)}{C_{HH}(t; \vec{g}^0)} + \dots \,, \tag{1.72}$$

where we have defined

$$\partial_t f(t) = f(t) - f(t-1) \tag{1.73}$$

and δ is defined in eq. (1.56).

In our lattice simulations we have enforced periodic (anti–periodic) boundary conditions for the gauge (matter) fields along the time direction. For this reason, we have extracted the correction to pseudoscalar meson masses by fitting the ratio $\delta C_{PP}(t)/C_{PP}(t; \vec{g}^0)$ of corrected over uncorrected pseudoscalar–pseudoscalar two–point functions according to the following functional form

$$\frac{\delta C_{PP}(t)}{C_{PP}(t; \vec{g}^0)} = const. + \delta M_P (T/2 - t) \tanh \left[M_P^0 (T/2 - t) \right] + \cdots \,, \tag{1.74}$$

where the constant term contains the correction to the residue of the pole corresponding to the lightest state of mass M_P and T is the extension of the time direction of the lattice. The formula above is obtained by noting that a pseudoscalar–pseudoscalar correlator is even under the symmetry $t \mapsto T - t$ and by using ordinary perturbation theory in order to predict the time dependence of corrected correlators, see ref. [8] for further details concerning this point.

In the following we continue to use the symbol ∂_t but, when referred to lattice correlators, we actually mean the operation that allows extracting the coefficient δM_P by a fit of the numerical correlators.

As explained in section 1.5, in order to minimize cutoff effects and optimize the numerical signal, we work in a mixed action setup. In addition in the meson two-point correlators the twisted Wilson quarks have opposite chirally rotated Wilson terms (i.e. opposite values of the Wilson parameter r). From our analysis this seems to be the best choice because in this case discretization effects are better under control, as we will discuss in the third chapter of the present work.

1.8 TUNING CRITICAL MASSES

In order to extract physical informations for the mass splittings of pseudoscalar mesons, we first need to obtain a numerical determination of the electromagnetic shift of the critical masses of the light quarks. Our results for the pseudoscalar mesons mass splittings have been obtained within the electro-quenched approximation that, consistently, has been employed to calculate $\delta m_{u,d}^{crit}$ in [9] as discussed in this section.

As mentioned before, the critical mass corrections have been calculated by imposing the WTI in eq. (1.51).

By applying the methods of section 1. 7 to the Ward-Takahashi identity $W_f(\vec{g}) = 0$, i.e. by applying the differential operator δ to the full theory parity-odd correlator (l.h.s. of eq. (1.51))

$$W_f(\vec{g}) = -\bar{\nabla}^0 \ \overset{+}{\underset{-}{\bigcirc}} \ = -\bar{\nabla}^0 \ \mathrm{Tr}\left\{\ \gamma^0\ S_f^+[U,A;\vec{g};t,\vec{p}=0]\ \gamma^5\ S_f^-[U,A;\vec{g};-t,\vec{p}=0]\ \right\} = 0\ ,$$

(1.75)

one obtains the following definition of δm_f^{crit}

$$\delta W_f = 0 \qquad \longrightarrow \qquad \delta m_f^{crit} = -\frac{e_f^2}{2}e^2 \frac{\bar{\nabla}^0 \left[\ \bigcirc + 2\ \bigcirc + 2\ \bigcirc\ \right]}{\bar{\nabla}_0\ \bigcirc} \ .$$

(1.76)

In eq. (1.75) the two quarks entering the correlator are chosen with opposite chirally rotated Wilson terms in order to minimize cutoff effects [42, 43]. From the numerical point of view, the parameters δm_f^{crit} have to be determined as accurately as possible because they are needed in order to cancel linear ultraviolet divergences present in the expressions used to compute pseudoscalar meson mass splittings. The great advantage of eq. (1.76) is that it holds at finite quark masses, thus not requiring chiral extrapolations.

1.9 QED FINITE VOLUME EFFECTS

The long-range nature of the electromagnetic interaction, i.e. the vanishing mass of the photon, induces finite-volume effects (FVE) which only fall off like inverse powers of the linear extent of the lattice [49, 50]. These are far more severe than the QCD finite volume effects for stable particles, which are exponentially suppressed [51], and require to be accurately

corrected. Furthermore the FVE depend on the specific prescription used to subtract the zero mode of the photon.

For the evaluation of the FVE we will follow the strategy described in [17]. Our photon field has periodic boundary conditions, while the quark fields are periodic in space and antiperiodic in time. Therefore, meson fields are periodic in all directions. As a result, the topology of our spacetime is the four-torus $\mathbb{T}^4$. As discussed in sec. 1.4 we consider the case where the four-momentum zero-mode of the photon field is eliminated, i.e. $\widetilde{A}^\mu(k_0, \vec{0}) = 0$, for all μ and k_0, which is denoted as QED_L.

Power–like FVE arise from the exchange of a photon around the torus, and they are obtained by comparing results obtained in finite volume (FV) with those of infinite volume (IV) QED.

The FV corrections to the mass m of a point particle of spin $J = 0$ and of charge q in units of e, on a torus of dimensions $T \times L^3$, is given by the difference of the FV self energy, $\Sigma_{J=0}(p, T, L)$, and its IV counterpart, $\Sigma_{J=0}(p)$, on shell:

$$
\begin{aligned}
\Delta m^2_{J=0}(T, L) \equiv m^2_{J=0}(T, L) - m^2 &= (qe)^2 \Delta\Sigma_{J=0}(p = im, T, L) \\
&\equiv (qe)^2 \left[\Sigma_{J=0}(p = im, T, L) - \Sigma_{J=0}(p = im) \right] ,
\end{aligned}
\tag{1.77}
$$

$p = im$ is a shorthand for $p = (im, \vec{0})$.

Because we only work in a regime where electromagnetic effects are linear in the fine structure constant α, the self-energy difference in eq. (1.77) is evaluated at one loop. At this order, differences of self energies or of contributions to self energies are generically written as

$$
\Delta\Sigma(p, T, L) = \left[\sum_{k}{}^{\prime}\!\!\!\!\!\!\!\!\int - \int \frac{d^4k}{(2\pi)^4} \right] \sigma(k, p) ,
\tag{1.78}
$$

where k is the momentum of the photon in the loop and $\sigma(k, p)$ is the appropriate IV self-energy integrand. The individual FV and IV terms in eq. (1.78) are generally UV and possibly IR divergent. Thus, individually they should be regularized, e.g. with dimensional regularization. However, on shell the IV integral is IR finite and in finite volume, the sums are IR finite because the FV formulations of QED that we consider are regulated by the space or spacetime volume. Moreover, for large k^2 the difference of the FV sums and IV integrals is also UV finite. In eq. (1.78) the information about the topology of the finite volume and the specific formulation of QED is contained in the definition of $\sum_{k}{}^{\prime}\!\!\!\!\!\!\!\int$; for QED_{TL} on $\mathbb{T}^4$ we have

$$
\sum_{k}{}^{\prime}\!\!\!\!\!\!\!\!\int \equiv \frac{1}{TL^3} \sum_{k_0 \in BZ_T} \sum_{\vec{k} \in BZ_L^{3*}} ,
\tag{1.79}
$$

where $BZ_T \equiv \frac{2\pi}{T}\mathbb{Z}$ and $BZ_L^{3*} \equiv \frac{2\pi}{T}\mathbb{Z}^{3*}$, the star indicates the removal of the zero element.

The last ingredient is the integrand of the self-energy $\sigma_{J=0}(k,p)$. This is obtained from the usual one-loop spinor self-energy Feynman diagrams, yielding the following expression:

$$\sigma_0(k,p) \quad = \quad 4\sigma_T(k) - \sigma_{S_0}(k,p) - 4p^2\sigma_{S_1}(k,p) - 4p_\mu\sigma_{S_2,\mu}(k,p) \tag{1.80}$$

with,

$$\begin{aligned} \sigma_T(k) &= \tfrac{1}{k^2} \,, & \sigma_{S_0}(k,p) &= \tfrac{1}{[(p+k)^2+m^2]} \,, \\ \sigma_{S_1}(k,p) &= \tfrac{1}{k^2[(p+k)^2+m^2]} \,, & \sigma_{S_2,\mu}(k,p) &= \tfrac{k_\mu}{k^2[(p+k)^2+m^2]} \,. \end{aligned} \tag{1.81}$$

It can be found that the FV corrections to a boson of spin 0 in terms of the infinite-volume mass m are given by [17]

$$m_0^2(T,L) \underset{T,L\to+\infty}{\sim} m^2 \left\{ 1 - q^2\alpha \left[\frac{\kappa}{mL} \left(1 + \frac{2}{mL} \right) \right] \right\} \,. \tag{1.82}$$

with $\kappa = 2.837297(1)$. At this order the result is valid for both point–like and composite particles. An other interesting observation is that the coefficient of the leading $1/L$ and $1/L^2$ corrections to the mass m of a particle of charge qe is the same for spin-1/2 fermions and spin-0 bosons at $O(\alpha_{em})$, i.e. these coefficients are always the same, independent of the spin and the point–like or composite nature of the particle: they are fixed by QED Ward-Takahashi identities.

1.10   DEFINING QCD IN THE FULL THEORY (QCD+QED)

Before concluding the present chapter and presenting the results of our calculations, we believe that it is useful to discuss the relation between the *"full"* QCD+QED theory, that includes explicit e.m. and strong isospin breaking effects, and QCD without electromagnetism (denoted in the following as the full theory and QCD, respectively). The ideas discussed in the this section have been extensively presented for the first time in Ref. [13].

The action of the full theory involving both quarks and leptons can be schematically written as

$$S^{\text{full}} = \frac{1}{g_s^2} S^{\text{YM}} + S^A + \sum_f \left\{ S_f^{\text{kin}} + m_f S_f^m \right\} + \sum_\ell \left\{ S_\ell^{\text{kin}} + m_\ell S_\ell^m \right\} \,. \tag{1.83}$$

Here g_s is the strong coupling constant, S^{YM} is a discretization of the gluon action, S^A is the preferred discretization of the Maxwell action of the photon, S_f^{kin} is the kinetic term for the quark with flavor f, including the interaction with the gluon and photon fields, $m_f S_f^m = m_f \sum_x \bar{q}_f(x)q_f(x)$ is the mass term, S_ℓ^{kin} and S_ℓ^m are respectively the kinetic and mass terms for the lepton ℓ. For fermion actions which break chiral symmetry, such as the Twisted-Mass action used in this work, a counterterm is needed to remove the critical mass and $m_f S_f^m$ has to be replaced with $m_f S_f^m + m_f^{\text{cr}} S_f^{\text{cr}}$. A mass counterterm is in principle needed also in the case of the lepton, but at leading order in α_{em} the lepton critical mass can be ignored.

At the level of precision to which we are currently working it is only the full theory, as defined in Eq. (1.83), which is expected to reproduce physical results and that is therefore unambiguous. Nevertheless, a frequently asked question is what is the difference between the results for a physical quantity computed in the full theory and in pure QCD, and how big are the strong isospin-breaking effects compared to the e.m. corrections. We particularly wish to underline that in order to properly formulate such questions it is necessary to carefully define what is meant by QCD. It is naturally to be expected that in QCD alone physical quantities will not be reproduced with a precision of better than $O(\alpha_{\mathrm{em}}) \simeq 1\%$ and this of course is the motivation for including QED. In order to define what is meant by QCD at this level of precision it is necessary to state the conditions which are used to determine the quark masses and the lattice spacing. The separation of the full theory into QCD and the rest is therefore prescription dependent.

In Ref. [9] the subtle issue of a precise definition of QCD has been discussed by using the GRS scheme originally proposed in Ref. [46], which has been widely used [7, 9, 16]. In the following we present an extended and detailed discussion by introducing alternative hadronic schemes, which could turn out to be convenient in light of the fact that hadron masses can nowadays be computed very precisely. At the end of this section we discuss the connection with the GRS scheme adopted in our calculations. A summary of the ideas discussed has been presented in Ref. [52].

1.10.1 RENORMALIZATION OF THE FULL THEORY

The main difference in the steps required to renormalize the full theory compared to the procedure in QCD is the presence of a massless photon and the corresponding finite-volume (FV) corrections which appear as inverse powers of L, where L is the spatial extent of the lattice and the volume $V = L^3$. By contrast, in QCD for mass spectra and (semi)leptonic decays the FV corrections are exponentially small in the volume. In the discussion below, if necessary, we imagine that the chiral Ward identities have been imposed to determine the critical masses m_f^{cr} [53].

A possible strategy in principle is the following:

1. Fix the number of lattice points N, e.g. $T = 2aN$ and $L = aN$, where T and L are the temporal and spatial extents of the lattice and the lattice spacing a will be determined later. (The specific choice $T = 2L$ is convenient for illustration but not necessary for the following argument.)

2. Using a four-flavor theory for illustration, we now need to determine the four physical bare quark masses, the bare electric charge and the lattice spacing. To this end we

need to compute six quantities, e.g. the five dimensionless ratios

$$R_1(aN; g_s, e, \mathbf{m}) = \frac{aM_{\pi^+}}{aM_\Omega}(aN; g_s, e, \mathbf{m}) \ ,$$

$$R_2(aN; g_s, e, \mathbf{m}) = \frac{aM_{K^0}}{aM_\Omega}(aN; g_s, e, \mathbf{m})$$

$$R_3(aN; g_s, e, \mathbf{m}) = \frac{aM_{D_s}}{aM_\Omega}(aN; g_s, e, \mathbf{m}) \ ,$$

$$R_4(aN; g_s, e, \mathbf{m}) = \frac{aM_{K^+} - aM_{K^0}}{aM_\Omega}(aN; g_s, e, \mathbf{m}) \ ,$$

$$R_5(aN; g_s, e, \mathbf{m}) = \frac{aM_{D^0} - aM_{D^+}}{aM_\Omega}(aN; g_s, e, \mathbf{m}) \ , \tag{1.84}$$

as well as a dimensionful quantity, e.g. the mass of the Ω baryon, computed in lattice units, from which the lattice spacing can be determined after extrapolation to the infinite volume limit (see below):

$$R_0(aN; g_s, e, \mathbf{m}) = \frac{aM_\Omega(aN; g_s, e, \mathbf{m})}{M_\Omega^{\text{phys}}} \ , \tag{1.85}$$

where $M_\Omega^{\text{phys}} = 1.672\,\text{GeV}$ is the physical value of the mass of the Ω baryon. For illustration we are considering the masses of QCD+QED stable pseudoscalar mesons in the numerators of the dimensionless ratios (1.84) and using M_Ω^{phys} to determine the lattice spacing, but of course other quantities can be used instead. For example, in the four flavor theory that we are considering here one can in principle avoid potentially very noisy baryon observables by using one of the charmed mesons masses already considered above to set the scale. On the other hand, the choice of setting the scale with a charmed-meson observable could generate large cutoff effects. In Eqs. (1.84) - (1.85) we have used aN instead of L to highlight that the infinite-volume limit should be taken at fixed lattice spacing (see Eq. (1.86) below). The quantity $\mathbf{m}$ represents the vector of bare quark masses $\mathbf{m} \equiv \{m_u, m_d, m_s, m_c\}$. Note that in the RM123 strategy, since one works at first order in α_{em}, it is not necessary to impose a renormalization condition to fix the e.m. coupling [7, 9]. In this case the electric charge can simply be fixed to the Thomson limit, i.e. $e = \sqrt{4\pi/137.036}$, and R_5 becomes a predictable quantity. For the remainder of this section, we assume that we are working to $O(\alpha_{\text{em}})$ and only consider the four ratios R_i (i=1,2,3,4) as well as R_0 when discussing the calibration of the lattices. Notice also that at first order in α_{em} the π^0 cannot decay in two photons, so that it can also be used in the calibration procedure.

3. Up to this point the procedure is the standard one used in QCD simulations. The difference here is in the FV effects which behave as inverse powers of L. We therefore envisage extrapolating the ratios R_i to the infinite-volume limit:

$$R_i(g_s, e, \mathbf{m}) \equiv \lim_{N \to \infty} R_i(aN; g_s, e, \mathbf{m}) \ , \qquad i = 0, 1, 2, 3, 4, 5 \ . \tag{1.86}$$

4. For a given discretization and choice of g_s, the *physical* bare quark masses, $\mathbf{m}^{\text{phys}}(g_s)$, and the electric charge, $e^{\text{phys}}(g_s)$, are defined by requiring that the five ratios $R_{1,2,3,4,5}$ take their physical values

$$R_i(g_s, e^{\text{phys}}(g_s), \mathbf{m}^{\text{phys}}(g_s)) = R_i^{\text{phys}} , \qquad i = 1, 2, 3, 4, 5 . \tag{1.87}$$

   In practice, of course, this will require some extrapolations of results obtained at different values of the bare quark masses and electric charge.

5. The lattice spacing a at this value of g_s can now be defined to be

$$a(g_s) = R_0(g_s, e^{\text{phys}}(g_s), \mathbf{m}^{\text{phys}}(g_s)) . \tag{1.88}$$

   Note that with such a procedure the bare parameters and the lattice spacing a do not depend on the lattice volume.

6. At first order in isospin breaking, i.e. $O(\alpha_{\text{em}}, m_d - m_u)$, the renormalization of the lepton masses is performed perturbatively, by requiring that the on-shell masses correspond to the physical ones. If one wishes to go beyond first order, when hadronic effects first enter, then the physical lepton masses should be added to the quantities used in the non-perturbative calibration. The bare lepton masses, together with the other parameters, should be chosen such that, in addition to satisfying the conditions in Eq. (1.84), the lepton-lepton correlators decay in time as $e^{-m_\ell t}$, where m_ℓ is the physical mass of the lepton ℓ.

In Eq. (1.86) we have taken the infinite-volume limit of the computed hadron masses. By working in the QED_L finite-volume formulation of QED, if for each hadron H the FV corrections of order $O(e^2/(M_H L)^3, e^4)$ can be neglected, then the extrapolation to the infinite-volume limit can be avoided by making use of the formula (1.82) [17, 54] (similar formulae also exist for other finite-volume formulations of the theory [55])

$$\frac{a M_H(L; g_s, e, \mathbf{m})}{a M_H(g_s, e, \mathbf{m})} = 1 - \kappa \, \alpha_{\text{em}} \, e_H^2 \left\{ \frac{1}{2L \, M_H(g_s, e, \mathbf{m})} + \frac{1}{L^2 \, M_H^2(g_s, e, \mathbf{m})} \right\} , \tag{1.89}$$

where e_H is the charge of the hadron H and $\kappa = 2.837297\,(1)$ is a known universal constant (independent of the structure of the hadron H). Equation (1.89) can be used to determine the infinite-volume mass of the hadron H from the value measured on the finite-volume L^3, up to corrections of order of $O(e^2/(m_H L)^3, e^4)$. (In any case, even if one wishes to study the behaviour with L by performing simulations at different volumes, the subtraction of the universal $O(e^2/(M_H L))$ and $O(e^2/(M_H L)^2)$ terms using Eq. (1.89) is a useful starting point; the residual leading behaviour of hadronic masses is then of $O(e^2/(M_H L)^3, e^4)$.)

1.10.2 DEFINING OBSERVABLES IN QCD

The procedure discussed in section 1.10.1 provides a full framework with which to perform lattice simulations of QCD together with isospin-breaking effects including radiative corrections. Nevertheless, one may wish to ask how different are the results for some physical

quantities in the full theory (QCD+QED) and in QCD alone. We stress again that, under the assumption that isospin breaking effects are not negligible, QCD by itself is an unphysical theory and requires a definition. Different prescriptions are possible and, of course, lead to different results in QCD. In this subsection we propose and advocate hadronic schemes, based on the non-perturbative evaluation of a set of hadronic masses in lattice simulations.

We recall that the QCD action is given by

$$S^{\mathrm{QCD}} = \frac{1}{g_0^2} S^{\mathrm{YM}} + \sum_f \left\{ S_{f,0}^{\mathrm{kin}} + m_{f,0} S_f^m \right\} \ , \tag{1.90}$$

where the kinetic term only includes the gluon links and the subscripts 0 indicate that the bare coupling and masses are different from those in the full theory of Eq. (1.83). Indeed the two theories have different dynamics that, in turn, generate a different pattern of ultraviolet divergences. The difference in the bare parameters of the two theories, for all schemes used to define QCD, can in fact be ascribed to the necessity of reabsorbing the different ultraviolet singularities. In what follows we present two different approaches to making the choice of the parameters g_0 and $m_{f,0}$.

1.10.2.1 DEFINING OBSERVABLES IN QCD: HADRONIC SCHEMES

In hadronic schemes we choose a value of g_0 and determine the bare quark masses $\mathbf{m}_0^{\mathrm{phys}}$ and the lattice spacing a_0 imposing the same conditions as for the full theory for the ratios $R_{0,...,4}$ evaluated at vanishing electric charge, i.e. following steps 1 - 5 in Sec. 1.10.1 without imposing any constraint on the ratio R_5. We repeat that, for illustration we define the bare quark masses and lattice spacing using the five ratios R_i, but other hadronic quantities could be used instead, both in the full theory and in QCD. These parameters differ by terms of order $O(\alpha_{\mathrm{em}})$ from those in the full theory. For this discussion, we make the natural and convenient choice $g_0 = g_s$. With this choice, the lattice spacings in QCD (a_0) and in the full theory (a) are therefore given by

$$a_0 = \frac{\langle a_0 M_\Omega \rangle^{\mathrm{QCD}}}{M_\Omega^{\mathrm{phys}}} \quad \text{and} \quad a = \frac{\langle a M_\Omega \rangle^{\mathrm{full}}}{M_\Omega^{\mathrm{phys}}} \equiv a_0 (1 + \delta a) \ . \tag{1.91}$$

To illustrate the procedure imagine that we wish to calculate an observable O of mass dimension 1, for example the mass of a hadron which has not been used for the calibration. At a fixed value of $g_s = g_0$, we denote the best estimate of the observable O, which is the one obtained in the full theory, by O^{phys}, and that obtained in QCD as defined above by O^{QCD}:

$$O^{\mathrm{phys}} \equiv \frac{\langle a O \rangle^{\mathrm{full}}}{a} \quad \text{and} \quad O^{\mathrm{QCD}} \equiv \frac{\langle a_0 O \rangle^{\mathrm{QCD}}}{a_0} \ . \tag{1.92}$$

We define the difference of the two as being due to QED effects, $\delta O^{\mathrm{QED}} \equiv O^{\mathrm{phys}} - O^{\mathrm{QCD}}$. There are 3 contributions to δO^{QED}:

1. The first contribution comes from the fact that the covariant derivatives in the kinetic terms in (1.83) and Eq. (1.90) are different. This generates the diagrams in the correlation functions which contain the explicit exchange of virtual photons.

2. The second contribution comes from the fact that the bare quark masses appearing in Eq. (1.83) and Eq. (1.90) are different. The corresponding quark-mass counterterms must therefore be inserted into the correlation functions used to determine O^{phys}. We stress that the need to include quark-mass counterterms is generic and arises from the requirement that the conditions being used to determine the quark masses must be satisfied both in the full theory and in QCD (for the hadronic scheme being used for illustration we impose that the conditions in Eq. (1.87) are satisfied in both theories).

3. Finally we must account for the difference in the lattice spacings $\delta a = a - a_0$ in the full theory and QCD.

Combining these contributions we arrive at

$$O^{\text{phys}} = O^{\text{QCD}} + \frac{\langle a_0\,\delta O\rangle^{\text{QCD}}}{a_0} - \frac{\delta a}{a_0^2}\langle a_0 O\rangle^{\text{QCD}} \ , \tag{1.93}$$

where we have combined the contributions to the correlation functions from the exchange of virtual photons and from the insertion of the mass counterterms into $\langle a_0\delta O\rangle^{\text{QCD}}$.

Further comments may be helpful here. The first term on the right-hand side is one that can be calculated within QCD alone. It has a well defined continuum limit as does the sum of all the terms in Eq. (1.93). This term allows us to define what is the difference between QCD (defined as above) and the full theory in the hadronic scheme: $\delta O^{\text{QED}} = O^{\text{phys}} - O^{\text{QCD}}$.

An important feature of the RM123 approach which we follow in the numerical studies presented in the next chapters, is that the $O(\alpha_{\text{em}})$ terms are computed explicitly and so we do not have to take the difference between numerical calculations performed in the full theory and in QCD. Each of the terms on the right-hand side of Eq. (1.93) is calculated directly. We now explain the procedure in some more detail by assuming that terms of order $O(\alpha_{\text{em}}^2)$ are negligible (the extension to higher orders in α_{em} is straightforward).

1. Correlation functions corresponding to diagrams with the exchange of a virtual photon and to the insertion of the mass counterterms are already of $O(\alpha_{\text{em}})$ and are calculated directly in QCD. The term proportional to the time separation in the correlation functions gives us the mass shift δM_{H_i} ($i = 1, 2, 3, 4$) and δM_Ω for the five masses (or mass differences) in the ratios R_i ($i = 1, 2, 3, 4$) in Eq. (1.84);

2. In the hadronic scheme being used for illustration, we impose the condition that the four ratios $R_i = m_{H_i}/m_\Omega$ are the same in QCD and in the full theory. This corresponds to requiring that

$$\frac{\delta M_{H_i}}{M_{H_i}} - \frac{\delta M_\Omega}{M_\Omega} = 0 \qquad (i = 1, 2, 3, 4) \ . \tag{1.94}$$

The QED contribution to the left-hand side is different from zero (and also ultraviolet divergent) and we require the terms proportional to the counterterms to cancel this contribution. We therefore (in principle) scan the values of the four mass counterterms $\delta m_f = m_f - m_{f,0}$ ($f = u, d, s, c$) until the four conditions (1.94) are satisfied. Also in this case no subtraction of results obtained in the full theory and in QCD is necessary.

3. Finally we determine the difference $\delta a \equiv a - a_0$ in the lattice spacing. Having determined the bare masses using item 2, we can calculate the shift in the Ω mass, δM_Ω due to both QED and the mass counterterms and use Eq. (1.91). Since $a\delta M_\Omega$ is calculated directly, there is again no subtraction.

We have devoted a considerable discussion to the definition of the isospin-breaking effects due to electromagnetism, δO^{QED}. Having done this, the subsequent definition of the strong isospin breaking effects is straightforward. To do this however, we need to define the isosymmetric theory (labelled by "ISO") by imposing appropriate conditions to determine the bare quark masses and the lattice spacing. Since $m_u = m_d$, in the $N_f = 2+1+1$ theory we need to determine only three quark masses and hence we only need three need conditions, e.g. we can use the ratios $R_{1,2,3}$ in Eq. (1.84) to determine the physical bare quark masses. For the determination of the lattice spacing we have two options. The simplest one is to work in a mass–independent scheme and set the lattice spacing in the isosymmetric theory, a_0^{ISO}, equal to the one of QCD with $m_u \neq m_d$, i.e. $a_0^{\mathrm{ISO}} = a_0$. Notice that this choice is fully consistent with renormalization because the ultraviolet divergences of the theories that we are considering do not depend on the quark masses. Note however, that they *do* depend instead on the electric charge. The other option is that we set the lattice spacing in the isosymmetric theory by using R_0 in Eq. (1.88). The difference between the two options is due to cutoff effects that disappear once the continuum limit is taken consistently. The strong isospin breaking correction δO^{SIB} to the observable O can now be defined by

$$\delta O^{\mathrm{SIB}} = O^{\mathrm{QCD}} - O^{\mathrm{ISO}} \, , \tag{1.95}$$

where $O^{\mathrm{ISO}} = \frac{\langle a_0^{\mathrm{ISO}} O \rangle^{\mathrm{ISO}}}{a_0^{\mathrm{ISO}}}$ is the value of the observable obtained in isosymmetric QCD. With these definitions we have the natural relation $O^{\mathrm{phys}} = O^{\mathrm{ISO}} + \delta O^{\mathrm{QED}} + \delta O^{\mathrm{SIB}}$. We underline however that δO^{SIB} depends on the quantities used for calibration, both in 4-flavor QCD and in isosymmetric QCD.

1.10.2.2   DEFINING QCD: THE GRS SCHEME

A different prescription, called the GRS scheme, was proposed in Ref. [46] to relate the bare quark masses and bare coupling of QCD ($m_{f,0}$ and g_0) to those in the full theory (m_f and g_s). This prescription has been adopted in Refs. [7, 9, 16]. In the GRS approach, instead of determining the bare parameters of QCD by requiring that the chosen hadronic masses in QCD are equal to their physical values, one imposes that the renormalized parameters in a given short–distance scheme (e.g. the $\overline{\mathrm{MS}}$ scheme) and at a given scale are equal in the full and QCD theories.

A consistent procedure is the following:

1. The full theory is renormalized by using a physical hadronic scheme as discussed in subsection 10.1. This means that for each chosen value of g_s we know the corresponding physical value of the bare electric charge $e^{\text{phys}}(g_s)$ and of the lattice spacing $a(g_s)$.

2. The renormalization constants (RCs) of the strong coupling constant and of the quark masses are computed in a short–distance mass–independent scheme both in the full theory and in the theory at vanishing electric charge.

3. In order to set the bare parameters of QCD at a given value of the lattice spacing we now chose a matching scale μ and impose that the renormalized strong coupling constant and the renormalized quark masses are the same as in the full theory. In practice we might want to simulate QCD at the same values of the lattice spacing used in the full theory simulations. In this case the matching conditions are

$$
\begin{aligned}
g(\mu) &= Z_g(0, g_0, a(g_s)\mu)g_0 = Z_g(e^{\text{phys}}(g_s), g_s, a(g_s)\mu)g_s = \widehat{g}(\mu) \\
m_f(\mu) &= Z_{m_f}(0, g_0, a(g_s)\mu)m_{f,0}(g_0) = Z_{m_f}(e^{\text{phys}}(g_s), g_s, a(g_s)\mu)m_f(g_s) = \widehat{m}_f(\mu) \,,
\end{aligned}
$$
(1.96)

where $\widehat{}$ indicates quantities in the QCD+QED theory. Notice that quarks with the same electric charge have the same RC, e.g. $Z_{m_u}(e, g_s, \mu) = Z_{m_c}(e, g_s, \mu)$, and that the quark mass RC at vanishing electric charge is flavor independent, $Z_{m_f}(0, g_0, \mu) = Z_m(g_0, \mu)$.

4. In order to define isosymmetric QCD by using this approach, the bare up–down quark mass is determined from

$$
Z_m(g_0, a(g_s)\mu)\, m_{ud,0}(g_0) = \frac{\widehat{m}_u(\mu) + \widehat{m}_d(\mu)}{2} \,.
$$
(1.97)

Some remarks are in order at this point. The GRS scheme is a short–distance matching procedure that can also be used to match the theories at unphysical values of the renormalized electric charge and/or quark masses with the physical theory.

By following the procedure outlined above one can perform lattice simulations of the full theory and of (isosymmetric) QCD at the same value of the lattice spacing but, consequently, at different values of the bare strong coupling constant. This is different from the strategy outlined in the previous subsection where, by using hadronic schemes, it was more natural to chose the same value of the bare strong coupling at the price of having two different lattice spacings. The absence of the lattice spacing counterterm (see Eq. (1.93) above) in the GRS scheme is compensated from the presence of the counterterm $(1/g_0^2 - 1/g_s^2)S^{\text{YM}}$ originating from the difference of the bare strong coupling constants in the two theories.

A remark of some practical relevance concerns the possibility of implementing hadronically the GRS scheme. To this end, note that in the GRS scheme the dimensionless ratios R_i

will not be equal to the corresponding physical values and the difference can be parametrized as follows

$$R_i^{\text{QCD-GRS}} = R_i^{\text{phys}}(1 + \epsilon_i^{\text{GRS}}), \tag{1.98}$$

where the ϵ_i^{GRS} are order $O(\alpha_{\text{em}})$ and depend on the chosen matching scheme and also on the chosen matching scale. Once the ϵ_i^{GRS} (and hence the $R_i^{\text{QCD-GRS}}$) are known, for example from a particularly accurate lattice simulation, then they can be used in other lattice computations. The bare quark masses are then determined by requiring that the R_i in (isosymmetric) QCD reproduce $R_i^{\text{QCD-GRS}}$ as given by Eq.(1.98), and, at this stage, the GRS scheme can be considered to be a hadronic one as it is defined in terms of non-perturbatively computed quantities (in this case meson masses). We stress however that this requires prior knowledge of the ϵ_i^{GRS}.

Of course other schemes are also possible. In general, the ϵ_i provide a unifying language to discuss the different schemes for the definition of (isosymmetric) QCD in the presence of electromagnetism; in hadronic schemes the $\epsilon_i = 0$ while in the GRS and other schemes they are of order $O(\alpha_{\text{em}})$. For later use, we make the simple observation that two schemes can be considered to be equivalent in practice if the ϵ_i in the two schemes are equal within the precision of the computations.

1.11 NON-PERTURBATIVE RENORMALIZATION IN THE RI'-MOM SCHEME

When quantizing a field theory, divergent quantities emerge such as quark masses, couplings and observables. In order to compute these quantities one has to regularize the theory. There are a lot of different regularizations to choose from. As it is often the case, the smartest ones are selected to preserve the symmetries of the action. LQCD is primarily a *regularization* of the QCD theory.

After regularization, i.e. at fixed cut-off, one can proceed in computing all the quantities of interest on the lattice, but the results would unphysically depend on the cut-off. Thus the next step consists in removing the cut-off performing the *continuum limit* for $a \to 0$. Performing this limit straight away would be disastrous. The only way to remove the cut-off properly is through the introduction of the so called *Renormalization Constants* (RCs) that are constructed to absorb the divergences in the continuum limit.

On the lattice, renormalization can be performed using both perturbative and non-perturbative methods. The most popular perturbative scheme is the $\overline{\text{MS}}$ scheme (modified Minimal Subtraction), which is naturally defined within dimensional regularization, at a given renormalization scale which is usually chosen to be $\mu = 2$ GeV. As any other renormalization scheme, $\overline{\text{MS}}$ can be also implemented perturbatively on the lattice. Lattice perturbation theory is however technically more difficult than in the continuum, so that in most of the cases only one-loop results are available. In addition, the convergence of lattice perturbation theory is tipically poor. Therefore, one often relies on non-perturbative approaches. The RI'-MOM (Regularization Independent at subtracted MOMentum), which we will consider here, is a

renormalization scheme suitable to be implemented non-perturbatively. In the remainder of this section we describe the main steps of the RI'-MOM renormalization procedure including $O(\alpha_{em})$ corrections.

1.11.1 RI'-MOM scheme in the QCD+QED theory

The basic idea of the RI'-MOM scheme is to impose renormalization conditions non-perturbatively directly on Green functions, computed in the chiral limit in a fixed gauge, with given off-shell external states, with large virtualities [14]. The method mimics what is usually done in perturbation theory: the renormalization conditions of a certain operator are fixed by imposing that, in a fixed gauge (usually Landau gauge), suitable Green functions computed between off-shell quark and gluon states, coincide with their tree level value[4]. The evaluation of the Green functions in the chiral limit ensures that the RI'-MOM scheme is a mass-independent scheme and the operator renormalization constant depends only on the renormalization scale μ and the coupling constant. The method is supposed to work properly whenever it is possible to fix the virtuality of the external states within a window

$$\Lambda_{\text{QCD}} \ll \mu \ll \frac{1}{a}, \tag{1.99}$$

in order to keep under control both non-perturbative and discretization effects. Indeed, in such a "window" discretization effects can be neglected because the renor- malization scale is small compared to the inverse of the lattice spacing. The fact that μ is much larger than the QCD scale guarantees that continuum perturbation theory can be used to connect different schemes.

Given the amputated Green function, Λ_O, of an operator O computed in a given gauge between external states with momentum p and a suitable projector on the relevant Dirac structure, P_O, we define the projected Green function as

$$\Gamma_O(pa) = \text{Tr} \left[\Lambda_O(pa) \, P_O \right] . \tag{1.100}$$

In the RI'-MOM scheme, the renormalization constant (RC) $Z_O(\mu a)$ is found by imposing the condition [14]

$$Z_{\Gamma_O}(\mu a) \Gamma_O(pa) |_{p^2 = \mu^2} = 1 \ , \tag{1.101}$$

where

$$Z_{\Gamma_O}(\mu a) = Z_O(\mu a) \prod_f Z_f^{-1/2}(\mu a) \ . \tag{1.102}$$

The Z_f are the RCs of the external fields and the index f runs over all external fields entering the expression of the composite operator O. In QCD+QED the RCs Z_O and Z_f depend both on the strong and the e.m. coupling constants.

---

[4]The choice of the tree level Green function is not mandatory. Indeed, one can impose this condition with any equivalent finite Green function.

We find it particularly convenient to write the RCs of any composite operator, and in particular of the fields, bilinear and four-fermion operators, in the generic decomposition

$$
\begin{aligned}
Z_O &= Z_O^{\text{QED}} \left[(Z_O^{\text{QED}})^{-1} Z_O (Z_O^{\text{QCD}})^{-1} \right] Z_O^{\text{QCD}} = \left[1 + \frac{\alpha_{\text{em}}}{4\pi} \left(\delta Z_O^{\text{QED}} + \eta_O \right) \right] Z_O^{\text{QCD}} \\
&= \left(1 + \frac{\alpha_{\text{em}}}{4\pi} \delta Z_O \right) Z_O^{\text{QCD}} ,
\end{aligned}
\tag{1.103}
$$

where Z_O^{QCD} and Z_O^{QED} are the RCs of the operator O in pure QCD and pure QED respectively and we have put

$$
\delta Z_O = \delta Z_O^{\text{QED}} + \eta_O .
\tag{1.104}
$$

The first term, δZ_O^{QED}, in Eq. (1.104) represents the pure QED contribution to the RC at $O(\alpha_{\text{em}})$, whereas η_O contains the $O(\alpha_{\text{em}})$ non-factorisable QCD+QED correction.

In Eq. (1.103) we have introduced the ratio

$$
\mathcal{R} = (Z_O^{\text{QED}})^{-1} Z_O (Z_O^{\text{QCD}})^{-1} \equiv 1 + \frac{\alpha_{\text{em}}}{4\pi} \eta_O ,
\tag{1.105}
$$

which encodes all the non-perturbative contributions of order $O(\alpha_{\text{em}} \alpha_s^n)$ with $n \geq 1$, other than the factorisable terms given by the product $Z_O^{\text{QED}} Z_O^{\text{QCD}}$. In other words if Z_O were simply given by $Z_O = Z_O^{\text{QED}} Z_O^{\text{QCD}}$ at first order in α_{em} then η_O would be zero. The case $\eta_O = 0$ thus corresponds to the *factorization approximation* that was first introduced in Refs. [7, 37]. Introducing this ratio $\mathcal{R}$ in the non-perturbative calculation is useful since by using the same photon fields in the lattice calculation of Z_O and Z_O^{QED} the statistical uncertainty due to the sampling of the photon field is significantly reduced. Note that the ratio is also free from cut-off effects of $O(\alpha_{\text{em}} a^n)$.

In terms of QCD renormalized operators O^χ, $O^\chi \equiv Z_O^{QCD} O^{bare}$, we define the QCD renormalized projected Green function Γ_O^χ, and expand it at first order in α_{em}

$$
\begin{aligned}
\Gamma_O^\chi(\mu a) &= Z_{\Gamma_O}^{\text{QCD}}(\mu a) \Gamma_O(pa)|_{p^2=\mu^2} = Z_{\Gamma_O}^{\text{QCD}}(\mu a) \left[\Gamma_O^{\text{QCD}}(\mu a) + \frac{\alpha_{\text{em}}}{4\pi} \delta \Gamma_O(\mu a) \right] = \\
&= 1 + \frac{\alpha_{\text{em}}}{4\pi} \delta \Gamma_O^\chi(\mu a) ,
\end{aligned}
\tag{1.106}
$$

where we have used the RI'-MOM renormalization condition $Z_{\Gamma_O}^{\text{QCD}}(\mu a) \Gamma_O^{\text{QCD}}(\mu a) = 1$ applied in the pure QCD theory and defined

$$
\delta \Gamma_O^\chi(\mu a) = Z_{\Gamma_O}^{\text{QCD}}(\mu a) \, \delta \Gamma_O(\mu a) .
\tag{1.107}
$$

Using Eqs. (1.103) and (1.106), we can rewrite Eq. (1.101) at first order in α_{em} as

$$
1 = Z_{\Gamma_O}(\mu a) \Gamma_O(\mu a) = 1 + \frac{\alpha_{\text{em}}}{4\pi} \left(\delta Z_{\Gamma_O}(\mu a) + \delta \Gamma_O^\chi(\mu a) \right)
\tag{1.108}
$$

which provides, in turn, the RI-MOM renormalization condition at order α_{em}

$$
\delta Z_{\Gamma_O}(\mu a) = -\delta \Gamma_O^\chi(\mu a) .
\tag{1.109}
$$

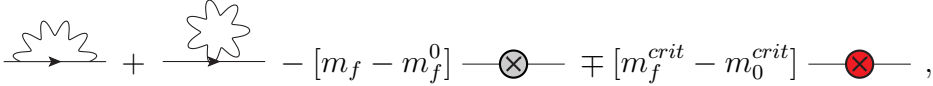Using the expression of Z_{Γ_O} in Eq. (1.102) in terms of Z_O and the external fields RCs one also obtains

$$\delta Z_O(\mu a) = -\delta\Gamma_O^\chi(\mu a) + \frac{1}{2}\sum_f \delta Z_f(\mu a)\,. \tag{1.110}$$

Thus, δZ_O is expressed directly in terms of the $O(\alpha_{\text{em}})$ contribution to the QCD renormalized projected Green function $\delta\Gamma_O^\chi = Z_{\Gamma_O}^{\text{QCD}}\delta\Gamma_O$ evaluated at $p^2 = \mu^2$.

In the following we describe a completely non-perturbative determination of the RCs $\delta Z_O(\mu a)$ to all orders in α_s. We will assume that all the relevant RCs of fields and composite operators in pure QCD have been already determined, by following the standard RI'-MOM renormalization procedure. With appropriate modifications to the kinematical conditions and projectors, the discussion can readily be adapted to similar schemes, such as SMOM [56].

1.11.2 RENORMALIZATION OF THE QUARK FIELD AND BILINEAR OPERATORS

We start with the renormalization of the quark fields. The e.m. corrections to a quark propagator can be represented schematically in the form (see Eq. (1.70))

$$\frac{\alpha_{\text{em}}}{4\pi}\,S^{\text{QCD}}(p)\delta S_q(p)S^{\text{QCD}}(p) =$$

 $+$ $- [m_f - m_f^0]$ $\mp [m_f^{crit} - m_0^{crit}]$ $,$ (1.111)

where the last two diagrams represent the mass and critical Wilson parameter counterterms [9].

The amputated one-particle irreducible two-point function is then given by

$$\delta\Sigma_q(p) = -\,\langle S^{\text{QCD}}(p)\rangle^{-1}\,\langle S^{\text{QCD}}(p)\delta S_q(p)S^{\text{QCD}}(p)\rangle\,\langle S^{\text{QCD}}(p)\rangle^{-1} \tag{1.112}$$

and the correction to the quark field RC in the RI'-MOM scheme is obtained, according to Eq. (1.109), as

$$\delta Z_q = -\frac{i}{12}\text{Tr}\left[\frac{\slashed{p}\,\delta\Sigma_q^\chi(p)}{p^2}\right]_{p^2=\mu^2} = -\frac{i}{12}(Z_q^{\text{QCD}})^{-1}\,\text{Tr}\left[\frac{\slashed{p}\,\delta\Sigma_q(p)}{p^2}\right]_{p^2=\mu^2}. \tag{1.113}$$

The e.m. correction to the RC Z_O of a generic bilinear operator $O_\Gamma = \bar{q}_2\,\Gamma\,q_1$, where Γ is one of the Dirac matrices ($\Gamma = 1, \gamma^5, \gamma^\mu, \gamma^\mu\gamma^5, \sigma^{\mu\nu}$), is given by Eq. (1.110), which in this case reads

$$\delta Z_O = -\delta\Gamma_O^\chi + \frac{1}{2}\left(\delta Z_{q_1} + \delta Z_{q_2}\right)\,. \tag{1.114}$$

Two kinds of corrections contribute to the amputated Green function: either the QCD Green function is amputated with the e.m. corrections on the inverse propagators, or the correction to the Green function itself is amputated with QCD propagators. Thus we have

$$\delta\Gamma_O^\chi = (Z_{q_1}^{\text{QCD}})^{-1/2}(Z_{q_2}^{\text{QCD}})^{-1/2}Z_O^{\text{QCD}}\,\text{Tr}\,[\delta\Lambda_O\,P_O] \tag{1.115}$$

with

$$\begin{aligned}
\delta\Lambda_O &= \delta\Sigma_{q_2}(p)\,G_O^{\text{QCD}}(p)\,\gamma_5\,\langle S^{\text{QCD}\dagger}(p)\rangle^{-1}\,\gamma_5 + \langle S^{\text{QCD}}(p)\rangle^{-1}\,G_O^{\text{QCD}}(p)\,\gamma_5\,\delta\Sigma_{q_1}^\dagger(p)\,\gamma_5\,+ \\
&\quad + \langle S^{\text{QCD}}(p)\rangle^{-1}\,\delta G_O(p)\,\gamma_5\langle S^{\text{QCD}\dagger}(p)\rangle^{-1}\,\gamma_5\,,
\end{aligned} \tag{1.116}$$

where G_O is the non-amputated Green function and δG_O is given diagrammatically by

$$\tag{1.117}$$

Before closing this subsection, we stress that in the calculation of the RC of the pseudoscalar density Z_P and its e.m. correction δZ_P, the Goldstone pole contamination has been taken into account and subtracted. In pure QCD, at each p^2 and for each combination of valence quark masses, μ_1 and μ_2, the amputated Green function has been fitted to the ansatz

$$\Gamma_P^{\text{QCD}} = A_0 + B_0\,M_P^2 + \frac{C_0}{M_P^2}\,, \tag{1.118}$$

where $M_P \equiv M_P(\mu_1, \mu_2)$ is the mass of the pseudoscalar meson composed of valence quarks of mass μ_1 and μ_2. When including QED in the calculation, Eq. (1.118) has to be modified to take into account the e.m. correction to the meson mass. By considering the ansatz in Eq. (1.118) in QCD+QED and expanding it in terms of α_{em} one finds

$$\delta\Gamma_P = A_1 + B_1\,M_P^2 + \frac{C_1}{M_P^2} + B_0\,\delta M_P^2 - C_0\,\frac{\delta M_P^2}{M_P^4}\,, \tag{1.119}$$

where δM_P^2 is the correction to M_P^2 evaluated in Ref. [7]. Note, in particular, that $\delta\Gamma_P$ also receives the contribution of a double pole. In Eq. (1.119) only the coefficients A_1, B_1, C_1 need to be fitted, since the values of B_0 and C_0 are already obtained from the QCD fit in Eq. (1.118).

1.11.3   RENORMALIZATION OF THE FOUR-FERMIONS OPERATORS

In this thesis we will address the lattice calculation of the radiative QED corrections to light-meson leptonic decay rates. In the Standard Model the effective Hamiltonian for

these processes is written in terms of the following four-fermion operator $O_1 = (\bar{q}_2\gamma_\mu(1 - \gamma_5)q_1)\,(\bar{\nu}_\ell\gamma^\mu(1-\gamma_5)\ell)$. In addition, for lattice formulations which break chiral symmetry, like the one used in the present study, the lattice weak operator O_1 mixes with other four-fermion operators of different chirality. Thus, we conclude this section by describing the calculation of the RCs of the weak four-fermion operators O_i ($i = 1,\ldots,5$), in the RI'-MOM scheme. In this case, the renormalization condition (1.110) for the renormalization matrix at $O(\alpha_{\rm em})$ reads:

$$\delta Z_O = -\delta\Gamma_O^\chi + \frac{1}{2}\left(\delta Z_{q_1} + \delta Z_{q_2} + \delta Z_\ell\right)\ , \tag{1.120}$$

where δZ_ℓ is only e.m. and can be computed in perturbation theory.

In Eq. (1.120) $\delta\Gamma_O^\chi$ is a matrix expressed by

$$(\delta\Gamma_O^\chi)_{ij} = (Z_{q_1}^{\rm QCD})^{-1/2}(Z_{q_2}^{\rm QCD})^{-1/2} \sum_{k=1,\ldots,5} (Z_O^{\rm QCD})_{ik}\,{\rm Tr}\left[\delta\Lambda_{O_k}\,P_{O_j}\right]\ . \tag{1.121}$$

As in the case of bilinear operators, the correction to the amputated Green function gets two kind of contributions,

$$\begin{aligned}
\delta\Lambda_{O_i} &= \delta\Sigma_{q_2}(p)\,G_{O_i}^{\rm QCD}(p)\gamma_5\,\langle S^{{\rm QCD}\dagger}(p)\rangle^{-1}\,\gamma_5 + \langle S^{\rm QCD}(p)\rangle^{-1}\,G_{O_i}^{\rm QCD}(p)\gamma_5\,\delta\Sigma_{q_1}^\dagger(p)\,\gamma_5\ + \\
&\quad + \langle S^{\rm QCD}(p)\rangle^{-1}\,\delta G_{O_i}(p)\,\gamma_5\langle S^{{\rm QCD}\dagger}(p)\rangle^{-1}\,\gamma_5\ ,
\end{aligned} \tag{1.122}$$

and in this case δG_{O_i} is given by

The fermionic lines on the left-hand side of the diagrams in Eq. (1.123) represent the ingoing and outgoing light quarks. The lepton self-energy is not reported in Eq. (1.123) since its contribution cancels out in the amputation.

49

2 ISOSPIN BREAKING CORRECTIONS TO MESON MASSES

2.1 INTRODUCTION

The issue of how to include electromagnetic effects in the hadron spectrum and in the determination of quark masses from *ab-initio* lattice calculations was addressed for the first time in Ref. [23]. Using a variety of different methods to include QED effects in lattice QCD simulations, several collaborations have recently obtained remarkably accurate results for the hadron spectrum, such as the determination of the charged-neutral mass splittings of light pseudoscalar (P) mesons and baryons [8, 9, 17, 25, 32, 57–63] (see Ref. [5, 39, 64] for recent reviews and a discussion of the different approaches used to perform QED+QCD lattice calculations of the spectrum).

Till now the inclusion of QED effects in lattice QCD simulations has been carried out following mainly two methods: in the first one QED is added directly to the action and QED+QCD simulations are performed at few values of the electric charge (see, e.g., Ref. [17, 63]), while the second one, the RM123 approach of Ref. [9], consists in an expansion of the lattice path-integral in powers of the two *small* parameters $(\widehat{m}_d - \widehat{m}_u)$ and α_{em}, namely $\alpha_{em} \approx (\widehat{m}_d - \widehat{m}_u)/\Lambda_{QCD} \approx 1\%$. Since it suffices to work at leading order in the perturbative expansion, the attractive feature of the RM123 method is that the small values of the two expansion parameters are factorized out, so that one can get relatively large numerical signals for the *slopes* of the corrections with respect to the two expansion parameters. Moreover the slopes can be determined using isospin symmetric QCD gauge configurations. In this work we adopt the RM123 method described in full details in the previous chapter.

Using the gauge ensembles generated by the European Twisted Mass Collaboration (ETMC) with $N_f = 2 + 1 + 1$ dynamical quarks [45, 65] and the quenched QED approximation, we have calculated the pion, kaon, charmed-meson mass splittings and various ϵ parameters describing the violations of the Dashen's theorem [6] (see Ref. [4]). The precise definition of the latter ones depend on the separation between QED and strong IB (SIB) effects, which we implement using the GRS prescription of Ref. [9].

Within the quenched QED approximation, which neglects the effects of the sea-quark

electric charges, our results[1] are [7, 13]:

$$M_{\pi^+} - M_{\pi^0} = 4.21\ (26)\ \text{MeV}\ \ [4.5936\ (5)\ \text{MeV}]_{exp}\ , \quad (2.1)$$

$$[M_{K^+} - M_{K^0}]^{QED}\ (\overline{MS}, 2\ \text{GeV}) = 2.07\ (15)\ \text{MeV}\ , \quad (2.2)$$

$$[M_{K^+} - M_{K^0}]^{SIB}\ (\overline{MS}, 2\ \text{GeV}) = -6.00\ (15)\ \text{MeV}\ , \quad (2.3)$$

$$(\widehat{m}_d - \widehat{m}_u)(\overline{MS}, 2\ \text{GeV}) = 2.38\ (18)\ \text{MeV}\ , \quad (2.4)$$

$$\frac{\widehat{m}_u}{\widehat{m}_d}(\overline{MS}, 2\ \text{GeV}) = 0.513\ (30)\ , \quad (2.5)$$

$$\widehat{m}_u(\overline{MS}, 2\ \text{GeV}) = 2.50\ (17)\ \text{MeV}\ , \quad (2.6)$$

$$\widehat{m}_d(\overline{MS}, 2\ \text{GeV}) = 4.88\ (20)\ \text{MeV}\ , \quad (2.7)$$

$$\epsilon_{\pi^0} = 0.01\ (4)\ , \quad (2.8)$$

$$\epsilon_{\gamma}(\overline{MS}, 2\ \text{GeV}) = 0.80\ (11)\ , \quad (2.9)$$

$$\epsilon_{K^0}(\overline{MS}, 2\ \text{GeV}) = 0.01\ (2)\ , \quad (2.10)$$

$$[M_{D^+} - M_{D^0}]^{QED}\ (\overline{MS}, 2\ \text{GeV}) = 2.42\ (51)\ \text{MeV}\ , \quad (2.11)$$

$$[M_{D^+} - M_{D^0}]^{SIB}\ (\overline{MS}, 2\ \text{GeV}) = 3.06\ (27)\ \text{MeV}\ , \quad (2.12)$$

$$M_{D^+} - M_{D^0} = 5.47\ (53)\ \text{MeV}\ \ [4.75\ (8)\ \text{MeV}]_{exp}\ , \quad (2.13)$$

$$\delta M_{D^+} + \delta M_{D^0} = 1.7\ (1.0)\ \text{MeV}\ , \quad (2.14)$$

$$\delta M_{D_s^+} = 2.3\ (4)\ \text{MeV}\ , \quad (2.15)$$

where the errors include an estimate of the effects of the QED quenching, while by $\widehat{m}$ we indicate a quark mass renormalized in QCD+QED. In Eqs. (2.1) and (2.13) the experimental values from PDG [3] are given in squared brackets for comparison. Instead the experimental value of the kaon mass splitting $M_{K^+} - M_{K^0} = -3.934(20)$ MeV [3] is used as the input to determine the quark mass difference $(\widehat{m}_d - \widehat{m}_u)$ given in Eq. (2.4).

Using the above results and the experimental values of the meson masses [3], we have estimated the pion, kaon, D- and D_s-meson masses in isospin-symmetric QCD within the

---

[1]The quark mass ratio m_u/m_d is renormalization group invariant in pure QCD only. In the presence of QED effects the running of the quark mass depends on its electric charge and, therefore, the ratio $\widehat{m}_u/\widehat{m}_d$ depends on the renormalization scheme and scale.

GRS prescription [7, 13]:

$$
\begin{aligned}
M_\pi^{QCD} &= 135.0\ (2)\ \text{MeV} & [134.8\ (3)\ \text{MeV}]_{FLAG}\ , & \qquad (2.16)\\
M_K^{QCD} &= 494.6\ (1)\ \text{MeV} & [494.2\ (3)\ \text{MeV}]_{FLAG}\ , & \qquad (2.17)\\
M_D^{QCD} &= 1866.4\ (6)\ \text{MeV}\ , & & \qquad (2.18)\\
M_{D_s}^{QCD} &= 1966.7\ (1.5)\ \text{MeV}\ , & & \qquad (2.19)
\end{aligned}
$$

where the current estimates from FLAG [4] are given in squared brackets for comparison.

This chapter is organized as follows. In section 2.2 we describe the lattice setup and give the simulation details. In section 2.3 we present the calculations of the relevant correlators within the RM123 approach. The results of our analysis for the pion mass splitting $M_{\pi^+} - M_{\pi^0}$ and for the ϵ_{π^0} parameter are given in sections 2.4 and 2.5, respectively. In section 2.6 we determine the light quark mass difference $\widehat{m}_d - \widehat{m}_u$ using the experimental value of the kaon mass splitting $M_{K^+} - M_{K^0}$, while section 2.7 is devoted to the evaluation of the ϵ_{K^0} parameter. In section 2.8 we evaluate the IB corrections in the charmed D^+, D^0 and D_s^+ mesons. Using our result for $\widehat{m}_d - \widehat{m}_u$, we present the first lattice determination of the D-meson mass difference $M_{D^+} - M_{D^0}$.

2.2 SIMULATION DETAILS

The gauge ensembles used in this work are the ones generated by ETMC with $N_f = 2+1+1$ dynamical quarks, which include in the sea, besides two light mass-degenerate quarks, also the strange and charm quarks with masses close to their physical values [45, 65].

The lattice actions for sea and valence quarks are the same used in Ref. [66] to determine the up, down, strange and charm quark masses in isospin symmetric QCD. They are the Iwasaki action for gluons and the Wilson Twisted Mass Action for sea quarks. In the valence sector, in order to avoid the mixing of strange and charm quarks a non-unitary set up was adopted, in which the valence strange and charm quarks are regularized as Osterwalder-Seiler fermions, while the valence up and down quarks have the same action of the sea. Working at maximal twist such a setup guarantees an automatic $O(a)$-improvement.

We considered three values of the inverse bare lattice coupling β and different lattice volumes, as shown in Table I, where the number of configurations analyzed (N_{cfg}) corresponds to a separation of 20 trajectories. At each lattice spacing, different values of the light sea quark masses have been considered. The light valence and sea quark masses are always taken to be degenerate. The bare mass of the strange valence quark $a\mu_s$ is obtained, at each β, using the physical strange mass and the mass renormalization constants determined in Ref. [66].

In Ref. [66] eight branches of the analysis were considered. They differ in:

- the continuum extrapolation adopting for the scale parameter either the Sommer parameter r_0 or the mass of a fictitious P meson made up of strange(charm)-like quarks;

ensemble	β	V/a^4	$a\mu_{sea} = a\mu_{val}$	$a\mu_\sigma$	$a\mu_\delta$	N_{cfg}	$a\mu_s$	$a\mu_c$
$A30.32$	1.90	$32^3 \times 64$	0.0030	0.15	0.19	150	0.02363	0.27903
$A40.32$			0.0040			100		
$A50.32$			0.0050			150		
$A40.24$		$24^3 \times 48$	0.0040			150		
$A60.24$			0.0060			150		
$A80.24$			0.0080			150		
$A100.24$			0.0100			150		
$A40.20$		$20^3 \times 48$	0.0040			150		
$B25.32$	1.95	$32^3 \times 64$	0.0025	0.135	0.170	150	0.02094	0.24725
$B35.32$			0.0035			150		
$B55.32$			0.0055			150		
$B75.32$			0.0075			80		
$B85.24$		$24^3 \times 48$	0.0085			150		
$D15.48$	2.10	$48^3 \times 96$	0.0015	0.1200	0.1385	100	0.01612	0.19037
$D20.48$			0.0020			100		
$D30.48$			0.0030			100		

Table I: *Values of the simulated sea and valence quark bare masses, of the pion (M_π) and kaon (M_K) masses for the 16 ETMC gauge ensembles with $N_f = 2 + 1 + 1$ dynamical quarks generated within the isospin symmetric theory (see Ref. [66] for details). The values of the strange and charm quark bare masses $a\mu_s$ and $a\mu_c$ correspond to the physical strange and charm quark masses, respectively, determined in Ref. [66].*

- the chiral extrapolation performed with fitting functions chosen to be either a polynomial expansion or a Chiral Perturbation Theory (ChPT) Ansatz in the light-quark mass;

- the choice between two methods, denoted as M1 and M2, which differ by $O(a^2)$ effects, used to determine in the RI'-MOM scheme the mass renormalization constant (RC) $Z_m = 1/Z_P$.

In the present analysis we made use of the input parameters corresponding to each of the eight branches of Ref. [66]. The central values and the errors of the input parameters, evaluated using bootstrap samplings with $O(100)$ events, are collected in Table II. Throughout this work all the results obtained within the above branches are averaged according to Eq. (28) of Ref. [66].

For each gauge ensemble the P meson masses are extracted from a single exponential fit (including the proper backward signal) in the range $t_{min} \leq t \leq t_{max}$. The values chosen for t_{min} and t_{max} at each β and lattice volume in the light, strange and charm sectors are collected in Table III, while the values of the pion, kaon and D-meson masses corresponding to pure iso-symmetric QCD, evaluated using the bootstrap samplings of Table II, are collected in Table IV.

	β	1st	2nd	3rd	4th
	1.90	2.224(68)	2.192(75)	2.269(86)	2.209(84)
a^{-1}(GeV)	1.95	2.416(63)	2.381(73)	2.464(85)	2.400(83)
	2.10	3.184(59)	3.137(64)	3.248(75)	3.163(75)
m_{ud}(GeV)		0.00372(13)	0.00386(17)	0.00365(10)	0.00375(13)
m_s(GeV)		0.1014(43)	0.1023(39)	0.0992(29)	0.1007(32)
m_c(GeV)		1.183(34)	1.193(28)	1.177(25)	1.219(21)
	1.90	0.5290(73)			
Z_P	1.95	0.5089(34)			
	2.10	0.5161(27)			

	β	5th	6th	7th	8th
	1.90	2.222(67)	2.195(75)	2.279(89)	2.219(87)
a^{-1}(GeV)	1.95	2.414(61)	2.384(73)	2.475(88)	2.411(86)
	2.10	3.181(57)	3.142(64)	3.262(79)	3.177(78)
m_{ud}(GeV)		0.00362(12)	0.00377(16)	0.00354(9)	0.00363(12)
m_s(GeV)		0.0989(44)	0.0995(39)	0.0962(27)	0.0975(30)
m_c(GeV)		1.150(35)	1.158(27)	1.144(29)	1.182(19)
	1.90	0.5730(42)			
Z_P	1.95	0.5440(17)			
	2.10	0.5420(10)			

Table II: *The input parameters for the eight branches of the analysis of Ref. [66]. The renormalized quark masses and the RC Z_P are given in the $\overline{\text{MS}}$ scheme at a renormalization scale of 2 GeV. With respect to Ref. [66] the table includes an update of the values of the lattice spacing and, consequently, of all the other quantities.*

β	T/a	$[t_{min}, t_{max}]_{(\ell\ell,\ell s)}/a$	$[t_{min}, t_{max}]_{(\ell c)}/a$	$[t_{min}, t_{max}]_{(sc)}/a$
1.90	48	[12, 23]	[15, 21]	[18, 23]
1.90	64	[12, 31]	[15, 24]	[18, 25]
1.95	48	[13, 23]	[16, 21]	[19, 21]
1.95	64	[13, 31]	[16, 24]	[19, 29]
2.10	96	[18, 40]	[20, 27]	[25, 40]

Table III: *Time intervals $[t_{min}, t_{max}]/a$ adopted for the extraction of the P meson masses in the light (ℓ), strange (s) and charm (c) sectors.*

Following Refs. [9, 46] we impose the GRS matching condition between the full QCD+QED and the isospin symmetric QCD theories: in the $\overline{\text{MS}}$ scheme at a renormalization scale $\mu = 2$ GeV we require $\widehat{m}_f(\overline{\text{MS}}, 2 \text{ GeV}) = m_f(\overline{\text{MS}}, 2 \text{ GeV})$ for $f = (ud), s, c$, where $\widehat{m}$ and m are the renormalized quark masses in the full theory and in isosymmetric QCD. A similar condition is imposed on the strong coupling constants of the two theories (i.e. the lattice spacing).

ensemble	β	V/a^4	M_π(MeV)	M_K(MeV)	M_D(MeV)
$A30.32$	1.90	$32^3 \times 64$	275 (10)	568 (22)	2012 (77)
$A40.32$			316 (12)	578 (22)	2008 (77)
$A50.32$			350 (13)	586 (22)	2014 (77)
$A40.24$		$24^3 \times 48$	322 (13)	582 (23)	2017 (77)
$A60.24$			386 (15)	599 (23)	2018 (77)
$A80.24$			442 (17)	618 (24)	2032 (78)
$A100.24$			495 (19)	639 (24)	2044 (78)
$A40.20$		$20^3 \times 48$	330 (13)	586 (23)	2029 (79)
$B25.32$	1.95	$32^3 \times 64$	259 (9)	546 (19)	1942 (67)
$B35.32$			302 (10)	555 (19)	1945 (67)
$B55.32$			375 (13)	578 (20)	1957 (68)
$B75.32$			436 (15)	599 (21)	1970 (68)
$B85.24$		$24^3 \times 48$	468 (16)	613 (21)	1972 (68)
$D15.48$	2.10	$48^3 \times 96$	223 (6)	529 (14)	1929 (49)
$D20.48$			255 (7)	535 (14)	1933 (50)
$D30.48$			318 (8)	550 (14)	1937 (49)

Table IV: *Values of the pion, kaon and D-meson masses evaluated using the bootstrap samplings of Table II for all the* 16 *ETMC gauge ensembles.*

These conditions fix the isosymmetric QCD bare parameters and a unique prescription to define the isosymmetric QCD contribution to each hadronic quantity (see for instance the first term on the r.h.s. of Eq. (2.20)). The parameters given in Table II have been obtained in Ref. [66] by using for the isosymmetric QCD contributions to the hadronic inputs the estimates given by FLAG [4]. In Ref. [7] we have provided new results for these inputs that can be used in the future to obtain (slightly) improved determinations of the isosymmetric bare couplings. We stress that in the calculation of leading IB observables it is fully legitimate to use the QCD parameters given in Ref. [66] because a change in the prescription that fixes these values has an effect only at higher orders in α_{em} and $(\widehat{m}_d - \widehat{m}_u)$.

2.3   EVALUATION OF THE ISOSPIN BREAKING CORRECTIONS

According to the RM123 approach of Ref. [9] the e.m. and strong IB corrections to the mass of a P meson with charge Qe can be written as

$$M_{PQ} = M_P + [\delta M_{PQ}]^{QED} + [\delta M_P]^{SIB} \tag{2.20}$$

with

$$[\delta M_{PQ}]^{QED} \equiv 4\pi\alpha_{em} [\delta M_{PQ}]^{em} + ... , \tag{2.21}$$

$$[\delta M_P]^{SIB} \equiv (\widehat{m}_d - \widehat{m}_u) [\delta M_P]^{QIB} + ... , \tag{2.22}$$

55

where the ellipses stand for higher order terms in α_{em} and $(\widehat{m}_d - \widehat{m}_u)$, while M_P stands for the P meson mass corresponding to the renormalized quark masses in the isosymmetric QCD theory. The separation in Eq. (2.20) between the QED and SIB contributions, $[\delta M_{PQ}]^{QED}$ and $[\delta M_P]^{SIB}$, is prescription and renormalization scheme and scale dependent [46, 67].

Throughout this work we adopt the quenched QED approximation, which neglects the sea-quark electric charges and corresponds to consider only (fermionic) connected diagrams. Including the contributions coming from the insertions of the e.m. current and tadpole operators, of the pseudoscalar and scalar densities (see Sec. 1.7) the basic diagrams are those depicted schematically in Fig. 4.6.8. The insertion of the pseudoscalar density is related to the the e.m. shift of the critical mass present in lattice formulations breaking chiral symmetry, as in the case of Wilson and twisted-mass fermions, as discussed in detail Sec. 1.8).
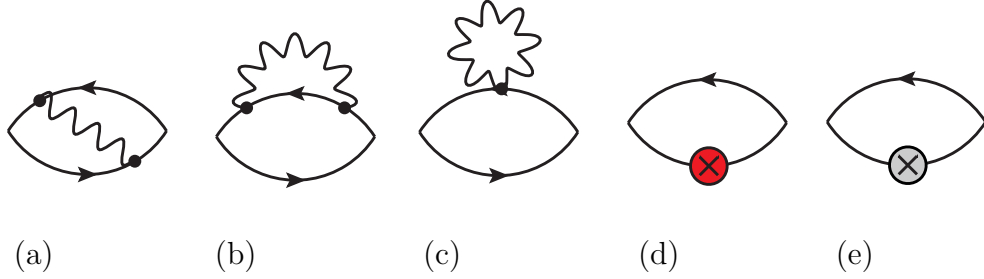

(a)   (b)   (c)   (d)   (e)

Figure 2.3.1: *Fermionic connected diagrams contributing at $O(e^2)$ and $O(m_d - m_u)$ to the IB corrections to meson masses: exchange (a), self energy (b), tadpole (c), pseudoscalar insertion (d) and scalar insertion (e).*

In order to evaluate the diagrams (4.6.8a)-(4.6.8e) the following correlators are considered:

$$\delta C^J(t) \;=\; \frac{1}{2} \sum_{\vec{x}, y_1, y_2} \langle 0| T \left\{ \phi_P^\dagger(\vec{x}, t) \; J_\mu(y_1) J_\nu(y_2) \; \phi_P(0) \right\} |0\rangle \Delta_{\mu\nu}(y_1, y_2), \qquad (2.23)$$

$$\delta C^T(t) \;=\; \sum_{\vec{x}, y} \langle 0| T \left\{ \phi_P^\dagger(\vec{x}, t) \; T_\nu(y) \; \phi_P(0) \right\} |0\rangle \Delta_{\nu\nu}(y, y), \qquad (2.24)$$

$$\delta C^{P_f}(t) \;=\; \sum_{\vec{x}, y} \langle 0| T \left\{ \phi_P^\dagger(\vec{x}, t) \; i\overline{\psi}_f(y)\gamma_5\psi_f(y) \; \phi_P(0) \right\} |0\rangle, \qquad (2.25)$$

$$\delta C^{S_f}(t) \;=\; -\sum_{\vec{x}, y} \langle 0| T \left\{ \phi_P^\dagger(\vec{x}, t) \; \left[\overline{\psi}_f(y)\psi_f(y)\right] \; \phi_P(0) \right\} |0\rangle, \qquad (2.26)$$

where $f = \{u, d, s, c\}$, $\Delta_{\mu\nu}(y_1, y_2)$ is the photon propagator and $J_\mu(y)$ and $T_\nu(y)$ are the lattice conserved e.m. current and the tadpole operator, respectively, defined in Eqs. (1.31), (1.39) with $\phi_P(x) = i\overline{\psi}_{f_1}(x)\gamma_5\psi_{f_2}(x)$ being the interpolating field for a P meson composed by two valence quarks f_1 and f_2 with charges $e_1 e$ and $e_2 e$. In our twisted-mass setup the Wilson parameters of the two valence quarks are chosen to be opposite ($r_1 = -r_2$) in order to guarantee that discretization effects on M_P are of order $O(a^2 m \Lambda_{QCD})$.

Within the quenched QED approximation the correlator $\delta C^J(t)$ corresponds to the sum of the diagrams (4.6.8a)-(4.6.8b), while the correlators $\delta C^T(t)$, $\delta C^{P_f}(t)$ and $\delta C^{S_f}(t)$ represent the contributions of the diagrams (4.6.8c), (4.6.8d) and (4.6.8e), respectively. The removal of the photon zero-mode is done according to QED_L [54], i.e. the photon field A_μ in momentum space satisfies $A_\mu(k_0, \vec{k} = \vec{0}) \equiv 0$ for all k_0.

The statistical accuracy of the meson correlators is based on the use of the so-called "one-end" stochastic method [68], which includes spatial stochastic sources at a single time slice chosen randomly. Four stochastic sources (diagonal in the spin variable and dense in the color one) were adopted per each gauge configuration.

In our analysis the correlators $\delta C^j(t)$ with $j = \{J, T, P, S\}$ are divided by the tree-level one (see Sec. 1.7.1)

$$C(t) \equiv \sum_{\vec{x}} \langle 0 | T \left\{ \phi_P^\dagger(\vec{x}, t) \phi_P(0) \right\} | 0 \rangle \ , \tag{2.27}$$

obtaining at large time distances, where the P ground-state is dominant,

$$\frac{\delta C^j(t)}{C(t)} \xrightarrow[t \gg a, (T-t) \gg a]{} \frac{\delta Z_P^j}{Z_P} + \frac{\delta M_P^j}{M_P} f_P(t) \tag{2.28}$$

where $Z_P \equiv \langle 0 | \phi_P(0) | P \rangle$ and

$$f_P(t) \equiv M_P \left(\frac{T}{2} - t \right) \frac{e^{-M_P t} - e^{-M_P(T-t)}}{e^{-M_P t} + e^{-M_P(T-t)}} - 1 - M_P \frac{T}{2} \tag{2.29}$$

is almost a linear function of the Euclidean time t. Thus, the various e.m. and strong IB corrections to the P mass, δM_P^j ($j = J, T, P_f, S_f$), can be extracted from the slope of the corresponding ratios $\delta C^j(t)/C(t)$ at large time distances (see Table III for the chosen fitting intervals).

The difference between the bare quark mass $\widehat{\mu}_f$ in QCD+QED and the bare mass μ_f in isosymmetric QCD is related to the corresponding difference between the renormalized masses $\widehat{m}_f$ and m_f by

$$\widehat{\mu}_f - \mu_f = \frac{\widehat{m}_f}{\widehat{Z}_{m_f}} - \frac{m_f}{Z_m} = \frac{1}{Z_m} \left[\frac{Z_m}{\widehat{Z}_{m_f}} \widehat{m}_f - m_f \right] \tag{2.30}$$

where $\widehat{Z}_{m_f}$ (Z_m) is the mass renormalization constant in QCD+QED (QCD). By defining

$$\frac{Z_m}{\widehat{Z}_{m_f}} = 1 + \frac{\alpha_{em}}{4\pi} \mathcal{Z}^f + O(\alpha_{em}^m \alpha_s^n) \qquad (m > 1, \ n \geq 0) \tag{2.31}$$

we get at first order in α_{em}

$$\widehat{\mu}_f - \mu_f = \frac{1}{Z_m} [\widehat{m}_f - m_f] + \frac{\alpha_{em}}{4\pi} \frac{\mathcal{Z}^f}{Z_m} \widehat{m}_f \ . \tag{2.32}$$

For our maximally twisted-mass setup one has $Z_m = 1/Z_P$, while $\mathcal{Z}^f$ can be written in the form

$$\mathcal{Z}^f = \mathcal{Z}^f_{\text{QED}} Z^{fact}_m \ , \tag{2.33}$$

where $\mathcal{Z}^f_{\text{QED}}$ is the pure QED contribution at leading order in α_{em}, given in the $\overline{\text{MS}}$ scheme at a renormalization scale μ by [69]

$$\mathcal{Z}^f_{\text{QED}}(\overline{\text{MS}}, \mu) = e^2_f \left[6\log(a\mu) - 22.5954 \right] \ , \tag{2.34}$$

and Z^{fact}_m takes into account all the corrections of order $O(\alpha^n_s)$ with $n \geq 1$. The quantity Z^{fact}_m has been computed non-perturbatively as described in Sec. 1.11.2 and represents the QCD corrections to the "naive factorization" approximation $\mathcal{Z}^f = \mathcal{Z}^f_{\text{QED}}$ (i.e. $Z^{fact}_m = 1$) introduced in Refs. [7, 37]. The values [13] of the coefficients Z^{fact}_m, corresponding to the non-factorisable e.m. corrections to the mass RC, are collected in Table V for the three values of the inverse coupling β adopted in this work and for $\mu = 1/a$. The two methods M1 and M2 correspond to different treatments of the $O(a^2\mu^2)$ discretization effects and are described in Ref. [66]. The difference of the results obtained with these two methods enters into a systematic uncertainty labelled as $()_{input}$ (see later on). The results in Table V show that the non-factorisable corrections are significant, of O(40‑60%), for Z_m.

	Z^{fact}_m	
β	Method 1	Method 2
1.90	1.629 (41)	1.637 (14)
1.95	1.514 (33)	1.585 (12)
2.10	1.459 (17)	1.462 (6)

Table V: *Values of the non-factorisable e.m. corrections to the mass RC in the $\overline{\text{MS}}(2\,\text{GeV})$, Z^{fact}_m (see Eq. (2.33)), calculated for the three values of the inverse coupling β adopted in this work and for $\mu = 1/a$. The evaluation of the RCs in the RI'-MOM scheme has been carried out in Ref. [13] using the methods M1 and M2 of Ref. [66].*

Once multiplied by the bare quantity $\delta M^{S_f}_P$ related to the insertion of the scalar density, the first term in the r.h.s. of Eq. (2.32) generates a finite term, which in our prescription [9] defines the SIB correction

$$[\delta M_P]^{SIB}(\overline{\text{MS}}, \mu) = \sum_{f=f_1,f_2} Z_P(\overline{\text{MS}}, \mu) \ \left[\widehat{m}_f(\overline{\text{MS}}, \mu) - m_f(\overline{\text{MS}}, \mu) \right] \ \delta M^{S_f}_P \ . \tag{2.35}$$

The second term in the r.h.s. of Eq. (2.32) generates a logarithmic divergent contribution that, when included in the QED correction, compensates the corresponding divergence of

the self-energy and tadpole diagrams. At leading order in α_{em} and $(\widehat{m}_d - \widehat{m}_u)$ one has

$$
\begin{aligned}
[\delta M_{PQ}]^{QED}\,(\overline{\text{MS}}, \mu) &= 4\pi\alpha_{em}\Bigg\{\delta M_P^J + \delta M_P^T + \sum_{f=f_1,f_2} \delta m_f^{crit}\,\delta M_P^{P_f} \\
&+ \frac{1}{16\pi^2}\sum_{f=f_1,f_2} Z_P(\overline{\text{MS}},\mu)\mathcal{Z}^f(\overline{\text{MS}},\mu)\,m_f(\overline{\text{MS}},\mu)\,\delta M_P^{S_f}\Bigg\}\,,
\end{aligned}
\tag{2.36}
$$

where δm_f^{crit} is the e.m. shift of the critical mass for the quark flavor f, which will be discussed in detail in the next Section. Note that, since we require $\widehat{m}_f(\overline{\text{MS}}, 2\text{ GeV}) = m_f(\overline{\text{MS}}, 2\text{ GeV})$ for $f = (ud), s, c$, the r.h.s. of Eq. (2.35) at the scale $\mu = 2$ GeV receives a non-vanishing contribution only when a valence light quark u or d is present in the P meson (since $m_d = m_u = m_{ud}$). In that case $[\delta M_P]^{SIB}\,(\overline{\text{MS}}, 2\text{ GeV})$ is proportional to $(\widehat{m}_d - \widehat{m}_u)(\overline{\text{MS}}, 2\text{ GeV})$, as anticipated in Eq. (2.22). When $P^Q = \pi^{0,+}$ the contributions coming from the u and d quarks cancel out and $[\delta M_\pi]^{SIB}\,(\overline{\text{MS}}, 2\text{ GeV}) = 0$ at leading order in $(\widehat{m}_d - \widehat{m}_u)(\overline{\text{MS}}, 2\text{ GeV})$.

2.3.1 DETERMINATION OF δm_f^{crit}

In order to extract physical information from Eq. (2.36) it is necessary to determine the e.m. shift of the critical mass of the quarks. The strategy chosen in [9] and described in Sec. 1.8 is to use the vector Ward-Takahashi identity, which allows to calculate δm_f^{crit} as

$$
\delta m_f^{crit} = -\frac{\nabla_0\left[\delta V_f^J(t) + \delta V_f^T(t)\right]}{\nabla_0\,\delta V_f^{P_f}(t)}
\tag{2.37}
$$

where ∇_0 is the backward time derivative and

$$
\delta V_f^J(t) = \sum_{\vec{x},y_1,y_2} \langle 0|T\left\{V_{\bar{f}f}^\dagger(\vec{x},t)\,J_\mu(y_1)J_\nu(y_2)\,\phi_{\bar{f}f}(0)\right\}|0\rangle\Delta_{\mu\nu}(y_1,y_2)\,,
\tag{2.38}
$$

$$
\delta V_f^T(t) = \sum_{\vec{x},y} \langle 0|T\left\{V_{\bar{f}f}^\dagger(\vec{x},t)\,T_\nu(y)\,\phi_{\bar{f}f}(0)\right\}|0\rangle\Delta_{\nu\nu}(y,y)\,,
\tag{2.39}
$$

$$
\delta V_f^{P_f}(t) = \sum_{\vec{x},y} \langle 0|T\left\{V_{\bar{f}f}^\dagger(\vec{x},t)\,i\overline{\psi}_f(y)\gamma_5\psi_f(y)\,\phi_{\bar{f}f}(0)\right\}|0\rangle\,,
\tag{2.40}
$$

with $V_{\bar{f}f}(x) \equiv \overline{\psi}_f(x)\gamma_0\psi_f(x)$.

Within the quenched QED approximation the shift δm_f^{crit} is proportional to e_f^2 and can be determined from the plateaux of the r.h.s of Eq. (2.37), as shown in Fig. 2.3.2 for the gauge ensembles B25.32 and D15.48.

The results of $\delta m_f^{crit}/e_f^2$ for all the ETMC gauge ensembles of Table I are collected in Fig. 2.3.3. It can be seen that: i) the values of $\delta m_f^{crit}/e_f^2$ are determined quite precisely (better than the per mille level), and   ii) at each value of the lattice spacing there is a very mild dependence on the value of the light-quark mass.
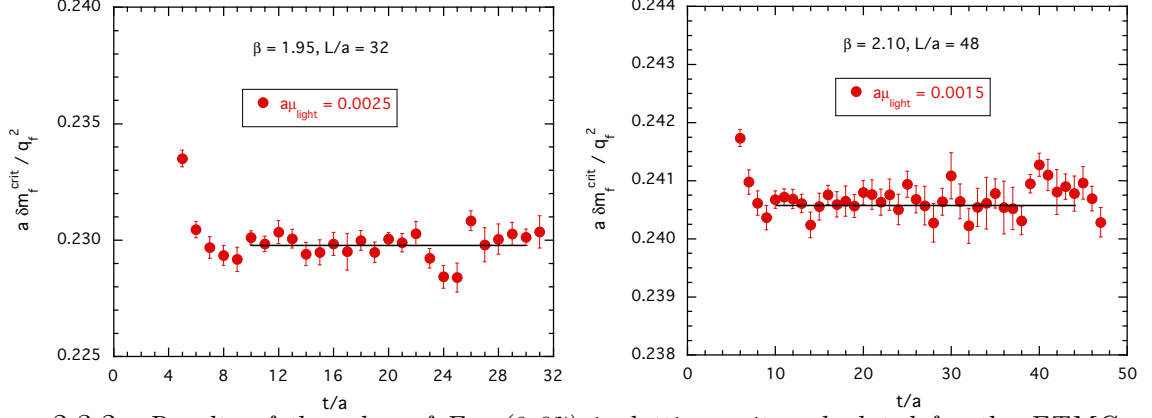
Figure 2.3.2: *Results of the r.h.s of Eq. (2.37) in lattice units calculated for the ETMC gauge ensembles B25.32 (left panel) and D15.48 (right panel). The solid lines represent the value of $\delta m_f^{crit}/e_f^2$ extracted from the corresponding plateau regions.*
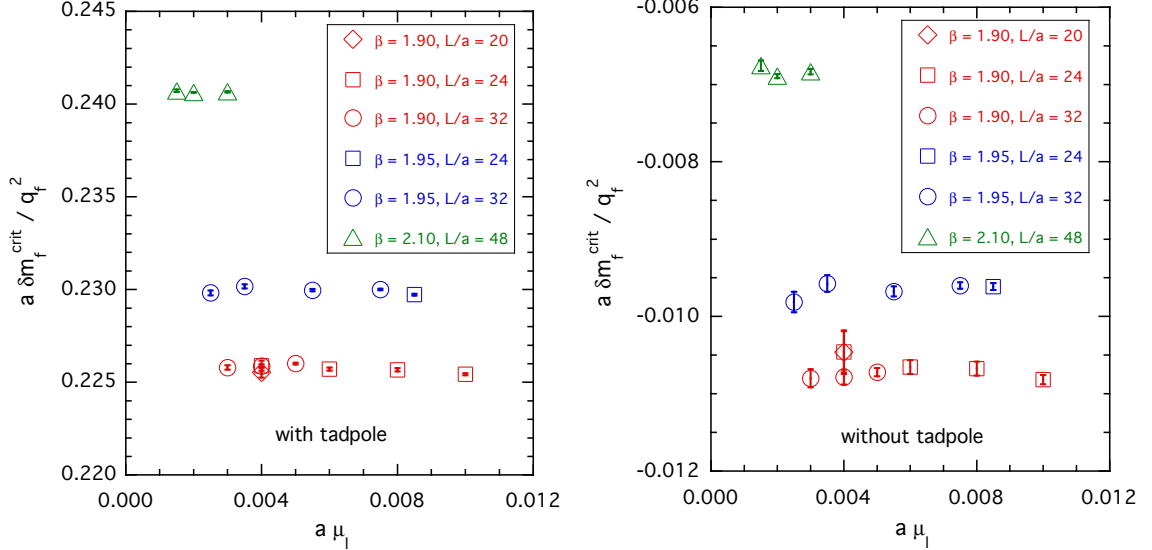

Figure 2.3.3: *Values of the e.m. shift of the critical mass $\delta m_f^{crit}/e_f^2$ versus the bare light-quark mass (in lattice units) calculated for the ETMC gauge ensembles of Table I. Left panel: with the tadpole contribution. Right panel: without the tadpole contribution.*

2.3.2 EXTRACTION OF THE ELECTROMAGNETIC AND STRONG ISOSPIN BREAKING CORRECTIONS

In this subsection we show some plots of the ratios $\delta C^j(t)/C(t)$, used in Eq. (2.28) in order to extract the IB corrections δM_P^j from the corresponding slopes. In Fig. 2.3.4 in the case of the kaon for the ensemble B35.32 we show the ratios $\delta C^J(t)/C(t)$ (exchange and self-energy contributions (4.6.8a)-(4.6.8b)) and $\delta C^S(t)/C(t)$ (scalar insertion (4.6.8e)) together with the almost linear fitting curve of Eq. (2.28), performed in the time interval where the

ground-state is dominant. In Fig. 2.3.5 the contributions of the tadpole diagram (4.6.8c) and of the shift of the critical mass are shown separately. It can be seen that the two terms are almost opposite. Thanks to the strong correlations due to the dominance of the tadpole contribution in δm^{crit} (see Fig. 2.3.3), their sum can be determined with a good precision and turns out to be small compared with the contributions of the self-energy and exchange diagrams.
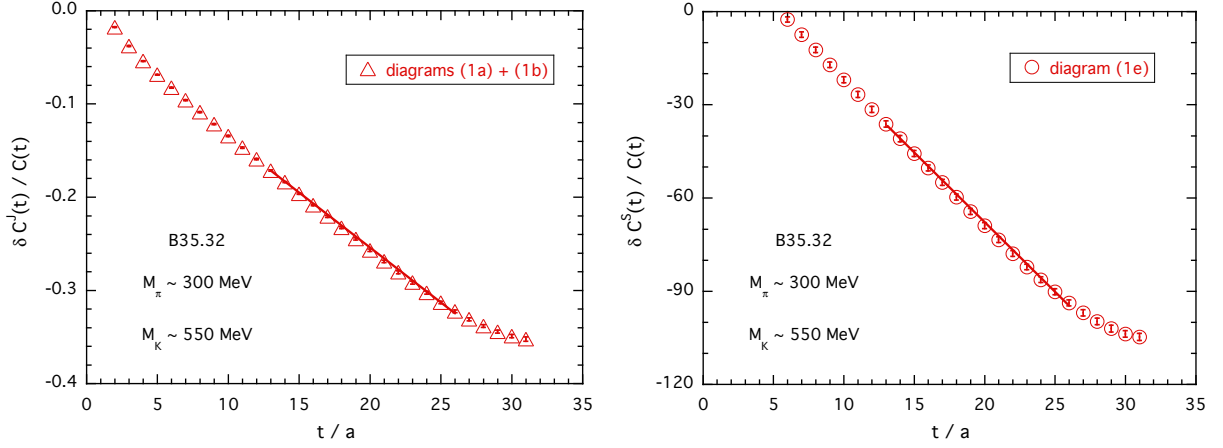

Figure 2.3.4: *Ratios $\delta C^J(t)/C(t)$ (left panel) and $\delta C^{S_\ell}(t)/C(t)$ (right panel) in the case of the charged kaon for the gauge ensemble B35.32. The solid lines represent the fit (2.28) applied in the time interval where the ground-state is dominant (see Table III).*

2.4 ANALYSIS OF THE PION MASS SPLITTING $M_{\pi^+} - M_{\pi^0}$

Given the observations made in the previous chapter, we now derive the leading isospin breaking corrections to pion masses by using the same technique employed to obtain the corrections to the quark propagator (see Sec. 1.7).
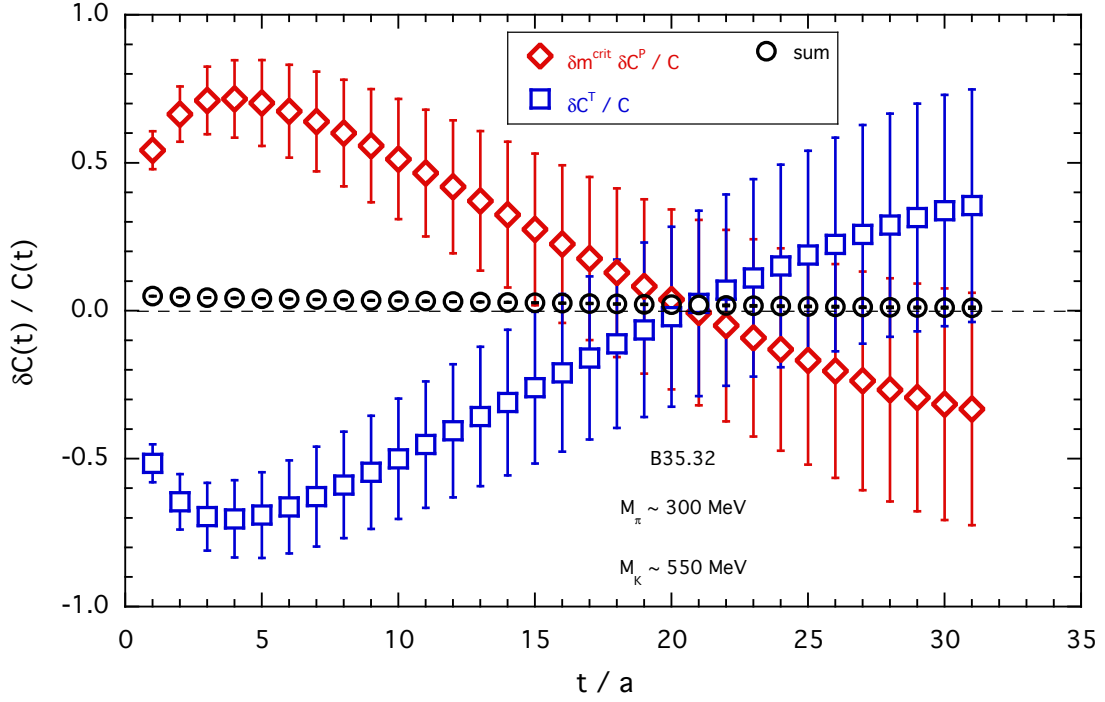
We get

$$(2.41)$$

Figure 2.3.5: *Ratios $\delta C^T(t)/C(t)$ and $\sum_f \delta m_f^{crit} \, \delta C^{P_f}(t)/C(t)$ in the case of the charged kaon for the gauge ensemble B35.32. Their sum, shown by the circles, is determined quite precisely.*

where $m_\ell = (m_d + m_u)/2$ is the renormalized isosymmetric light quark mass. In the case of the neutral pion we obtain

The sea quark propagators have been drawn in blue (and with a different line) and the isosymmetric vacuum polarization diagrams have not been displayed explicitly. By combin-

ing the previous expressions we find the elegant formula

$$M_{\pi^+} - M_{\pi^0} = \frac{(e_u - e_d)^2}{2} e^2 \partial_t \frac{\text{}}{\text{}} \, ,$$

(2.43)

where, following the notation of Ref. [9], $(-\partial_t)$ stands for the operator corresponding to the extraction of the slope δM_P from the ratio $\delta C(t)/C(t)$ (see Eq. (2.28)). All the isosymmetric vacuum polarization diagrams cancel by taking the difference of δM_{π^+} and δM_{π^0} together with the disconnected sea quark loop contributions explicitly shown in eqs. (2.41) and (2.42). Note, in particular, the cancellation of the corrections/counter–terms corresponding to the variation of the symmetric up–down quark mass and to the variation of the strong coupling constant $g_s^2 - (g_s^0)^2$. This is a general feature: at first order of the perturbative expansion in $\widehat{\alpha}_{em}$ and $\widehat{m}_d - \widehat{m}_u$, the isosymmetric corrections coming from the variation of the stong gauge coupling (the lattice spacing), of m_ℓ and of the heavier quark masses do not contribute to observables that vanish in the isosymmetric theory, like the mass splitting $M_{\pi^+} - M_{\pi^0}$. Furthermore, as already stressed, the electric charge does not need to be renormalized at this order and, for all these reasons, the expression for the pion mass splitting can be considered a "clean" theoretical prediction.

On the other hand, the lattice calculation of the disconnected diagram present in eq. (2.43) is a highly non trivial numerical problem and we shall neglect this contribution in this work. Relying on the flavor $SU(3)$ version of the Dashen's theorem, according to which, even in the presence of electromagnetic interactions, the neutral pion and the neutral kaons are non-singlet Goldstone's bosons, it can be shown that the neutral pion mass has to vanish in the limit $\widehat{m}_u = \widehat{m}_d = 0$ for arbitrary values of e_u, e_d as well as the masses $\widehat{m}_f$ and the electric charges e_f of the heavier quarks. This happens because the electric charge operator is diagonal in the up–down space and commutes with the isospin generator τ^3. Once the critical mass counter–terms $m_{u,d}^{crit} - m_0^{crit}$ have been properly tuned, the contributions to eq. (2.42) can be separated by the dependence with respect to e_u, e_d and e_f of the different coefficients. It follows that the disconnected diagram of eq. (2.43) vanishes in the $SU(2)$ chiral limit and, consequently, it is of $O(\widehat{\alpha}_{em}\widehat{m}_\ell)$. Neglecting this $O(\widehat{\alpha}_{em}\widehat{m}_\ell)$ diagram we are thus introducing a small systematic error that, from the phenomenological point of view, can be considered of the same order of magnitude of the other $O(\widehat{\alpha}_{em}[\widehat{m}_d - \widehat{m}_u])$ contributions neglected in this paper.

Disregarding the disconnected diagram in the r.h.s. of Eq. (2.43), the results for $M_{\pi^+}^2 - M_{\pi^0}^2 = 2M_\pi (M_{\pi^+} - M_{\pi^0})$ are shown in Fig. 2.4.1 for the ETMC gauge ensembles of Table I as a function of the renormalized light-quark mass.

Putting a massless photon in a finite box yields sizeable finite volume effects (FVEs), which have been investigated in Ref. [54], using QED$_L$ for the infrared regularization, and for other choices of the zero-mode subtraction in Ref. [17]. The main outcome discussed in Sec. 1.9 is that FVEs on hadron masses start at order $O(1/L)$ and they are *universal* up to order $O(1/L^2)$, i.e. they depend only on the charge of the hadron and not on its structure.
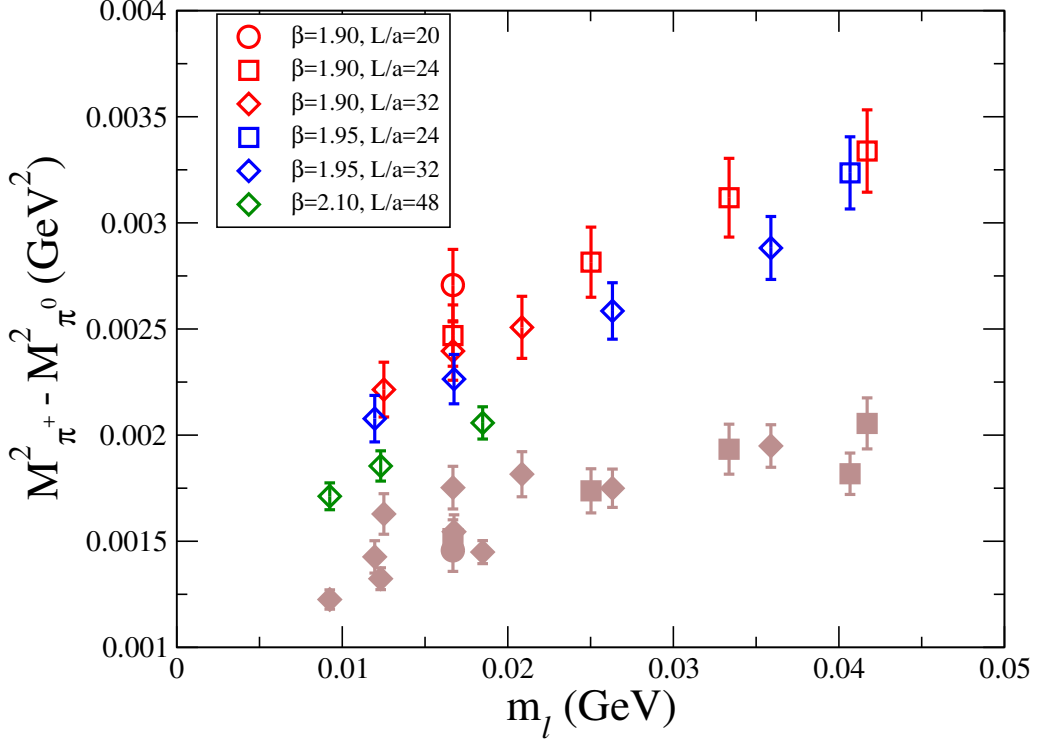
Figure 2.4.1: *Results for the pion mass splitting $M_{\pi^+}^2 - M_{\pi^0}^2$ versus the renormalized light-quark mass m_ℓ, obtained using Eq. (2.43) and neglecting the contribution coming from the disconnected diagram. Brown full points correspond to the data without any correction for FVEs, while open markers represent the lattice data subtracted by the universal FVEs given by Eq. (2.44).*

In the case of QED_L the universal FVEs are given by (see Eq. (1.82))

$$M_{PQ}^2(L) - M_{PQ}^2(\infty) = -Q^2 \alpha_{em} \frac{\kappa}{L^2} (2 + M_P L) \tag{2.44}$$

where $\kappa = 2.837297$ [54]. The universal FVEs are thus present only for the charged pion. The effect of their subtraction from our lattice data is shown in Fig. 2.4.1 by the open markers. It can be clearly seen that the correction is quite large, approaching $\simeq 40\%$ at the heaviest light-quark masses. In Fig. 2.4.2 the data corresponding to the gauge ensembles A40.20, A40.24 and A40.32, which share a common value of the pion mass and the lattice spacing, but differ for the lattice size L, are shown. The presence of residual FVEs after the subtraction of the universal ones is visible, but its impact does not exceed few percent at the largest lattice sizes. According to the non-relativistic expansion of Ref. [50], the structure-dependent (SD) FVEs are expected to be proportional at order $O(1/L^3)$ to the squared pion charge radius $\langle r^2 \rangle_{\pi^+}$, namely

$$\left[M_{\pi^+}^2(L) - M_{\pi^0}^2(L) \right]^{(SD)} = F \frac{4\pi\alpha_{em}}{3} \frac{M_\pi}{L^3} \langle r^2 \rangle_{\pi^+} + O(\frac{1}{L^4}, \frac{M_\pi}{L^4}), \tag{2.45}$$

where at the physical pion mass $\langle r^2 \rangle_{\pi^+} = (0.672 \pm 0.008 \text{ fm})^2$ [3]. In Eq. (2.45) we have included the multiplicative factor F to account for possible deviations from the theoretical
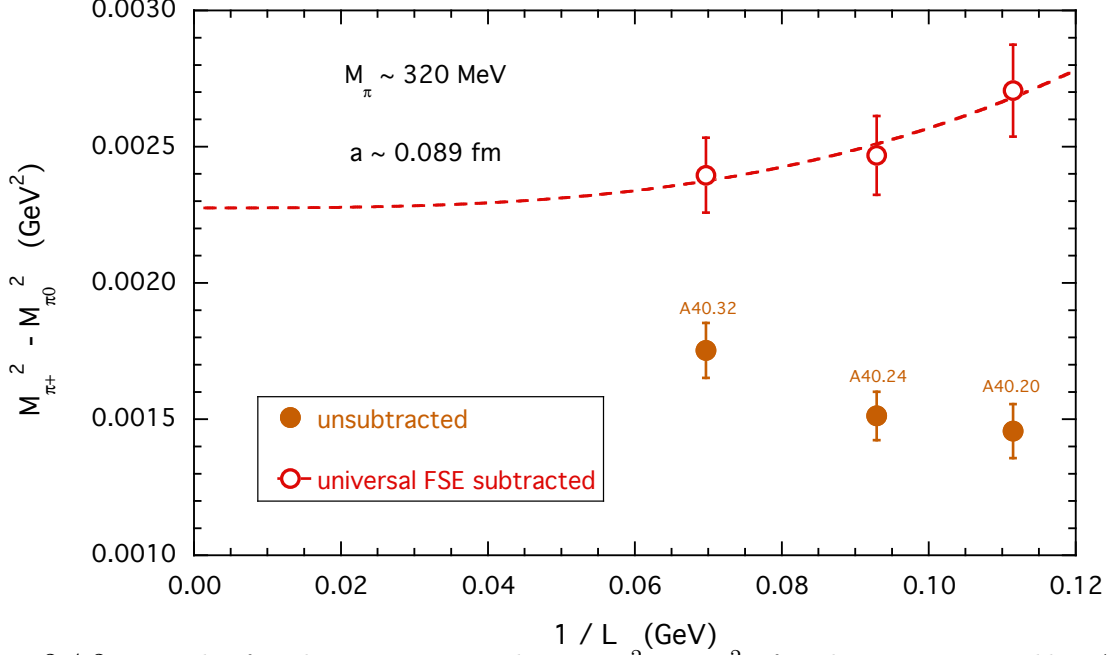
Figure 2.4.2: *Results for the pion mass splitting $M_{\pi^+}^2 - M_{\pi^0}^2$ for the gauge ensembles A40.20, A40.24 and A40.32, which share a common value of the pion mass and the lattice spacing, but differ for the lattice size L. The brown full points correspond to the data without any correction for FVEs, while the open dots represent the lattice data corrected by the universal FVEs given by Eq. (2.44). The dotted line corresponds to the result of a simple linear fit in $1/L^3$ (see Eq. (2.45)).*

expectation. The lattice data can be fitted by Eq. (2.45) with $F = 2.9 \pm 0.3$, as shown by the dashed line in Fig. 2.4.2. This highlights a significative deviation of the observed residual SD FVEs from the non-relativistic result.

From now on we always refer to the data for $M_{\pi^+}^2 - M_{\pi^0}^2$ as to the charged/neutral pion mass splitting subtracted by the universal FVEs (2.44).

Inspired by the Chiral Perturbation Theory (ChPT) analysis of Ref. [54], we have performed combined extrapolations to the physical pion mass and to the continuum and infinite volume limits adopting the following fitting function

$$
\begin{aligned}
M_{\pi^+}^2 - M_{\pi^0}^2 &= 4\pi\alpha_{em}f_0^2 \left\{ 4\frac{C}{f_0^4} - \left(3 + 16\frac{C}{f_0^4}\right) \frac{\overline{M}^2}{16\pi^2 f_0^2} \log\left(\frac{\overline{M}^2}{16\pi^2 f_0^2}\right) \right. \\
&+ \left. A_1^\pi \frac{\overline{M}^2}{16\pi^2 f_0^2} + A_2^\pi \frac{\overline{M}^4}{(4\pi f_0)^4} \right\} + D^\pi a^2 + D_m^\pi a^2 m_\ell \\
&+ \frac{4\pi\alpha_{em}}{3} \frac{M_\pi}{L^3} \langle r^2 \rangle_{\pi^+} + F^\pi a^2 \frac{M_\pi}{L^3}
\end{aligned}
\tag{2.46}
$$

where $\overline{M}^2 \equiv 2B_0 m_\ell$, B_0 and f_0 are the QCD low-energy constants (LECs) at leading order (LO), C is the e.m. LEC at LO, A_1^π is a combination of the e.m. LECs at order $O(\alpha_{em}m_\ell)$ (at a ChPT renormalization scale equal to $4\pi f_0$), A_2^π is an effective NNLO LEC, D^π and

D_m^π are fitting parameters that take into account discretization effects. In Eq. (2.46) the SD FVEs are represented by the last two terms in its r.h.s.: the first one is directly given by the non-relativistic result of Ref. [50], while the second term, expected from the FVEs related to a heavy intermediate state with mass $\propto 1/a$ [70], is added as a correction with a fitting multiplicative parameter F^π.

In Fig. 2.4.3 the results obtained using the combined fitting function (2.46) assuming $A_2^\pi = 0$ are shown, i.e. with C, A_1^π, D^π, D_m^π and F^π being free parameters.
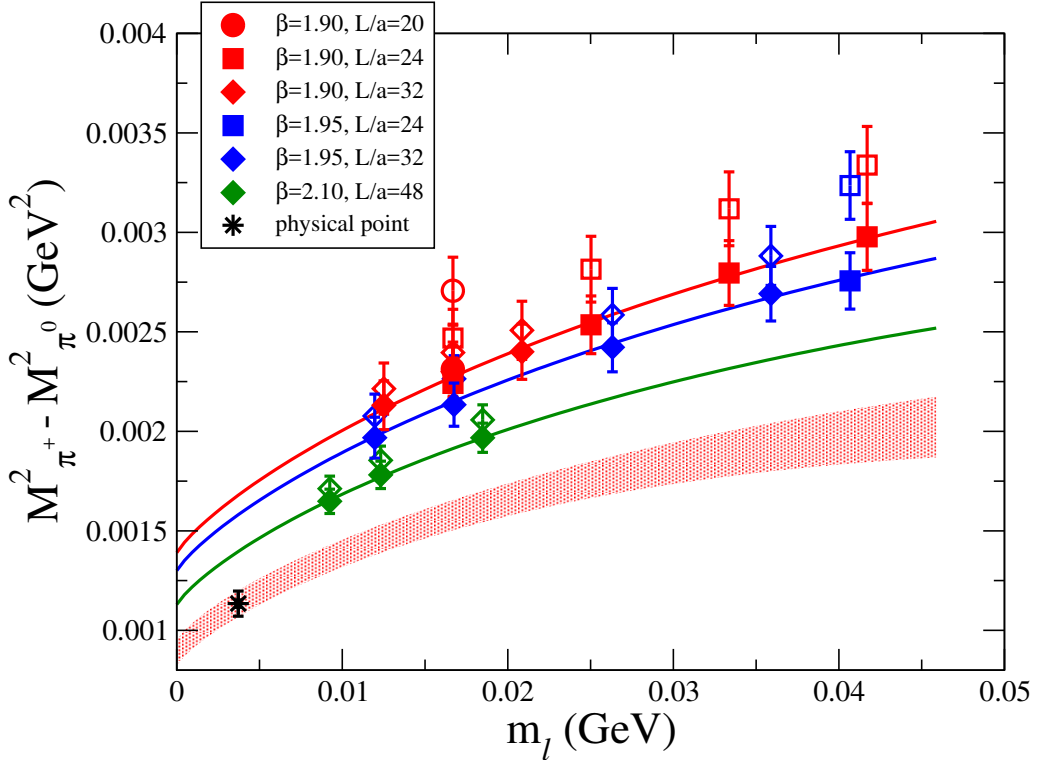

Figure 2.4.3: *Results for the pion mass splitting $M_{\pi^+}^2 - M_{\pi^0}^2$ versus the renomalized light-quark mass m_ℓ. The empty markers correspond to the data after the subtraction of the universal FVEs, while the filled markers represent the lattice data corrected also by the SD FVEs obtained in the fitting procedure (2.46). The solid lines correspond to the results of the combined fit (2.46) assuming $A_2^\pi = 0$ obtained in the infinite volume limit at each value of the lattice spacing. The black asterisk represents the pion mass splitting extrapolated at the physical pion mass (corresponding to $m_\ell = m_{ud} = 3.70(17)$ MeV) and to the continuum limit, while the red area indicates the corresponding uncertainty as a function of m_ℓ at the level of one standard deviation.*

As for the lattice spacing a and the renormalization constants Z_P, their uncertainties (see Table II) are taken into account as follows. First, we have randomly generated the values a^i and Z_P^i for the bootstrap event i assuming gaussian distributions corresponding to the central values and the standard deviations of Table II. Then, we add to the definition of the

χ^2 variable the following contribution

$$\sum_\beta \frac{\left(\overline{a}^i - a^i\right)^2}{\sigma_a^2} + \sum_\beta \frac{\left(\overline{Z}_P^i - Z_P^i\right)^2}{\sigma_{Z_P}^2} \ , \tag{2.47}$$

where $\overline{a}^i$ and $\overline{Z}_P^i$ are free parameters of the fitting procedure. The use of Eq. (2.47) allows the quantities a and Z_P to slightly change from their central values (in the given bootstrap event) with a weight in the χ^2 given by their uncertainties. This procedure corresponds to impose a gaussian prior for a and Z_P.

At the physical pion mass and in the continuum and infinite volume limits our result is

$$\begin{aligned}
M_{\pi^+}^2 - M_{\pi^0}^2 &= 1.137 \ (63)_{stat+fit} \ (24)_{disc} \ (22)_{chir} \ (10)_{FVE} \cdot 10^{-3} \ \text{GeV}^2 \ , \\
&= 1.137 \ (63)_{stat+fit} \ (34)_{syst} \cdot 10^{-3} \ \text{GeV}^2 \ , \\
&= 1.137 \ (72) \cdot 10^{-3} \ \text{GeV}^2 \ , \tag{2.48}
\end{aligned}$$

where

- $()_{stat+fit}$ indicates the statistical uncertainty including also the ones induced by the fitting procedure and by the errors of the input parameters of Table II, namely the values of the average u/d quark mass m_{ud}, the lattice spacing and the quark mass RC $1/Z_P$.

- $()_{disc}$ is the uncertainty due to discretization effects estimated by comparing the results obtained either including or excluding the $D_m^\pi a^2 m_\ell$ term in Eq. (2.46);

- $()_{chir}$ is the error coming from including $(A_2^\pi \neq 0)$ or excluding $(A_2^\pi = 0)$ the term proportional to m_ℓ^2 in Eq. (2.46);

- $()_{FVE}$ is the uncertainty due to FVEs estimated by comparing the results obtained including or excluding the two SD terms in Eq. (2.46). In the latter case only the ensembles with $L/a = 32, \ 48$ have been included in the fit.

Our result (2.48) implies

$$\begin{aligned}
M_{\pi^+} - M_{\pi^0} &= 4.21 \ (23)_{stat+fit} \ (13)_{syst} \ \text{MeV} \ , \\
&= 4.21 \ (26) \ \text{MeV} \ , \tag{2.49}
\end{aligned}$$

which agrees with the experimental determination

$$[M_{\pi^+} - M_{\pi^0}]^{exp} = 4.5936 \ (5) \ \text{MeV} \tag{2.50}$$

within ≈ 1.5 standard deviations. The difference among the central values, which is equal to $\approx 8\%$, may be of statistical origin, but it may be due also to the disconnected contribution at order $O(\alpha_{em} m_\ell)$ in Eq. (2.43) as well as to possible higher-order effects proportional to $\alpha_{em}(\widehat{m}_d - \widehat{m}_u)$ and to $(\widehat{m}_d - \widehat{m}_u)^2$, which have been neglected. The latter ones are estimated to be of the order of $\simeq 4\%$ in Ref. [4] and therefore the disconnected contribution at order $O(\alpha_{em} m_\ell)$ is expected to be of the same size $\approx 4\%$, which corresponds to ≈ 0.2 MeV.

2.5 DETERMINATION OF ϵ_{π^0}

The Dashen's theorem [6] states that in the chiral limit the self-energies of the neutral Nambu-Goldstone bosons vanish. Thus, the violation of the Dashen's theorem in the pion sector can be measured through the quantity ϵ_{π^0} defined as [4]

$$\epsilon_{\pi^0} = \frac{\left[\delta M_{\pi^0}^2\right]^{QED}}{M_{\pi^+}^2 - M_{\pi^0}^2} \ . \tag{2.51}$$

In our analysis the e.m. contribution $\left[\delta M_{\pi^0}^2\right]^{QED}$ is computed in the quenched QED approximation and neglecting also the disconnected diagram of Eq. (2.42), namely

$$\left[\delta M_{\pi^0}^2\right]^{QED} = 8\pi\alpha_{em}M_\pi\left[\delta M_{\pi^0}\right]^{em} \ , \tag{2.52}$$

where (see Eq. (2.42))

$$\tag{2.53}$$

The lattice data for $\left[\delta M_{\pi^0}^2\right]^{QED}$ are shown by filled markers in Fig. 2.5.1. It can be seen that the data exhibit an almost linear behavior as a function of the light-quark mass m_ℓ without any significant FVEs. Thus for the combined chiral and continuum limit extrapolations we use the following simple Ansatz

$$\left[\delta M_{\pi^0}^2\right]^{QED} = \widetilde{A}_1^\pi \frac{\overline{M}^2}{16\pi^2 f_0^2}\left(1 + \widetilde{A}_2^\pi \frac{\overline{M}^2}{16\pi^2 f_0^2}\right) + \widetilde{D}^\pi a^2 + \widetilde{D}_m^\pi a^2 m_\ell, \tag{2.54}$$

where $\overline{M}^2 \equiv 2B_0 m_\ell$ and $\widetilde{A}_1^\pi$, $\widetilde{A}_2^\pi$, $\widetilde{D}^\pi$ and $\widetilde{D}_m^\pi$ are free parameters. The results of the fitting procedure assuming $\widetilde{A}_2^\pi = 0$ are shown in Fig. 2.5.1 by the solid lines at each value of the lattice spacing and by the black asterisk at the physical pion mass and in the continuum limit.

At the physical pion mass and in the continuum limit we obtain

$$\begin{aligned}
\left[\delta M_{\pi^0}^2\right]^{QED} &= 0.008\,(4)_{stat+fit}\,(4)_{chir}\,(3)_{disc}\,(50)_{qQED} \cdot 10^{-3}\,\text{GeV}^2 \ , \\
&= 0.008\,(4)_{stat+fit}\,(5)_{syst}\,(50)_{qQED} \cdot 10^{-3}\,\text{GeV}^2 \ , \\
&= 0.008\,(50) \cdot 10^{-3}\,\text{GeV}^2 \ , \tag{2.55}
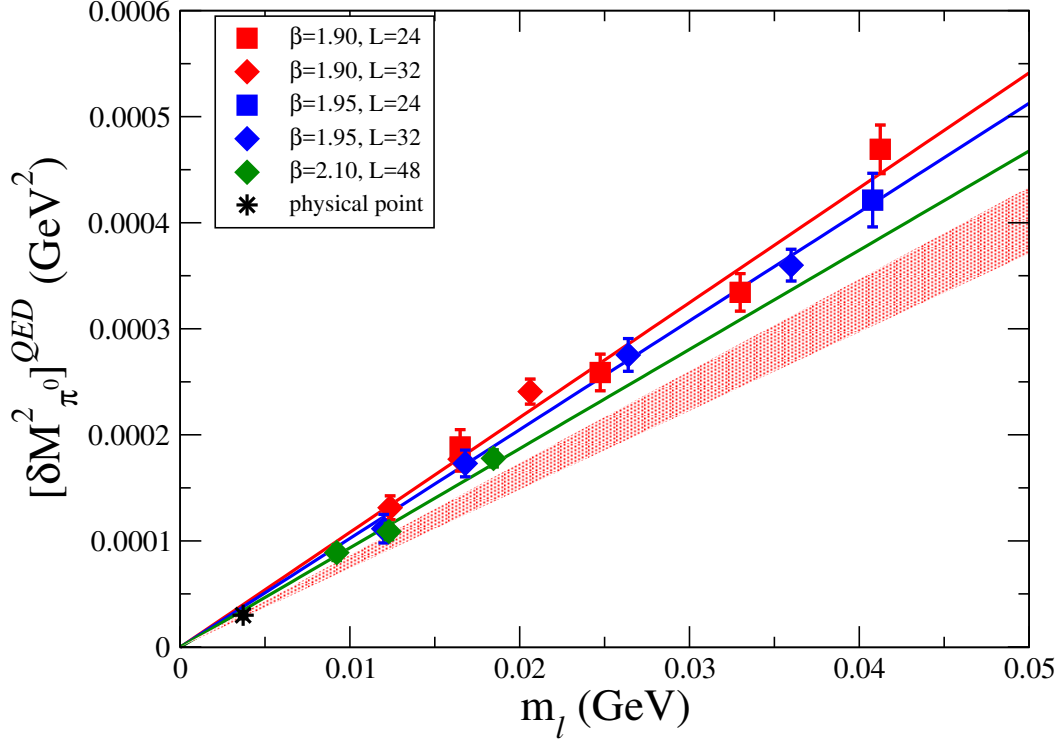\end{aligned}$$

where

Figure 2.5.1: *Results for the quantity $\left[\delta M_{\pi^0}^2\right]^{QED}$ versus the renomalized light-quark mass m_ℓ. The filled markers represent the lattice data without FVE corrections. The solid lines correspond to the results of the combined fit (2.54) assuming $\widetilde{A}_2^\pi = 0$ obtained at each value of the lattice spacing. The black asterisk represents the value extrapolated at the physical pion mass $m_\ell = m_{ud} = 3.70(17)$ MeV and to the continuum limit, while the red area indicates the corresponding uncertainty as a function of m_ℓ at the level of one standard deviation.*

- $()_{stat+fit}$ indicates the statistical uncertainty including also the ones induced by the fitting procedure and by the determination of the input parameters of Table II;

- $()_{chir}$ is the error coming from including ($\widetilde{A}_2^\pi \neq 0$) or excluding ($\widetilde{A}_2^\pi = 0$) the quadratic term;

- $()_{disc}$ is the uncertainty due to discretization effects estimated by comparing the results obtained including both the $\widetilde{D}^\pi a^2$ and $\widetilde{D}_m^\pi a^2 m_\ell$ terms in Eq. (2.54) or excluding one out of them.

- $()_{qQED}$ comes from our estimate of the neglect of the neutral pion, disconnected diagram ($0.05 \cdot 10^{-3}$ GeV^2), which dominates over all other uncertainties.

Using the experimental value $M_{\pi^0} = 134.98$ MeV [3] our result (2.55) corresponds to a pion mass in pure QCD equal to $M_\pi = 135.0(2)$ MeV in agreement with the FLAG estimate $M_\pi = 134.8(3)$ MeV.

Dividing our result (2.55) by Eq. (2.48), we obtain

$$\epsilon_{\pi^0} = 0.01 \ (4) \ ,$$

which is consistent with the FLAG estimate $\epsilon_{\pi^0} = 0.07(7)$ [4], based on the old determination of Ref. [23] (corrected by FLAG into the value $\epsilon_{\pi^0} = 0.10(7)$) and on the more recent result $\epsilon_{\pi^0} = 0.03(2)$ obtained by the QCDSF/UKQCD collaboration [71].

2.6 ANALYSIS OF ϵ_γ AND DETERMINATION OF $m_d - m_u$

The Dashen's theorem predicts that in the chiral limit the e.m. corrections to the charged kaon and pion are equal to each other, while the ones for the neutral mesons are vanishing. Therefore, in the kaon sector the violation of the Dashen's theorem is parameterized in terms of the quantity ϵ_γ defined as [4]

$$\epsilon_\gamma(\overline{\text{MS}}, \mu) = \frac{\left[M_{K^+}^2 - M_{K^0}^2\right]^{QED} (\overline{\text{MS}}, \mu)}{M_{\pi^+}^2 - M_{\pi^0}^2} - 1 \ , \tag{2.56}$$

where $\left[M_{K^+}^2 - M_{K^0}^2\right]^{QED} (\overline{\text{MS}}, \mu)$ is the QED contribution to the kaon mass splitting. Within the quenched QED approximation one has

$$\left[M_{K^+}^2 - M_{K^0}^2\right]^{QED} = 8\pi\alpha_{em} M_K \left[M_{K^+} - M_{K^0}\right]^{em} \ , \tag{2.57}$$

where

$$\tag{2.58}$$

with the red lines representing the strange quark propagator.

The results for $\left[M_{K^+}^2 - M_{K^0}^2\right]^{QED}$ are shown in Fig. 2.6.1 with and without the subtraction of the universal FVEs, given by Eq. (2.44). It can be clearly seen that, as in the case of the pion mass splitting, the universal FVE correction is quite large, approaching $\simeq 40\%$ at the heaviest light-quark masses.

From now on we always refer to the data for $\left[M_{K^+}^2 - M_{K^0}^2\right]^{QED}$ as to the QED part of the charged/neutral kaon mass splitting subtracted by the universal FVEs.
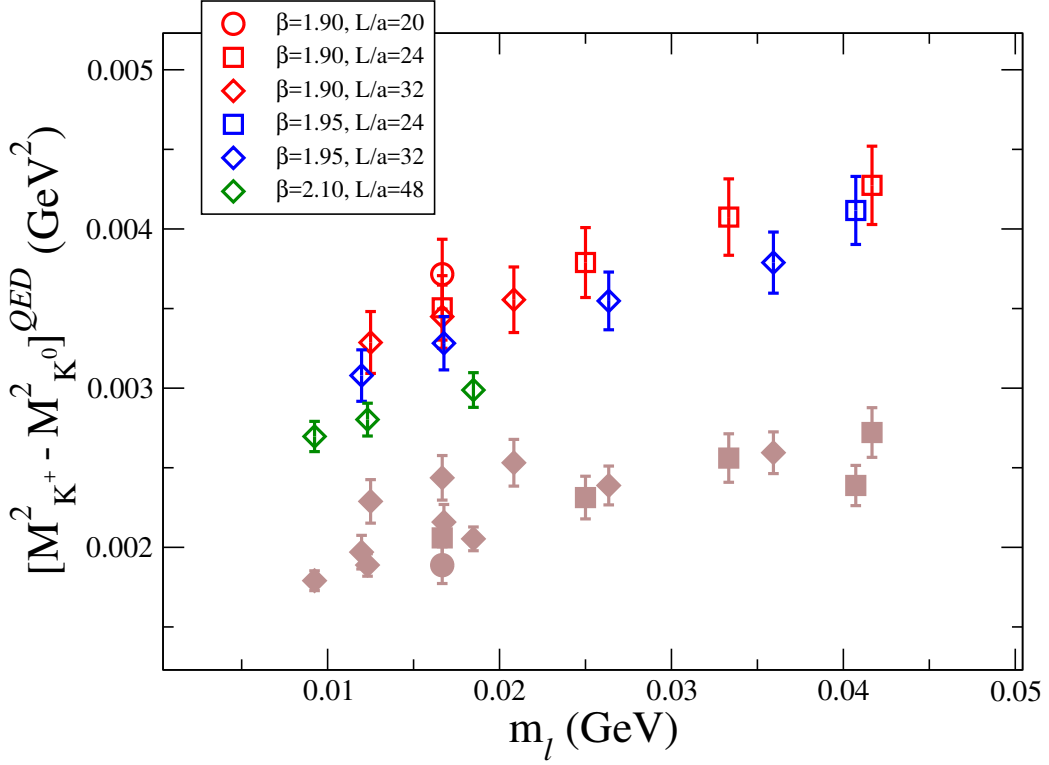
Figure 2.6.1: *Results for the kaon mass splitting $\left[M^2_{K^+} - M^2_{K^0}\right]^{QED}$ versus the renormalized light-quark mass m_ℓ, obtained using Eq. (2.58) in the quenched QED approximation. Brown full points correspond to the data without any correction for FVEs, while open markers represent the lattice data corrected by the universal FVEs given by Eq. (2.44).*

Inspired by the ChPT analysis of Ref. [54] we have performed combined extrapolations to the physical pion mass and to the continuum and infinite volume limits adopting the following fitting function

$$
\begin{aligned}
\left[M^2_{K^+} - M^2_{K^0}\right]^{QED} & = 16\pi\alpha_{em}\frac{C}{f_0^2}\left[A_0^K - \frac{8}{3}\frac{\overline{M}^2}{16\pi^2 f_0^2}\log\left(\frac{\overline{M}^2}{16\pi^2 f_0^2}\right)\right. \\
& + \left. A_1^K\frac{\overline{M}^2}{16\pi^2 f_0^2} + A_2^K\frac{\overline{M}^4}{(4\pi f_0)^4}\right] + D^K a^2 + D_m^K a^2 m_\ell \\
& + \frac{4\pi\alpha_{em}}{3}\frac{M_K}{L^3}\langle r^2\rangle_{K^+} + F^K a^2\frac{M_K}{L^3} ,
\end{aligned}
\tag{2.59}
$$

where the residual SD FVEs are estimated using two terms similar to the ones appearing in Eq. (2.46) and with $\langle r^2\rangle_{K^+} = (0.560 \pm 0.031 \text{ fm})^2$ [3]. The free parameters to be determined by the fitting procedure are A_0^K, A_1^K, A_2^K, D^K, D_m^K and F^K, while the LEC C is taken from the analysis of the pion mass splitting. In Fig. 2.6.2 we show the results obtained using the combined fitting function (2.59) assuming $A_2^K = 0$. As in the case of the pion mass splitting we obtain a value for the parameter F^K significantly different from zero, which confirms the

presence of a deviation from the non-relativistic expansion prediction of Ref. [50].
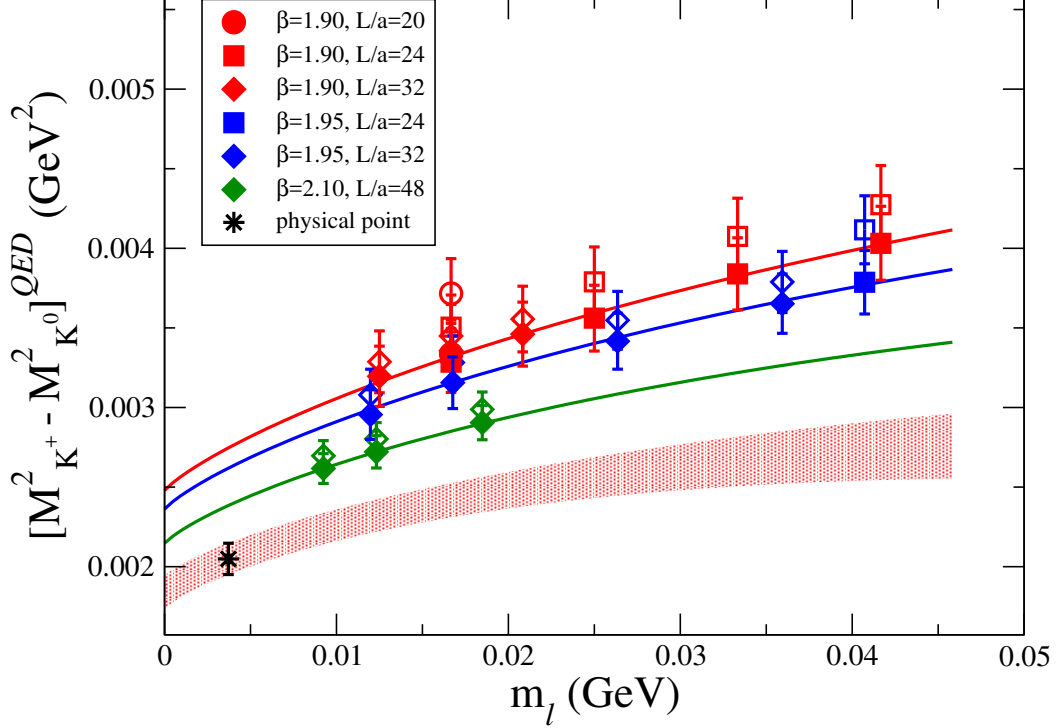

Figure 2.6.2: *Results for the kaon mass splitting $\left[M_{K^+}^2 - M_{K^0}^2\right]^{QED}$ versus the renormalized light-quark mass m_ℓ in the $\overline{MS}$ scheme at a renormalization scale equal to $\mu = 2$ GeV. The empty markers correspond to the data after the subtraction of the universal FVEs, while the filled markers represent the lattice data corrected also by the SD FVEs obtained in the fitting procedure (2.59). The solid lines correspond to the results of the combined fit (2.59) assuming $A_2^K = 0$ obtained in the infinite volume limit at each value of the lattice spacing. The black asterisk represents the kaon mass splitting extrapolated at the physical pion mass $m_\ell = m_{ud} = 3.70(17)$ MeV and to the continuum limit, while the red area indicates the corresponding uncertainty as a function of m_ℓ at the level of one standard deviation.*

At the physical pion mass and in the continuum and infinite volume limits our result in the $\overline{MS}$ scheme at a renormalization scale equal to $\mu = 2$ GeV is

$$
\begin{aligned}
\left[M_{K^+}^2 - M_{K^0}^2\right]^{QED} &= 2.047 \ (99)_{stat+fit} \ (43)_{disc} \ (23)_{chir} \ (3)_{FVE} \ (102)_{qQED} \cdot 10^{-3} \ \text{GeV}^2 \ , \\
&= 2.047 \ (99)_{stat+fit} \ (49)_{syst} \ (102)_{qQED} \cdot 10^{-3} \ \text{GeV}^2 \ , \\
&= 2.047 \ (150) \cdot 10^{-3} \ \text{GeV}^2 \ ,
\end{aligned}
\tag{2.60}
$$

where

- $()_{stat+fit}$ indicates the statistical uncertainty including also the ones induced by the fitting procedure and by the determination of the input parameters of Table II;

- $()_{disc}$ is the uncertainty due to discretization effects estimated by comparing the results assuming either $D^K \neq 0$ or $D_m^K = 0$ in Eq. (2.59);

- $()_{chir}$ is the error coming from including ($A_2^K \neq 0$) or excluding ($A_2^K = 0$) the term proportional to m_ℓ^2;

- $()_{FVE}$ is the uncertainty due to FVE estimated by comparing the results obtained including or excluding the two phenomenological terms (2.59) for the SD FVEs. In the latter case only the ensembles with $L/a = 32$, 48 are considered.

- $()_{qQED}$ is the estimate of the effects due to the quenched QED approximation (5%) taken from Refs. [33, 62].

Recent results available in the literature for $\left[M_{K^+}^2 - M_{K^0}^2\right]^{QED}$ are: $2.075(395) \cdot 10^{-3}$ GeV^2, obtained using the FLAG inputs [4], $2.186(231) \cdot 10^{-3}$ GeV^2 from the BMW collaboration [62] at $N_f = 2 + 1$, and $2.38(38) \cdot 10^{-3}$ GeV^2 from the latest update of the dispersive analysis of the $\eta \to 3\pi$ decays [72]. Note that in Ref. [62] a "hadronic" scheme is adopted in which the quark mass difference $(\widehat{m}_d - \widehat{m}_u)$ is replaced by the mass difference of the "connected" $\bar{u}u$ and $\bar{d}d$ mesons. Using our results of Sec. 2.5 the conversion from the hadronic BMW scheme to the $(\overline{\mathrm{MS}}, 2\ \mathrm{GeV})$ one amounts to add $0.018(3) \cdot 10^{-3}$ GeV^2 to the result of Ref. [62], leading to $\left[M_{K^+}^2 - M_{K^0}^2\right]^{QED} (\overline{\mathrm{MS}}, 2\ \mathrm{GeV}) = 2.204(231) \cdot 10^{-3}$ GeV^2. For the other results either the prescription used for evaluating the QED contribution is not clearly defined or the conversion to the $(\overline{\mathrm{MS}}, 2\ \mathrm{GeV})$ scheme is not known precisely.

Using Eqs. (2.48) and (2.60) our estimate for ϵ_γ is

$$
\begin{aligned}
\epsilon_\gamma(\overline{\mathrm{MS}}, 2\ \mathrm{GeV}) &= 0.801\ (48)_{stat+fit}\ (8)_{disc}\ (16)_{chir}\ (18)_{FVE}\ (96)_{qQED}, \\
&= 0.801\ (48)_{stat+fit}\ (25)_{syst}\ (96)_{qQED}, \\
&= 0.801\ (110)\ ,
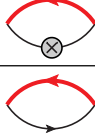\end{aligned}
\tag{2.61}
$$

where now the $()_{qQED}$ error includes also the 4% effect (added in quadrature) coming from the neglect of the neutral pion, disconnected diagram. Our result (2.61) is consistent with the recent result, converted in the $(\overline{\mathrm{MS}}, 2\ \mathrm{GeV})$ scheme, $\epsilon_\gamma(\overline{\mathrm{MS}}, 2\ \mathrm{GeV}) = 0.74(18)$ from the BMW collaboration [62] and larger than the recent QCDSF/UKQCD result $\epsilon_\gamma(\overline{\mathrm{MS}}, 2\ \mathrm{GeV}) = 0.50(6)$ [71] by $\simeq 2.4$ standard deviations. Note that in Ref. [71] the QED contributions to kaon masses are evaluated in the so-called Dashen scheme, which differs from the $(\overline{\mathrm{MS}}, 2\ \mathrm{GeV})$ one. The conversion between the two schemes is taken into account by a perturbative matching performed at leading order in α_{em} in Ref. [71].

Other results present in the literature are the FLAG estimate $\epsilon_\gamma = 0.7(3)$ [4] and the two recent findings $\epsilon_\gamma = 0.78(10)$ from the MILC collaboration [73] and $\epsilon_\gamma = 0.9(3)$ from the latest update of the dispersive analysis of the $\eta \to 3\pi$ decays [72]. For the above results either the prescription used for evaluating the QED contribution is not clearly defined or the conversion to the $(\overline{\mathrm{MS}}, 2\ \mathrm{GeV})$ scheme is not known precisely.

Using the experimental value for the charged/neutral kaon mass splitting, $M_{K^+}^2 - M_{K^0}^2 = -3.903(3) \cdot 10^{-3}$ GeV^2 [3], one gets

$$
\left[M_{K^+}^2 - M_{K^0}^2\right]^{SIB} (\overline{MS}, 2\ \mathrm{GeV}) = -5.950\ (150) \cdot 10^{-3}\ \mathrm{GeV}^2\ .
\tag{2.62}
$$

In order to estimate the light-quark mass difference $(\widehat{m}_d - \widehat{m}_u)$ from the result (2.62) we need to compute the *QCD isospin breaking slope* (see Eq. (2.22))

$$\left[M_{K^+}^2 - M_{K^0}^2\right]^{QIB} \equiv \frac{\left[M_{K^+}^2 - M_{K^0}^2\right]^{SIB}}{\widehat{m}_d - \widehat{m}_u} = -2M_K \, Z_P \, \partial_t \raisebox{-0.5em}{\includegraphics{diagram}} \ . \tag{2.63}$$

The lattice data for $\left[M_{K^+}^2 - M_{K^0}^2\right]^{QIB}$ have been fitted according to the following Ansatz:

$$\begin{aligned}
\left[M_{K^+}^2 - M_{K^0}^2\right]^{QIB} &= \overline{A}_0^K \left[1 - \frac{\overline{M}^2}{16\pi^2 f_0^2} \log\left(\frac{\overline{M}^2}{16\pi^2 f_0^2}\right) + \overline{A}_1^K \frac{\overline{M}^2}{16\pi^2 f_0^2}\right] \\
&+ \overline{D}^K a^2 + \overline{F}^K \frac{\overline{M}^2}{16\pi^2 f_0^2} \frac{e^{-\overline{M}L}}{(\overline{M}L)^{3/2}}
\end{aligned} \tag{2.64}$$

where the chiral extrapolation is based on the SU(3) ChPT formulae of Ref. [74] expanded as a power series in terms of the quantity m_ℓ/m_s, while FVEs are described by a phenomenological term inspired by the leading FVE correction in QCD to the pion and kaon masses in the p-regime ($\overline{M}L \gg 1$) [75].

The results of the fitting procedure (2.64), using $\overline{A}_0^K$, $\overline{A}_1^K$, $\overline{D}^K$ and $\overline{F}^K$ as free parameters, are shown in Fig. 2.6.3.

At the physical pion mass and in the continuum and infinite volume limits we get

$$\begin{aligned}
\left[M_{K^+}^2 - M_{K^0}^2\right]^{QIB} &= -2.51 \, (10)_{stat+fit} \, (15)_{disc} \, (1)_{chir} \, (1)_{FVE} \text{ GeV} \\
&= -2.51 \, (10)_{stat+fit} \, (15)_{syst} \text{ GeV} , \\
&= -2.51 \, (18) \text{ GeV} ,
\end{aligned} \tag{2.65}$$

where

- $()_{stat+fit}$ indicates the statistical uncertainty including also the ones induced by the fitting procedure and by the determination of the input parameters of Table II;

- $()_{disc}$ is the uncertainty due to discretization effects estimated by including ($\overline{D}^K \neq 0$) or excluding ($\overline{D}^K = 0$) the discretization term in Eq. (2.64);

- $()_{chir}$ is the error coming from including the term proportional to the chiral log in Eq. (2.64) or substituting it with a quadratic term in m_ℓ (i.e., $\overline{A}_2^K \overline{M}^4/(4\pi f_0)^4$);

- $()_{FVE}$ is the uncertainty obtained including ($\overline{F}^K \neq 0$) or excluding ($\overline{F}^K = 0$) the FVE term in Eq. (2.64).

Our $N_f = 2 + 1 + 1$ result (2.65) agrees with the corresponding BMW result, 2.53(7) GeV, obtained at $N_f = 2 + 1$ [62].
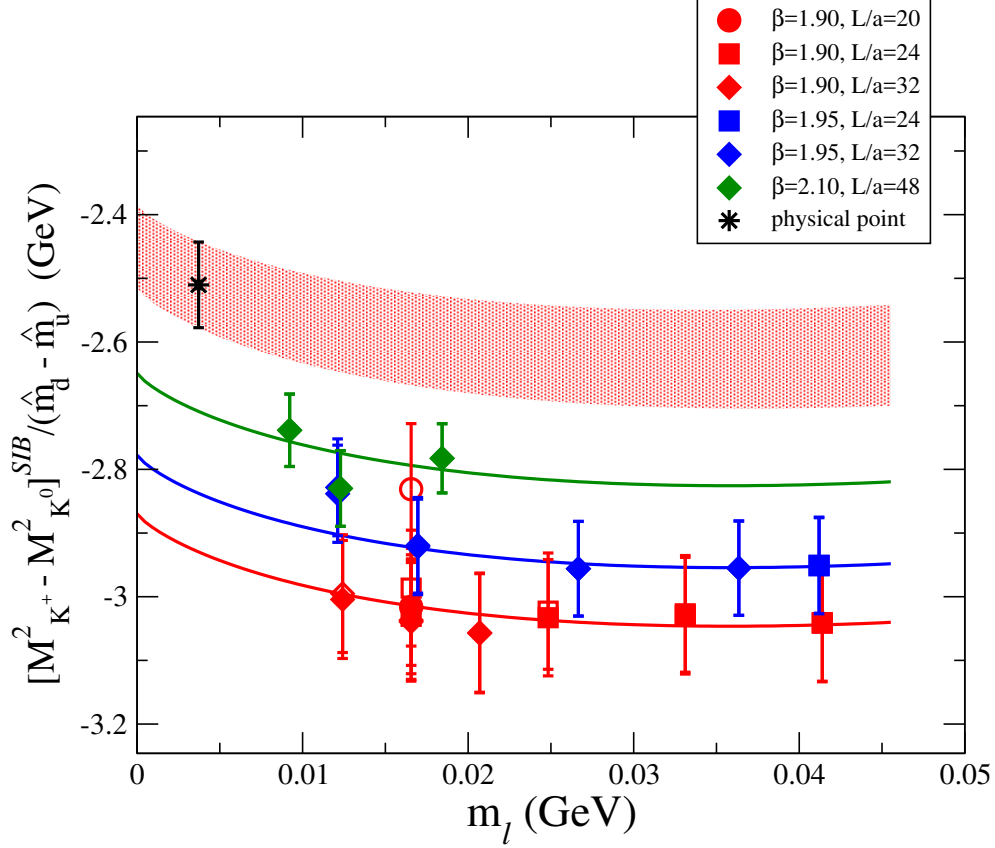
Figure 2.6.3: *Results for the QIB slope $\left[M_{K^+}^2 - M_{K^0}^2\right]^{QIB} = \left[M_{K^+}^2 - M_{K^0}^2\right]^{SIB}/(\widehat{m}_d - \widehat{m}_u)$ versus the renomalized light-quark mass m_ℓ. The empty markers correspond to the lattice data, while the filled ones represent the data corrected for the FVEs obtained in the fitting procedure (2.64). The solid lines correspond to the results of the combined fit (2.64) obtained in the infinite volume limit at each value of the lattice spacing. The black asterisk represents the QIB slope extrapolated at the physical pion mass $m_\ell = m_{ud} = 3.70(17)$ MeV and to the continuum limit, while the red area indicates the corresponding uncertainty as a function of m_ℓ at the level of one standard deviation.*

Putting together the results (2.62) and (2.65) with Eq. (2.22), we get

$$
\begin{aligned}
\left[\widehat{m}_d - \widehat{m}_u\right](\overline{MS}, 2 \text{ GeV}) &= 2.380 \; (87)_{stat+fit} \; (154)_{disc} \; (11)_{chir} \; (11)_{FVE} \; (41)_{qQED} \text{ MeV} , \\
&= 2.380 \; (87)_{stat+fit} \; (155)_{syst} \; (41)_{qQED} \text{ MeV} , \\
&= 2.380 \; (182) \text{ MeV} , \quad\quad\quad\quad\quad\quad\quad\quad\quad\quad (2.66)
\end{aligned}
$$

which is consistent with the previous ETMC determination 2.67(35) MeV [66] at $N_f = 2 + 1 + 1$ and with the recent BMW result, converted in the $(\overline{MS}, 2 \text{ GeV})$ scheme, 2.40(12) MeV [62] at $N_f = 2 + 1$.

Combining the result (2.66) with our ETMC determination of the average up/down quark mass $m_{ud}(\overline{MS}, 2 \text{ GeV}) = 3.70(17)$ MeV from Ref. [66], we can also compute the u-

and d-quark masses

$$\begin{aligned}
\widehat{m}_u(\overline{MS}, 2 \text{ GeV}) &= 2.50 \ (15)_{stat+fit} \ (8)_{syst} \ (2)_{qQED} \text{ MeV} , \\
&= 2.50 \ (17) \text{ MeV} , && (2.67) \\
\widehat{m}_d(\overline{MS}, 2 \text{ GeV}) &= 4.88 \ (18)_{stat+fit} \ (8)_{syst} \ (2)_{qQED} \text{ MeV} , \\
&= 4.88 \ (20) \text{ MeV} && (2.68)
\end{aligned}$$

and the ratio

$$\begin{aligned}
\frac{\widehat{m}_u}{\widehat{m}_d}(\overline{MS}, 2 \text{ GeV}) &= 0.513 \ (18)_{stat+fit} \ (24)_{syst} \ (6)_{qQED} , \\
&= 0.513 \ (30) , && (2.69)
\end{aligned}$$

which are consistent within the uncertainties with the current FLAG estimates [4] at $N_f = 2 + 1 + 1$, based on the ETMC results of Ref. [66], and with the recent BMW results [62] at $N_f = 2 + 1$.

Finally, using the ETMC result $m_s(\overline{MS}, 2 \text{ GeV}) = 99.6(4.3)$ MeV [66] we can obtain a determination of the flavor symmetry breaking parameters R and Q, namely

$$R(\overline{MS}, 2 \text{ GeV}) \equiv \frac{m_s - m_{ud}}{\widehat{m}_d - \widehat{m}_u}(\overline{MS}, 2 \text{ GeV}) = 40.4 \ (3.3) , \qquad (2.70)$$

$$Q(\overline{MS}, 2 \text{ GeV}) \equiv \sqrt{\frac{m_s^2 - m_{ud}^2}{\widehat{m}_d^2 - \widehat{m}_u^2}}(\overline{MS}, 2 \text{ GeV}) = 23.8 \ (1.1) , \qquad (2.71)$$

which are consistent within the errors with the current FLAG estimate $R = 35.6(5.1)$ and $Q = 22.2(1.6)$ [4] as well as with the recent BMW results $R = 38.20(1.95)$ and $Q = 23.40(64)$ [62].

Our central value (2.71) for the parameter Q is $\approx 8\%$ higher than the recent result of Ref. [72], $Q = 22.0(7)$, based on the latest update of the dispersive analysis of the $\eta \to 3\pi$ decay and on the use of the SU(3) ChPT relation

$$\left[M_{K^+}^2 - M_{K^0}^2\right]^{SIB} = \frac{1}{Q^2} \frac{M_K^2}{M_\pi^2} (M_\pi^2 - M_K^2) \left[1 + O(m_s^2)\right] . \qquad (2.72)$$

Had we used our result (2.62) in Eq. (2.72), the value of the parameter Q would have been $Q = 22.6 \ (3)$, which is $\approx 5\%$ below the result (2.71) based on the use of the QIB slope (2.65) evaluated directly on the lattice. This seems to suggest that the higher-order corrections to the SU(3) ChPT relation (2.72) may be at the level of $\approx 10\%$ or equivalently about one unit for Q (see also Ref. [76]).

We are here in position of evaluating the leading SIB corrections to the kaon decay constant. It is possible to extract this information by studying the ratio of the correlators

$$\frac{\delta C_K^{S_\ell}(t)}{C_K^{(0)}(t)} \equiv \frac{\text{}}{\text{}} , \qquad (2.73)$$

with the red line representing the strange quark propagator. The IB correction $\delta f_K/f_K$ can be computed by extracting the slope and intercept from the large time behavior of $\delta C_K^{S_\ell}(t)/C_K^{(0)}(t)$ (see Eq. (2.28)) according to

$$\frac{\delta f_K}{f_K} \equiv \frac{1}{\widehat{m}_d - \widehat{m}_u} \frac{[f_{K^+} - f_{K^0}]^{SIB}}{f_K} = \frac{1}{m_s + m_\ell} + \frac{\delta Z_K^{S_\ell}}{Z_K} - 2 \frac{\delta M_K^{S_\ell}}{M_K} \ , \qquad (2.74)$$

where f_K is given by $f_K = (m_s + m_\ell) \ Z_K/M_K^2$. The lattice data have been fitted according to the following ansatz:

$$\frac{\delta f_K}{f_K} = A + B \ \frac{\overline{M}^2}{16\pi^2 f_0^2} - \frac{3}{4m_s} \ \frac{\overline{M}^2}{16\pi^2 f_0^2} \log\left(\frac{\overline{M}^2}{16\pi^2 f_0^2}\right) + D \ a^2 + F \ \frac{\overline{M}^2}{16\pi^2 f_0^2} \frac{e^{-\overline{M}L}}{(\overline{M}L)^{3/2}} \ , \quad (2.75)$$

where $\overline{M}^2 \equiv 2B_0 m_\ell$, B_0, f_0 are the QCD low-energy constants at leading order and A, B, C, D, F are free parameters to be determined by the fitting procedure. In Eq. (2.75) the chiral extrapolation is based on the SU(3) ChPT formulae of Ref. [74] expanded as a power series in terms of the quantity m_ℓ/m_s, while FVEs are described by a phenomenological term inspired by the leading FVE correction in QCD kaon decay constant in the p-regime ($\overline{M}L \gg 1$) [75]. The results of the fitting procedure are shown in Fig. 2.6.4.

At the physical pion mass and in the continuum and infinite volume limits we obtain [36]

$$\delta f_K/f_K = -2.77 \ (16)_{stat+fit} \ (22)_{disc} \ (10)_{chir} \ (1)_{FVE} \ \text{GeV}^{-1} = -2.77 \ (29) \ \text{GeV}^{-1} \ , \quad (2.76)$$

where

- $()_{stat+fit}$ indicates the statistical uncertainty including also the one induced by the fitting procedure;

- $()_{disc}$ is the uncertainty due to discretization effects estimated by including or excluding the term proportional to a^2 in Eq. (2.75);

- $()_{chir}$ is the error coming from including the term proportional to the chiral log or substituting it with a quadratic term in m_ℓ and iv) $()_{FVE}$ is the uncertainty obtained including or excluding the FVE term in Eq. (2.75).

By using the determination of the light-quark mass difference (see Eq. (2.66)) and the result (2.76) we get the following estimate

$$\left[\frac{f_{K^+} - f_{K^0}}{f_K}\right]^{SIB} (\overline{\text{MS}}, 2 \ \text{GeV}) = -0.00656 \ (48)_{stat+fit} \ (9)_{disc} \ (22)_{chir} \ (6)_{FVE} \ (12)_{qQED} \ .$$
$$(2.77)$$

At order $O(\widehat{m}_d - \widehat{m}_u)$, thanks to the fact that pions don't get strong IB corrections, we have

$$\left[\frac{f_{K^+}/f_{\pi^+}}{f_K/f_\pi} - 1\right]^{SIB} (\overline{\text{MS}}, 2 \ \text{GeV}) = -0.00328 \ (28) \ , \qquad (2.78)$$
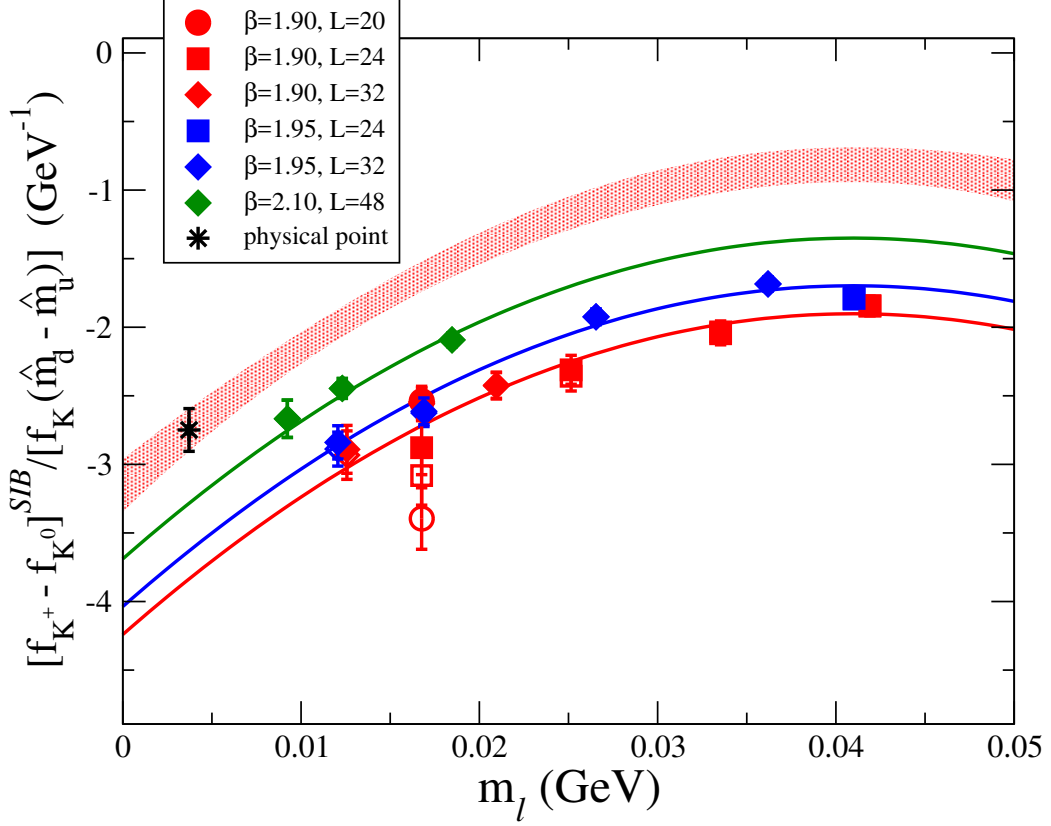
Figure 2.6.4: *Results for the IB correction $[f_{K^+} - f_{K^0}]^{SIB} / [f_K \, (\widehat{m}_d - \widehat{m}_u)]$ versus the renormalized light-quark mass m_ℓ. The empty markers correspond to the lattice data, while the filled ones represent the data corrected for the FVEs obtained in the fitting procedure (2.75). The solid lines correspond to the results of the combined fit (2.75) obtained in the infinite volume limit at each value of the lattice spacing. The black asterisk represents the result extrapolated at the physical pion mass $m_\ell = m_{ud} = 3.70(17)$ MeV and to the continuum limit, while the red area indicates the corresponding uncertainty as a function of m_ℓ at the level of one standard deviation.*

a value that is higher (by about 1.6 standard deviations) than the estimate obtained in Ref. [22] by using ChPT, namely

$$\left[\frac{f_{K^+}/f_{\pi^+}}{f_K/f_\pi} - 1 \right]^{\chi pt} = -0.0022 \ (6) \tag{2.79}$$

and in agreement with (and more precise than) our previous determination at $N_f = 2$ [9].

2.7 DETERMINATION OF ϵ_{K^0}

The violation of the Dashen's theorem for the neutral kaon mass can be represented by the quantity ϵ_{K^0} defined as [4]

$$\epsilon_{K^0} = \frac{\left[\delta M_{K^0}^2\right]^{QED}}{M_{\pi^+}^2 - M_{\pi^0}^2} \; . \tag{2.80}$$

The e.m. contribution $\left[\delta M_{K^0}^2\right]^{QED}$ is given within the quenched QED approximation by

$$\left[\delta M_{K^0}^2\right]^{QED} = 8\pi\alpha_{em} M_K \left[\delta M_{K^0}\right]^{em} , \tag{2.81}$$

where

$$
[\delta M_{K^0}]^{em} \;\;=\;\; e_d e_s \partial_t \frac{}{} - e_d^2 \partial_t \frac{}{}
$$

$$
-\;\; [\delta m_d^{crit}]\partial_t \frac{}{} + [\delta m_s^{crit}]\partial_t \frac{}{}
$$

$$
-\;\; e_s^2 \partial_t \frac{}{} + Z_P \mathcal{Z}^s m_s \partial_t \frac{}{}
$$

$$
+\;\; Z_P \mathcal{Z}^d m_\ell \partial_t \frac{}{} \; . \tag{2.82}
$$

The lattice data for $\left[\delta M_{K^0}^2\right]^{QED}$ are shown by filled markers in Fig. 2.7.1. No significant FVEs are visible and therefore for the combined chiral and continuum limit fitting procedure we use the following simple Ansatz

$$\left[\delta M_{K^0}^2\right]^{QED} = \widetilde{A}_0^K \left[1 + \widetilde{A}_L^K \frac{\overline{M}^2}{16\pi^2 f_0^2} \log\left(\frac{\overline{M}^2}{16\pi^2 f_0^2}\right) + \widetilde{A}_1^K \frac{\overline{M}^2}{16\pi^2 f_0^2} \right] + \widetilde{D}^K a^2 \; , \tag{2.83}$$

where $\widetilde{A}_0^K$, $\widetilde{A}_L^K$, $\widetilde{A}_1^K$ and $\widetilde{D}^K$ are free parameters. The results of the fitting procedure are shown in Fig. 2.5.1 by the solid lines at each value of the lattice spacing and by the black asterisk at the physical pion mass and in the continuum limit.
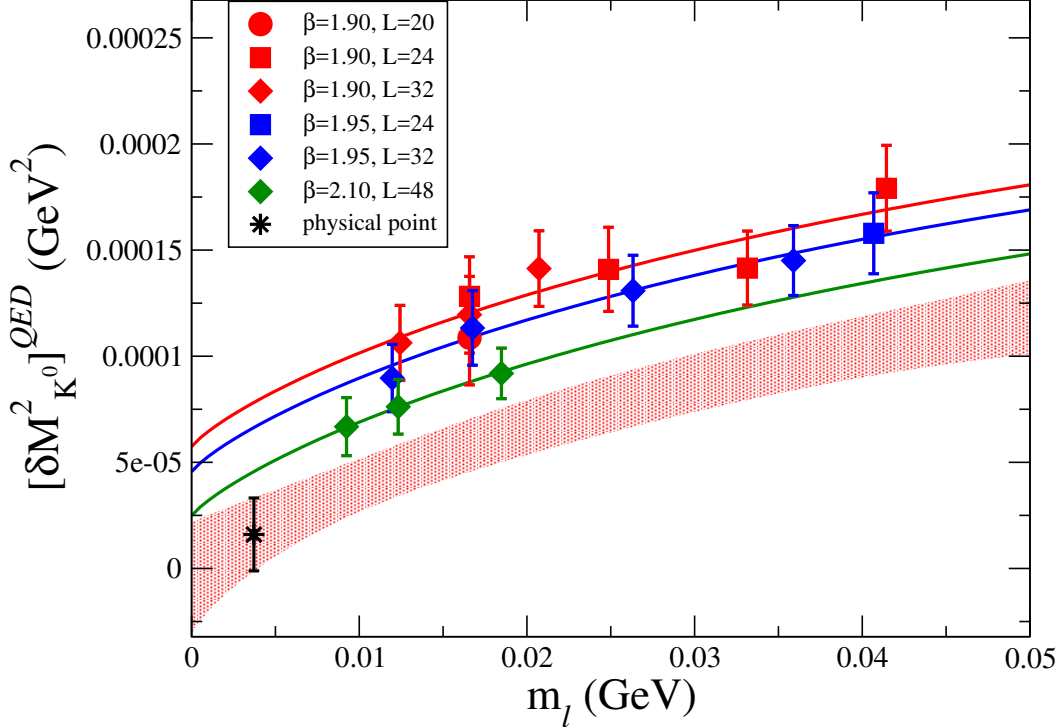
Figure 2.7.1: *Results for the quantity* $\left[\delta M_{K^0}^2\right]^{QED}$ *versus the renormalized light-quark mass* m_ℓ. *The filled markers represent the lattice data without FVE corrections. The solid lines correspond to the results of the combined fit (2.83) obtained at each value of the lattice spacing. The black asterisk represents the value extrapolated at the physical pion mass* $m_\ell = m_{ud} = 3.70(17)$ *MeV and to the continuum limit, while the red area identifies the corresponding uncertainty at the level of one standard deviation.*

At the physical pion mass and in the continuum limit we obtain

$$
\begin{aligned}
\left[\delta M_{K^0}^2\right]^{QED} (\overline{MS}, 2 \text{ GeV}) &= 0.016\,(17)_{stat+fit}\,(18)_{disc}\,(2)_{chir}\,(1)_{qQED} \cdot 10^{-3} \text{ GeV}^2 , \\
&= 0.016\,(17)_{stat+fit}\,(18)_{syst}\,(1)_{qQED} \cdot 10^{-3} \text{ GeV}^2 , \\
&= 0.016\,(25) \cdot 10^{-3} \text{ GeV}^2 , \quad\quad (2.84)
\end{aligned}
$$

where

- $()_{stat+fit}$ indicates the statistical uncertainty including also the ones induced by the fitting procedure and by the determination of the input parameters of Table II;

- $()_{disc}$ is the uncertainty due to discretization effects estimated by comparing the results obtained including ($\widetilde{D}^K \neq 0$) or excluding ($\widetilde{D}^K = 0$) the discretization term in Eq. (2.83);

- $()_{chir}$ is the error coming from including the term proportional to the chiral log in Eq. (2.83) or substituting it with a quadratic term in m_ℓ (i.e., $\widetilde{A}_2^K \overline{M}^4/(4\pi f_0)^4$);

- $()_{qQED}$ is the 5% estimate of the effects due to the quenched QED approximation taken from Refs. [33, 62].

Using the experimental value $M_{K^0} = 497.611(13)$ MeV [3] our results (2.84) and (2.62) correspond to a kaon mass in pure QCD equal to $M_K = 494.6(1)$ MeV in agreement with the FLAG estimate $M_K = 494.2(3)$ MeV.

Dividing our result (2.83) by Eq. (2.48), we obtain

$$
\begin{aligned}
\epsilon_{K^0}(\overline{MS}, 2 \text{ GeV}) &= 0.01 \ (2)_{stat+fit} \ (1)_{syst} \ (1)_{qQED} \ , \\
&= 0.01 \ (2) \ ,
\end{aligned}
\tag{2.85}
$$

where now the $()_{qQED}$ error includes also the 4% effect coming from the disconnected diagram neglected in the pion mass splitting analysis. Our result (2.85) is in agreement with the estimate quoted by FLAG, namely $\epsilon_{K^0} = 0.3(3)$ [4]; the QCDSF/UKQCD result $\epsilon_{K^0}(\overline{MS}, 2 \text{ GeV}) = 0.2(1)$ [71] and the recent determination $\epsilon_{K^0} = 0.035(20)$ from the MILC collaboration [73].

2.8 ISOSPIN BREAKING CORRECTIONS IN CHARMED MESONS

In this section using the RM123 approach we address the evaluation of the leading-order e.m. and strong IB corrections to the D-meson mass splitting $(M_{D^+} - M_{D^0})$, and the determination of the leading-order e.m. corrections to the D-meson mass combination $(M_{D^+} + M_{D^0})$ and to the D_s-meson mass $M_{D_s^+}$. In the case of D-meson mass splitting we make use of the determination (2.66) of the u- and d-quark mass difference done in the kaon sector (see Section 6) to evaluate the strong IB correction and therefore to predict the physical mass splitting $(M_{D^+} - M_{D^0})$ on the lattice.

2.8.1 ELECTROMAGNETIC AND STRONG ISOSPIN BREAKING CORRECTIONS TO $M_{D^+} - M_{D^0}$

Within the quenched QED approximation and the RM123 prescription described in Sec. 2.3, the QED contribution to the D-meson mass splitting is given by

$$
\left[M_{D^+}^2 - M_{D^0}^2\right]^{QED} = 8\pi\alpha_{em}M_D\left[M_{D^+} - M_{D^0}\right]^{em} \ ,
\tag{2.86}
$$

where

$$[M_{D^+} - M_{D^0}]^{em} = (e_u - e_d)e_c\partial_t \frac{\text{\raisebox{2pt}{(diagram)}}}{\text{(diagram)}} - (e_d^2 - e_u^2)\partial_t \frac{\text{(diagram)} + \text{(diagram)}}{\text{(diagram)}}$$

$$- (\delta m_d^{crit} - \delta m_u^{crit})\partial_t \frac{\text{(diagram)}}{\text{(diagram)}} + Z_P \left(\mathcal{Z}^d - \mathcal{Z}^u\right) m_\ell \partial_t \frac{\text{(diagram)}}{\text{(diagram)}}$$

(2.87)

with the green lines representing the charm quark propagator.

In Fig. 2.8.1 the data for $\left[M_{D^+}^2 - M_{D^0}^2\right]^{QED}$ are shown before and after the subtraction of the universal FVEs, given by Eq. (2.44). It can be clearly seen that, as in the case of the pion and kaon mass splittings, the universal FVE correction is quite large, approaching $\simeq 30\%$ at the heaviest light-quark masses.

Figure 2.8.1: *Results for the D-meson mass splitting* $\left[M_{D^+}^2 - M_{D^0}^2\right]^{QED}$ *versus the renormalized light-quark mass* m_ℓ, *obtained using Eq. (2.87) in the quenched QED approximation. Brown full points correspond to the data without any correction for FVEs, while open markers represent the lattice data corrected by the universal FVEs given by Eq. (2.44).*

From now on we always refer to the data for $\left[M_{D^+}^2 - M_{D^0}^2\right]^{QED}$ as to the QED part of the charged/neutral D-meson mass splitting already subtracted by the universal FVEs.

We have performed combined chiral, continuum and infinite volume extrapolations adopting the following fitting function

$$\left[M_{D^+}^2 - M_{D^0}^2\right]^{QED} = 4\pi\alpha_{em}\left[A_0^D + A_1^D m_\ell + D^D a^2 + F^D \frac{M_D}{L^3}\right] , \qquad (2.88)$$

where A_0^D, A_1^D, D^D and F^D are free parameters. In Fig. 2.8.2 we show the results obtained using the combined fitting function (2.88).
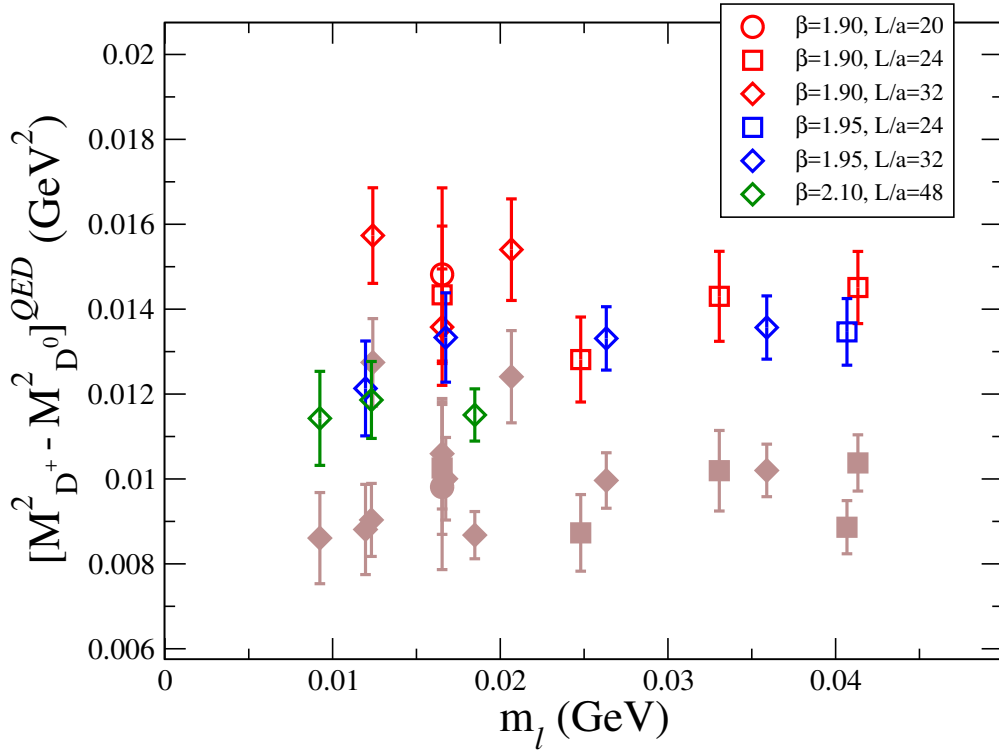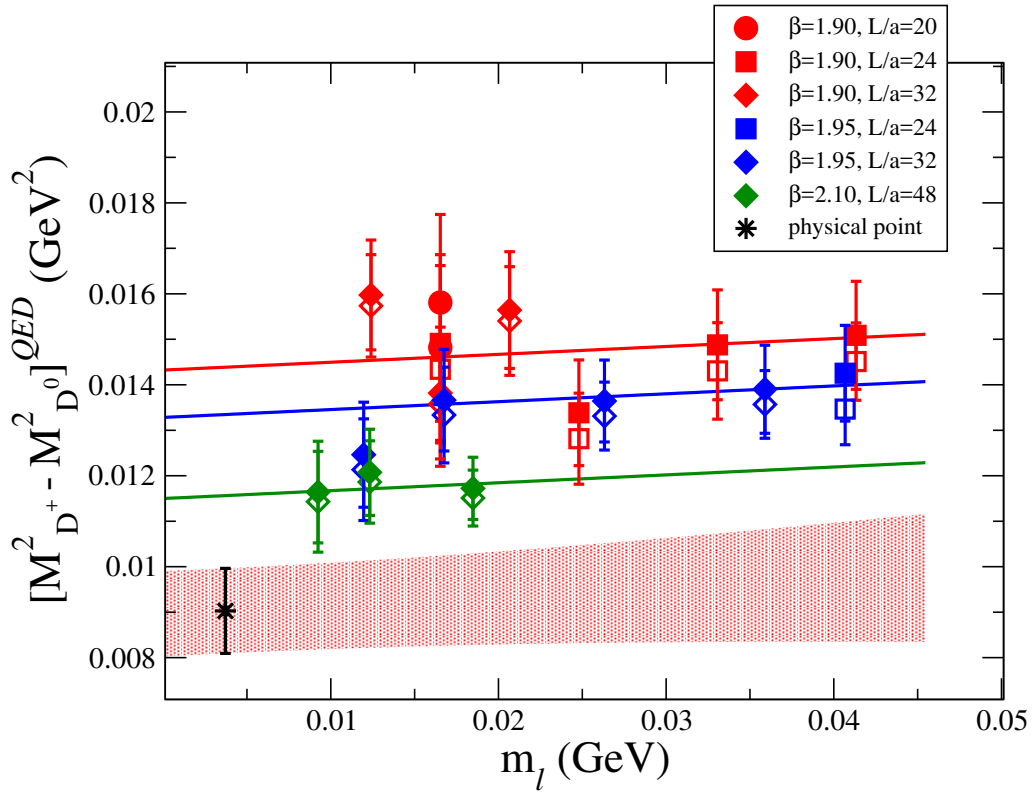

Figure 2.8.2: *Results for the D-meson mass splitting* $\left[M_{D^+}^2 - M_{D^0}^2\right]^{QED}$ *versus the renormalized light-quark mass* m_ℓ. *The empty markers correspond to the data after the subtraction of the universal FVEs, while the filled markers represent the lattice data corrected also by the SD FVEs obtained in the fitting procedure. The solid lines correspond to the results of the combined fit (2.88) obtained in the infinite volume limit at each value of the lattice spacing. The black asterisk represents the D-meson mass splitting extrapolated at the physical pion mass* $m_\ell = m_{ud} = 3.70(17)$ *MeV and to the continuum limit, while the red area identifies the corresponding uncertainty at the level of one standard deviation.*

At the physical pion mass and in the continuum and infinite volume limits our result in

the $\overline{MS}$ scheme at a renormalization scale equal to $\mu = 2$ GeV is

$$
\begin{aligned}
\left[M_{D^+}^2 - M_{D^0}^2\right]^{QED} &= 9.03 \ (0.84)_{stat+fit} \ (1.65)_{disc} \ (0.12)_{chir} \ (0.07)_{FVE} \ (0.45)_{qQED} \cdot 10^{-3} \ \text{GeV}^2 \ , \\
&= 9.03 \ (0.84)_{stat+fit} \ (1.65)_{syst} \ (0.45)_{qQED} \cdot 10^{-3} \ \text{GeV}^2 \ , \\
&= 9.03 \ (1.90) \cdot 10^{-3} \ \text{GeV}^2 \ ,
\end{aligned} \tag{2.89}
$$

where

- $()_{stat+fit}$ indicates the statistical uncertainty including also the ones induced by the fitting procedure and by the determination of the input parameters of Table II;

- $()_{disc}$ is the uncertainty due to discretization effects estimated by comparing the results assuming either $D^D \neq 0$ or $D^D = 0$ in Eq. (2.88);

- $()_{chir}$ is the error coming from including $(A_1^D \neq 0)$ or excluding $(A_1^D = 0)$ the linear term in the light-quark mass;

- $()_{FVE}$ is the uncertainty due to FVE estimated by comparing the results obtained including $(F^D \neq 0)$ or excluding $(F^D = 0)$ the phenomenological term for the SD FVEs;

- $()_{qQED}$ is the estimate of the effects due to the quenched QED approximation (5%) taken from Refs. [33, 62] and extended to the case of charmed mesons.

We need now to compute the SIB contribution

$$
\left[M_{D^+}^2 - M_{D^0}^2\right]^{SIB} = 2M_D \ Z_P \ (\widehat{m}_d - \widehat{m}_u) \ \partial_t \underset{\otimes}{\underline{}} \ , \tag{2.90}
$$

where for $(\widehat{m}_d - \widehat{m}_u)$ we make use of the result (2.66). The lattice data for $\left[M_{D^+}^2 - M_{D^0}^2\right]^{SIB}$ are shown in Fig. 2.8.3 and FVEs are visible. Thus the data have been fitted according to the following simple Ansatz:

$$
\left[M_{D^+}^2 - M_{D^0}^2\right]^{SIB} = \overline{A}_0^D + \overline{A}_1^D \, m_\ell + \overline{D}^D a^2 + \overline{F}^D \frac{\overline{M}^2}{16\pi^2 f_0^2} \frac{e^{-\overline{M}L}}{(\overline{M}L)^{3/2}} \ , \tag{2.91}
$$

where we recall $\overline{M}^2 = 2B_0 m_\ell$. The results of the linear fit (2.91) with the four free parameters $\overline{A}_0^D$, $\overline{A}_1^D$, $\overline{D}^D$ and $\overline{F}^D$, are shown in Fig. 2.8.3.

At the physical pion mass and in the continuum and infinite volume limits we get

$$
\begin{aligned}
\left[M_{D^+}^2 - M_{D^0}^2\right]^{SIB} (\overline{MS}, 2 \ \text{GeV}) &= 11.41 \ (99)_{stat+fit} \ (21)_{disc} \ (13)_{chir} \ (9)_{FVE} \cdot 10^{-3} \ \text{GeV}^2 \\
&= 11.41 \ (99)_{stat+fit} \ (26)_{syst} \cdot 10^{-3} \ \text{GeV}^2 \ , \\
&= 11.41 \ (1.02) \cdot 10^{-3} \ \text{GeV}^2 \ .
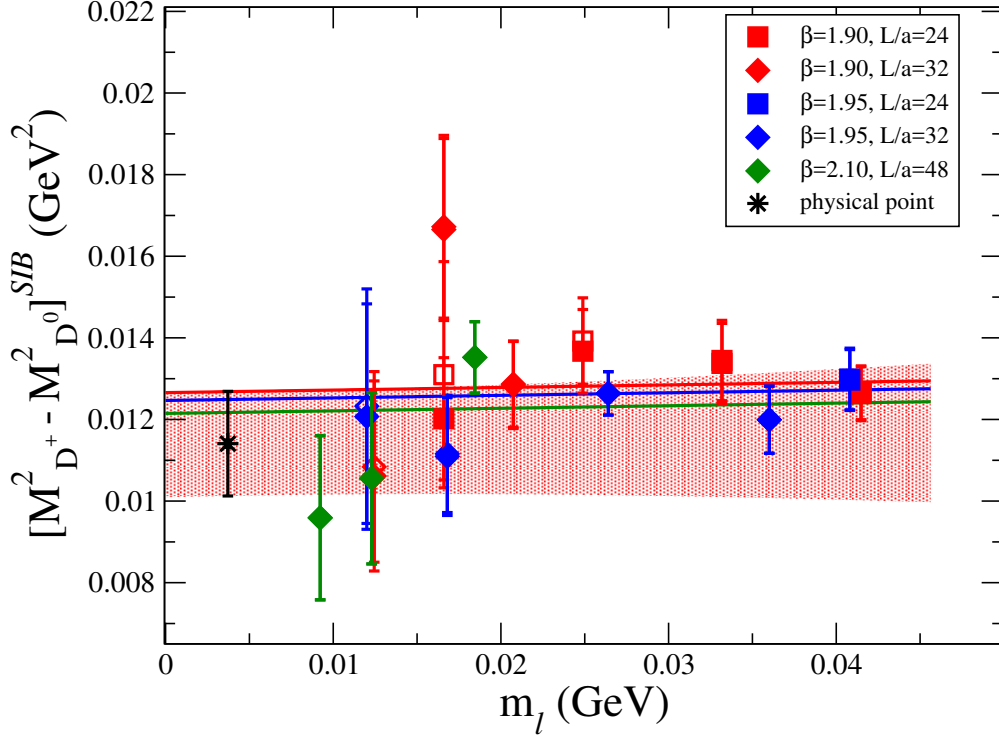\end{aligned} \tag{2.92}
$$

where

Figure 2.8.3: *Results for the SIB contribution $\left[M_{D^+}^2 - M_{D^0}^2\right]^{SIB}$ versus the renomalized light-quark mass m_ℓ. The empty markers correspond to the lattice data, while the filled ones represent the data corrected for the FVEs obtained in the fitting procedure (2.91). The solid lines correspond to the results of the combined fit (2.91) obtained in the infinite volume limit at each value of the lattice spacing. The black asterisk represents the SIB contribution extrapolated at the physical pion mass $m_\ell = m_{ud} = 3.70(17)$ MeV and to the continuum limit, while the red area identifies the corresponding uncertainty at the level of one standard deviation.*

- $()_{stat+fit}$ indicates the statistical uncertainty including also the ones induced by the fitting procedure and by the determination of the input parameters of Table II;

- $()_{disc}$ is the uncertainty due to discretization effects estimated by including $(\overline{D}^D \neq 0)$ or excluding $(\overline{D}^D = 0)$ the discretization term in Eq. (2.91);

- $()_{chir}$ is the error coming from including $(\overline{A}_1^D \neq 0)$ or excluding $(\overline{A}_1^D = 0)$ the linear term in the light-quark mass.

- $()_{FVE}$ is the uncertainty obtained including $(\overline{F}^D \neq 0)$ or excluding $(\overline{F}^D = 0)$ the FVE term in Eq. (2.91).

Thus, putting together the results (2.89) and (2.92) we get the prediction [7]

$$
\begin{aligned}
M_{D^+} - M_{D^0} &= 5.47\,(30)_{stat+fit}\,(40)_{disc}\,(6)_{chir}\,(3)_{FVE}\,(12)_{qQED}\ \text{MeV}\,, \\
&= 5.47\,(30)_{stat+fit}\,(42)_{syst}\,(12)_{qQED}\ \text{MeV}\,, \\
&= 5.47\,(53)\ \text{MeV}\,, \tag{2.93}
\end{aligned}
$$

which is consistent with the experimental value $M_{D^+} - M_{D^0} = 4.75(8)$ MeV [3] and with the unquenched QED estimate $M_{D^+} - M_{D^0} = 4.68(16)$ MeV from the BMW collaboration [17] at $N_f = 1+1+1+1$ within $\simeq 1.4$ standard deviations.

2.8.2 ELECTROMAGNETIC CORRECTIONS TO $M_{D^+} + M_{D^0}$

The D-meson mass combination $(M_{D^+} + M_{D^0})$, being isospin symmetric, does not receive any strong IB correction at leading order $O(\widehat{m}_d - \widehat{m}_u)$. Within the quenched QED approximation one has

$$
\delta M_{D^+} + \delta M_{D^0} = 4\pi\alpha_{em} \left\{ -(e_u + e_d)e_c\partial_t \frac{\text{⬡}}{\text{⬡}} - (e_d^2 + e_u^2)\partial_t \frac{\text{⬡} + \text{⬡}}{\text{⬡}} \right.
$$

$$
- \; 2\,e_c^2\partial_t \frac{\text{⬡} + \text{⬡}}{\text{⬡}} + 2\delta m_c^{crit}\partial_t \frac{\text{⬡}}{\text{⬡}}
$$

$$
- \; (\delta m_d^{crit} + \delta m_u^{crit})\partial_t \frac{\text{⬡}}{\text{⬡}} + 2Z_P \mathcal{Z}^c m_c\partial_t \frac{\text{⬡}}{\text{⬡}}
$$

$$
\left. + \; Z_P \left(\mathcal{Z}^u + \mathcal{Z}^d \right) m_\ell\partial_t \frac{\text{⬡}}{\text{⬡}} \right\} . \tag{2.94}
$$

The data for $\delta M_{D^+} + \delta M_{D^0}$ after the subtraction of the universal FVEs are shown in Fig. 2.8.4.

We have performed combined chiral, continuum and infinite volume extrapolations adopting the following fitting function

$$
\delta M_{D^+} + \delta M_{D^0} = \widetilde{A}_0^D + \widetilde{A}_1^D m_\ell + \widetilde{D}^D a^2 + \widetilde{F}^D \frac{M_D}{L^3} , \tag{2.95}
$$

where $\widetilde{A}_0^D$, $\widetilde{A}_1^D$, $\widetilde{D}^D$ and $\widetilde{F}^D$ are free parameters. In Fig. 2.8.5 we show the results obtained using the combined fitting function (2.95).

At the physical pion mass and in the continuum and infinite volume limits our result is

$$
\begin{aligned}
\delta M_{D^+} + \delta M_{D^0} &= 1.7\,(6)_{stat+fit}\,(8)_{disc}\,(1)_{chir}\,(1)_{FVE}\,(1)_{qQED} \text{ MeV} , \\
&= 1.7\,(6)_{stat+fit}\,(8)_{syst}\,(1)_{qQED} \text{ MeV} , \\
&= 1.7\,(1.0) \text{ MeV} ,
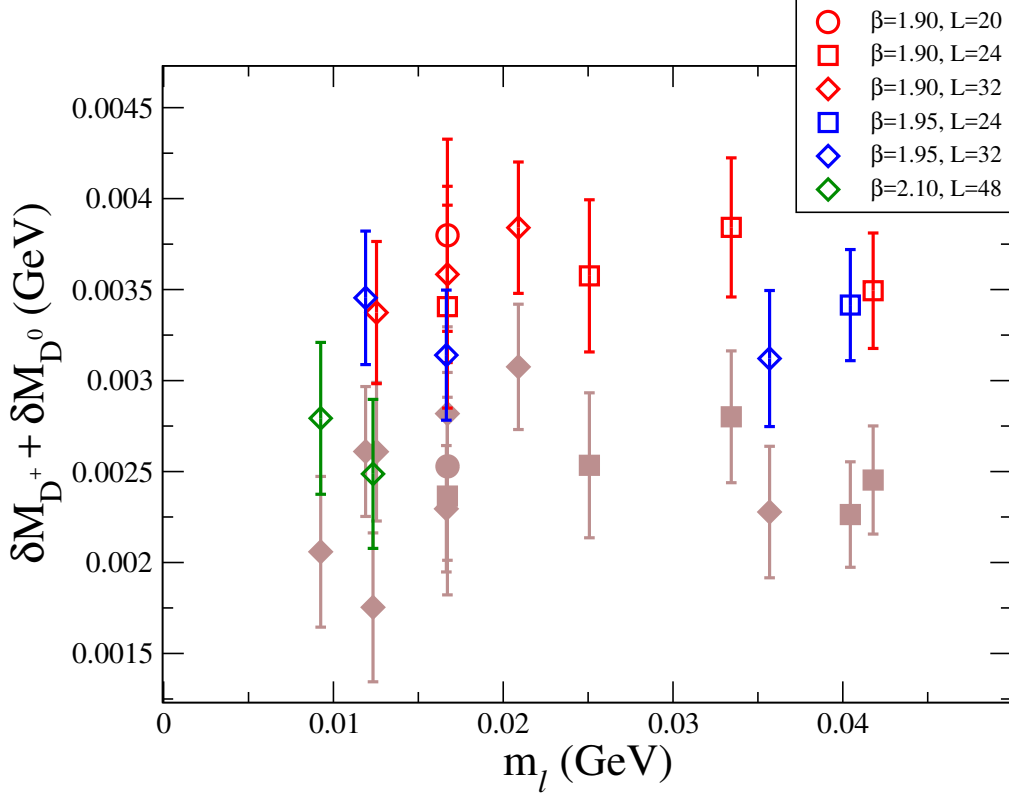\end{aligned} \tag{2.96}
$$

Figure 2.8.4: *Results for the e.m. correction to the charge-averaged D-meson mass $\delta M_{D^+} + \delta M_{D^0}$ versus the renormalized light-quark mass m_ℓ, obtained using Eq. (2.94) in the quenched QED approximation. Brown full points correspond to the data without any correction for FVEs, while open markers represent the lattice data corrected by the universal FVEs given by Eq. (2.44).*

where

- $()_{stat+fit}$ indicates the statistical uncertainty including also the ones induced by the fitting procedure and by the determination of the input parameters of Table II;

- $()_{disc}$ is the uncertainty due to discretization effects estimated by comparing the results assuming either $\widetilde{D}^D \neq 0$ or $\widetilde{D}^D = 0$ in Eq. (2.95);

- $()_{chir}$ is the error coming from including ($\widetilde{A}_1^D \neq 0$) or excluding ($\widetilde{A}_1^D = 0$) the linear term in the light-quark mass;

- $()_{FVE}$ is the uncertainty due to FVE estimated by comparing the results obtained including ($\widetilde{F}^D \neq 0$) or excluding ($\widetilde{F}^D = 0$) the phenomenological term for the SD FVEs;

- $()_{qQED}$ is the estimate of the effects due to the quenched QED approximation (5%) taken from Refs. [33, 62] and extended to the case of charmed mesons.
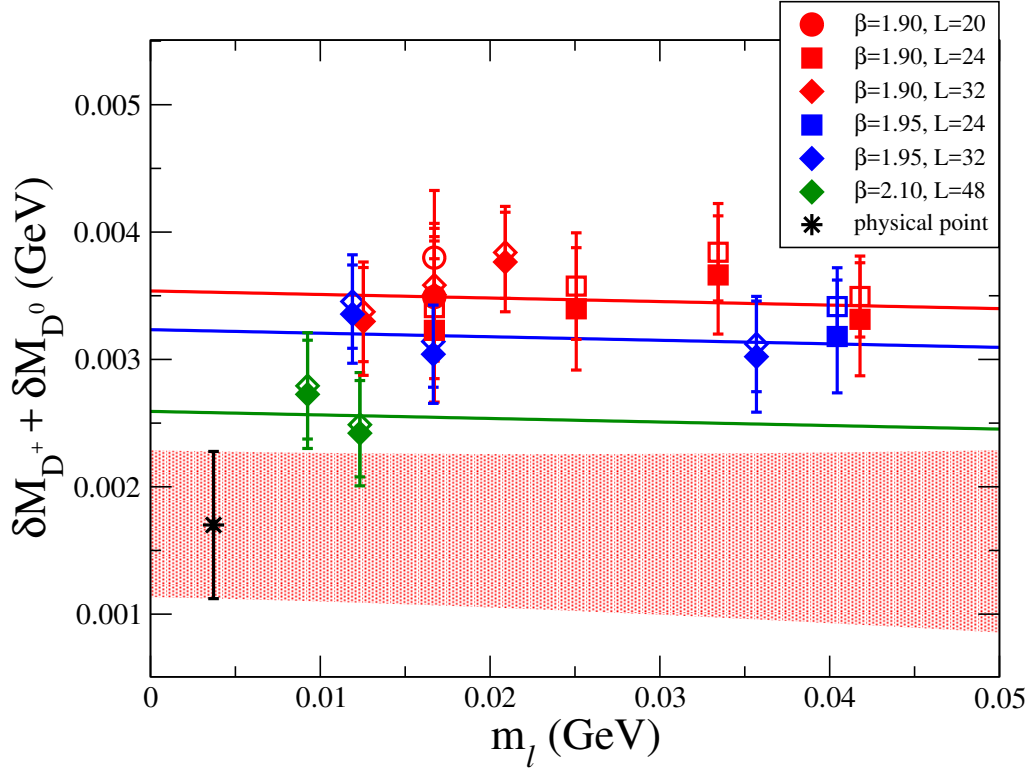
Figure 2.8.5: *Results for the e.m. correction to the charge-averaged D-meson mass $\delta M_{D^+} + \delta M_{D^0}$ versus the renormalized light-quark mass m_ℓ. The empty markers correspond to the data after the subtraction of the universal FVEs, while the filled markers represent the lattice data corrected also by the SD FVEs obtained in the fitting procedure. The solid lines correspond to the results of the combined fit (2.95) obtained in the infinite volume limit at each value of the lattice spacing. The black asterisk represents the value extrapolated at the physical pion mass $m_\ell = m_{ud} = 3.70(17)$ MeV and to the continuum limit, while the red area identifies the corresponding uncertainty at the level of one standard deviation.*

Using the experimental value $(M_{D^+} + M_{D^0})/2 = 1867.2(4)$ MeV [3] our result (2.96) corresponds to a D-meson mass in pure QCD equal to 1866.4(6) MeV.

2.8.3 ELECTROMAGNETIC CORRECTIONS TO THE D_s^+-MESON MASS

Finally we have computed also the e.m. corrections to the mass of the D_s^+-meson, that, within the quenched QED approximation, are given by

$$
\delta M_{D_s^+} = 4\pi\alpha_{em} \left\{ -e_c e_s \partial_t \frac{}{} - e_s^2 \partial_t \frac{}{} \right.
$$

$$
- e_c^2 \partial_t \frac{}{} - \delta m_s^{crit} \partial_t \frac{}{} + \delta m_c^{crit} \partial_t \frac{}{}
$$

$$
\left. + Z_P \mathcal{Z}^s m_s \partial_t \frac{}{} + Z_P \mathcal{Z}^c m_c \partial_t \frac{}{} \right\} . \tag{2.97}
$$

The data for $\delta M_{D_s^+}$ after the subtraction of the universal FVEs are shown in Fig. 2.8.6.

We have performed combined chiral, continuum and infinite volume extrapolations adopting the following fitting function

$$
\delta M_{D_s^+} = A_0^{D_s} + A_1^{D_s} m_\ell + D^{D_s} a^2 + F^{D_s} \frac{M_{D_s}}{L^3} , \tag{2.98}
$$

where $A_0^{D_s}$, $A_1^{D_s}$, D^{D_s} and F^{D_s} are free parameters. In Fig. 2.8.7 we show the results obtained using the combined fitting function (2.98).

At the physical pion mass and in the continuum and infinite volume limits our result is

$$
\begin{aligned}
\delta M_{D_s^+} &= 2.3 \, (3)_{stat+fit} \, (1)_{disc} \, (1)_{chir} \, (1)_{FVE} \, (1)_{qQED} \text{ MeV} , \\
&= 2.3 \, (3)_{stat+fit} \, (2)_{syst} \, (1)_{qQED} \text{ MeV} , \\
&= 2.3 \, (4) \text{ MeV} , \tag{2.99}
\end{aligned}
$$

where

- $()_{stat+fit}$ indicates the statistical uncertainty including also the ones induced by the fitting procedure and by the determination of the input parameters of Table II;

- $()_{disc}$ is the uncertainty due to discretization effects estimated by comparing the results assuming either $D^{D_s} \neq 0$ or $D^{D_s} = 0$ in Eq. (2.98);
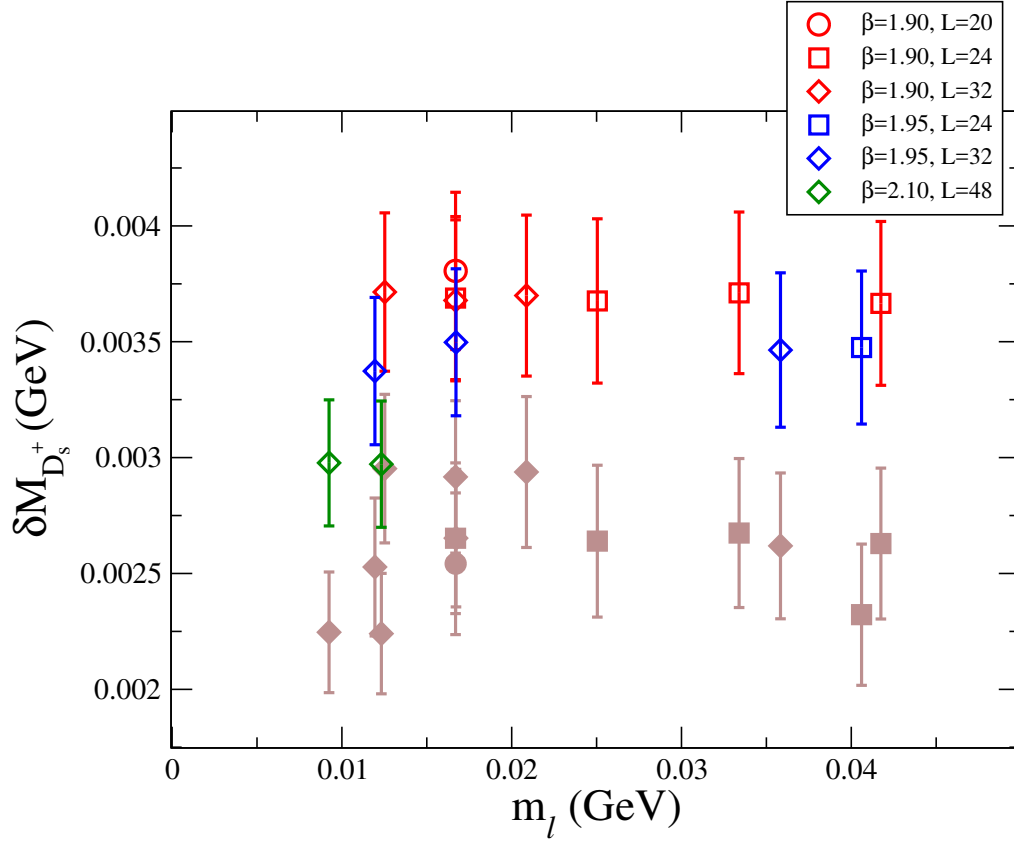
Figure 2.8.6: *Results for the e.m. correction $\delta M_{D_s^+}$ versus the renormalized light-quark mass m_ℓ, obtained using Eq. (2.97) in the quenched QED approximation. Brown full points correspond to the data without any correction for FVEs, while open markers represent the lattice data corrected by the universal FVEs given by Eq. (2.44).*

- $()_{chir}$ is the error coming from including $(A_1^{D_s} \neq 0)$ or excluding $(A_1^{D_s} = 0)$ the linear term in the light-quark mass;

- $()_{FVE}$ is the uncertainty due to FVE estimated by comparing the results obtained including $(F^{D_s} \neq 0)$ or excluding $(F^{D_s} = 0)$ the phenomenological term for the SD FVEs;

- $()_{qQED}$ is the estimate of the effects due to the quenched QED approximation (5%) taken from Refs. [33, 62] and extended to the case of charmed mesons.

Using the experimental value $M_{D_s^+} = 1969.0(1.4)$ MeV [3] our result (2.99) corresponds to a D_s-meson mass in pure QCD equal to 1966.7(1.5) MeV.
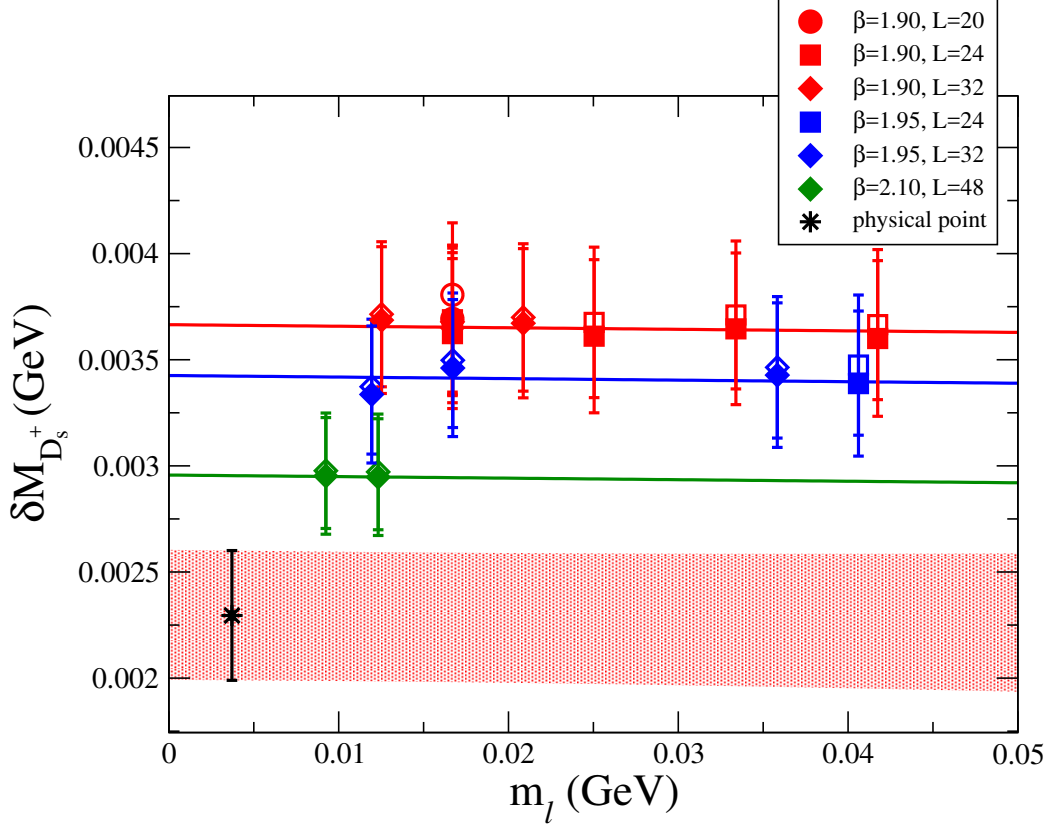
Figure 2.8.7: *Results for the e.m. correction $\delta M_{D_s^+}$ versus the renormalized light-quark mass m_ℓ. The empty markers correspond to the data after the subtraction of the universal FVEs, while the filled markers represent the lattice data corrected also by the SD FVEs obtained in the fitting procedure. The solid lines correspond to the results of the combined fit (2.98) obtained in the infinite volume limit at each value of the lattice spacing. The black asterisk represents the value extrapolated at the physical pion mass $m_\ell = m_{ud} = 3.70(17)$ MeV and to the continuum limit, while the red area identifies the corresponding uncertainty at the level of one standard deviation.*

QED Corrections to Hadronic Decay Rates on the Lattice

<div style="text-align: right">3</div>

3.1 Introduction

Precision flavor physics is a particularly powerful tool for exploring the limits of the Standard Model (SM) of particle physics and in searching for inconsistencies which would signal the existence of new physics. An important component of this endeavour is the over-determination of the elements of the Cabibbo-Kobayashi-Maskawa (CKM) matrix from a wide range of weak processes. The precision in extracting CKM matrix elements is generally limited by our ability to quantify hadronic effects and the main goal of large-scale simulations using the lattice formulation of QCD is the *ab-initio* evaluation of the non-perturbative QCD effects in physical processes. The recent, very impressive, improvement in lattice computations has led to a precision approaching $O(1\%)$ for a number of quantities (see e.g. Ref. [4] and references therein) and therefore in order to make further progress electromagnetic effects (and other isospin-breaking contributions) have to be considered. The question of how to include electromagnetic effects in the hadron spectrum and in the determination of quark masses in ab-initio lattice calculations has been addressed in the previous chapter 2 of this thesis.

In the computation of the hadron spectrum there is a very significant simplification in that there are no infrared divergences. In Ref. [10] it has been proposed for the first time a strategy to include electromagnetic effects in processes for which infrared divergences are present but which cancel in the standard way between diagrams containing different numbers of real and virtual photons [11]. The presence of infrared divergences in intermediate steps of the calculation requires the development of new methods. Indeed, in order to cancel the infrared divergences and obtain results for physical quantities, radiative corrections from virtual and real photons must be combined. We stress that it is not sufficient simply to add the electromagnetic interaction to the quark action because amplitudes with different numbers of real photons must be evaluated separately, before being combined in the inclusive rate for a given process. In this chapter we discuss in full detail the strategy envisaged in Ref. [10] to compute electromagnetic radiative corrections to leptonic decays of pseudoscalar mesons which can then be used to determine the corresponding CKM matrix elements. In the next chapter we will show the results for the first application of the method here described in the case of the light-meson leptonic decay rates [13, 16]. Although we present the explicit

discussion for this specific set of processes, the method is more general and can be extended to generic processes including, for example, to semileptonic decays. Before concluding the present chapter we will provide some hints on the theoretical framework required for the computation of radiative corrections to semileptonic decay rates in lattice simulations. In this respect we will review the ongoing work on the new theoretical issues which arise in this case [52].

We now focus on the leptonic decay of the charged pseudoscalar meson P^+. Let Γ_0 be the partial width for the decay $P^+ \to \ell^+ \nu_\ell$ where the charged lepton ℓ is an electron or a muon (or possibly a τ) and ν_ℓ is the corresponding neutrino. The subscript 0 indicates that there are no photons in the final state. In the absence of electromagnetism, the non-perturbative QCD effects are contained in a single number, the decay constant f_P, defined by

$$\langle 0 \,|\, \bar{q}_1 \gamma^\mu \gamma^5 \, q_2 \,|\, P^+(p) \rangle = i p^\mu f_P \,, \tag{3.1}$$

where P^+ is composed of the valence quarks $\bar{q}_1$ and q_2, and the axial current in (3.1) is composed of the corresponding quark fields. There have been very many lattice calculations of the decay constants $f_\pi, f_K, f_{D_{(s)}}$ and $f_{B_{(s)}}$ [4], some of which are approaching $O(1\%)$ precision. As noted above, in order to determine the corresponding CKM matrix elements at this level of precision isospin breaking effects, including electromagnetic corrections, must be considered. It will become clear in the following, and has been stressed in [48, 67], that it is not possible to give a physical definition of the decay constant f_P in the presence of electromagnetism, because of the contributions from diagrams in which the photon is emitted by the hadron and absorbed by the charged lepton. Thus the physical width is not just given in terms of the matrix element of the axial current and can only be obtained by a full calculation of the electromagnetic corrections at a given order.

The calculation of electromagnetic effects leads to an immediate difficulty: Γ_0 contains infrared divergences and by itself is therefore unphysical. The well-known solution to this problem is to include the contributions from real photons. We therefore define $\Gamma_1(\Delta E)$ to be the partial width for the decay $P^+ \to \ell^+ \nu_\ell \gamma$ where the energy of the photon in the rest frame of P^+ is integrated from 0 to ΔE. The sum $\Gamma_0 + \Gamma_1(\Delta E)$ is free from infrared divergences (although, of course, it does depend on the energy cut-off ΔE). We restrict the discussion to $O(\alpha_{em})$ corrections, where α is the electromagnetic fine-structure constant, and hence only consider a single photon.

The previous paragraph reminds us that the determination of the CKM matrix elements $V_{q_1 q_2}$ at $O(\alpha_{em})$ (i.e. at $O(1\%)$ or better) from leptonic decays requires the evaluation of amplitudes with a real photon. The main goal of the pioneering paper [10] has been to suggest how such a calculation might be performed with non-perturbative accuracy. There are a number of technicalities which will be explained in the following sections, but here we present a general outline of the proposed method. We start with the experimental observable $\Gamma(\Delta E)$, the partial width for $P^+ \to \ell^+ \nu_\ell(\gamma)$. The final state consists either of $\ell^+ \nu_\ell$ or of $\ell^+ \nu_\ell \gamma$ where the energy of the photon in the centre-of-mass frame is smaller than ΔE:

$$\Gamma(\Delta E) = \Gamma_0 + \Gamma_1(\Delta E) \,. \tag{3.2}$$

The exchange of a virtual photon depends on the structure of the decaying meson, since all momentum modes are included, and the corresponding amplitude must therefore be computed non-perturbatively. On the other hand, the non-perturbative evaluation of the emission of a real photon is not strictly necessary. In principle, $\Gamma_1(\Delta E)$ can be evaluated in lattice simulations by computing the amplitudes for a range of photon momenta and using the results to perform the integral over phase space. Since such computations are necessarily performed in finite volumes the available momenta are discrete, so that it is necessary to choose the volumes appropriately and compute several correlation functions. In the next chapter we will expand more on our recent efforts to compute non-perturbatively the form factors contributing to the amplitudes for the radiative decays $P \to \ell\nu_\ell\gamma$. This $O(a)$-improved lattice calculation is currently ongoing and preliminary results have been presented at the *Lattice 2019* conference [77]. As a first approach we have implemented the method of Ref. [10] choosing instead to make use of the fact that a very soft photon couples to a charged hadron as if to an elementary particle; it does not resolve the structure of the hadron. We therefore propose to choose ΔE to be sufficiently small that the pointlike approximation can be used to calculate $\Gamma_1(\Delta E)$ in perturbation theory, treating P^+ as an elementary particle. On the other hand, ΔE must be sufficiently large that $\Gamma(\Delta E)$ can be measured experimentally. We imagine setting $\Delta E = O(10\text{-}20\,\mathrm{MeV})$ which satisfies both requirements. From Refs. [78, 79] we learn that resolutions on the energy of the photon in the rest frame of the decaying particle of this order are experimentally accessible. Later on we will present a discussion, based on phenomenological analyses, of the uncertainties induced by treating the meson as elementary as a function of ΔE.

It is necessary to ensure that the cancellation of infrared divergences occurs with good numerical precision leading to an accurate result for $\Gamma(\Delta E)$. Since Γ_0 is to be calculated in a Monte-Carlo simulation and $\Gamma_1(\Delta E)$ in perturbation theory using the pointlike approximation, this requires an intermediate step. In Ref. [10] it has been proposed to rewrite Eq. (3.2) in the form

$$\Gamma(\Delta E) = \lim_{V \to \infty} \left(\Gamma_0 - \Gamma_0^{\mathrm{pt}} \right) + \lim_{V \to \infty} \left(\Gamma_0^{\mathrm{pt}} + \Gamma_1(\Delta E) \right), \tag{3.3}$$

where V is the volume of the lattice. Γ_0^{pt} is an unphysical quantity; it is the perturbatively calculated amplitude at $O(\alpha_{em})$ for the decay $P^+ \to \ell^+\nu_\ell$ with the P^+ treated as an elementary particle. In Γ_0^{pt} the finite-volume sum over the momenta of the photon is performed over the full range. The contributions from small momenta to Γ_0 and Γ_0^{pt} are the same and thus the infrared divergences cancel in the first term on the right-hand side of Eq. (4.9). Moreover, the infrared divergences in Γ_0 and Γ_0^{pt} are both equal and opposite to that in $\Gamma_1(\Delta E)$. The infrared divergences therefore cancel separately in each of the two terms on the right-hand side of Eq. (4.9) and indeed we treat each of these terms separately. $\Gamma_0^{\mathrm{pt}} + \Gamma_1(\Delta E)$ is calculated in perturbation theory directly in infinite volume. The QCD effects in Γ_0 are calculated stochastically in a lattice simulation and the virtual photon is included explicitly in the Feynman gauge. For each photon momentum this is combined with Γ_0^{pt} and the difference is summed over the momenta and then the infinite-volume limit is taken. This completes the sketch of the proposed method, and in the remainder of this chapter we will explain the many technical issues which must be addressed.

It will be helpful in the following to define $\Delta\Gamma_0(L)$ in terms of the first term on the right-hand side of Eq. (4.9):

$$\Delta\Gamma_0(L) = \Gamma_0(L) - \Gamma_0^{\mathrm{pt}}(L) , \tag{3.4}$$

where we have made the dependence on the lattice size. In analogy to Eq. (3.2) we also define the perturbative quantity

$$\Gamma^{\mathrm{pt}}(\Delta E) \equiv \Gamma_0^{\mathrm{pt}} + \Gamma_1(\Delta E) . \tag{3.5}$$

We note that, since the sum of all the terms in Eq. (4.9) is gauge invariant as is the perturbative rate $\Gamma^{\mathrm{pt}}(\Delta E)$, the combination $\Delta\Gamma_0(L)$ is also gauge invariant, although each of the two terms is not.

The plan of this chapter is as follows. In the next section we discuss the effective weak Hamiltonian and its renormalization in the presence of electromagnetism. We discuss the matching of the bare lattice operators used in the calculation of correlation functions and those defined in the W-regularization which is a natural scheme used in the definition of the Fermi constant G_F in the presence of electromagnetism. The structure of the calculation and the correlation functions which need to be calculated are presented in Sec. 3.3. In Sec. 3.4 we describe the calculation of the first term on the right-hand side of Eq. (4.9), $\Delta\Gamma_0(L)$. The evaluation of the second term, $\Gamma^{\mathrm{pt}}(\Delta E)$, directly in infinite volume, is theoretically straightforward and in Sec. 3.5 we briefly sketch the main steps of the calculation performed in Ref. [10]. Sec. 3.6 contains a detailed discussion of the regularization and cancellation of infrared divergences in a finite volume. In Sec. 3.7 we present some phenomenological estimates of the uncertainties due to the use of the point-like approximation for P^+ in the decay $P^+ \to \ell^+\nu\gamma$. Finally, in Sec. 3.8 we discuss the additional theoretical issues which arise when including electromagnetic corrections to semileptonic decays, such as $K_{\ell 3}$.

In the remainder of the chapter, to be specific we choose $P^+ = \pi^+$, unless explicitly stated, but the discussion generalizes trivially to other pseudoscalar mesons with the obvious changes of flavor labels. The method does not require P^+ to be a light psuedo-Goldstone Boson nor on the use of chiral perturbation theory.

3.2 MATCHING THE EFFECTIVE LOCAL FOUR-QUARK OPERATOR(S) ONTO THE STANDARD MODEL

At lowest order in electromagnetic (and strong) perturbation theory the process $u\bar{d} \to \ell^+\nu_\ell$ proceeds by an s-channel W exchange, see the left-hand diagram in Fig. 4.2.1. Since the energy-momentum exchanged in this process are much smaller than M_W, it is standard practice to rewrite the amplitude in terms of a four-fermion local interaction:

$$\mathcal{L}_W = -\frac{4G_F}{\sqrt{2}} V_{ud}^* \left(\bar{d}_L\gamma_\mu u_L\right)\left(\bar{\nu}_{\ell L}\gamma^\mu \ell_L\right) , \tag{3.6}$$

where the subscript L represents *left*, $\psi_L = \frac{(1-\gamma_5)}{2}\psi$, and G_F is the Fermi constant. In performing lattice computations this replacement is necessary, since the lattice spacing a
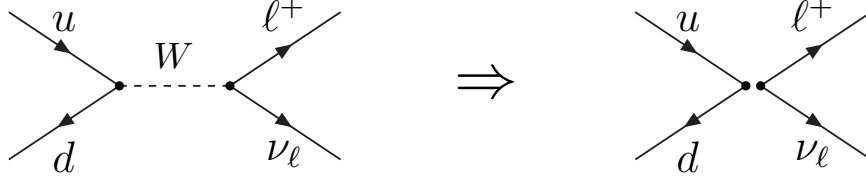
Figure 3.2.1: Tree-level diagram for the process $u\bar{d} \to \ell^+ \nu_\ell$ (left-hand diagram). In the effective theory the interaction is replaced by a local four-fermion operator (right-hand diagram).

is much greater than $1/M_W$, where M_W is the mass of the W-Boson. When including the $O(\alpha_{em})$ corrections, the ultra-violet contributions to the matrix element of the local operator are different to those in the Standard Model and in this section we discuss the matching factors which must be computed to determine the $O(\alpha_{em})$ corrections to the $\pi^+ \to \ell^+ \nu_\ell$ decay from lattice computations of correlation functions containing the local operator in (3.6). Since the pion decay width is written in terms of G_F, it is necessary to start by revisiting the determination of the Fermi constant at $O(\alpha_{em})$.

3.2.1 DETERMINATION OF THE FERMI CONSTANT, G_F

G_F is conventionally taken from the measured value of the muon lifetime using the expression [80, 81]

$$\frac{1}{\tau_\mu} = \frac{G_F^2 m_\mu^5}{192\pi^3} \left[1 - \frac{8m_e^2}{m_\mu^2} \right] \left[1 + \frac{\alpha_{em}}{2\pi} \left(\frac{25}{4} - \pi^2 \right) \right], \tag{3.7}$$

leading to the value $G_F = 1.16634 \times 10^{-5}\,\text{GeV}^{-2}$. For an extension of Eq. (3.7) to $O(\alpha_{em}^2)$ and the inclusion of higher powers of $\rho \equiv (m_e/m_\mu)^2$ see Sec. 10.2 of [3]. The Particle Data Group [3] quote the corresponding value of the Fermi constant to be $G_F = 1.1663787(6) \times 10^{-5}\,\text{GeV}^{-2}$.

Eq. (3.7) can be viewed as the definition of G_F. When calculating the Standard Model corrections to the muon lifetime many of the contributions are absorbed into G_F and the remaining terms on the right-hand side of (3.7) come from the diagrams in Fig. 3.2.2. Specifically in these diagrams the factor $1/k^2$ in the Feynman-gauge photon propagator is replaced by $1/k^2 \times M_W^2/(M_W^2 - k^2)$, where k is the momentum in the propagator; this is called the W-regularization of ultra-violet divergences. These diagrams are evaluated in the effective theory with the local four-fermion operator $(\bar{\nu}_\mu \gamma^\mu (1 - \gamma^5)\mu)(\bar{e}\gamma^\mu(1-\gamma^5)\nu_e)$; the two currents are represented by the filled black circles in Fig. 3.2.2.

An explanation of the reasoning behind the introduction of the W-regularization is given in [82]. The Feynman-gauge photon propagator is rewritten as two terms:

$$\frac{1}{k^2} = \frac{1}{k^2 - M_W^2} + \frac{M_W^2}{M_W^2 - k^2} \frac{1}{k^2} \tag{3.8}$$
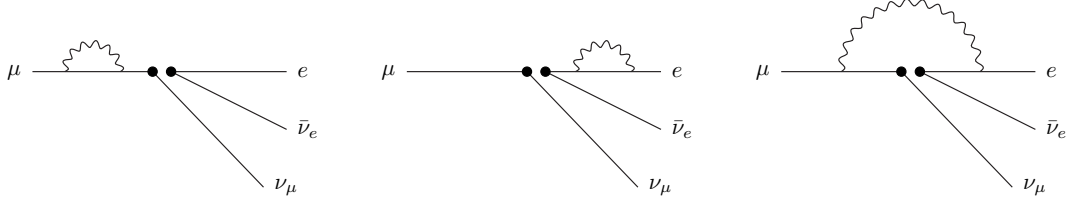
Figure 3.2.2: Diagrams contributing to the $O(\alpha_{em})$ corrections to muon decay; see Eq. (3.7). The curly line represents the photon.
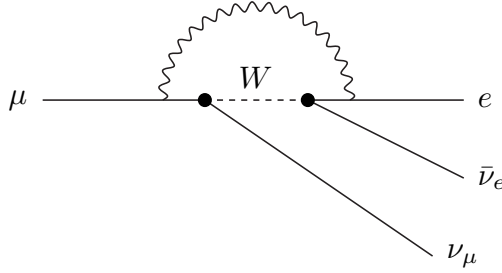

Figure 3.2.3: Photon-W box diagrams contributing to the $O(\alpha_{em})$ corrections to muon decay in the Standard Model. The curly line represents the photon.

and the ultra-violet divergent contributions come from the first term and are absorbed in the definition of G_F. In addition, the Standard-Model γ-W box diagram in Fig. 3.2.3 is ultra-violet convergent and is equal to the corresponding diagram in the effective theory (i.e. the third diagram in Fig. 3.2.2) with the W-regularization, up to negligible corrections of $O(q^2/M_W^2)$, where q is the four-momentum of the electron and its neutrino. Other electroweak corrections not explicitly mentioned above are all absorbed into G_F.

3.2.2 W-regularization and weak decays of hadrons

It is a particularly helpful feature that most of the terms which are absorbed into the definition of G_F are common to other processes, including the leptonic decays of pseudoscalar mesons [12, 83]. There are however, some short-distance contributions which do depend on the electric charges of the individual fields in the four-fermion operators and these lead to a correction factor of $(1 + \frac{2\alpha_{em}}{\pi} \log \frac{M_Z}{M_W})$ to Γ_0 [12]. This is a tiny correction ($\simeq 0.06\%$), but one which nevertheless can readily be included explicitly.

The conclusion of the above discussion is that the evaluation of the amplitude for the process $\pi^+ \to \ell^+ \nu$ up to $O(\alpha_{em})$ can be performed in the effective theory with the effective

Hamiltonian

$$H_{\text{eff}} = \frac{G_F}{\sqrt{2}} V_{ud}^* \left(1 + \frac{\alpha_{em}}{\pi} \log \frac{M_Z}{M_W} \right) O_1^{\text{W-reg}}(M_W), \tag{3.9}$$

where $O_1^{\text{W-reg}}(M_W)$ is the operator $(\bar{d}\gamma^\mu(1 - \gamma^5)u)\,(\bar{\nu}_\ell\gamma_\mu(1 - \gamma^5)\ell)$ renormalized in the W-regularization scheme, which is used to regularize the Feynman-gauge photon propagator. The value of G_F is obtained from the muon lifetime as discussed around Eq. (3.7). Of course we are not able to implement the W-regularization directly in present day lattice simulations in which the inverse lattice spacing is much smaller than M_W. Thus, a matching of the lattice weak operator O_1 to the W-regularization scheme is necessary. In addition, for lattice formulations which break chiral symmetry, like the one used in the present study, the lattice weak operator O_1 mixes with other four-fermion operators of different chirality.

3.2.3 THE RENORMALIZED WEAK OPERATOR IN THE W-REGULARIZATION SCHEME

In order to obtain the operator renormalized in the W-regularization scheme, we start by renormalizing the lattice four-fermion operator O_1 in the RI'-MOM scheme [14] up to order $O(\alpha_{\text{em}})$ and to all orders in α_s, as discussed in Sec. 1.11, obtaining $O_1^{\text{RI'}}(\mu)$, and then perturbatively match the operator $O_1^{\text{RI'}}(\mu)$ to the one in the W-regularization [10]

$$O_1^{\text{W-reg}}(M_W) = Z^{\text{W-RI'}} \left(\frac{M_W}{\mu}, \alpha_s(\mu), \alpha_{\text{em}} \right) O_1^{\text{RI'}}(\mu). \tag{3.10}$$

In Ref. [13] we have calculated the coefficient of the term proportional to $\alpha_{\text{em}}\alpha_s \log(M_W^2/\mu^2)$ in the matching coefficient $Z^{\text{W-RI'}}(M_W/\mu, \alpha_s(\mu), \alpha_{\text{em}})$. Following this calculation the error due to the renormalization of the effective hamiltonian is of the order of $O(\alpha_{\text{em}}\alpha_s(M_W))$. The matching coefficient in Eq. (3.10) can be computed by first evolving the operator in the RI' scheme to the scale M_W and then matching it to the corresponding operator in the W-scheme. The coefficient can therefore be written as the product of a matching coefficient and an evolution operator

$$Z^{\text{W-RI'}} \left(\frac{M_W}{\mu}, \alpha_s(\mu), \alpha_{\text{em}} \right) = Z^{\text{W-RI'}} \left(1, \alpha_s(M_W), \alpha_{\text{em}} \right) U^{\text{RI'}} \left(M_W, \mu, \alpha_{\text{em}} \right). \tag{3.11}$$

Below we will only consider terms of first order in α_{em} and, therefore we will consistently neglect the running of α_{em}.

We note that the original bare lattice operators and $O_1^{\text{W-reg}}(M_W)$ are gauge invariant, and thus the corresponding matching coefficients are gauge invariant. This is not the case for $O_1^{\text{RI'}}(\mu)$ that instead depends not only on the external states chosen to define the renormalization conditions, but also on the gauge. Consequently the matching coefficient $Z^{\text{W-RI'}} \left(\frac{M_W}{\mu}, \alpha_s(\mu), \alpha_{\text{em}} \right)$ and the evolution operator $U^{\text{RI'}} (M_W, \mu, \alpha_{\text{em}})$ are in general gauge dependent. However, at the order of perturbation theory to which we are working, the evolution operator turns out to be both scheme and gauge independent.

In the following, we discuss in turn the matching coefficient, $Z^{\text{W-RI'}}\left(1, \alpha_s(M_W), \alpha_{\text{em}}\right)$, the evolution operator $U^{\text{RI'}}\left(M_W, \mu, \alpha_{\text{em}}\right)$, and the definition of the renormalized operator $O_1^{\text{RI'}}(\mu)$, obtained non-perturbatively.

a) The matching coefficient. At first order (one loop) in α_{em}

$$Z^{\text{W-RI'}}\left(1, \alpha_s(M_W), \alpha_{\text{em}}\right) = 1 + \frac{\alpha_{\text{em}}}{4\pi}\, C^{\text{W-RI'}} \, , \tag{3.12}$$

where the strong interaction corrections for the RI'-MOM operator vanish, at this order, because of the Ward identities of the quark vector and axial vector currents appearing in the operator O_1 in the massless limit. We recall that we currently do not include terms of $O(\alpha_s(M_W)\alpha_{\text{em}})$ in the matching coefficient $Z^{\text{W-RI'}}$.

b) The evolution operator. The evolution operator $U^{\text{RI'}}\left(M_W, \mu, \alpha_{\text{em}}\right)$ is the solution of the renormalization group equation

$$\left[\mu^2\frac{\partial}{\partial\mu^2} + \beta(\alpha_s, \alpha_{\text{em}})\frac{\partial}{\partial\alpha_s}\right] U^{\text{RI'}}\left(M_W, \mu, \alpha_{\text{em}}\right) = \gamma(\alpha_s, \alpha_{\text{em}})\, U^{\text{RI'}}\left(M_W, \mu, \alpha_{\text{em}}\right) \, , \tag{3.13}$$

where $U^{\text{RI'}}\left(M_W, \mu, \alpha_{\text{em}}\right)$ satisfies the initial condition $U^{\text{RI'}}\left(M_W, M_W, \alpha_{\text{em}}\right) = 1$, $\gamma(\alpha_s, \alpha_{\text{em}})$ is, in general, the anomalous dimension matrix [84, 85], although in our particular case it is actually a number (and not a matrix), and $\beta(\alpha_s, \alpha_{\text{em}})$ is the QCD β-function:

$$\beta(\alpha_s, \alpha_{\text{em}}) = \frac{d\alpha_s}{d\log\mu^2} = -\beta_0\frac{\alpha_s^2}{4\pi} - \beta_1\frac{\alpha_s^3}{(4\pi)^2} - \beta_1^{se}\frac{\alpha_s^2\alpha_{\text{em}}}{(4\pi)^2} \, , \tag{3.14}$$

with

$$\beta_0 = 11 - \frac{2}{3}N_f \, , \quad \beta_1 = 102 - \frac{38}{3}N_f \, , \quad \beta_1^{se} = -\frac{8}{9}\left(N_u + \frac{N_d}{4}\right) \, , \tag{3.15}$$

where N_f denotes the number of active flavors, and N_u and N_d denote the number of up-like and down-like active quarks respectively so that $N_f = N_u + N_d$. We may expand $\gamma(\alpha_s, \alpha_{\text{em}})$ in powers of the couplings as follows

$$\gamma(\alpha_s, \alpha_{\text{em}}) = \frac{\alpha_s}{4\pi}\gamma_s^{(0)} + \frac{\alpha_s^2}{(4\pi)^2}\gamma_s^{(1)} + \frac{\alpha_{\text{em}}}{4\pi}\gamma_e^{(0)} + \frac{\alpha_s\alpha_{\text{em}}}{(4\pi)^2}\gamma_{se}^{(1)} \, , \tag{3.16}$$

where $\gamma_{se}^{(1)}$ has been previously calculated in Ref. [86]. In the case of the operator O_1 both $\gamma_s^{(0)}$ and $\gamma_s^{(1)}$ vanish whereas

$$\gamma_e^{(0)} = -2 \, , \qquad \gamma_{se}^{(1)} = +2 \, . \tag{3.17}$$

It can be demonstrated that, in addition to the leading anomalous dimension $\gamma_e^{(0)}$, $\gamma_{se}^{(1)}$ is also independent of the renormalization scheme, thus in particular it is the same in RI' and

in the W-regularization schemes. It is then straightforward to derive $U^{\text{RI'}}(M_W, \mu, \alpha_{\text{em}})$

$$
\begin{aligned}
U^{\text{RI'}}(M_W, \mu, \alpha_{\text{em}}) &= 1 - \frac{\alpha_{\text{em}}}{4\pi} \gamma_e^{(0)} \log\left(\frac{M_W^2}{\mu^2}\right) - \frac{\alpha_s(\mu)\alpha_{\text{em}}}{(4\pi)^2} \gamma_{se}^{(1)} \log\left(\frac{M_W^2}{\mu^2}\right) \\
&= 1 + \frac{\alpha_{\text{em}}}{4\pi} 2\left(1 - \frac{\alpha_s(\mu)}{4\pi}\right) \log\left(\frac{M_W^2}{\mu^2}\right) \; .
\end{aligned}
\tag{3.18}
$$

Note that at this order the evolution operator is independent of the QCD β-function. This is a consequence of the fact that the QCD anomalous dimension vanishes for the operator O_1.

Combining Eqs. (3.10) - (3.12) and (3.18) we obtain the relation between the operator O_1 in the W-regularization scheme and the one in the RI' scheme,

$$
O_1^{\text{W-reg}}(M_W) = \left\{ 1 + \frac{\alpha_{\text{em}}}{4\pi} \left[2\left(1 - \frac{\alpha_s(\mu)}{4\pi}\right) \log\left(\frac{M_W^2}{\mu^2}\right) + C^{\text{W-RI'}} \right] \right\} O_1^{\text{RI'}}(\mu) \; ,
\tag{3.19}
$$

which is valid at first order in α_{em} and up to and including terms of $O(\alpha_{\text{em}}\alpha_s(M_W))$ in the strong coupling constant.

c) The renormalized operator in the RI'-MOM scheme. When we include QCD and e.m. corrections at $O(\alpha_{\text{em}})$, the operator O_1 on the lattice with Wilson fermions mixes with a complete basis of operators with different chiralities. The mixing involves the following operators

$$
\begin{aligned}
O_1^{\text{bare}} &= \bar{q}_2 \gamma^\mu (1 - \gamma_5) q_1 \; \bar{\nu}_\ell \gamma_\mu (1 - \gamma_5)\ell \; , \\
O_2^{\text{bare}} &= \bar{q}_2 \gamma^\mu (1 + \gamma_5) q_1 \; \bar{\nu}_\ell \gamma_\mu (1 - \gamma_5)\ell \; , \\
O_3^{\text{bare}} &= \bar{q}_2 (1 - \gamma_5) q_1 \; \bar{\nu}_\ell (1 + \gamma_5)\ell \; , \\
O_4^{\text{bare}} &= \bar{q}_2 (1 + \gamma_5) q_1 \; \bar{\nu}_\ell (1 + \gamma_5)\ell \; , \\
O_5^{\text{bare}} &= \bar{q}_2 \sigma^{\mu\nu} (1 + \gamma_5) q_1 \; \bar{\nu}_\ell \sigma_{\mu\nu} (1 + \gamma_5)\ell \; .
\end{aligned}
\tag{3.20}
$$

The complete basis is made up of ten operators. The five additional operators are obtained from O_1 - O_5 by the exchange $(1 - \gamma^5) \leftrightarrow (1 + \gamma^5)$. Since the neutrino is electrically neutral its chirality is conserved and the operators O_1 - O_5 do not mix under renormalization with the remaining 5 operators and invariance under parity transformations ensures that the two 5×5 renormalization matrices are equal. For this reason, in the following we focus the discussion on the five operators of Eq. (3.20). Moreover, the basis of operators in Eq. (3.20) is the complete basis of operators for a left-handed neutrino.

The mixing is a consequence of the explicit chiral symmetry breaking of Wilson-like fermions on the lattice. Therefore, the renormalized operators in the RI'-MOM scheme, $\vec{O}^{\text{RI'}}(\mu)$, with $\vec{O} = (O_1, \ldots O_5)$, can be written in terms of bare lattice operators $\vec{O}^{\text{bare}}(a)$ as

$$
\vec{O}^{\text{RI'}}(\mu) = Z_O(\mu a) \vec{O}^{\text{bare}}(a)
\tag{3.21}
$$

where $Z_O(\mu a)$ is a 5×5 renormalization matrix. We note that in pure QCD the operator O_1 mixes only with O_2, with scale independent coefficients, whereas the full 5×5 renormalization matrix is necessary in general when e.m. corrections are included.

With regularizations which respect chiral symmetry the four-fermion operator relevant for the leptonic weak decay, O_1, renormalizes multiplicatively. If instead of using Wilson fermions, we used a lattice formulation with good chiral properties, such as domain wall fermions, the corresponding discussion would be restricted to the single operator O_1 which transforms as the $(8,1)$ representation under $SU(3)_L \times SU(3)_R$ chiral symmetry for the quarks.

According to Eqs. (1.103), (1.105) we rewrite Eq. (3.21) in the form

$$\vec{O}^{\mathrm{RI'}} = Z_O^{\mathrm{QED}} \left[(Z_O^{\mathrm{QED}})^{-1} Z_O (Z_O^{\mathrm{QCD}})^{-1}\right] Z_O^{\mathrm{QCD}} \vec{O}^{\mathrm{bare}} = Z_O^{\mathrm{QED}} \, \mathcal{R} \, Z_O^{\mathrm{QCD}} \, \vec{O}^{\mathrm{bare}} \tag{3.22}$$

where Z_O^{QCD} is the mixing matrix in pure QCD (corresponding to $\alpha_{\mathrm{em}} = 0$), and

$$Z_O^{\mathrm{QED}} \equiv 1 + \frac{\alpha_{\mathrm{em}}}{4\pi} \delta Z_O^{\mathrm{QED}} \tag{3.23}$$

is the pure, perturbative QED mixing matrix (corresponding to $\alpha_s = 0$). Using Eq. (1.105) , Eq. (3.22) is written as

$$\vec{O}^{\mathrm{RI'}} = \left[1 + \frac{\alpha_{\mathrm{em}}}{4\pi} \left(\delta Z_O^{\mathrm{QED}} + \eta_O\right)\right] Z_O^{\mathrm{QCD}} \, \vec{O}^{\mathrm{bare}} \, . \tag{3.24}$$

As already mentioned, pure QCD corrections in Eq. (3.24) only induce the mixing of the operator O_1 with the operator O_2. This mixing produces the renormalized QCD operators

$$O_1^\chi \equiv (Z_O^{\mathrm{QCD}} \vec{O}^{\mathrm{bare}})_1 = \bar{q}_2 \gamma^\mu \left[Z_V^{(0)} - Z_A^{(0)} \gamma_5\right] q_1 \, \bar{\nu}_\ell \gamma_\mu (1 - \gamma_5)\ell \, ,$$

$$O_2^\chi \equiv (Z_O^{\mathrm{QCD}} \vec{O}^{\mathrm{bare}})_2 = \bar{q}_2 \gamma^\mu \left[Z_V^{(0)} + Z_A^{(0)} \gamma_5\right] q_1 \, \bar{\nu}_\ell \gamma_\mu (1 - \gamma_5)\ell \, , \tag{3.25}$$

which, similarly to the corresponding continuum operators, belong respectively to the $(8,1)$ and $(1,8)$ chiral representations with respect to a rotation of the quark fields [53]. These are the combinations entering on the r.h.s. of Eq. (3.24).

When we include the e.m. corrections at $O(\alpha_{\mathrm{em}})$, the matrices $\delta Z_O^{\mathrm{QED}}$ and η_O in Eq. (3.24) induce, in general, the mixing of O_1^χ with the full basis of operators in Eq. (3.20). As shown in Appendix 6.2, however, in the twisted-mass formulation used in this work the only relevant chirality mixing is the one between the operators O_1 with O_2. Indeed, the mixing coefficients with the operators O_3 and O_4 are found to be odd in the parameter $\bar{r} \equiv r_1 r_\ell = -r_2 r_\ell$, defined by the product of the Wilson r-parameters of the valence quarks and the lepton (with $r_2 = -r_1$ in our procedure). Therefore, taking the average over the values of the parameter $\bar{r}$ (with $\bar{r} = \pm 1$) when computing the amplitude, eliminates the mixing with O_3 and O_4. Moreover, the matrix element of the operator O_5 between a pseudoscalar meson and the vacuum vanishes, so that the mixing with the operator O_5 cannot contribute to the decay rate. Therefore, Eq. (3.24) for the renormalized operator $O_1^{\mathrm{RI'}}$ simplifies to

$$
\begin{aligned}
O_1^{\mathrm{RI'}}(\mu) &= \left[1 + \frac{\alpha_{\mathrm{em}}}{4\pi} \left(\delta Z^{\mathrm{QED}}(\mu a)_{11} + \eta(\mu a, \alpha_s(1/a))_{11}\right)\right] O_1^\chi(a) + \\
&+ \frac{\alpha_{\mathrm{em}}}{4\pi} \left(\delta Z_{12}^{\mathrm{QED}} + \eta(\alpha_s(1/a))_{12}\right) O_2^\chi(a) ,
\end{aligned} \tag{3.26}
$$

where we have explicitly indicated the dependence of the various terms on α_s and the renormalization scale. Since the mixing of the *bona fide* $(8,1)$ operator O_1^χ with O_2^χ is a consequence of the explicit chiral symmetry breaking of Wilson-like fermions on the lattice, the corresponding coefficient is due to lattice artefacts and can only be a function of the lattice bare coupling constant $\alpha_s(1/a)$ [53].

We are now in a position to collect the results of the previous subsections in order to provide the final expression relating the renormalized operator $O_1^{\text{W-reg}}$ in the W-regularization to the lattice bare operators O_1 and O_2 in Eq. (3.20) at first order in α_{em}. Combining Eqs. (3.19) and (3.26) and choosing $\mu = 1/a$ as renormalization scale in the intermediate RI'-MOM scheme we obtain:

$$
\begin{aligned}
O_1^{\text{W-reg}}(M_W) &= O_1^\chi(a) + \frac{\alpha_{\text{em}}}{4\pi}\left[2\left(1 - \frac{\alpha_s(1/a)}{4\pi}\right)\log\left(a^2 M_W^2\right) + C^{\text{W-RI'}} + \delta Z_{11}^{\text{QED}}(1/a) + \right. \\
&\quad + \left. \eta_{11}(\alpha_s(1/a))\right]O_1^\chi(a) + \frac{\alpha_{\text{em}}}{4\pi}\left[\delta Z_{12}^{\text{QED}} + \eta_{12}(\alpha_s(1/a))\right]O_2^\chi(a) ,
\end{aligned} \tag{3.27}
$$

where $O_{1,2}^\chi$ are the renormalized QCD operators defined in Eq. (3.25). Using the results of Ref. [10], obtained in perturbation theory at order $O(\alpha_s^0)$ and collected in Appendix 6.2, we have determined the values for the matching and mixing coefficients,

$$
\begin{aligned}
C^{\text{W-RI'}} &= -5.7825 + 1.2373\,\xi , \\
\delta Z_{11}^{\text{QED}}(1/a) &= -9.7565 - 1.2373\,\xi \quad , \quad \delta Z_{12}^{\text{QED}} = -0.5357 ,
\end{aligned} \tag{3.28}
$$

where ξ is the photon gauge parameter ($\xi = 0\,(1)$ in the Feynman (Landau) gauge). Such matching factors depend, of course, on the lattice discretization of the full theory action. The above results are valid for twisted-mass (or Wilson) fermions and naive QED gauge action. It is worth noting that the renormalized operator in the W-regularization scheme is gauge independent, at any order of perturbation theory. In particular, as shown by Eq. (3.28), at first order in α_{em} and at zero order in α_s the gauge dependence of the matching coefficient of O_1^χ cancels in the sum $C^{\text{W-RI'}} + \delta Z_{11}^{\text{QED}} = -15.539$. By contrast, for the matching coefficient of O_2^χ, the two terms $\delta Z_{12}^{\text{QED}}$ and η_{12} are separately gauge independent.

Since the renormalization corrections here discussed are related to the operators O_i defined in Eq. (3.20) and mediating the physical process of interest, we stress that the above expression (3.27) is valid also for semileptonic decays of hadrons.

In the next chapter we will use the results of the present section in order to provide the final numerical expression relating the renormalized operator $O_1^{\text{W-reg}}$ in the W-regularization to the lattice bare operators O_1 and O_2 at first order in α_{em} which enter in our calculation.

Having formulated the problem of calculating Γ_0 in terms of the evaluation of correlation functions involving the effective Hamiltonian in Eq. (3.9) we are now in a position to discuss the calculation of $\Delta\Gamma_0(L)$, the first term on the right-hand side of the master formula Eq. (4.9).
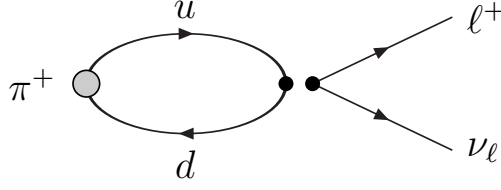
Figure 3.3.1: Correlation function used to calculate the amplitude for the leptonic decay of the pion in pure QCD. The two black filled circles represent the local current-current operator $(\bar{d}\gamma_L^{\mu}u)\,(\bar{\nu}_\ell\gamma_\mu\ell)$; the circles are displaced for convenience.

3.3 STRUCTURE OF THE CALCULATION

In this section we begin our explanation of how the calculations of the amplitudes for the processes $\pi^+ \to \ell^+\nu$ and $\pi^+ \to \ell^+\nu\gamma$ are to be performed. Before entering into the details however, we discuss more extensively the structure of the different terms appearing in Eq. (4.9).

Since we add and subtract the same perturbative quantity Γ_0^{pt}, we find it convenient to choose this to be the virtual decay rate for a point-like pion computed in the W-regularization. In this way we obtain the important advantage that the difference of the first two terms $(\Delta\Gamma_0(L))$ and the sum of the last two terms $(\Gamma^{\mathrm{pt}}(\Delta E))$ on the r.h.s. of Eq. (4.9) are separately ultraviolet and infrared finite.

Let $\sqrt{Z_\ell}$ be the contribution to the decay amplitude from the electromagnetic wave-function renormalization of the final state lepton (see the diagram in Fig. 3.4.1(d)). An important simplifying feature of this calculation is that Z_ℓ cancels in the difference $\Gamma_0 - \Gamma_0^{\mathrm{pt}}$. This is because in any scheme and using the same value of the decay constant f_π, the contribution from the diagram in Fig. 3.4.1(d) computed non-perturbatively or perturbatively with the point-like approximation are the same. Thus we only need to calculate Z_ℓ directly in infinite volume and include it in the second term on the right-hand side of Eq. (4.9). As a result of this cancellation it is convenient to rewrite Γ_0 and Γ_0^{pt} in the form:

$$\Gamma_0 = \Gamma_0^{\mathrm{tree}} + \Gamma_0^{\alpha} + \Gamma_0^{(\mathrm{d})} \quad \text{and} \quad \Gamma_0^{\mathrm{pt}} = \Gamma_0^{\mathrm{tree}} + \Gamma_0^{\alpha,\mathrm{pt}} + \Gamma_0^{(\mathrm{d}),\mathrm{pt}}, \tag{3.29}$$

where the superscript tree indicates the width in the absence of electromagnetic effects, (d) denotes the contribution from the leptonic wave function renormalization and the index α represents the remaining contributions of $O(\alpha_{em})$ other than those proportional to Z_ℓ. In this notation the above discussion can be summarized by saying that $\Gamma_0^{(\mathrm{d})} = \Gamma_0^{(\mathrm{d}),\mathrm{pt}}$ and that the calculation of $\Delta\Gamma_0(L)$ at $O(\alpha_{em})$ reduces to that of computing $\Gamma_0^{\alpha} - \Gamma_0^{\alpha,\mathrm{pt}}$.

Having eliminated the need to include the effects of the lepton's wave-function renormalization from the evaluation of $\Delta\Gamma_0(L)$, we need to make the corresponding modification in the factor(s) relating the lattice and W regularizations. This simply amounts to subtracting the term corresponding to the matching between the lattice to W regularizations of the lepton wave function renormalization diagram. Thus, we can avoid calculating the effects of the lepton's wave-function renormalization in $\Delta\Gamma_0(L)$ by neglecting the diagram in Fig. 3.4.1(d)

and the corresponding diagram with the point-like pion, and simply replacing $O_1^{\text{W}-\text{reg}}$ in Eq.(3.10) by $\tilde{O}_1^{\text{W}-\text{reg}}$ in which the contribution to the matching factor from the lepton wave function renormalization constant is subtracted.

Of course $\Gamma_0^{\text{(d),pt}}$ needs to be computed for the second term on the right-hand side of Eq. (4.9). This is a straightforward perturbative calculation in infinite-volume and gives [10]

$$\Gamma_0^{\text{(d),pt}} = \Gamma_0^{\text{tree}} \frac{\alpha_{em}}{4\pi} \left\{ \log \left(\frac{m_\ell^2}{M_W^2} \right) - 2 \log \left(\frac{m_\gamma^2}{m_\ell^2} \right) - \frac{9}{2} \right\} , \tag{3.30}$$

where we use the W-regularization for the ultra-violet divergences and have introduced a mass m_γ for the photon in order to regulate the infrared divergences. The explicit expression for Γ_0^{tree} is given in Eq. (3.35) below. Using the W-regularization we naturally work in the Feynman gauge, but note that with m_γ as the infrared regulator the result for Z_ℓ is generally gauge-dependent. For example, using dimensional regularization for the ultraviolet divergences and m_γ as the infrared regulator leads to a gauge dependent result for this single diagram (gauge invariance is restored of course for $\Gamma^{\text{pt}}(\Delta E)$).

In summary therefore, we need to compute the two quantities

$$\Delta \Gamma_0(L) = \tilde{\Gamma}_0^\alpha - \Gamma_0^{\alpha,\text{pt}} \qquad \text{and} \qquad \Gamma^{\text{pt}}(\Delta E) = \Gamma_0^{\text{tree}} + \Gamma_0^{\alpha,\text{pt}} + \Gamma_0^{\text{(d),pt}} + \Gamma_1(\Delta E) , \tag{3.31}$$

where $\tilde{\Gamma}_0^\alpha$ corresponds to Γ_0^α using $\tilde{O}_1^{\text{W}-\text{reg}}$ instead of $O_1^{\text{W}-\text{reg}}$. Note that $\Delta \Gamma_0(L)$ and $\Gamma^{\text{pt}}(\Delta E)$ are separately infrared finite and the result of the calculation of these two quantities does not depend on the infrared cutoff. In particular, this means that the infrared cutoff can be chosen in two different ways for the two quantities. We have decided to give a mass to the photon in the perturbative calculation of $\Gamma^{\text{pt}}(\Delta E)$, whereas for $\Delta \Gamma_0(L)$ a possible convenient choice is to use the finite volume as the infrared regulator.

In the following two sections we discuss the calculation of $\Delta \Gamma_0(L)$ and $\Gamma^{\text{pt}}(\Delta E)$ respectively.

3.4 CALCULATION OF $\Delta \Gamma_0(L)$

In this section we describe the calculation of the first term on the right-hand side of Eq. (4.9), $\Delta \Gamma_0(L)$, at $O(\alpha_{em})$. We start however, by briefly recalling the calculation of Γ_0 at $O(\alpha_{em}^0)$, i.e. without electromagnetism.

3.4.1 CALCULATION OF Γ_0 AT $O(\alpha_{em}^0)$

Without electromagnetic corrections we need to compute the correlation function sketched in Fig. 3.3.1, which is a completely standard calculation. Since the leptonic terms are factorized from the hadronic ones, the amplitude is simply given by

$$\begin{aligned} \bar{u}_{\nu_\ell \, \alpha}(p_{\nu_\ell}) \, (M_0)_{\alpha\beta} \, v_{\ell \, \beta}(p_\ell) &= \frac{G_F}{\sqrt{2}} V_{ud}^* \, \langle \, 0 \, | \, \bar{d}\gamma^\nu \gamma^5 u \, | \pi^+(p_\pi) \rangle \, \left[\bar{u}_{\nu_\ell}(p_{\nu_\ell}) \gamma_\nu (1 - \gamma^5) \, v_\ell(p_\ell) \right] \\ &= \frac{iG_F f_\pi}{\sqrt{2}} V_{ud}^* p_\pi^\nu \, \left[\bar{u}_{\nu_\ell}(p_{\nu_\ell}) \gamma_\nu (1 - \gamma^5) \, v_\ell(p_\ell) \right] . \end{aligned} \tag{3.32}$$

Here u, d in the matrix element represent the quark fields with the corresponding flavor quantum numbers and u_{ν_ℓ} and v_ℓ the spinors of the leptons defined by the subscript. The hadronic matrix element, and hence the decay constant f_π, are obtained in the standard way by computing the correlation function

$$C_0(t) \equiv \sum_{\vec{x}} \langle 0 \,|\left(\bar{d}(\vec{0},0)\gamma^4\gamma^5\, u(\vec{0},0)\right) \phi^\dagger(\vec{x},-t) \,|0\rangle \simeq \frac{Z_0^\phi}{2m_\pi^0} e^{-m_\pi^0 t}\, A_0\,, \qquad (3.33)$$

where $\phi^\dagger$ is an interpolating operator which can create the pion out of the vacuum, $Z_0^\phi \equiv \langle \pi^+(\vec{0})|\phi^\dagger(0,\vec{0})\,|0\rangle$ and $A_0 \equiv \langle 0\,|\,\bar{d}\gamma^4\gamma^5\, u\,|\pi^+(\vec{0})\rangle_0$. We have chosen to place the weak current at the origin and to create the pion at negative time $-t$, where t and $T-t$ are sufficiently large to suppress the contributions from heavier states and from the backward propagating pions (this latter condition may be convenient but is not necessary). The subscript or superscript 0 here denotes the fact that the calculation is performed at $O(\alpha_{em}^0)$, i.e. in the absence of electromagnetism. Z_0^ϕ is obtained from the two-point correlation function of two ϕ operators:

$$C_0^{\phi\phi}(t) \equiv \sum_{\vec{x}} \langle 0\,|T\{\phi(\vec{0},0)\,\phi^\dagger(\vec{x},-t)\}\,|0\rangle \simeq \frac{(Z_0^\phi)^2}{2m_\pi^0}\, e^{-m_\pi^0 t}\,. \qquad (3.34)$$

For convenience we take ϕ to be a local operator (e.g. at $(\vec{x}, -t)$ in Eq. (4.23)), but this is not necessary for our discussion. Any interpolating operator for the pion on the chosen time slice would do equally well.

Having determined A_0 and hence the amplitude $\bar{u}_{\nu_\ell\,\alpha}(p_{\nu_\ell})(M_0)_{\alpha\beta}\,v_{\ell\,\beta}(p_\ell)$, the $O(\alpha_{em}^0)$ contribution to the decay width is readily obtained

$$\Gamma_0^{\text{tree}}(\pi^+ \to \ell^+\nu_\ell) = \frac{G_F^2\,|V_{ud}|^2 f_\pi^2}{8\pi}\, m_\pi\, m_\ell^2 \left(1 - \frac{m_\ell^2}{m_\pi^2}\right)^2\,. \qquad (3.35)$$

In this equation we use the label tree to denote the absence of electromagnetic effects since the subscript 0 here indicates that there are no photons in the final state.

3.4.2 CALCULATION AT $O(\alpha_{em})$

We now consider the one-photon exchange contributions to the decay $\pi^+ \to \ell^+\nu_\ell$ and show the corresponding six connected diagrams in Fig. 3.4.1 and the disconnected diagrams in Fig. 3.4.2. By "disconnected" here we mean that there is a sea-quark loop connected, as usual, to the remainder of the diagram by a photon and/or gluons (the presence of the gluons is implicit in the diagrams). The photon propagator in these diagrams in the Feynman gauge and in infinite (Euclidean) volume is given by

$$\Delta_{\mu\nu}(x_1, x_2) = \delta_{\mu\nu} \int \frac{d^4 k}{(2\pi)^4}\, \frac{e^{ik\cdot(x_1-x_2)}}{k^2}\,. \qquad (3.36)$$
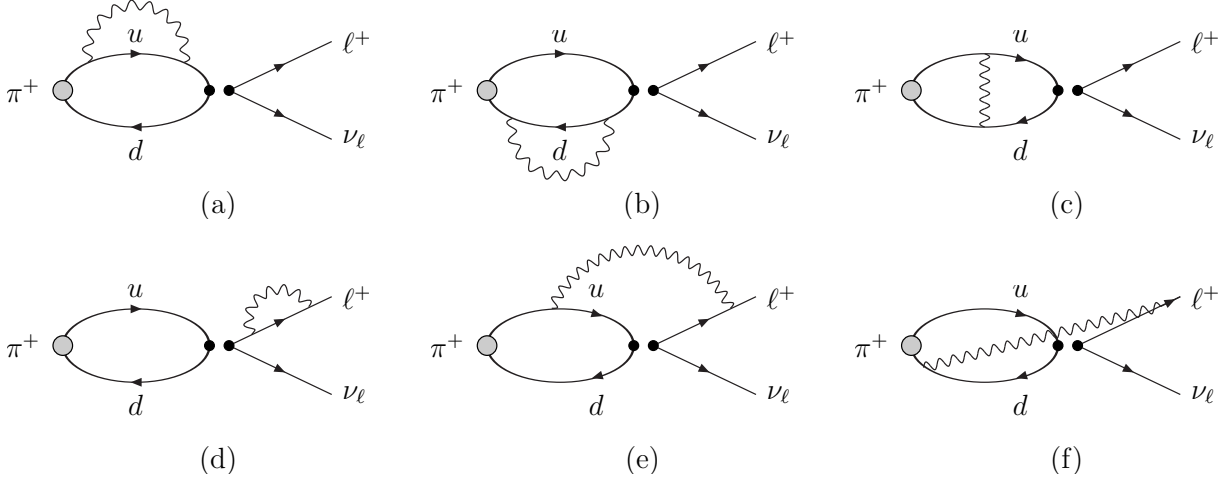
Figure 3.4.1: Connected diagrams contributing at $O(\alpha_{em})$ contribution to the amplitude for the decay $\pi^+ \to \ell^+ \nu_l$.

In a finite volume the momentum integration is replaced by a summation over the momenta which are allowed by the boundary conditions. For periodic boundary conditions, we can neglect the contributions from the zero-mode $k = 0$ since a very soft photon does not resolve the structure of the pion and its effects cancel in $\Gamma_0 - \Gamma_0^{\text{pt}}$ in Eq. (4.9). Although we evaluate $\Gamma_0 + \Gamma_1(\Delta E)$ (see Eq. (3.2)) in perturbation theory directly in infinite volume, we note that the same cancellation would happen if one were to compute $\Gamma_1(\Delta E)$ also in a finite volume. Moreover from a spectral analysis we conclude that such a cancellation also occurs in the Euclidean correlators from which the different contributions to the decay rates are extracted. For this reason in the following Γ_0 and Γ_0^{pt} are evaluated separately but using the following expression for the photon propagator in finite volume:

$$\Delta_{\mu\nu}(x_1, x_2) = \delta_{\mu\nu} \frac{1}{L^4} \sum_{k=\frac{2\pi}{L}n;\, k \neq 0} \frac{e^{ik\cdot(x_1-x_2)}}{4\sum_\rho \sin^2 \frac{k_\rho}{2}} , \tag{3.37}$$

where all quantities are in lattice units and the expression corresponds to the simplest lattice discretization. k, n, x_1 and x_2 are four component vectors and for illustration we have taken the temporal and spatial extents of the lattice to be the same (L).

For other quantities, the presence of zero momentum excitations of the photon field is a subtle issue that has to be handled with some care (see Sec. 1.9). In the case of the hadron spectrum the problem has been studied in [54] and, more recently in [17, 58], where it has been shown, at $O(\alpha_{em})$, that the quenching of zero momentum modes corresponds in the infinite-volume limit to the removal of sets of measure zero from the functional integral and that finite volume effects are different for the different prescriptions.

We now divide the discussion of the diagrams in Fig. 3.4.1 and Fig. 3.4.2 into three classes: those in which the photon is attached at both ends to the quarks (diagrams 3.4.1(a)-3.4.1(c) and 3.4.2(a), (b) and (d)), those in which the photon propagates between one of the quarks
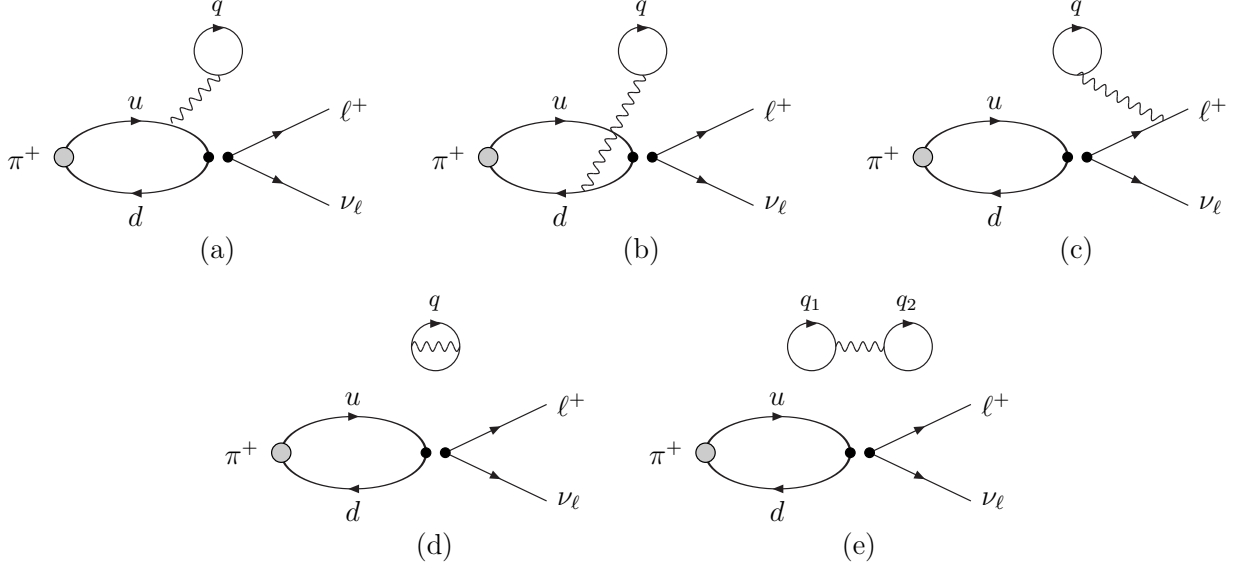
Figure 3.4.2: Disconnected diagrams contributing at $O(\alpha_{em})$ contribution to the amplitude for the decay $\pi^+ \to \ell^+ \nu_\ell$. The curly line represents the photon and a sum over quark flavors q, q_1 and q_2 is to be performed.

and the outgoing lepton (diagrams 3.4.1(e), 3.4.1(f) and 3.4.2(c)) and finally diagram 3.4.1(d) which corresponds to the mass and wave-function normalization of the charged lepton. We have already discussed the treatment of the wave function renormalization of the lepton in Sec. 3.3 so we now turn to the remaining diagrams.

3.4.2.1 THE EVALUATION OF DIAGRAMS FIG. 3.4.1(A)-(C) AND FIG. 3.4.2(A),(B) AND (D)

We start by considering the connected diagrams 3.4.1(a)-(c). For these diagrams, the leptonic contribution to the amplitude is contained in the factor $\left[\bar{u}_{\nu_\ell}(p_{\nu_\ell})\gamma^\nu(1 - \gamma^5)\, v_\ell(p_\ell)\right]$ and we need to compute the Euclidean hadronic correlation function

$$C_1(t) = -\frac{1}{2} \int d^3\vec{x}\, d^4x_1\, d^4x_2\; \langle 0|T\{J_W^\nu(0)\, j_\mu(x_1)j_\nu(x_2)\phi^\dagger(\vec{x}, -t)\}\,|\,0\rangle\; \Delta_{\mu\nu}(x_1, x_2)\,. \tag{3.38}$$

where T represents time-ordering, J_W^ν is the V–A current $\bar{d}\gamma^\nu(1 - \gamma^5)\, u$ and we take $-t < 0$. j_μ is the hadronic component of the electromagnetic current and we find it convenient to include the charges of the quarks e_f in the definition of j:

$$j_\mu(x) = \sum_f e_f e\, \bar{f}(x)\gamma_\mu f(x)\,, \tag{3.39}$$

where the sum is over all quark flavors f. The factor of $1/2$ is the standard combinatorial one.

The computations are performed in Euclidean space and in a finite-volume with the photon propagator $\Delta_{\mu\nu}$ given in Eq. (3.37) (or the corresponding expression for other lattice discretizations). The absence of the zero mode in the photon propagator implies a gap between M_π and the energies of the other eigenstates. Provided one can separate the contributions of these heavier states from that of the pion, one can perform the continuation of the correlation function in Eq. (3.38) from Minkowski to Euclidean space without encountering any singularities. From the correlation function $C_1(t)$ we obtain the electromagnetic shift in the mass of the pion and also a contribution to the physical decay amplitude, as we now explain. For sufficiently large t the correlation function is dominated by the ground state, i.e. the pion, and we have

$$C_0(t) + C_1(t) \simeq \frac{e^{-M_\pi t}}{2M_\pi} Z^\phi \langle 0 | J_W^0(0) | \pi^+ \rangle , \tag{3.40}$$

where the electromagnetic terms are included in all factors (up to $O(\alpha_{em})$). Writing $M_\pi = M_\pi^0 + \delta M_\pi$, where δM_π is the $O(\alpha_{em})$ mass shift,

$$e^{-M_\pi t} \simeq e^{-M_\pi^0 t} \left(1 - \delta M_\pi \, t\right) \tag{3.41}$$

so that $C_1(t)$ is of the schematic form

$$C_1(t) = C_0(t) \left(c_1 \, t + c_2\right) . \tag{3.42}$$

By determining c_1 we obtain the electromagnetic mass shift, $\delta M_\pi = -c_1$, and from c_2 we obtain the electromagnetic correction to $Z^\phi \langle 0 | J_W(0) | \pi^+ \rangle / 2M_\pi$. Note that δM_π is gauge invariant and infrared finite, whereas the coefficient c_2 obtained from these diagrams is neither.

In order to obtain the contribution to the $\pi \to \ell\nu_\ell$ decay amplitude A we need to remove the factor $(e^{-M_\pi t}/2M_\pi)Z^\phi$ on the right-hand side of Eq. (3.40), including the $O(\alpha_{em})$ corrections to this factor. Having determined c_1, we are in a position to subtract the corrections present in M_π. The $O(\alpha_{em})$ corrections to Z^ϕ are determined in the standard way, by performing the corresponding calculation to $C_1(t)$ but with the axial current A replaced by ϕ:

$$
\begin{aligned}
C_1^{\phi\phi}(t) &= -\frac{1}{2} \int d^3\vec{x} \, d^4x_1 \, d^4x_2 \, \langle 0|T\{\phi(\vec{0},0) \, j_\mu(x_1) j_\nu(x_2) \phi^\dagger(\vec{x},t)\} \, |0\rangle \, \Delta_{\mu\nu}(x_1, x_2) \\
&= C_0^{\phi\phi}(t)(c_1 t + c_2^{\phi\phi}) .
\end{aligned}
\tag{3.43}
$$

We finally obtain

$$Z^\phi = Z_0^\phi \left(1 + \frac{1}{2}\left(c_2^{\phi\phi} - \frac{c_1}{M_\pi^0}\right)\right) , \tag{3.44}$$

and the $O(\alpha_{em})$ contribution to the amplitude from these three diagrams is

$$\delta A = A_0 \left(c_2 - \frac{c_2^{\phi\phi}}{2} - \frac{c_1}{2M_\pi^0}\right) . \tag{3.45}$$

For these three diagrams the $O(\alpha_{em})$ term can be simply considered as a correction to f_π. Note however, that such an "f_π" would not be a physical quantity as it contains infrared divergences.

The treatment of the disconnected diagrams in Figs. 3.4.2(a), (b) and (d) follows in exactly the same way. These diagrams contribute to the electromagnetic corrections to both the pion mass and the decay amplitude in an analogous way to the discussion of the connected diagrams above. It is standard and straightforward to write down the corresponding correlation functions in terms of quark propagators. We do not discuss here the different possibilities for generating the necessary quark propagators to evaluate the diagrams; for example we can imagine using sequential propagators or some techniques to generate all-to-all quark propagators.

3.4.2.2 THE EVALUATION OF DIAGRAMS FIG. 3.4.1(E)-(F)

For these diagrams the leptonic and hadronic contributions do not factorize and indeed the contribution cannot be written simply in terms of the parameter f_π. We start by considering the Minkowski space quantity

$$
\begin{aligned}
\bar{u}_{\nu_\ell \alpha}(p_{\nu_\ell})(\bar{M}_1)_{\alpha\beta} v_{\ell\beta}(p_\ell) &= -\int d^4x_1 \, d^4x_2 \, \langle 0| \, T(j_\mu(x_1) J_W^\nu(0)) \, |\pi\rangle \\
&\times iD_{\mu\rho}(x_1,x_2)\big\{\bar{u}_{\nu_\ell}(p_{\nu_\ell})\gamma^\nu(1-\gamma^5)(iS_M(x_2))\gamma_\rho v_\ell(p_\ell)\big\}e^{ip_\ell \cdot x_2} ,
\end{aligned}
\tag{3.46}
$$

where iS_M and iD are the lepton and (Feynman gauge) photon propagators respectively in Minkowski space. In order to demonstrate that we can obtain the $O(\alpha_{em})$ corrections to the decay amplitude from a Euclidean space correlation function, we use the reduction formula to rewrite the expression in Eq. (3.46) as

$$
\bar{u}_{\nu_\ell \alpha}(p_{\nu_\ell})(\bar{M}_1)_{\alpha\beta} v_{\ell\beta}(p_\ell) = i \lim_{k_0 \to m_\pi}(k_0{}^2 - M_\pi^2)\int d^4x_1 \, d^4x_2 \, d^4x \, e^{-ik^0 x^0}
$$

$$
\langle 0|T(j_\mu(x_1)J_W^\nu(0)\pi(x))|0\rangle \, iD_{\mu\rho}(x_1,x_2)\big[\bar{u}_{\nu_\ell}(p_{\nu_\ell})\gamma^\nu(1-\gamma^5)(iS_M(x_2))\gamma_\rho v_\ell(p_\ell)\big]e^{ip_\ell \cdot x_2} ,
\tag{3.47}
$$

where $\pi(x)$ is the field which creates a pion with amplitude 1. On the other hand the Euclidean space correlation function which we propose to compute is

$$
\begin{aligned}
\bar{C}_1(t)_{\alpha\beta} &= -\int d^3\vec{x} \, d^4x_1 \, d^4x_2 \, \langle 0|T\big\{J_W^\nu(0) \, j_\mu(x_1)\phi^\dagger(\vec{x},-t)\big\}|0\rangle \, \Delta_{\mu\rho}(x_1,x_2) \\
&\times \big(\gamma^\nu(1-\gamma^5)S(0,x_2)\gamma_\rho\big)_{\alpha\beta} \, e^{E_\ell t_2}e^{-i\vec{p}_\ell \cdot \vec{x}_2}.
\end{aligned}
\tag{3.48}
$$

Here S and Δ are Euclidean propagators, and α, β are spinor indices. Similarly to the discussion in Sec. 4.2.1, provided that the pion is the lightest hadronic state then for large t, $\bar{C}_1(t)$ is dominated by the matrix element with a single pion in the initial state.

In view of the factor $e^{E_\ell t_2}$ on the right-hand side of Eq. (3.48), the new feature in the evaluation of the diagrams in Fig. 3.4.1 (e) and (f) is that we need to ensure that the t_2
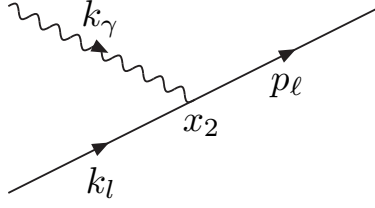
Figure 3.4.3: Zoom of the lepton-photon vertex at x_2 from the diagrams in Fig. 3.4.1(e) and (f).

integration converges as $|t_2| \to \infty$. For $t_2 < 0$ the convergence of the integral is improved by the presence of the exponential factor and so we limit the discussion to the case $t_2 \to \infty$. $E_\ell = \sqrt{m_\ell^2 + \vec{p}_\ell^2}$ is the energy of the outgoing charged lepton with three-momentum $\vec{p}_\ell$. To determine the $t_2 \to \infty$ behaviour, consider the lepton-photon vertex at x_2 from the diagrams in Fig. 3.4.1(e) and (f), redrawn in Fig. 3.4.3. k_ℓ and k_γ are the four-momentum variables in the Fourier transform of the propagators $S(x_2)$ and $\Delta_{\mu\rho}(x_1, x_2)$ respectively in Eqs. (3.46) - (3.48). The t_2 integration is indeed convergent as explicitly shown in [10].

1. The integration over $\vec{x}_2$ implies three-momentum conservation at this vertex so that in the sum over the momenta $\vec{k}_\ell + \vec{k}_\gamma = \vec{p}_\ell$, where p_ℓ is the momentum of the outgoing charged lepton.

2. The integrations over the energies $k_{4\ell}$ and $k_{4\gamma}$ lead to the exponential factor $e^{-(\omega_\ell + \omega_\gamma)t_2}$, where $\omega_\ell = \sqrt{\vec{k}_\ell^2 + m_\ell^2}$, $\omega_\gamma = \sqrt{\vec{k}_\gamma^2 + m_\gamma^2}$, and m_γ is the mass of the photon introduced as an infra-red cut-off. The large t_2 behaviour is therefore given by the factor $e^{-(\omega_\ell + \omega_\gamma - E_\ell)t_2}$.

3. A simple kinematical exercise shows that in the sum over $\vec{k}_\gamma$ (with $\vec{k}_\ell = \vec{p}_\ell - \vec{k}_\gamma$), the minimum value of $\omega_\ell + \omega_\gamma$ is given by

$$(\omega_\ell + \omega_\gamma)_{\min} = \sqrt{(m_\ell + m_\gamma)^2 + \vec{p}_\ell^2} \,. \tag{3.49}$$

4. Thus for non-zero m_γ, the exponent in $e^{-(\omega_\ell + \omega_\gamma - E_\ell)t_2}$ for large t_2 is negative for every term in the summation over k_γ and the integral over t_2 is convergent so that the continuation from Minkowski to Euclidean space can be performed.

5. Note that the integration over t_2 is also convergent if we set $m_\gamma = 0$ but remove the $\vec{k} = 0$ mode in finite volume. In this case $\omega_\ell + \omega_\gamma > E_\ell + [1 - (p_\ell/E_\ell)]|\vec{k}_{\min}|$.

In summary the t_2 integration is convergent because for every term in the sum over momenta $\omega_\ell + \omega_\gamma > E_\ell$ and so for sufficiently large t we can write

$$\bar{C}_1(t)_{\alpha\beta} \simeq Z_0^\phi \frac{e^{-M_\pi^0 t}}{2M_\pi^0} (\bar{M}_1)_{\alpha\beta} \tag{3.50}$$

and the contribution from the diagrams of Fig. 3.4.1(e) and 3.4.1(f) is $\bar{u}_\alpha(p_{\nu_\ell})(\bar{M}_1)_{\alpha\beta} v_\beta(p_\ell)$. This completes the demonstration that the Minkowski-space amplitude (3.47) is equal to the pion contribution to the Euclidean correlation function (3.48), up to a factor Z_0^ϕ which accounts for the normalization of the pion field.

Again the evaluation of the correction to the amplitude from the disconnected diagram in Fig. 3.4.2(c) follows in an analogous way.

3.5 CALCULATION OF $\Gamma^{\mathrm{pt}}(\Delta E)$

The evaluation in perturbation theory of the total width $\Gamma^{\mathrm{pt}} = \Gamma_0^{\mathrm{pt}} + \Gamma_1^{\mathrm{pt}}$ in infinite volume, was performed by Berman and Kinoshita in 1958/9 [80, 87], using the Pauli-Villars regulator for the ultraviolet divergences and a photon mass to regulate the infrared divergences in both Γ_0^{pt} and Γ_1^{pt}. Γ_1^{pt} is the rate for process $\pi^+ \to \ell^+ \nu_\ell \gamma$ for a pointlike pion with the energy of the photon integrated over the full kinematic range. We have added the label pt in Γ_1^{pt} to remind us that the integration includes contributions from regions of phase space in which the photon is not sufficiently soft for the structure of the pion to be reliably neglected. We do not include this label when writing $\Gamma_1(\Delta E)$ because we envisage that ΔE is sufficiently small so that the pointlike approximation reproduces the full calculation.

In our calculation, Γ_0^{pt} is evaluated in the W-regularization, so that the ultra-violet divergences are replaced by logarithms of M_W. For convenience we rewrite here the expression for $\Gamma^{\mathrm{pt}}(\Delta E)$ from Eq. (3.31)

$$\Gamma^{\mathrm{pt}}(\Delta E) = \Gamma_0^{\mathrm{pt}} + \Gamma_1(\Delta E) = \Gamma_0^{\mathrm{tree}} + \Gamma_0^{\alpha,\mathrm{pt}} + \Gamma_0^{(\mathrm{d}),\mathrm{pt}} + \Gamma_1(\Delta E). \tag{3.51}$$

Γ_0^{tree} and $\Gamma_0^{(\mathrm{d}),\mathrm{pt}}$ have already been presented in Eqs. (3.35) and (3.30) respectively. In Ref. [10] the results of the remaining contributions to $\Gamma^{\mathrm{pt}}(\Delta E)$ have been given separately using a photon mass m_γ as the infrared regulator.

In the perturbative calculation the following Lagrangian for the interaction of a point-like pion with the leptons has been used:

$$\mathcal{L}_{\pi-\ell-\nu_\ell} = i\, G_F f_\pi V_{ud}^* \left\{ (\partial_\mu - ieA_\mu)\pi \right\} \left\{ \bar{\psi}_{\nu_\ell} \frac{1+\gamma_5}{2} \gamma^\mu \psi_\ell \right\} + \text{Hermitian conjugate}. \tag{3.52}$$

The corresponding Feynman rules are:

$$\pi^+ \;\text{----}\!\!\blacktriangleright\!\!\text{--}\bullet\!\!\!<^{\ell^+}_{\nu_\ell} \;=\; -iG_F f_\pi V_{ud}^* \, p_\pi^\mu \, \tfrac{1+\gamma^5}{2} \gamma_\mu$$

$$\pi^+ \;\text{----}\!\!\blacktriangleright\!\!\text{--}\bullet\!\!\!<^{\ell^+}_{\nu_\ell}{}^{\gamma^*} \;=\; ie\, G_F f_\pi V_{ud}^* \, g^{\mu\nu} \, \tfrac{1+\gamma^5}{2} \gamma_\mu \tag{3.53}$$

In addition the standard Feynman rules of scalar electromagnetism for the interactions of charged pions in an electromagnetic field have been used.

The $O(\alpha_{em})$ contribution of the pion wave function renormalization to $\Gamma_0^{\alpha,\mathrm{pt}}$ is obtained from the diagrams in Fig. 3.5.1, corresponding to those in Fig. 3.4.1(a), Fig. 3.4.1(b) and Fig. 3.4.1(c) in the composite case. The remaining graphs contributing to $\Gamma_0^{\alpha,\mathrm{pt}}$ are the π-ℓ vertex corrections from the diagrams shown in Fig. 3.5.2 and their complex conjugates. These diagrams correspond to the diagrams Fig. 3.4.1(e) and Fig. 3.4.1(f) in the composite pion case. As for the contributions to $\Gamma_1(\Delta E)$, the real photon is emitted and absorbed by the pion (diagram (a) in Fig. 3.5.3), the charged lepton (diagram (b) in Fig. 3.5.3) or emitted by the pion and absorbed by the lepton or vice-versa (diagrams (c)–(f) in Fig. 3.5.3).
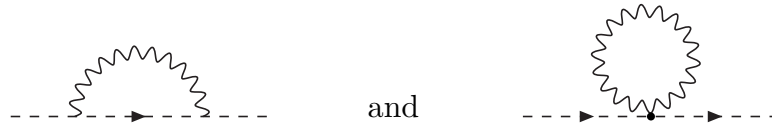
Figure 3.5.1: One loop diagrams contributing to the wave-function renormalization of a point-like pion.
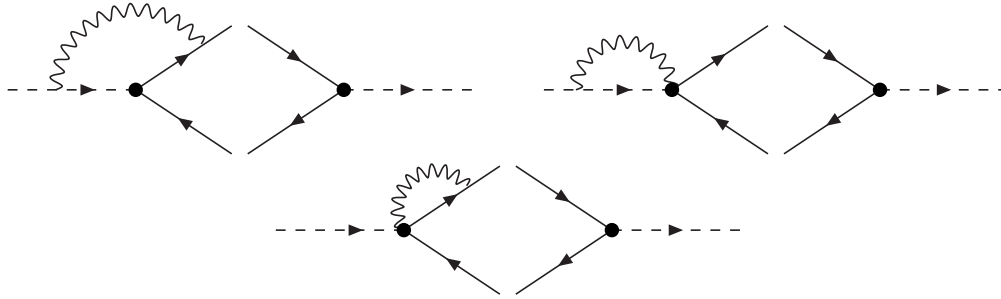
Figure 3.5.2: Radiative corrections to the pion-lepton vertex. The diagrams represent $O(\alpha_{em})$ contributions to Γ_0^{pt}. The left part of each diagram represents a contribution to the amplitude and the right part the tree-level contribution to the hermitian conjugate of the amplitude. The corresponding diagrams containing the radiative correction on the right-hand side of each diagram are also included.

We do not give here the separate expressions for the contributions to $\Gamma_0^{\alpha,\mathrm{pt}}$ and $\Gamma_1(\Delta E)$, referring the interested reader to [10] for further details on the calculation. We limit ourselves to combine the results in [10] in order to provide the final expression for $\Gamma^{\mathrm{pt}}(\Delta E)$. As
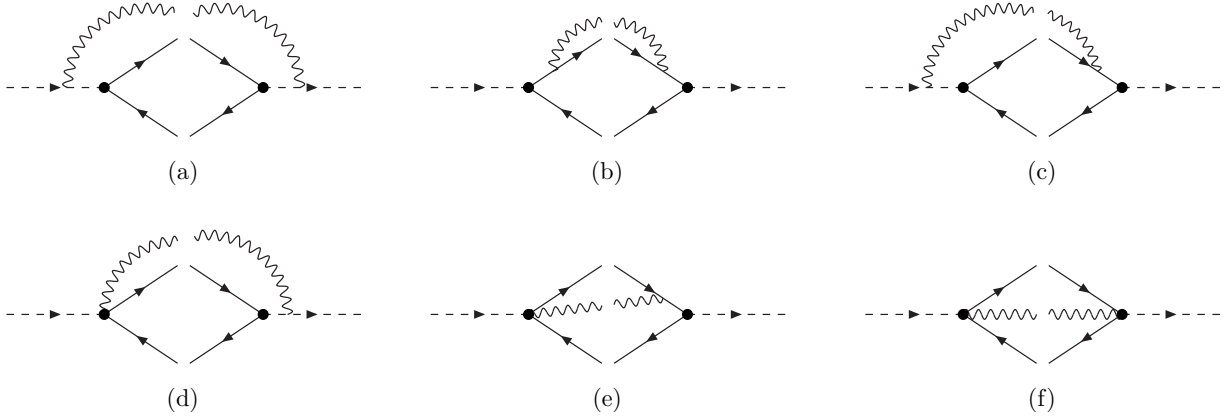
Figure 3.5.3: Diagrams contributing to $\Gamma_1(\Delta E)$. For diagrams (c), (d) and (e) the "conjugate" contributions in which the photon vertices on the left and right of each diagram are interchanged are also to be included.

expected the infrared cutoff cancels and one gets

$$
\Gamma^{\mathrm{pt}}(\Delta E) = \Gamma_0^{\mathrm{tree}} \times \left(1 + \frac{\alpha_{em}}{4\pi} \left\{ 3\log\left(\frac{M_\pi^2}{M_W^2}\right) + \log\left(r_\ell^2\right) - 4\log(r_E^2) + \frac{2 - 10 r_\ell^2}{1 - r_\ell^2}\log(r_\ell^2) \right. \right.
$$

$$
- 2\frac{1 + r_\ell^2}{1 - r_\ell^2}\ \log(r_E^2)\log(r_\ell^2) - 4\frac{1 + r_\ell^2}{1 - r_\ell^2}\ \mathrm{Li}_2(1 - r_\ell^2) - 3
$$

$$
+ \left[\frac{3 + r_E^2 - 6 r_\ell^2 + 4 r_E(-1 + r_\ell^2)}{(1 - r_\ell^2)^2}\ \log(1 - r_E) + \frac{r_E(4 - r_E - 4 r_\ell^2)}{(1 - r_\ell^2)^2}\ \log(r_\ell^2) \right.
$$

$$
\left. \left. \left. - \frac{r_E(-22 + 3 r_E + 28 r_\ell^2)}{2(1 - r_\ell^2)^2} - 4\frac{1 + r_\ell^2}{1 - r_\ell^2}\ \mathrm{Li}_2(r_E) \right] \right\} \right) , \tag{3.54}
$$

where $r_\ell = m_\ell/M_\pi$ and $r_E = 2\Delta E/M_\pi$ with $0 \leq r_E \leq 1 - r_\ell^2$. Note that the terms in square brackets in eq. (3.54) vanish when r_E goes to zero; in this limit $\Gamma^{\mathrm{pt}}(\Delta E)$ is given by its eikonal approximation.

The total rate is readily computed by setting r_E to its maximum value, namely $r_E = 1 - r_\ell^2$, giving

$$
\Gamma^{\mathrm{pt}} = \Gamma_0^{\mathrm{tree}} \times \left\{ 1 + \frac{\alpha_{em}}{4\pi} \left(3\log\left(\frac{M_\pi^2}{M_W^2}\right) - 8\log(1 - r_\ell^2) - \frac{3 r_\ell^4}{(1 - r_\ell^2)^2}\log(r_\ell^2) \right. \right. \tag{3.55}
$$

$$
\left. \left. - 8\frac{1 + r_\ell^2}{1 - r_\ell^2}\ \mathrm{Li}_2(1 - r_\ell^2) + \frac{13 - 19 r_\ell^2}{2(1 - r_\ell^2)} + \frac{6 - 14 r_\ell^2 - 4(1 + r_\ell^2)\log(1 - r_\ell^2)}{1 - r_\ell^2}\ \log(r_\ell^2) \right) \right\} .
$$

The result in Eq. (3.55) agrees with the well known results in literature [80, 81], which provides an important check of our calculation.

In the description of our method above, we limit the photon's energy to be smaller than ΔE to ensure that the photon is sufficiently soft for the pointlike approximation to be valid in the evaluation of $\Gamma_1(\Delta E)$. It is of course possible instead to impose a cut-off on the energy of the final-state lepton, requiring it to be close to its maximum value $E_\ell^{\max} = \frac{M_\pi}{2}(1 + r_\ell^2)$. For completeness we also give, up to $O(\Delta E_\ell)$, the distribution for $\Gamma^{\mathrm{pt}}(\Delta E_\ell)$ defined as

$$\Gamma^{\mathrm{pt}}(\Delta E_\ell) = \int_{E_\ell^{max} - \Delta E_\ell}^{E_\ell^{max}} dE' \, \frac{d\Gamma^{\mathrm{pt}}}{dE'_\ell} \,, \tag{3.56}$$

where $0 \le \Delta E_\ell \le (M_\pi - m_\ell)^2/(2M_\pi)$;

$$
\begin{aligned}
\Gamma^{\mathrm{pt}}(\Delta E_\ell) = \Gamma_0^{\mathrm{tree}} \times \Bigg\{ & 1 + \frac{\alpha_{em}}{4\pi} \Bigg[3\log\left(\frac{M_\pi^2}{M_W^2}\right) + 8\log\left(1 - r_\ell^2\right) - 7 \\
& + \log\left(r_\ell^2\right) \frac{3 - 7r_\ell^2 + 8\Delta E_\ell + 4\left(1 + r_\ell^2\right)\log\left(1 - r_\ell^2\right)}{1 - r_\ell^2} \\
& + \log\left(2\Delta E_\ell\right)\left(-8 - 4\frac{1 + r_\ell^2}{1 - r_\ell^2}\log\left(r_\ell^2\right)\right) \Bigg] \Bigg\}.
\end{aligned}
\tag{3.57}
$$

3.6 REGULARIZATION AND CANCELLATION OF INFRARED DIVERGENCES IN FINITE VOLUMES

In the previous section we have explicitly demonstrated the cancellation of infrared divergences in the perturbative quantity $\Gamma^{\mathrm{pt}}(\Delta E)$. This of course is simply the standard Bloch-Nordsieck cancellation [11]. In this section we discuss in more detail the cancellation of infrared divergences in

$$\Delta\Gamma_0(L) = \tilde{\Gamma}_0^\alpha - \Gamma_0^{\alpha,\mathrm{pt}} \,. \tag{3.58}$$

We have already explained in Sec. 3 that the contribution of the lepton's wave function renormalization in $\Delta\Gamma_0(L)$ is simply to introduce the tilde in $\tilde{\Gamma}_0^\alpha$, denoting that the corresponding contribution to the matching factor between the lattice and W-regularizations is to be removed. Here we concentrate on the remaining diagrams in Figs. 3.4.1 and 3.4.2 and the corresponding diagrams for the point-like meson.

Although the right-hand side of Eq. (3.58) is a difference of decay widths, since at this order the widths are linear in the $O(\alpha_{em})$ virtual amplitude, we can equivalently consider the difference of the $O(\alpha_{em})$ contributions to the amplitudes. In order to reduce statistical fluctuations when performing the sum over the gauge field configurations, we define the ratios

$$R^\alpha = \frac{\delta\tilde{A}^\alpha}{A^0} \,, \qquad R^{\alpha,\mathrm{pt}} = \frac{\delta A^{\alpha,\mathrm{pt}}}{A^0} \,, \tag{3.59}$$

where $\delta \tilde{A}^\alpha$ and $\delta A^{\alpha,\text{pt}}$ are the $O(\alpha_{em})$ amplitudes corresponding to the widths in Eq. (3.58). The non-perturbative amplitude $\delta \tilde{A}^\alpha$ is precisely the quantity that we have computed numerically in a lattice simulation [13, 16] (see Chapter 4). It is then combined with $\delta A^{\alpha,\text{pt}}$, for which we have given the explicit expression in infinite volume in Sec. 3.5.

In the calculation of $\delta A^{\alpha,\text{pt}}$ we set the mass of the photon to zero and consider the theory on a finite volume of length L, which will be used as an infrared regulator. The form of the vertices and propagators is the same as in the infinite volume (the ultraviolet cutoff is provided by the W-regularization), but the momenta are quantized $k_\mu = 2\pi/L \times n_\mu = 2\pi/(Na) \times n_\mu$ where $-\infty \leq n_\mu \leq +\infty$ and N is the number of lattice sites in one direction, which for simplicity we take to be the same in all directions.

The calculation of $\delta \tilde{A}^\alpha$ is performed non perturbatively on the same finite volume as in the perturbative case, but in a numerical simulation and with the photon propagator defined as in Eq. (3.37), which does not contain the zero mode. Indeed, as already discussed in Sec. 4.2, the zero mode does not contribute to the difference

$$\Delta R(L) = R^\alpha - R^{\alpha,\text{pt}} \,. \tag{3.60}$$

This is a gauge invariant, ultraviolet and infrared finite quantity and for these reasons its finite volume effects are expected to be comparable to those affecting the $O(\alpha_{em})$ corrections to the hadron masses (that are also gauge invariant, ultraviolet and infrared finite).

We should add that in principle any consistent regularization of the infrared divergences is acceptable. The main criterion for the choice of the infrared regulator will be determined by the precision of the terms remaining after the cancellation of the infrared divergences in a numerical simulation.

In the lattice simulation which we will present in the next chapter we have worked in the QED_L formulation of QED on a finite volume and the same zero-mode regularization for the photon propagator has been adopted in Ref. [88] for the perturbative calculation of $\Gamma_0^{\text{pt}}(L)$ (ultraviolet divergences have been regulated in the W-regularization scheme).

We conclude the present section illustrating the main results obtained in [88] (see also Ref. [70]). The point-like decay rate $\Gamma_0^{\text{pt}}(L)$ is given by

$$\Gamma_0^{\text{pt}}(L) = \left(1 + Y_\pi^\ell(L)\right) \, \Gamma_0^{\text{tree}} \,. \tag{3.61}$$

The function $Y_\pi^\ell(L)$ is expanded in inverse powers of L as follows

$$Y_\pi^\ell(L) = b_{\text{IR}} \log(M_\pi^2 L^2) + b_0 + \frac{b_1}{M_\pi L} + \frac{b_2^{\text{pt}}}{(M_\pi L)^2} + \frac{b_3^{\text{pt}}}{(M_\pi L)^3} + O(e^{-M_\pi L}) \,, \tag{3.62}$$

where the coefficients b_j ($j = \text{IR}, 0, 1$) and b_j^{pt} ($j = 2, 3$), depending on the dimensionless ratio $r_\ell = m_\ell/M_\pi$, are given explicitly in [70, 88] after the subtraction of the lepton self-energy contribution in the Feynman gauge. Note that the lepton wave function renormalization is also not computed in $\Gamma_0(L)$ since it cancels exactly in the difference $\Gamma_0(L) - \Gamma_0^{\text{pt}}(L)$.

In addition to the presence of infrared divergences, even in the rest-frame of the meson there is a dependence on the three-momentum of the final-state lepton from the diagram in

which the photon is emitted from the meson and absorbed by the lepton. When evaluating the FV corrections, the summand in the summation over the spatial momentum modes of the photon, $\vec{k}$, depends not only on $|\vec{k}|$ but also on $\vec{p}_\ell \cdot \vec{k}$, i.e. on the direction of the final state lepton's momentum, $\vec{p}_\ell$, with respect to the axes of the cubic lattice. This complicates the calculation significantly and leads to results which also depend on the direction of $\vec{p}_\ell$. We believe that the techniques developed in this paper, which extend those of Ref. [89], have a wider applicability and will be useful for many other processes.

The calculation of the coefficients $b_{IR,0,1}$ and $b_{2,3}^{\text{pt}}$ in Eq. (4.53) is technically involved, thus we here limit ourselves to only give the final results referring the reader to the quoted papers for greater detail. In [70, 88] it has been obtained

$$
\begin{aligned}
b_{IR} &= \frac{1}{8\pi^2} \left\{ \frac{(1+r_\ell^2)\log(r_\ell^2)}{(1-r_\ell^2)} + 1 \right\}, \\
b_0 &= \frac{1}{16\pi^2} \left\{ 2\log\left(\frac{M_\pi^2}{M_W^2}\right) + \frac{(2-6r_\ell^2)\log(r_\ell^2) + (1+r_\ell^2)\log^2(r_\ell^2)}{1-r_\ell^2} - \frac{5}{2} \right\} + \frac{\zeta_C(\vec{0}) - 2\zeta_C(\vec{\beta}_\ell)}{2}, \\
b_1 &= -\frac{2(1+r_\ell^2)\zeta_B(\vec{0})}{1-r_\ell^2} + \frac{8r_\ell^2\zeta_B(\vec{\beta}_\ell)}{1-r_\ell^4}, \quad b_2^{\text{pt}} = \frac{4\zeta_A(\vec{0})}{1-r_\ell^2} - \frac{8\zeta_B^{P\ell}(\vec{\beta}_\ell)}{1-r_\ell^4}, \quad b_3^{\text{pt}} = \frac{-5 - 5r_\ell^2 - 3r_\ell^4 + r_\ell^6}{(1+r_\ell^2)^3},
\end{aligned}
$$

$$(3.63)$$

where the generalized ζ-functions appearing in the previous expressions are dimensionless functions of the kinematical variable $\vec{\beta}_\ell = \vec{p}_\ell/E_\ell$, where $E_\ell = M_\pi(1+r_\ell^2)/2$ and $\vec{p}_\ell$ is the spatial momentum of the lepton when $p_\pi = (iM_\pi, \vec{0})$. These arise in the calculation of finite-volume one-loop master integrals and can be computed with arbitrary numerical precision. We quote below the numerical results for the ζ-functions needed in order to use Eqs. (3.63).

$$
\begin{aligned}
\zeta_A(\vec{0}) &= -0.22578495944(1), & \zeta_B(\vec{0}) &= -0.05644623986(1), \\
\zeta_C(\vec{0}) &= -0.06215473226(1),
\end{aligned}
$$

$$(3.64)$$

while at the physical values of the pion, $M_{\pi^+} = 139.57018$ MeV, kaon, $M_{K^+} = 493.677$ MeV, and muon, $m_\mu = 105.65837$ MeV, masses, for a lepton moving diagonally across the box, $\vec{p}_\mu = p_\mu \frac{(1,1,1)}{\sqrt{3}}$

$$
\begin{aligned}
\zeta_B^{P\ell}(\vec{\beta}_\mu^{\vec{\pi}}) &= -0.23173738346(1), & \zeta_B^{P\ell}(\vec{\beta}_\mu^{\vec{K}}) &= -0.45599283983(1), \\
\zeta_B(\vec{\beta}_\mu^{\vec{\pi}}) &= -0.05791071589(1), & \zeta_B(\vec{\beta}_\mu^{\vec{K}}) &= -0.10350847338(1), \\
\zeta_C(\vec{\beta}_\mu^{\vec{\pi}}) &= -0.06331584128(1), & \zeta_C(\vec{\beta}_\mu^{\vec{K}}) &= -0.09037019089(1).
\end{aligned}
$$

$$(3.65)$$

The above findings have been used in our lattice calculation of the QED radiative corrections to the $\pi_{\mu 2}$ and $K_{\mu 2}$ decay rates, described in Chapter 4.

An important result of Ref. [88] is that the structure-dependent FVEs start at order $O(1/(M_\pi L)^2)$. Consequently the coefficients $b_{\text{IR},0,1}$ in the factor $Y_\pi^\ell(L)$ are "universal",

i.e. they are the same as in the full theory when the structure of the meson is considered[1], and, therefore, cancel in the difference $\Gamma_0(L) - \Gamma_0^{\text{pt}}(L)$. The remaining, non-universal, $O(1/L^2)$ FV effects are milder and can be determined by performing simulations on different volumes and fitting the observed volume dependence (see Chapter 4). The universality of the leading and next-to-leading FV effects has been proved in [88] using the electromagnetic Ward identities of the full theory and the QED skeleton expansion, in which the meson propagator and the vertices to which the photon couples, are defined in terms of QCD correlation functions and then inserted into one-loop diagrams. Note that b_{IR} does not depend on the regularization, while $b_{0,1}$ and $b_{2,3}^{\text{pt}}$ depend on the choice of QED_L as the regulator of the momentum zero-mode.

3.7 STRUCTURE DEPENDENT CONTRIBUTIONS TO THE REAL DECAY

When studying radiative corrections to leptonic decays of pseudoscalar mesons at $O(\alpha_{em})$ the presence of infrared divergences requires us to consider the rates for both the processes $P \to \ell\nu_\ell$ and $P \to \ell\nu_\ell\gamma$. In the previous sections we have described in detail a strategy to include electromagnetic effects in such processes in a lattice simulation. Our initial proposal was to restrict the maximum energy of the final-state photon in the meson rest frame, ΔE, to be sufficiently small for the dependence on the structure of the meson to be negligible and yet to be within the experimental resolution. However, the introduction of the soft energy cut-off ΔE can be avoided by computing amplitudes with a real photon in the final state. Such a calculation is now in progress and we will present some preliminary results in Sec. 4.6. As a first numerical implementation of our method to evaluate the isospin-breaking corrections to the light meson leptonic decay rates (see Chapter 4 of this thesis) we have used the pointlike approximation to calculate $\Gamma_1(\Delta E)$ in perturbation theory. In this section the size of the neglected $O(\alpha_{em}\Delta E/\Lambda_{\text{QCD}})$ structure-dependent contributions to the decay $P^+ \to \ell^+\nu_\ell\gamma$ for light mesons, $P^+ = \pi^+, K^+$ is estimated [10]. We base the estimates on the results of the phenomenological analyses performed in Refs. [90–92] based on the use of chiral perturbation theory at $O(p^4)$.

Although the relevant expressions have also been derived at $O(p^6)$ [93, 94] (see also page 10 of [95]), in that case there are too many unknown low-energy constants to be useful in making an estimate. As was done in the previous sections of this chapter, for the general framework we give the explicit formulae for pion decays; the generalization of the framework to kaons, and indeed also to D-mesons and B-mesons decays is straightforward. We then make the numerical estimates of the structure dependent effects for pions and kaons based on chiral perturbation theory. Finally we make some comments about structure dependent terms when P^+ is a heavy-light meson, D^+ or B^+. In this section we will follow the description in Appendix B of Ref. [10].

---

[1] Notice that the decay rate in the full theory, $\Gamma_0(L)$, can be affected also by non-universal FVEs of order $O[1/(M_\pi L)^n]$ with $n \geq 4$ that do not appear in $\Gamma_0^{pt}(L)$.

The starting point of the analysis is the decomposition in terms of Lorenz invariant form factors of the hadronic matrix element (see also Eq. (3.46))

$$H^{\mu\nu}(k, p_\pi) \;=\; \int d^4x \, e^{ikx} \, T\langle 0| J^\mu(x) J^\nu_W(0) |\pi(p_\pi)\rangle \;. \tag{3.66}$$

We follow the standard convention of separating the contribution corresponding to the approximation of a point-like pion (also frequently called *inner bremsstrahlung*) $H^{\mu\nu}_{\rm pt}$, from the structure dependent part $H^{\mu\nu}_{\rm SD}$,

$$H^{\mu\nu} = H^{\mu\nu}_{\rm SD} + H^{\mu\nu}_{\rm pt} \;. \tag{3.67}$$

$H^{\mu\nu}_{\rm pt}$ is simply given by

$$H^{\mu\nu}_{\rm pt} = f_\pi \left[g^{\mu\nu} - \frac{(2p_\pi - k)^\mu (p_\pi - k)^\nu}{(p_\pi - k)^2 - M^2_\pi} \right] \;. \tag{3.68}$$

The structure dependent component can be parametrized by four independent invariant form factors which we define as

$$
\begin{aligned}
H^{\mu\nu}_{\rm SD} \;=\;\; & H_1 \left[k^2 g^{\mu\nu} - k^\mu k^\nu \right] + H_2 \left\{ \left[(k \cdot p_\pi - k^2) k^\mu - k^2 (p_\pi - k)^\mu \right] (p_\pi - k)^\nu \right\} \\
& - i \frac{F_V}{M_\pi} \epsilon^{\mu\nu\alpha\beta} k_\alpha p_{\pi\beta} + \frac{F_A}{M_\pi} \left[(k \cdot p_\pi - k^2) g^{\mu\nu} - (p_\pi - k)^\mu k^\nu \right] \;.
\end{aligned} \tag{3.69}
$$

Note that the vector Ward Identity $k_\mu H^{\mu\nu} = f_\pi p^\nu_\pi$, derived in Ref. [90], is saturated by $H^{\mu\nu}_{\rm pt}$

$$k_\mu H^{\mu\nu}_{\rm pt} = f_\pi p^\nu_\pi \;, \qquad k_\mu H^{\mu\nu}_{\rm SD} = 0 \;. \tag{3.70}$$

$H^{\mu\nu}_{\rm pt}$ also contains the infrared divergences which appear in the virtual- and real-photon contributions to the decay rate. These observations motivate the decomposition in Eq. (3.67).

In the calculation of the decay rate for $\pi^+ \to \ell^+ \nu_\ell \gamma$ the tensor $H^{\mu\nu}$ is contracted with the polarization vector of the real photon. In physical gauges with $\varepsilon^\star \cdot k = 0$ we define

$$H^\nu \equiv \varepsilon^\star_\mu H^{\mu\nu} \;, \tag{3.71}$$

so that

$$H^\nu_{SD} \;=\; -\varepsilon^\star_\mu \left\{ i \frac{F_V}{M_\pi} \epsilon^{\mu\nu\alpha\beta} k_\alpha p_{\pi\beta} - \frac{F_A}{M_\pi} \left[(k \cdot p_\pi - k^2) g^{\mu\nu} - (p_\pi - k)^\mu k^\nu \right] \right\} \;, \tag{3.72}$$

showing that the structure dependent part of the decay rate can be parametrized in terms of the two form factors F_V and F_A.

Before performing the integrations over the three-body phase space, the differential decay rate can be expressed as a function of the two independent Dalitz variables ($p_\pi = p_\ell + p_\nu + k$)

$$x_\ell = -\frac{(p_\pi - p_\ell)^2}{M^2_\pi} + 1 \;, \qquad x_\gamma = -\frac{(p_\pi - k)^2}{M^2_\pi} + 1 \;. \tag{3.73}$$

The decay rate as a function of the photon's energy in the pion's rest frame can be obtained by performing the integration over x_ℓ with the limits $x_\ell \in \left[x_\ell^{\min}, x_\ell^{\max}\right]$ where

$$
\begin{aligned}
x_\ell^{\min} &= 1 - r_\gamma^2 - \frac{1 - x_\gamma - r_\ell^2}{2(1 - x_\gamma)}\left[x_\gamma - r_\gamma^2 + \sqrt{(x_\gamma + r_\gamma^2)^2 - 4r_\gamma^2}\right] \,, \\
x_\ell^{\max} &= 1 - r_\gamma^2 - \frac{1 - x_\gamma - r_\ell^2}{2(1 - x_\gamma)}\left[x_\gamma - r_\gamma^2 - \sqrt{(x_\gamma + r_\gamma^2)^2 - 4r_\gamma^2}\right] \,,
\end{aligned}
\tag{3.74}
$$

$r_\ell = m_\ell/M_\pi$ and $r_\gamma = m_\gamma/M_\pi$. The total decay rate is obtained by performing the integral over x_γ in the range $x_\gamma \in \left[x_\gamma^{\min}, x_\gamma^{\max}\right]$ with

$$
x_\gamma^{\min} = r_\gamma(2 - r_\gamma) \,, \qquad x_\gamma^{\max} = 1 - r_\ell^2 \,.
\tag{3.75}
$$

The photon's mass m_γ was introduced in the definition of r_γ to regulate the infrared divergences in the point-like contribution. For the structure dependent contribution, which is infrared finite we can set $m_\gamma \to 0$ and simplify the above expressions by making the replacements

$$
\begin{aligned}
x_\ell^{\min} &\mapsto (1 - x_\gamma) + \frac{x_\gamma r_\ell^2}{(1 - x_\gamma)} \,, \qquad x_\ell^{\max} \mapsto 1 \,. \\
x_\gamma^{\min} &\mapsto 0 \,, \qquad x_\gamma^{\max} \mapsto 1 - r_\ell^2 \,.
\end{aligned}
\tag{3.76}
$$

The different contributions to the differential decay rate have been obtained in Ref. [90]. Writing $\Gamma_1 = \Gamma_1^{\mathrm{pt}} + \Gamma_1^{\mathrm{SD}} + \Gamma_1^{\mathrm{INT}}$, where Γ_1^{INT} is the contribution to the decay rate coming from the interference between the point-like and the structure-dependent amplitudes, we confirm the following results:

$$
\begin{aligned}
\frac{4\pi}{\alpha_{em}\,\Gamma_0^{\mathrm{tree}}}\frac{d^2\Gamma_1^{\mathrm{pt}}}{dx_\gamma dx_\ell} &= \frac{2\,f_{\mathrm{pt}}(x_\gamma, x_\ell)}{(1 - r_\ell^2)^2} \,, \\
\frac{4\pi}{\alpha_{em}\,\Gamma_0^{\mathrm{tree}}}\frac{d^2\Gamma_1^{\mathrm{SD}}}{dx_\gamma dx_\ell} &= \frac{M_\pi^2\left\{[F_V(x_\gamma) + F_A(x_\gamma)]^2\,f_{\mathrm{SD}}^+(x_\gamma, x_\ell) + [F_V(x_\gamma) - F_A(x_\gamma)]^2\,f_{\mathrm{SD}}^-(x_\gamma, x_\ell)\right\}}{2f_\pi^2\,r_\ell^2(1 - r_\ell^2)^2} \,, \\
\frac{4\pi}{\alpha_{em}\,\Gamma_0^{\mathrm{tree}}}\frac{d^2\Gamma_1^{\mathrm{INT}}}{dx_\gamma dx_\ell} &= -\frac{2M_\pi\left\{[F_V(x_\gamma) + F_A(x_\gamma)]\,f_{\mathrm{INT}}^+(x_\gamma, x_\ell) + [F_V(x_\gamma) - F_A(x_\gamma)]\,f_{\mathrm{INT}}^-(x_\gamma, x_\ell)\right\}}{f_\pi\,(1 - r_\ell^2)^2} \,.
\end{aligned}
\tag{3.77}
$$

The functions appearing in Eq. (3.77) are

$$f_{\text{pt}}(x_\gamma, x_\ell) = \frac{1 - x_\ell}{x_\gamma^2(x_\gamma + x_\ell - 1)} \left[x_\gamma^2 + 2(1 - x_\gamma)(1 - r_\ell^2) - \frac{2x_\gamma r_\ell^2(1 - r_\ell^2)}{x_\gamma + x_\ell - 1} \right] ,$$

$$f_{\text{SD}}^+(x_\gamma, x_\ell) = (x_\gamma + x_\ell - 1) \left[(x_\gamma + x_\ell - 1 + r_\ell^2)(1 - x_\gamma) - r_\ell^2 \right] ,$$

$$f_{SD}^-(x_\gamma, x_\ell) = -(1 - x_\ell) \left[(x_\ell - 1 + r_\ell^2)(1 - x_\gamma) - r_\ell^2 \right] , \qquad (3.78)$$

$$f_{\text{INT}}^+(x_\gamma, x_\ell) = -\frac{1 - x_\ell}{x_\gamma(x_\gamma + x_\ell - 1)} \left[(x_\gamma + x_\ell - 1 + r_\ell^2)(1 - x_\gamma) - r_\ell^2 \right] ,$$

$$f_{\text{INT}}^-(x_\gamma, x_\ell) = \frac{1 - x_\ell}{x_\gamma(x_\gamma + x_\ell - 1)} \left[x_\gamma^2 + (x_\gamma + x_\ell - 1 + r_\ell^2)(1 - x_\gamma) - r_\ell^2 \right] ,$$

in agreement with the results of Ref. [90].

It will be useful below to define the following quantities,

$$Q_1^A(x_\gamma) = \frac{4\pi}{\alpha_{em}\,\Gamma_0^{\text{tree}}} \frac{d\Gamma_1^A(x_\gamma)}{dx_\gamma} , \qquad\qquad A = \{\text{pt,SD,INT}\} , \qquad (3.79)$$

$$R_1^A(\Delta E) = \frac{\Gamma_1^A(\Delta E)}{\Gamma_0^{\alpha,\text{pt}} + \Gamma_0^{(d),\text{pt}} + \Gamma_1^{\text{pt}}(\Delta E)} , \qquad A = \{\text{SD,INT}\} , \qquad (3.80)$$

where $\Delta E = r_E\, M_\pi/2$ and $\Gamma_0^{\alpha,\text{pt}}$ and $\Gamma_0^{(d),\text{pt}}$ have been defined in the main body of the paper (see Eq. (3.51)). Notice that the quantity in the denominator of $R_1^A(\Delta E)$ is infrared finite (although it does depend on M_W, the ultraviolet cutoff in the W-regularization).

In the following we use phenomenological parametrizations of the form factors in order to estimate the size of the structure-dependent contributions to the decay rate Γ_1. For the case of light mesons, we can use the results of the calculations of refs. [90–92] (see also ref. [95]) based on chiral perturbation theory and approximate the form factors as constants. At $O(p^4)$ in chiral perturbation theory,

$$F_V = \frac{M_P}{4\pi^2 f_\pi} \quad \text{and} \quad F_A = \frac{8M_P}{f_\pi}\left(L_9^r + L_{10}^r\right), \qquad (3.81)$$

where $P = \pi$ or K and L_9^r, L_{10}^r are Gasser-Leutwyler coefficients. The numerical values of these constants have been taken from the review by M.Bychkov and G.D'Ambrosio in Ref. [3]; the values of F_V and F_A are 0.0254 and 0.0119 for the pion and 0.096 and 0.042 for the Kaon (for the pion these values of the form factors, obtained from direct measurements, can be found in the supplement to [3] found in [96]). In Figs. 3.7.1 and 3.7.2 we compare the point-like, structure-dependent and interference contributions to the decays $\pi \to \ell\nu\gamma$ and $K \to \ell\nu\gamma$ respectively. As can be seen, interference contributions are negligible in all the decays. The structure-dependent contributions can be sizeable because they are chirally enhanced with respect to the point-like contribution (notice the factor $1/r_\ell^2$ in the second equation in (3.77)). From the phenomenological estimates of the form factors, this
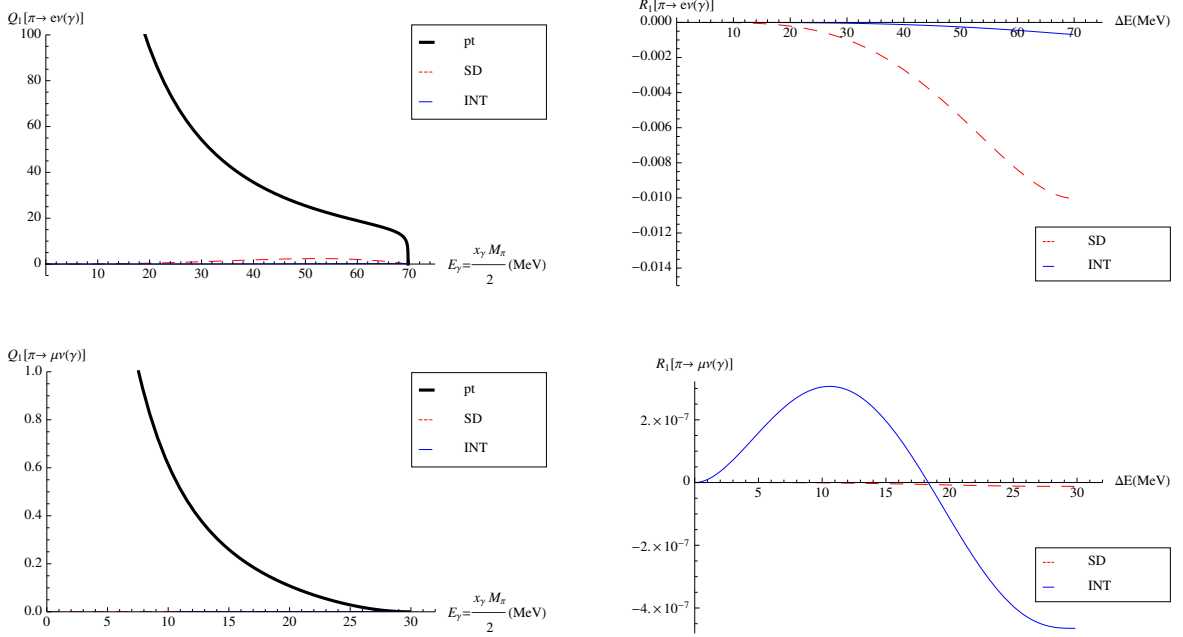
Figure 3.7.1: Point-like (pt), structure-dependent (SD) and interference (INT) contributions to the decay $\pi \to \ell\nu\gamma$. The first (second) row corresponds to $\ell = e$ ($\ell = \mu$).

happens for the real decay $K \to e\nu_e\gamma$. On the other hand, for $E_\gamma < 20$ MeV both structure dependent and interference contributions can be safely neglected with respect to the point-like contributions for all the decays of pions and the decay $K \to \mu\nu\gamma$. We learn from Refs. [78, 79] that a cutoff on the energy of the photon in the rest frame of the decaying particle of $O(20\,\mathrm{MeV})$ is experimentally accessible.

The application of chiral perturbation theory described above does not apply to the decays of D and B mesons and for these decays a lattice calculation of $F_{V,A}(x_\gamma)$ for a range of values of x_γ will prove to be very useful as a check of the range of validity of the point-like approximation. Furthermore, it is likely that in order to make experimental measurements feasible, ΔE may have to be sufficiently large that the structure dependence of the heavy meson can no longer be neglected and therefore that the emission of real "hard" photons, with energies of $E_\gamma \geq \Lambda_{\mathrm{QCD}}$ should be implemented in the lattice simulation. Such a lattice calculation, starting from Euclidean correlators is indeed possible and we refer the reader to Sec. 4.6 for further details. A new feature in the case of B-decays in particular, one which is a consequence of the heavy-quark symmetry, is that the B^* and B are almost degenerate $(M_{B^*} - M_B \simeq 45\,\mathrm{MeV})$. The radiation of a relatively soft photon can therefore cause the transition from a B-meson to an internal B^* close to its mass-shell. Lattice calculations of the form factors allow us to investigate the effect this small hyperfine splitting has on the size of the structure dependent terms as a function of ΔE.
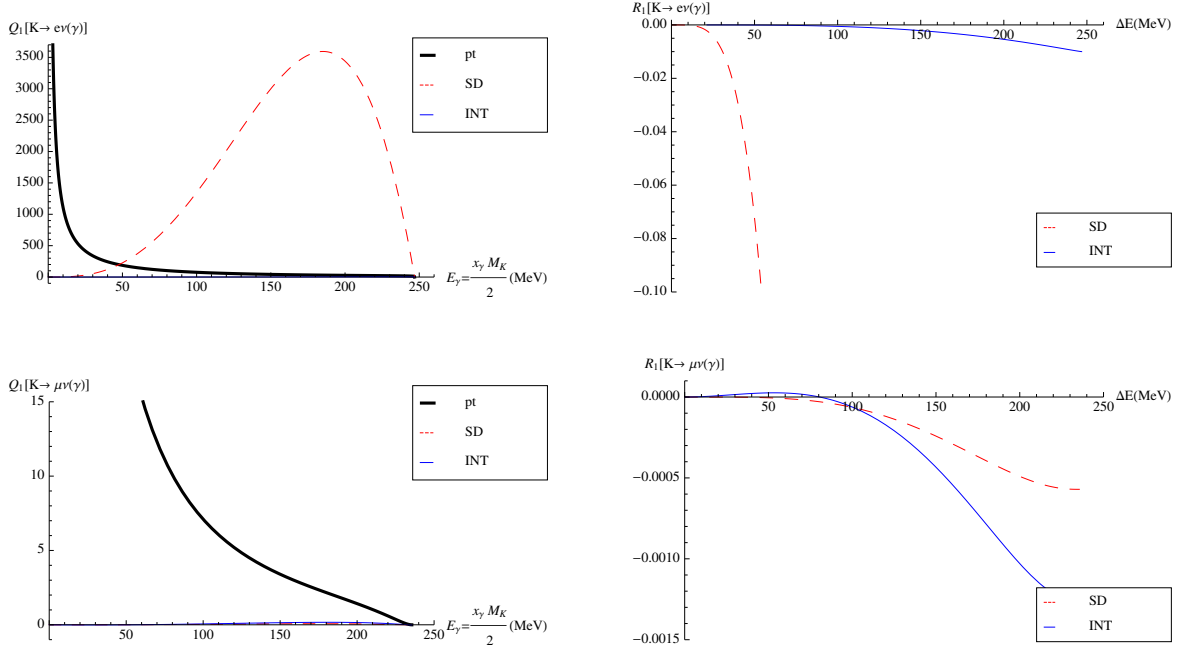
121

Figure 3.7.2: Point-like (pt), structure-dependent (SD) and interference (INT) contributions to the decay $K \to \ell\nu\gamma$. The first (second) row corresponds to $\ell = e$ ($\ell = \mu$).

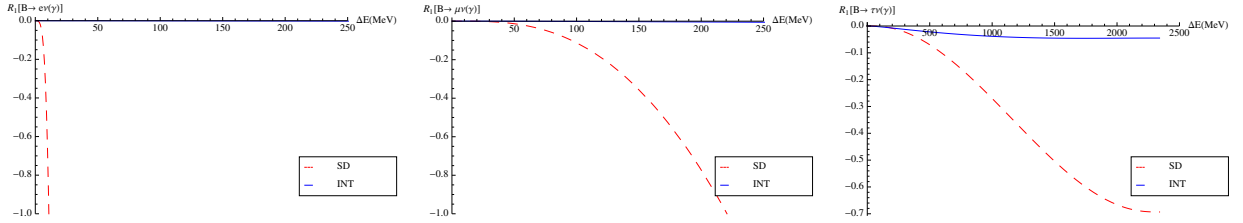Figure 3.7.3: Structure-dependent (SD) and interference (INT) contributions to R_1 for the decays $B \to \ell\nu\gamma$. Going from left to right, the plots correspond to $\ell = e$, $\ell = \mu$ and $\ell = \tau$ respectively.

Still in the absence of lattice calculations of the form factors, we note the phenomenological analysis of Ref. [97], based on the extreme assumption of the single pole dominance, B^* for F_V and $B_1(5721)$ for F_A (in reality many other virtual states contribute to the form factors):

$$F_V(x_\gamma) \simeq \frac{C_V}{x_\gamma - 1 + M_{B^\star}^2/M_B^2} \,, \qquad F_A(x_\gamma) \simeq \frac{C_A}{x_\gamma - 1 + M_{B_1(5721)}^2/M_B^2} \,, \qquad (3.82)$$

with $C_V = 0.24$ and $C_A = 0.20$. The corresponding ratios R_1 are shown in Figure 3.7.3, from

which it can be seen that under this assumption the structure-dependent contributions to $B \to e\nu_e\gamma$ for $E_\gamma \simeq 20\,\mathrm{MeV}$ can be very large, but are small for $B \to \mu\nu_\mu\gamma$ and $B \to \tau\nu_\tau\gamma$.

3.8 RADIATIVE CORRECTIONS IN SEMILEPTONIC DECAY RATES

We are now generalising the framework developed for leptonic decays and described in the previous sections to semileptonic decays, such as $\bar{K}^0 \to \pi^+\ell^-\bar{\nu}_\ell$ which we will here use for illustration. Although the main ideas presented above are also applicable in this case, several new features arise which have been presented in Refs. [52?] and we now explain.
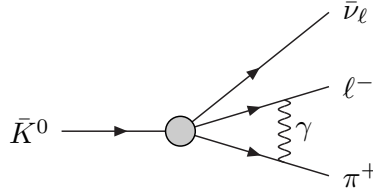
Figure 3.8.1: One of the diagrams contributing to radiative corrections to $K_{\ell 3}$ decays.

In QCD the amplitude depends on two form factors $f_{0,+}(q^2)$, where $q = p_K - p_\pi = p_\ell + p_\nu$:

$$\langle \pi(p_\pi) | \bar{s}\gamma_\mu u | K(p_K) \rangle = f_0(q^2) \frac{M_K^2 - M_\pi^2}{q^2} q_\mu + f_+(q^2) \left[(p_\pi + p_K)_\mu - \frac{M_K^2 - M_\pi^2}{q^2} q_\mu \right] . \quad (3.83)$$

When including radiative corrections, the natural observable to consider is $d^2\Gamma/dq^2 ds_{\pi\ell}$, where $s_{\pi\ell} = (p_\pi + p_\ell)^2$ and we follow the same procedure as for leptonic decays and write:

$$\frac{d^2\Gamma}{dq^2 ds_{\pi\ell}} = \lim_{V\to\infty} \left(\frac{d^2\Gamma_0}{dq^2 ds_{\pi\ell}} - \frac{d^2\Gamma_0^{\mathrm{pt}}}{dq^2 ds_{\pi\ell}} \right) + \lim_{V\to\infty} \left(\frac{d^2\Gamma_0^{\mathrm{pt}}}{dq^2 ds_{\pi\ell}} + \frac{d^2\Gamma_1(\Delta E)}{dq^2 ds_{\pi\ell}} \right) \quad (3.84)$$

where where again "pt" denotes pointlike and ΔE is the cut-off on the energy of the real photon. The infrared divergences cancel separately in each of the two terms on the right-hand side. The second term has been calculated in infinite volume in the eikonal approximation: $(p - k)^2 - m^2 \to -2p \cdot k$, where p is the momentum of an external on-shell particle and k is the momentum of the photon [98, 99].

We now discuss a number of issues which arise when considering semileptonic decays which are absent for leptonic decays.

3.8.1 THE PRESENCE OF UNPHYSICAL TERMS WHICH GROW EXPONENTIALLY IN TIME

Consider for illustration the diagram in Fig. 3.8.2. The integration over the times $t_{1,2}$ yields terms in the momentum sum which are proportional to $e^{-(E_{\pi\ell}^{\mathrm{int}} - E_{\pi\ell}^{\mathrm{ext}})(t_{\pi\ell} - t_H)}$, where $E_{\pi\ell}^{\mathrm{int}}$ and

$E^{\text{ext}}_{\pi\ell}$ are the internal and external energies of the pion-lepton pair and $t_{\pi\ell}$ and t_H are the times of the insertion of the pion-lepton sink and of the weak Hamiltonian H. Depending on the choice of the momenta of the final-state pion and lepton, it is possible that the exchange of the photon with an allowed finite-volume momentum can result in the internal energy being smaller than the external one, $E^{\text{int}}_{\pi\ell} < E^{\text{ext}}_{\pi\ell}$, leading to unphysical terms which grow exponentially with $t_{\pi\ell} - t_H$. This is a generic feature when calculating long-distance contributions in Euclidean space and such terms must be identified and subtracted. The presence of such contributions is a manifestation of the Maiani-Testa theorem [100]. The number of such states depends on the choice of the kinematic variables q^2 and $s_{\pi\ell}$ as well as on the volume. Note that no such exponentially growing terms are present for leptonic decays.
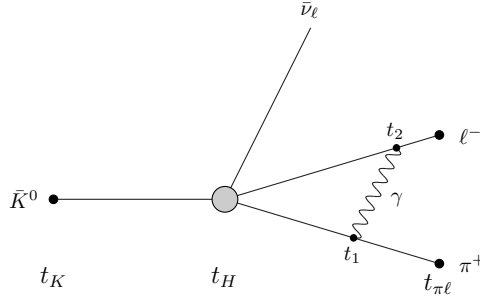

Figure 3.8.2: Diagram contributing to the $K \to \pi\ell\bar{\nu}_\ell$ correlation function, illustrating the presence of unphysical terms which grow exponentially in time (see text).

For $K_{\ell 3}$ decays, in some corners of phase space, there may also be multi-hadron intermediate states with energies smaller than the external one, and hence containing exponentials which grow with the time separation, but these are expected to be small. For example the $K \to \pi\pi\ell \to \pi\ell\nu(\gamma)$ sequence only contributes at high order (p^6) in ChPT and is present due to the Wess-Zumino-Witten term in the action. More importantly however, we can restrict the values of $s_{\pi\ell}$ to a range below the multi-hadron threshold. Note that for D and B decays the large number of such terms which need to be subtracted in most of phase space, makes it very difficult to perform a non-perturbative lattice calculation.

3.8.2 FINITE VOLUME CORRECTIONS

As observed in Sec. 3.6 the leading structure-dependent FV effects in $\Gamma_0 - \Gamma_0^{\text{pt}}$ are of $O(1/L^2)$.

The following scaling law is useful in determining which terms need to be evaluated to obtain the universal coefficients. If the leading behavior of the infinite-volume integrand and finite-volume summand is proportional to $1/(k^2)^{n/2}$ as $k \to 0$ then the corresponding difference between the infinite-volume integral and finite-volume sum of $O(1/L^{4-n})$ [88]. In the calculation of the mass spectrum $n = 3$ and the leading finite-volume correction is of

$O(1/L)$ and is universal, as is the subleading term of $O(1/L^2)$. In decay amplitudes $n = 4$, corresponding to the presence of infrared divergences.
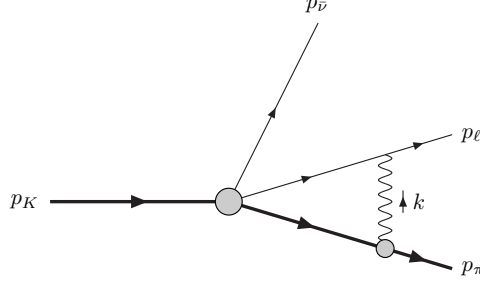

Figure 3.8.3: Diagram contributing to the $K \to \pi \ell \bar{\nu}_\ell$ correlation function used in the discussion of finite-volume effects (see text).

For illustration consider the diagram in Fig. 3.8.3. At small photon momentum k, the pion and lepton internal propagators scale as $1/k$ and the photon propagator as $1/k^2$, so that the loop integrand/summand scales as $1/k^4$ corresponding to an infrared divergence. There are also subleading terms which scale as $1/k^3$ which lead to $1/L$ finite-volume effects. These arise by expanding the propagators and vertices, including the vertex containing the weak Hamiltonian, to $O(k)$. Since the $1/L^2$ finite-volume corrections depend on the structure of the pion we do consider these further.
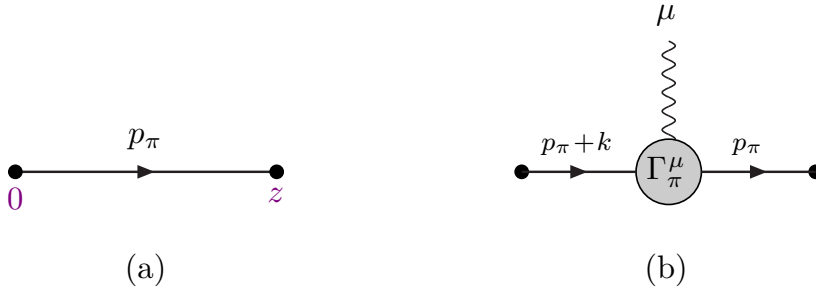

Figure 3.8.4: (a) The pion propagator, (b) $\pi\gamma\pi$ vertex

Electromagnetic Ward identities are particularly useful in the study of the universality of the $O(1/L)$ finite-volume corrections. To illustrate this consider the pion propagator in Fig. 3.8.4(a). We define the Euclidean pion propagator $\Delta_\pi(p_\pi)$ by:

$$
\begin{aligned}
C_{\pi\pi}(p_\pi) &= \int d^4z \, e^{-ip_\pi \cdot z} \langle 0|T\{\phi_\pi(z)\phi_\pi^\dagger(0)\}|0\rangle \\
&\equiv |\langle 0|\phi_\pi(0)|\pi(\vec{p}_\pi)\rangle|^2 \Delta_\pi(p_\pi) \\
&\equiv |\langle 0|\phi_\pi(0)|\pi(\vec{p}_\pi)\rangle|^2 \frac{Z_\pi(p_\pi^2)}{p_\pi^2 + M_\pi^2} \, .
\end{aligned}
\tag{3.85}
$$

Z_π parametrises the structure dependence of the pion propagator. We now expand the propagator for small values of k and off-shellness $\varepsilon_\pi^2 = p_\pi^2 + M_\pi^2$ to obtain

$$\Delta_\pi(p_\pi + k) = \frac{1 - 2z_{\pi_1}p_\pi \cdot k - \varepsilon_\pi^2 z_{\pi_1} + O(k^2, \varepsilon_\pi^4, \varepsilon_\pi^2 k)}{\varepsilon_\pi^2 + 2p_\pi \cdot k + k^2} \ , \tag{3.86}$$

where the structure dependent parameter z_{π_1} is given by

$$z_{\pi_1} = \left. \frac{dZ_\pi^{-1}(p_\pi^2)}{dp_\pi^2} \right|_{p_\pi^2 = -M_\pi^2} . \tag{3.87}$$

Similarly we define the amputated $\pi\gamma\pi$ vertex Γ_π^μ, by amputating the propagators and matrix elements of the interpolating operators in the correlation function (see Fig. 3.8.4(b))

$$C_\pi^\mu(p_\pi, k) = i \int d^4z \, d^4x \, e^{-ip_\pi \cdot z} e^{-ik \cdot x} \langle 0|T\{\phi_\pi(z)j^\mu(x)\phi_\pi^\dagger(0)\}|0\rangle \ . \tag{3.88}$$

We now expand Γ_π^μ for small k (and ε_π). The key result is obtained from the Ward identity

$$k_\mu \Gamma_\pi^\mu(p_\pi, k) = Q_\pi \{\Delta_\pi^{-1}(p_\pi + k) - \Delta_\pi^{-1}(p_\pi)\} \ , \tag{3.89}$$

which relates the first-order expansion coefficients and yields

$$Z_\pi(p_\pi + k)\Gamma_\pi^\mu(p_\pi, k) = Q_\pi(2p_\pi + k)^\mu + O(k^2, \varepsilon_\pi^2) \ . \tag{3.90}$$

Here Q_π is the electric charge of the pion. Thus, since we are neglecting the structure dependent $O(1/L^2)$ corrections, the pion propagator and $\pi\gamma\pi$ vertex combine to give the same result as in the point-like theory.

We have seen that, as a result of the Ward identity, we do not need the derivatives of the pion form-factors to obtain the $O(1/L)$ corrections. However, we also need to expand the weak-vertex which, in QCD without QED, is a linear combination of two form-factors $f_{0,+}(q^2)$. Off-shell, the $K\pi\ell\bar{\nu}$ weak vertex is a linear combination of two functions $F_{0,+}(p_\pi^2, p_K^2, 2p_K \cdot p_\pi)$ (which on-shell reduce to the form-factors $f_{0,+}(q^2)$). The Ward identity relates the $K\pi\ell\bar{\nu}$ and $K\pi\ell\bar{\nu}\gamma$ vertices and does lead to a partial, but not complete, cancellation of the $O(1/L)$ terms. The remaining $O(1/L)$ corrections are found to depend on the derivatives of the form factors $df_{0,+}(q^2)/dq^2$, as well as on the form factors $f_{0,+}(q^2)$ themselves; this will be demonstrated in a publication in preparation. Such derivative terms are a generic consequence of the Low theorem and are absent only in particularly simple cases, such as leptonic decays as explained below. These corrections are "universal" since the coefficients are physical, i.e. the form factors and their derivatives can be measured experimentally or computed in lattice simulations. On the other hand, there are no corrections of the form $df_{0,+}/dM_\pi^2$ or $df_{0,+}/dM_K^2$, which would not be physical. It is instructive to contrast the situation for semileptonic decays with the corresponding one for leptonic decays, e.g. for $K^+ \to \ell^+\nu_\ell$ decays. In that case the leading isospin-breaking corrections are proportional to the decay constant f_K computed in QCD simulations and again there are no

$O(1/L)$ terms proportional to df_K/dM_K^2. In that case however, there is no scope for terms analogous to $df_{0,+}(q^2)/dq^2$.

For leptonic decays the $O(1/L)$ finite-volume corrections have been calculated analytically using the Poisson summation formula [88]. For semileptonic decays, the evaluation of the coefficients of the $O(1/L)$ corrections could be tough due to the appearance of new integrands/summands. In the ignorance of the analytic coefficients, the subtraction of the $O(1/L)$ effects can be performed instead by fitting data obtained at different volumes with however, some loss of precision. For leptonic decays, where the $O(1/L)$ corrections are known and can be subtracted explicitly, we have checked that fitting these finite-volume effects numerically leads instead to an approximate doubling of the uncertainty in the theoretical prediction extrapolated to physical masses in the infinite volume limit. This may be disappointing, but recalling that isospin breaking corrections are of $O(1\%)$, it is not a major problem.

4 ISOSPIN BREAKING CORRECTIONS TO LEPTONIC DECAY RATES

4.1 INTRODUCTION

In flavor physics the determination of the elements of the CKM matrix [1, 2], which contains just 4 parameters, from a wide range of weak processes represents a crucial test of the limits of the Standard Model (SM) of particle physics. Inconsistencies with theoretical expectations would indeed signal the existence of new physics beyond the SM and subsequently a detailed comparison of experimental measurements and theoretical predictions would provide a guide towards uncovering the underlying theory beyond the SM. For this to be possible non-perturbative hadronic effects need to be evaluated as precisely as possible and in this chapter we report on progress in improving the precision of lattice computations of leptonic decay rates by including radiative corrections and strong IB effects.

The extraction of the CKM elements from experimental data requires an accurate knowledge of a number of hadronic quantities and the main goal of large-scale QCD simulations on the lattice is the *ab initio* evaluation of the nonperturbative QCD effects in physical processes. For several quantities relevant for flavor physics phenomenology, lattice QCD has recently reached the impressive level of precision of $O(1\%)$ or even better. Important examples are the ratio f_K/f_π of kaon and pion leptonic decay constants and the $K_{\ell 3}$ vector form factor $f_+(0)$ [4], which play the central role in the accurate determination of the CKM entries $|V_{us}/V_{ud}|$ and $|V_{us}|$, respectively. Such lattice computations are typically performed in the isospin symmetric limit of QCD, in which the up and down quarks are mass degenerate ($m_u = m_d$) and electromagnetic (e.m.) effects are neglected ($\alpha_{em} = 0$).

Isospin breaking effects arise because of radiative corrections and because $m_u \neq m_d$; the latter contributions are referred to as strong isospin breaking effects throughout this thesis. Since both α_{em} and $(m_d - m_u)/\Lambda_{QCD}$ are of $O(1\%)$, IB effects need to be included in lattice simulations to make further progress in flavor physics phenomenology, beyond the currently impressive precision obtained in isosymmetric QCD.

Since the electric charges of the up and down quarks are different, the presence of electromagnetism itself induces a difference in their masses, in addition to any explicit difference in the bare masses input into the action being simulated. The separation of IB effects into strong and e.m. components therefore requires a convention. We have discussed this in detail

in Sec. 1.10, defining QCD in the presence of electromagnetism.

In the previous chapter we have presented a method to compute electromagnetic effects in hadronic processes. For these quantities the presence of infrared divergences in the intermediate stages of the calculation makes the procedure much more complicated than is the case for the hadronic spectrum, for which calculations in several different approaches [7–9, 17, 25, 32, 57, 58, 101, 102] already exist. In order to obtain physical decay widths (or cross sections) diagrams containing virtual photons must be combined with those corresponding to the emission of real photons. Only in this way are the infrared divergences cancelled. We stress that it is not sufficient simply to add the electromagnetic interaction to the quark action because, for any given process, the contributions corresponding to different numbers of real photons must be evaluated separately.

We have discussed in detail a specific case, namely the $O(\alpha_{em})$ radiative corrections to the leptonic decay of charged pseudoscalar mesons. The method can however, be extended to many other processes, for example to semileptonic decays (see Sec. 3.8). The condition for the applicability of the proposed strategy is that there is a mass gap between the decaying particle and the intermediate states generated by the emission of the photon, so that all of these states have higher energies than the mass of the initial hadron (in the rest frame of the initial hadron).

In the previous chapter, we have limited the discussion to real photons with energies which are much smaller than the QCD scale Λ_{QCD}. This is not a limitation of the method and one can envisage numerical simulations of contributions to the inclusive width from the emission of real photons with energies which do resolve the structure of the initial hadron. Such calculations can be performed in Euclidean space under the same conditions as above, i.e. providing that there is a mass gap, and are currently in progress. In the present chapter we will present some preliminary results for the axial and vector form factors contributing to the amplitudes for the radiative decays of pseudoscalar mesons $P \to \ell \bar{\nu}_\ell \gamma$.

We here illustrate the first implementation of the method so far described in an actual numerical simulation. The leading e.m. and strong IB corrections to the $\pi^+ \to \mu^+ \nu_\mu(\gamma)$ and $K^+ \to \mu^+ \nu_\mu(\gamma)$ leptonic decay rates have been evaluated for the first time on the lattice, using the gauge ensembles produced by the European Twisted Mass Collaboration with $N_f = 2 + 1 + 1$ dynamical quarks [13, 16]. The QED effects are included by adopting the RM123 approach described in Chapter 1. The attractive feature of that approach is that it allows one naturally to work at first order in isospin breaking, computing the coefficients of the two small parameters α_{em} and $(m_d - m_u)/\Lambda_{\mathrm{QCD}}$ directly from simulations of isosymmetric QCD.

Before presenting the details of our lattice calculation, for reader's reference we briefly sketch the outline of the adopted strategy. When computing hadronic amplitudes, the e.m. corrections due to the exchange of a virtual photon and to the emission of a real one can be computed non-perturbatively, by numerical simulations, on a finite lattice with the corresponding uncertainties. The exchange of a virtual photon depends on the structure of the decaying meson, since all momentum modes are included, and the corresponding amplitude must therefore be computed non-perturbatively. On the other hand, the non-perturbative

evaluation of the emission of a real photon is not strictly necessary [10]. Indeed, it is possible to compute the real emission amplitudes in perturbation theory by limiting the maximum energy of the emitted photon in the meson rest-frame, ΔE_γ, to a value small enough so that the internal structure of the decaying meson is not resolved. The IR divergences in the non-perturbative calculation of the corrections due to the exchange of a virtual photon are cancelled by the corrections due to the real photon emission even when the latter is computed perturbatively, because of the universality of the IR behaviour of the theory (i.e., the IR divergences do not depend on the structure of the decaying hadron). Such a strategy, which requires an experimental cut on the energy of the real photon, makes the extraction of the relevant CKM element(s) cleaner.

In the intermediate steps of the calculation it is necessary to introduce an IR regulator. In order to work with quantities that are finite when the IR regulator is removed, the inclusive rate $\Gamma(P^+ \to \ell^+ \nu_\ell[\gamma])$ is written as [10]

$$
\begin{aligned}
\Gamma(P^\pm \to \ell^\pm \nu_\ell[\gamma]) &= \Gamma_0 + \Gamma_1^{\mathrm{pt}}(\Delta E_\gamma) \\
&= \lim_{L \to \infty} \left[\Gamma_0(L) - \Gamma_0^{\mathrm{pt}}(L) \right] + \lim_{\mu_\gamma \to 0} \left[\Gamma_0^{\mathrm{pt}}(\mu_\gamma) + \Gamma_1^{\mathrm{pt}}(\Delta E_\gamma, \mu_\gamma) \right] ,
\end{aligned}
\tag{4.1}
$$

where the subscripts $0, 1$ indicate the number of photons in the final state, while the superscript pt denotes the point-like approximation of the decaying meson and μ_γ is an IR regulator. In the first term on the r.h.s. of Eq. (4.1) the quantities $\Gamma_0(L)$ and $\Gamma_0^{\mathrm{pt}}(L)$ are evaluated on the lattice. Both have the same IR divergences which therefore cancel in the difference. We use the lattice size L as the intermediate IR regulator by working in the QED_L [54] formulation of QED on a finite volume. The difference $\left[\Gamma_0 - \Gamma_0^{\mathrm{pt}} \right]$ is independent of the regulator as this is removed [88]. As already pointed out, since all momentum modes contribute to it, $\Gamma_0(L)$ depends on the structure of the decaying meson and must be computed non-perturbatively. The numerical determination of $\Gamma_0(L)$ for several lattice spacings, physical volumes and quark masses is indeed the focus of our study.

In the second term on the r.h.s. of Eq. (4.1) P is a point-like meson and both $\Gamma_0^{\mathrm{pt}}(\mu_\gamma)$ and $\Gamma_1^{\mathrm{pt}}(\Delta E_\gamma, \mu_\gamma)$ can be calculated directly in infinite volume in perturbation theory, using a photon mass μ_γ as the IR regulator. Each term is IR divergent, but the sum is convergent [11] and independent of the IR regulator. In Refs. [10] and [88] the explicit perturbative calculations of $\left[\Gamma_0^{\mathrm{pt}} + \Gamma_1^{\mathrm{pt}}(\Delta E_\gamma) \right]$ and $\Gamma_0^{\mathrm{pt}}(L)$ have been performed with a small photon mass μ_γ or by using the finite volume respectively, as the IR cutoffs (see, e.g., Secs. 3.5 and 3.6).

In Ref. [16] we have calculated the e.m. and IB corrections to the ratio of $K_{\mu2}$ and $\pi_{\mu2}$ decay rates of charged pions and kaons into muons [16], using the $N_f = 2+1+1$ ETMC gauge ensembles [45, 65] in the quenched QED (qQED) approximation in which the charges of the sea quarks are set to 0. The ratio is less sensitive to various sources of uncertainty than the IB corrections to $\pi_{\mu2}$ and $K_{\mu2}$ decay rates separately. In Ref. [13], we have evaluated the e.m. and strong IB corrections to the decay processes $\pi_{\mu2}$ and $K_{\mu2}$ separately. Since the corresponding experimental rates are fully inclusive in the real photon energy, structure-dependent (SD) contributions to the real photon emission should be included, however according to the ChPT

predictions of Ref. [103] these SD contributions are negligible for both kaon and pion decays into muons (see the bottom right panels of Figs. 3.7.1 and 3.7.2 in Sec. 3.7). The same is not true to the same extent for decays into final-state electrons and so in our calculations we have focused on decays into muons. The SD contributions to Γ_1 are being investigated in an ongoing dedicated lattice study of light and heavy P-meson leptonic decays and preliminary results will be presented at the end of this chapter (see Sec. 4.6 later on).

The main results of the calculation are presented in Sec. 4.5 together with a detailed discussion of their implications. Here, we anticipate some key results: After extrapolation of the data to the physical pion mass, and to the continuum and infinite-volume limits, the isospin-breaking corrections to the leptonic decay rates can be written in the form:

$$\Gamma(\pi^\pm \to \mu^\pm \nu_\mu[\gamma]) = (1.0153 \pm 0.0019)\, \Gamma^{(0)}(\pi^\pm \to \mu^\pm \nu_\mu), \tag{4.2}$$

$$\Gamma(K^\pm \to \mu^\pm \nu_\mu[\gamma]) = (1.0024 \pm 0.0010)\Gamma^{(0)}(K^\pm \to \mu^\pm \nu_\mu), \tag{4.3}$$

where $\Gamma^{(0)}$ is the leptonic decay rate at tree level in the Gasser-Rusetsky-Scimemi scheme [46] (see Sec. 1.10.2.2 below). The corrections are about 1.6% for the pion decays and 0.3% for the kaon decay, in line with naive expectations. Taking the experimental value of the rate for the $K_{\mu2}$ decay, Eq. (4.3) together with $\Gamma^{(0)}(K^\pm \to \mu^\pm \nu_\mu)$ obtained using the lattice determination of the kaon decay constant we obtain $|V_{us}| = 0.22567(42)$, in agreement with the latest estimate $|V_{us}| = 0.2253(7)$, recently updated by the PDG [3] but with better precision. Alternatively, by taking the ratio of $K_{\mu2}$ and $\pi_{\mu2}$ decay rates and the updated value $|V_{ud}| = 0.97420\,(21)$ from super-allowed nuclear beta decays [15], we obtain $|V_{us}| = 0.22538(46)$. The unitarity of the first row of the CKM matrix is satisfied at the per-mille level; e.g. taking the value of V_{us} from the ratio of decay rates and $|V_{ub}| = 0.00413(49)$ [3], we obtain $|V_{ud}|^2 + |V_{us}|^2 + |V_{ub}|^2 = 0.99988(46)$. See Sec. 4.5 for a more detailed discussion of our results and their implications.

The plan for the remainder of this chapter is as follows. In Sec. 4.2 we present the calculation of the relevant amplitudes using the RM123 approach. The renormalization of the bare lattice operators necessary to obtain the effective weak Hamiltonian in the W-regularization scheme is performed in Sec. 4.3, while the subtraction of the universal IR-divergent finite volume effects (FVEs) is described in Sec. 4.4. The lattice data for the e.m. and strong IB corrections to the leptonic decay rates of pions and kaons are extrapolated to the physical pion mass, to the continuum and infinite volume limits in Sec. 4.5.

4.2 Evaluation of the amplitudes

At first order in $\alpha_{\rm em}$ and $(m_d - m_u)/\Lambda_{\rm QCD}$ the inclusive decay rate (4.1) can be written as

$$\Gamma(P^\pm \to \ell^\pm \bar{\nu}_\ell[\gamma]) = \Gamma^{\rm QCD} \cdot \left[1 + \overline{\delta R}_P\right] + O\left[\alpha_{\rm em}^2, (m_d - m_u)^2, \alpha_{\rm em}(m_d - m_u)\right], \tag{4.4}$$

where $\Gamma^{\rm QCD}$ is the tree-level decay rate given by

$$\Gamma^{\rm QCD} = \frac{G_F^2}{8\pi}|V_{q_1 q_2}|^2 m_\ell^2 \left(1 - \frac{m_\ell^2}{M_P^{(0)\,2}}\right)^2 f_P^{(0)\,2} M_P^{(0)}, \tag{4.5}$$

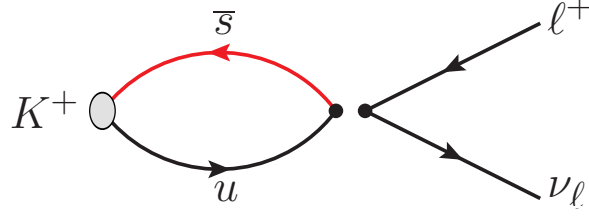Figure 4.2.1: *Feynman diagram for the process $K^+ \to \ell^+ \nu_\ell$. In the effective theory the interaction is given by a local four-fermion operator denoted by the two full dots in the figure.*

and $M_P^{(0)}$ and $f_P^{(0)}$ are the mass and decay constant of the charged P-meson mass defined in isosymmetric QCD in the chosen scheme.

The decay constant $f_P^{(0)}$ is defined in terms of the matrix element of the QCD axial current $A_P^{(0)}$ (in the continuum) as

$$A_P^{(0)} \equiv \langle 0|\bar{q}_2\gamma_0\gamma_5 q_1|P^{(0)}\rangle \equiv f_P^{(0)}M_P^{(0)} , \qquad (4.6)$$

where the initial state meson $P^{(0)}$ is at rest. The decay rate is obtained from the insertion of the lowest-order effective Hamiltonian

$$\mathcal{H}_W = \frac{G_F}{\sqrt{2}} V_{q_1 q_2}^* \, O_1 = \frac{G_F}{\sqrt{2}} V_{q_1 q_2}^* \left(\bar{q}_2\gamma_\mu(1-\gamma_5)q_1\right)\left(\bar{\nu}_\ell\gamma^\mu(1-\gamma_5)\ell\right) , \qquad (4.7)$$

as depicted in the Feynman diagram of Fig. 4.2.1, where the decay of a charged kaon is shown as an example. At lowest order in $\alpha_{\rm em}$ the two full dots in the figure represent the two currents in the bare four-fermion operator

$$O_1 = \left(\bar{q}_2\gamma_\mu(1-\gamma_5)q_1\right)\left(\bar{\nu}_\ell\gamma^\mu(1-\gamma_5)\ell\right) , \qquad (4.8)$$

whereas at order $\alpha_{\rm em}$ they will denote the insertion of the renormalized operator in the W-regularization as defined in Sec. 3.2.

In order to compare our results for the e.m. and strong IB corrections to those obtained in Ref. [22] and adopted by the PDG [3, 104] however, we will use a modified expression:

$$\Gamma(P^\pm \to \ell^\pm \bar{\nu}_\ell[\gamma]) = \Gamma^{(0)} \cdot [1 + \delta R_P] + O\left[\alpha_{\rm em}^2, (m_d - m_u)^2, \alpha_{\rm em}(m_d - m_u)\right] , \qquad (4.9)$$

where $\Gamma^{(0)}$ is given by

$$\Gamma^{(0)} = \frac{G_F^2}{8\pi}|V_{q_1 q_2}|^2 m_\ell^2 \left(1 - \frac{m_\ell^2}{M_P^2}\right)^2 \left[f_P^{(0)}\right]^2 M_P , \qquad (4.10)$$

and M_P is the physical mass of the charged P-meson including both e.m. and leading-order strong IB corrections.

The quantity δR_P encodes both the e.m. and the strong IB leading-order corrections to the tree-level decay rate. Its value depends on the prescription used for the separation

between the QED and QCD corrections, while the quantity

$$\mathcal{F}_P^2 \equiv \frac{\Gamma(P^\pm \to \ell^\pm \bar{\nu}_\ell[\gamma])}{\frac{G_F^2}{8\pi}|V_{q_1 q_2}|^2 m_\ell^2 \left(1 - \frac{m_\ell^2}{M_P^2}\right)^2 M_P} = \left[f_P^{(0)}\right]^2 (1 + \delta R_P) \tag{4.11}$$

is prescription independent [48] to all orders in both $\alpha_{\rm em}$ and $(m_d - m_u)$.

The quantity $\mathcal{F}_\pi$ may be used to set the lattice scale instead of the Ω baryon mass. The physical value $\mathcal{F}_\pi^{\rm phys}$ can be obtained by taking the experimental pion decay rate $\Gamma(\pi^- \to \mu^- \bar{\nu}_\mu[\gamma]) = 3.8408(7) \cdot 10^7$ s^{-1} from the PDG [3] and the result for $|V_{ud}| = 0.97420(21)$ determined accurately from super-allowed β-decays in Ref. [15]. Consequently, one may replace M_Ω with $\mathcal{F}_\pi$ (as the denominator of the ratios $R_{1,...,4}$ in Eqs. (1.84)), M_{π^+} with M_{π^0} in the ratio R_1 (when working at leading order in $\alpha_{\rm em}$) and set the electron charge directly to its Thomson's limit (instead of using the ratio R_5), namely

$$R_1(aN; g_s, e, \mathbf{m}) = \frac{aM_{\pi^0}}{a\mathcal{F}_\pi}(aN; g_s, e, \mathbf{m}),$$

$$R_2(aN; g_s, e, \mathbf{m}) = \frac{aM_{K^0}}{a\mathcal{F}_\pi}(aN; g_s, e, \mathbf{m})$$

$$R_3(aN; g_s, e, \mathbf{m}) = \frac{aM_{D_s}}{a\mathcal{F}_\pi}(aN; g_s, e, \mathbf{m}),$$

$$R_4(aN; g_s, e, \mathbf{m}) = \frac{aM_{K^+} - aM_{K^0}}{a\mathcal{F}_\pi}(aN; g_s, e, \mathbf{m}). \tag{4.12}$$

Note that for the present study we were unable to use M_Ω to determine the lattice spacing because the corresponding baryon correlators were unavailable. The choice of using $\mathcal{F}_\pi$ instead to set the scale clearly prevents us from being able to predict the value of $|V_{ud}|$. As already explained above, in this work we renormalize the QCD theory using the same set of hadronic inputs adopted in our quark-mass analysis in Ref. [66], since we started the present calculations using the RM123 method on previously generated isosymmetric QCD gauge configurations from ETMC (see Sec. 2.2). The bare parameters of these QCD gauge ensembles were fixed in Ref. [66] by using the hadronic scheme corresponding to $M_\pi^{(0),\rm FLAG} = 134.98$ MeV, $M_K^{(0),\rm FLAG} = 494.2(3)$ MeV and $f_\pi^{(0),\rm FLAG} = 130.41(20)$ MeV, while $M_{D_s}^{(0)}$ was chosen to be equal to the experimental D_s^+-meson mass, $M_{D_s^+} = 1969.0(1.4)$ MeV [3]. Note that in the absence of QED radiative corrections $\mathcal{F}_\pi$ reduces to the conventional definition of the pion decay constant $f_\pi^{(0)}$. The superscript FLAG has been used because the chosen values of three out of the four hadronic inputs had been suggested in the previous editions of the FLAG review [4]. For this reason we refer to the scheme defined from these inputs as the FLAG scheme.

We have calculated the same input parameters (4.12) used in the FLAG scheme also in the GRS scheme (corresponding to the $\overline{\rm MS}$ scheme at $\mu = 2$ GeV) obtaining: $M_\pi^{(0),\rm GRS} = 135.0(2)$ MeV, $M_K^{(0),\rm GRS} = 494.6(1)$ MeV, $M_{D_s}^{(0),\rm GRS} = 1966.7(1.5)$ MeV and $f_\pi^{(0),\rm GRS} = 130.65(12)$ MeV (see Eqs. (2.16), (2.17), (2.19) in Sec. 2.1 and Eq. (4.70) in Sec. 4.5 below). Therefore, the

values of the inputs determined in the GRS scheme differ at most by $\sim 0.15\%$ from the corresponding values adopted in Ref. [66] for the isosymmetric QCD theory and the differences are at the level of our statistical precision. Thus, the result of our analysis of the scheme dependence can be summarized by the conclusion that the FLAG and GRS schemes can be considered to be equivalent at the current level of precision. Nevertheless, we have used the results of this analysis to estimate the systematic error on our final determinations of the isospin breaking corrections δR_P induced by residual scheme uncertainties (see the discussion at the end of Sec. 4.5).

In light of this quantitative analysis, given the numerical equivalence of the two schemes at the current level of precision, in the rest of the chapter we shall compare our results obtained in the GRS scheme with the results obtained by other groups using the FLAG scheme and we shall not use superscripts to distinguish between the two schemes.

The correction δR_P, defined in Eq. (4.9), is given by (see Ref. [10])

$$\delta R_P = \frac{\alpha_{\rm em}}{\pi}\log\left(\frac{M_Z^2}{M_W^2}\right) + 2\frac{\delta A_P}{A_P^{(0)}} - 2\frac{\delta M_P}{M_P^{(0)}} + \delta\Gamma_P^{(\rm pt)}(\Delta E_\gamma) \,, \qquad (4.13)$$

where

   i) the term containing $\log(M_Z^2/M_W^2)$ comes from the short-distance matching (3.9) between the full theory (the Standard Model) and the effective theory in the W-regularization [12];

  ii) the quantity $\delta\Gamma_P^{(\rm pt)}(\Delta E_\gamma)$ represents the $O(\alpha_{\rm em})$ correction to the tree-level decay rate for a point-like meson (see Eq. (4.1)), which can be read off from Eq. (3.54). The cut-off on the final-state photon's energy, ΔE_γ, must be sufficiently small for the point like-approximation to be valid;

 iii) δA_P is the e.m. and strong IB correction to the decay amplitude $P \to \ell\nu$ with the corresponding correction to the amplitude with a point-like meson subtracted (this subtraction term is added back in the term $\delta\Gamma_P^{(\rm pt)}(\Delta E_\gamma)$, see Eq. (4.1)).

 iv) δM_P are the e.m. and strong IB corrections to the mass of the P-meson. The correction proportional to $2\,\delta M_P/M_P^{(0)}$ is present because of the definition of $f_P^{(0)}$ in terms of the amplitude and of the meson mass in Eq. (4.6).

Since we adopt the qQED approximation, which neglects the effects of the sea-quark electric charges, the calculation of δA_P and δM_P only requires the evaluation of the connected diagrams. These are shown in Figs. 4.2.1 - 4.2.5 for the case of $K_{\ell 2}$ decays. At $O(\alpha_{\rm em})$ the diagram in Fig. 4.2.1 corresponds to the insertion of the operator renormalized in the W-renormalization scheme.

In Eq. (4.13) δA_P and δM_P contain both the e.m. and the strong IB leading-order corrections

$$\delta A_P = \delta A_P^W + \delta A_P^{\rm SIB} + \sum_{i=J,T,P,S} \delta A_P^i + \delta A_P^\ell + \delta A_P^{\ell,{\rm self}} \,, \qquad (4.14)$$

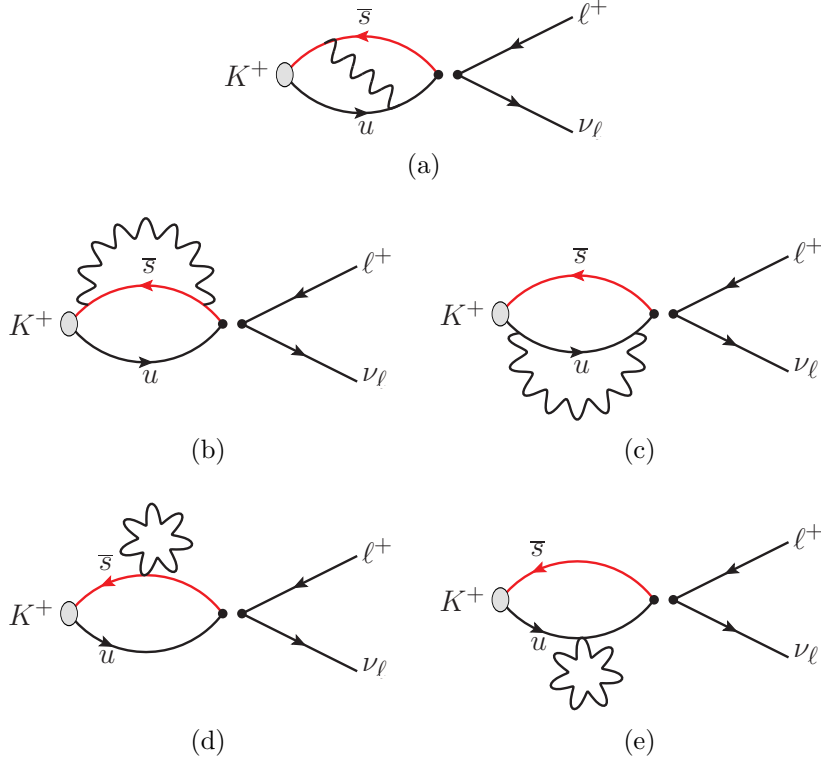$$\delta M_P = \delta M_P^{\rm SIB} + \sum_{i=J,T,P,S} \delta M_P^i \,, \qquad (4.15)$$

Figure 4.2.2: *Connected diagrams contributing at $O(\alpha_{\rm em})$ to the $K^+ \to \ell^+ \nu_\ell$ decay amplitude, in which the photon is attached to quark lines: (a) exchange, (b, c) self-energy and (d, e) tadpole diagrams. The labels are introduced to identify the individual diagrams when describing their evaluation in the text.*
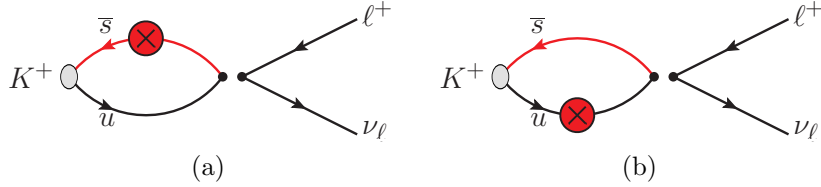

Figure 4.2.3: *Connected diagrams contributing at $O(\alpha_{\rm em})$ to the $K^+ \to \ell^+ \nu_\ell$ decay amplitude corresponding to the insertion of the pseudoscalar density related to the e.m. shift of the critical mass, δm_f^{crit}, determined in Ref. [7] (see Sec. 2.3.1).*

where δA_P^W is the e.m. correction from both the matching of the four-fermion lattice weak operator to the W-renormalization scheme and from the mixing with several bare lattice four-fermion operators generated by the breaking of chiral symmetry with the twisted-mass fermion action which we are using. Both the matching and the mixing will be discussed and calculated in Sec. 4.3. As already pointed out, the renormalized operator, defined in the W-renormalization scheme, is inserted in the diagram of Fig. 4.2.1. As for the diagrams of Figs. 4.2.2 - 4.2.5, which are already of order $O(\alpha_{\rm em})$ and $O((m_d - m_u)/\Lambda_{\rm QCD})$, it is sufficient to insert the weak current operator renormalized in QCD only.
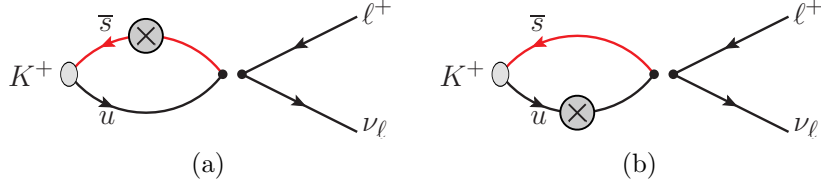
Figure 4.2.4: *Connected diagrams contributing at $O(\alpha_{\rm em})$ and $O(m_d - m_u)$ to the $K^+ \to \ell^+ \nu_\ell$ decay amplitude related to the insertion of the scalar density (see Ref. [7]).*
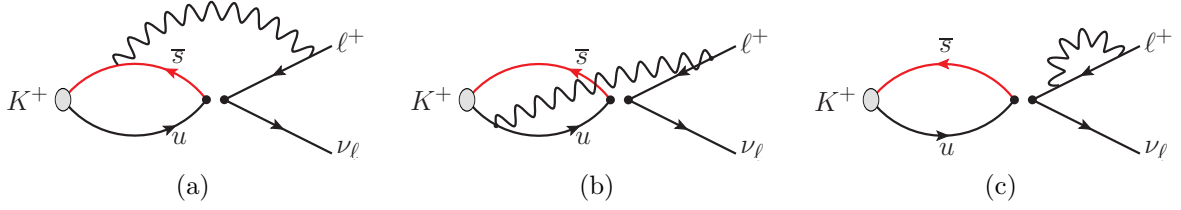

Figure 4.2.5: *Connected diagrams contributing at $O(\alpha_{\rm em})$ to the $K^+ \to \ell^+ \nu_\ell$ decay amplitude corresponding to photon exchanges involving the final-state lepton.*

In Eqs. (4.14) and (4.15) the quantity $\delta A_P^{\rm SIB}$ ($\delta M_P^{\rm SIB}$) represents the strong IB corrections proportional to $m_d - m_u$ and to the diagram of Fig. 4.2.4(b), while the other terms are QED corrections coming from the insertions of the e.m. current and tadpole operators, of the pseudoscalar and scalar densities (see Refs. [8, 9]). The term δA_P^J (δM_P^J) is generated by the diagrams of Fig. 4.2.2(a-c), δA_P^T (δM_P^T) by the diagrams of Fig. 4.2.2(d-e), δA_P^P (δM_P^P) by the diagrams of Fig. 4.2.3(a-b) and δA_P^S (δM_P^S) by the diagrams of Fig. 4.2.4(a-b). The term δA_P^ℓ corresponds to the exchange of a photon between the quarks and the final-state lepton and arises from the diagrams in Fig. 4.2.5(a-b). The term $\delta A_P^{\ell,\rm self}$ corresponds to the contribution to the amplitude from the lepton's wave function renormalization; it arises from the self-energy diagram of Fig. 4.2.5(c). The contribution of this term cancels out in the difference $\Gamma_0(L) - \Gamma_0^{\rm pt}(L)$ and could be therefore omitted, as explained Sec. 3.3. The different insertions of the scalar density encode the strong IB effects together with the counter terms necessary to fix the masses of the quarks. The insertion of the pseudoscalar density is peculiar to twisted mass quarks and would be absent in standard Wilson (improved) formulations of QCD.

In the following subsection we discuss the calculation of all the diagrams that do not involve the photon attached to the charged lepton line. The determination of the contributions δA_P^ℓ and $\delta A_P^{\ell,\rm self}$ will be described later in subsection 2.2.

4.2.1 QUARK-QUARK PHOTON EXCHANGE DIAGRAMS AND SCALAR AND PSEUDOSCALAR INSERTIONS

The terms δA_P^i and δM_P^i ($i = J, T, P, S$) can be extracted from the following correlators:

$$\delta C_P^J(t) = 4\pi\alpha_{em} \frac{1}{2} \sum_{\vec{x},y_1,y_2} \langle 0|T\left\{J_W^\rho(0)\ J_\mu(y_1)J_\nu(y_2)\ \phi_P^\dagger(\vec{x},-t)\right\}|0\rangle \Delta_{\mu\nu}(y_1,y_2)\frac{p_P^\rho}{M_P} \quad (4.16)$$

$$\delta C_P^T(t) = 4\pi\alpha_{em} \sum_{\vec{x},y} \langle 0|T\left\{J_W^\rho(0)\ T_\mu(y)\ \phi_P^\dagger(\vec{x},-t)\right\}|0\rangle \Delta_{\mu\mu}(y,y)\frac{p_P^\rho}{M_P} , \quad (4.17)$$

$$\delta C_P^P(t) = 4\pi\alpha_{em} \sum_{f=f_1,f_2} \delta m_f^{crit} \cdot \sum_{\vec{x},y} \langle 0|T\left\{J_W^\rho(0)\ i\bar{q}_f(y)\gamma_5 q_f(y)\ \phi_P^\dagger(\vec{x},-t)\right\}|0\rangle \frac{p_P^\rho}{M_P} \quad (4.18)$$

$$\delta C_P^S(t) = -4\pi\alpha_{em} \sum_{f=f_1,f_2} m_f \frac{\mathcal{Z}^f}{Z_m} \cdot \sum_{\vec{x},y} \langle 0|T\left\{J_W^\rho(0)\ [\bar{q}_f(y)q_f(y)]\ \phi_P^\dagger(\vec{x},-t)\right\}|0\rangle \frac{p_P^\rho}{M_P} , \quad (4.19)$$

where $\Delta_{\mu\nu}(y_1,y_2)$ is the photon propagator, $J_W^\rho(x)$ is the local version of the hadronic $(V-A)$ weak current renormalized in QCD only[1]

$$J_W^\rho(x) = \bar{q}_{f_2}(x)\gamma^\rho\left[Z_V^{(0)} - Z_A^{(0)}\gamma^5\right]q_{f_1}(x) , \quad (4.20)$$

and J_μ and T_μ are the lattice conserved e.m. current[2] and the tadpole operator, respectively, defined in Eqs. (1.31), (1.39). In Eqs. (4.16)-(4.19) $\phi_P^\dagger(\vec{x},-t) = i\bar{q}_{f_1}(\vec{x},-t)\gamma_5 q_{f_2}(\vec{x},-t)$ is the interpolating field for a P-meson composed by two valence quarks f_1 and f_2 with charges $e_1 e$ and $e_2 e$. The Wilson r-parameters r_{f_1} and r_{f_2} are always chosen to be opposite $r_{f_1} = -r_{f_2}$. We have also chosen to place the weak current at the origin and to create the P-meson at a negative time $-t$, where t and $T-t$ are sufficiently large to suppress the contributions from heavier states and from the backward propagating P-meson (this latter condition may be convenient but is not necessary). In Eq. (4.19) Z_m is the mass RC in pure QCD, which for our maximally twisted-mass setup is given by $Z_m = 1/Z_P$, where Z_P is the RC of the pseudoscalar density determined in Ref. [66]. The quantity $\mathcal{Z}^f$ is related to the e.m. correction to the mass RC according to Eq. (2.33). The values of the coefficients Z_m^{fact}, corresponding to the non-factorisable e.m. corrections to the mass RC, are collected in Table V.

Analogously, the term $[\delta A_P]^{\text{SIB}}$ and $[\delta M_P]^{\text{SIB}}$ can be extracted from the correlator

$$\delta C_P^{\text{SIB}}(t) = -\sum_{f=f_1,f_2} \frac{\widehat{m}_f - m_f}{Z_m} \cdot \sum_{\vec{x},y} \langle 0|T\left\{J_w^\rho(0)\ [\bar{q}_f(y)q_f(y)]\ \phi_P^\dagger(\vec{x},-t)\right\}|0\rangle \frac{p_P^\rho}{M_P} , \quad (4.21)$$

---

[1]In our maximally twisted-mass setup, in which the Wilson r-parameters r_{f_1} and r_{f_2} are always chosen to be opposite $r_{f_1} = -r_{f_2}$, the vector (axial) weak current in the physical basis renormalizes multiplicatively with the RC Z_A (Z_V) of the axial (vector) current for Wilson-like fermions, i.e. $Z_V^{(0)} = Z_A$ and $Z_A^{(0)} = Z_V$ (see Appendix 6.2).

[2]The use of the conserved e.m. current guarantees the absence of additional contact terms in the product $J_\mu(y_1)J_\nu(y_2)$.

where, following the notation of Ref. [7], we indicate with $\widehat{m}_f$ and m_f the renomalized masses of the quark with flavor f in the full theory and in isosymmetric QCD only, respectively. We stress again that the separation between QCD and QED corrections is prescription dependent and in this work we adopt the GRS prescription of Refs. [7, 9, 16], where

$$
\begin{aligned}
\widehat{m}_u(\overline{\text{MS}}, 2\,\text{GeV}) + \widehat{m}_d(\overline{\text{MS}}, 2\,\text{GeV}) &= 2\widehat{m}_{ud}(\overline{\text{MS}}, 2\,\text{GeV}) = 2m_{ud}(\overline{\text{MS}}, 2\,\text{GeV}), \\
\widehat{m}_s(\overline{\text{MS}}, 2\,\text{GeV}) = m_s(\overline{\text{MS}}, 2\,\text{GeV}), &\qquad \widehat{m}_c(\overline{\text{MS}}, 2\,\text{GeV}) = m_c(\overline{\text{MS}}, 2\,\text{GeV}).
\end{aligned}
\tag{4.22}
$$

Thus, in Eq. (4.21), the only relevant quark mass difference is $\widehat{m}_d - m_{ud} = -(\widehat{m}_u - m_{ud})$, whose value in the $(\overline{\text{MS}}, 2\,\text{GeV})$ scheme was found to be equal to $1.19(9)$ MeV [7] (see Eq. (2.66)) using as inputs the experimental values of the charged and neutral kaon masses.

Following Ref. [9] we form the ratio of $\delta C_P^i(t)$ with the corresponding tree-level correlator

$$
C_P^{(0)}(t) = \sum_{\vec{x}} \langle 0|T\left\{ J_W^\rho(0)\phi_P^\dagger(\vec{x}, -t) \right\}|0\rangle \frac{p_P^\rho}{M_P}
\tag{4.23}
$$

and at large time distances t we obtain ($i = J, T, P, S, QCD$)

$$
\frac{\delta C_P^i(t)}{C_P^{(0)}(t)} \xrightarrow[t\gg a,(T-t)\gg a]{} \frac{\delta[G_P^i A_P^i]}{G_P^{(0)} A_P^{(0)}} +
$$
$$
\frac{\delta M_P^i}{M_P^{(0)}}\left[M_P^{(0)}\left(\frac{T}{2} - t\right)\frac{e^{-M_P^{(0)}t} + e^{-M_P^{(0)}(T-t)}}{e^{-M_P^{(0)}t} - e^{-M_P^{(0)}(T-t)}} - 1 - M_P^{(0)}\frac{T}{2} \right]
\tag{4.24}
$$

where

$$
G_P^{(0)} \equiv \langle 0|\phi_P(0)|P^{(0)}\rangle
\tag{4.25}
$$

is the coupling of the interpolating field of the P-meson with its ground-state in isosymmetric QCD. The term proportional to δM_P^i in the r.h.s. of Eq. (4.24) is related to the e.m. and strong IB corrections of the meson mass.

The function in the square brackets on the r.h.s. of Eq. (4.24) is an almost linear function of t. Thus, the correction to the P-meson mass, δM_P^i, can be extracted from the slope of the ratio $\delta C_P^i(t)/C_P^{(0)}(t)$ and the quantity $\delta[G_P^i A_P^i]$ from its intercept. As explained in Ref. [10], in order to obtain the quantity δA_P^i the correction δG_P^i is separately determined by evaluating a correlator similar to those of Eqs. (4.16)-(4.19), in which the weak operator $J_W^\rho p_P^\rho/M_P$ is replaced by the P-meson interpolating field ϕ_P.

For illustration, in Fig. 4.2.6 we show the ratios C_P^i for the charged kaon ($P = K$) obtained from the ensemble D20.48 (see Sec. 2.2). The top panel contains the ratio $\delta C_K^{\text{SIB}}(t)/C_K^{(0)}(t)$, the ratio $\delta C_K^J(t)/C_K^{(0)}(t)$ is shown in the middle panel and the ratios $\delta C_K^T(t)/C_K^{(0)}(t)$ and $\delta C_K^P(t)/C_K^{(0)}(t)$ are presented in the bottom panel.

We find: i) the contributions $\delta C_K^T(t)/C_P^{(0)}(t)$ and $\delta C_K^P(t)/C_P^{(0)}(t)$ are separately large, but strongly correlated, since the tadpole insertion dominates the values of the e.m. shift of
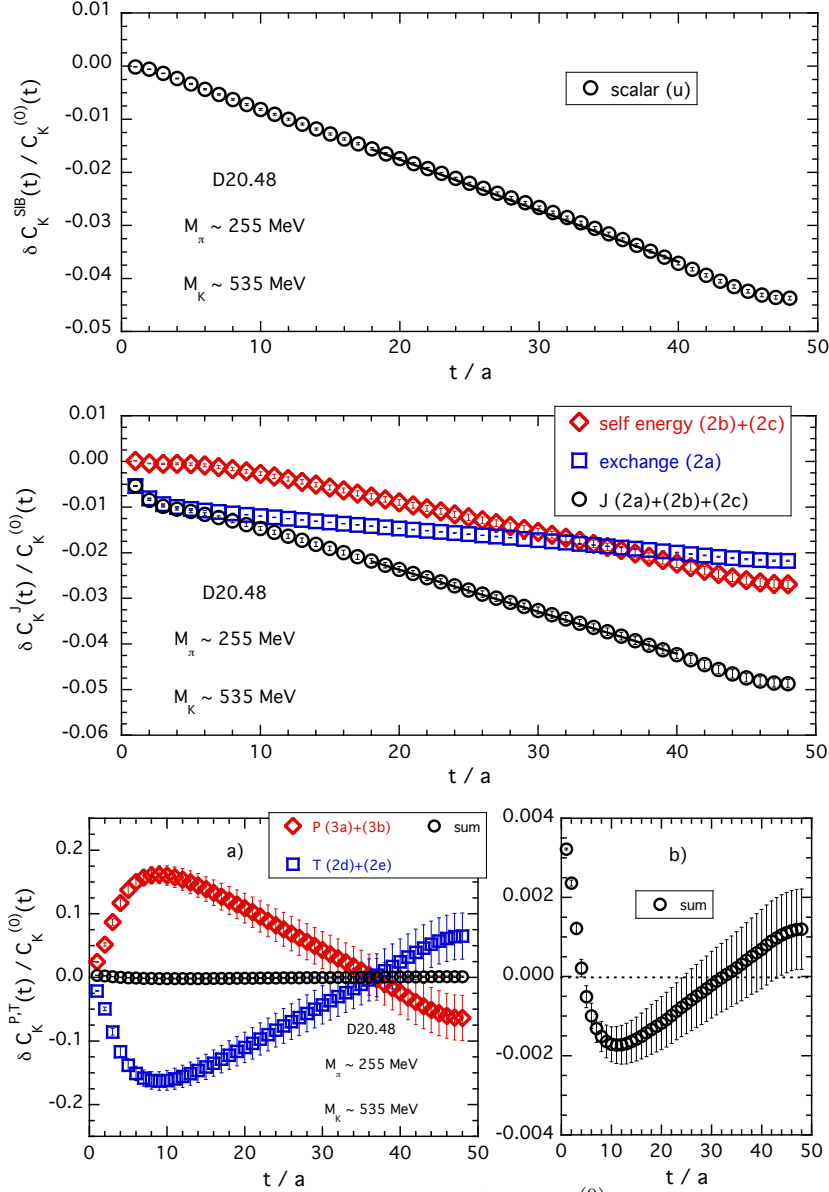
Figure 4.2.6: *Top panel: The strong IB correction $\delta C_K^{\text{SIB}}(t)/C_K^{(0)}(t)$ for the charged kaon obtained on the ensemble D20.48 (see Sec. 2.2). The solid line is the "linear" fit (4.24) applied in the time interval where the ground-state is dominant. Middle panel: contributions of the exchange (4.2.2a) and self-energy (4.2.2b)+(4.2.2c) diagrams. The circles represent the sum (4.2.2a)+(4.2.2b)+(4.2.2c), i.e. the ratio $\delta C_K^J(t)/C_K^{(0)}(t)$. Bottom panel: contributions of the tadpole operator $\delta C_K^T(t)/C_K^{(0)}(t)$, i.e. diagrams (4.2.2d)+(4.2.2e), and of the e.m. shift of the critical mass $\delta C_K^P(t)/C_K^{(0)}(t)$, i.e. diagrams (4.2.3a)+(4.2.3b). The sum $\delta[C_K^T(t)+C_K^P(t)]/C_K^{(0)}(t)$, shown by the circles, is non vanishing and it is determined quite precisely (see the right-hand plot where it is presented on an expanded scale). Errors are statistical only.*

the critical mass δm_f^{crit} (see Sec. 2.3.1). In the chiral limit they would cancel, but at finite masses the sum is small and linear in t. Because of the correlations it can nevertheless, be determined quite precisely (see the bottom right-hand plot of Fig. 4.2.6) where the sum

is presented on an expanded scale. ii) the time dependence of the ratio $\delta C_K^J(t)/C_K^{(0)}(t)$ is almost linear in the time interval where the ground state is dominant.

4.2.2 CROSSED DIAGRAMS AND LEPTON SELF-ENERGY

The evaluation of the diagrams 4.2.5(a)‑(b), corresponding to the term δA_P^ℓ in Eq. (4.14), can be obtained by studying the correlator [10]

$$
\delta C_P^\ell(t) = -4\pi\alpha_{\mathrm{em}} \sum_{\vec{x},x_1,x_2} \langle 0|\, T\left\{ J_W^\rho(0) J_\mu(x_1) \phi_P^\dagger(\vec{x},-t) \right\} |0\rangle \Delta_{\mu\nu}(x_1,x_2) e^{E_\ell t_2 - i\vec{p}_\ell\cdot\vec{x}_2}
$$

$$
\cdot\ \ \overline{u}(p_\nu)\gamma_\rho(1-\gamma_5) S^\ell(0,x_2)\gamma_\nu v(p_\ell) \left[\overline{v}(p_\ell)\gamma_\sigma(1-\gamma_5) u(p_\nu) \frac{p_P^\sigma}{M_P} \right] , \qquad (4.26)
$$

where $S^\ell(0,x_2)$ stands for the free twisted-mass propagator of the charged lepton. For the numerical analysis we have found it to be convenient to saturate the Dirac indices by inserting on the r.h.s. of Eq. (4.26) the factor $[\overline{v}(p_\ell)\gamma_\sigma(1-\gamma_5)u(p_\nu)]$, which represents the lowest order "conjugate" leptonic $(V-A)$ amplitude, and to sum over the lepton polarizations. In this way we are able to study the time behaviour of the single function $\delta C_P^\ell(t)$.

The corresponding correlator at lowest order $(O(\alpha_{\mathrm{em}}^0))$ is

$$
C_P^{\ell(0)}(t) = \sum_{\vec{x}} \langle 0|\, T\left\{ J_W^\rho(0) \phi_P^\dagger(\vec{x},-t) \right\} |0\rangle\ \overline{u}(p_\nu)\gamma_\rho(1-\gamma_5) v(p_\ell) \left[\overline{v}(p_\ell)\gamma_\sigma(1-\gamma_5) u(p_\nu) \frac{p_P^\sigma}{M_P} \right] .
$$
$$(4.27)$$

In Eqs. (4.26) and (4.27) the contraction between the weak hadronic current $J_W^\rho(0)$ [see Eq. (4.20)] and its leptonic $(V-A)$ counterpart gives rise to two terms corresponding to the product of either the temporal or spatial components of these two weak currents, which are odd and even under time reversal, respectively. Thus, on a lattice with finite time extension T, for $t \gg a$ and $(T-t) \gg a$ one has

$$
\delta C_P^\ell(t) \xrightarrow[t\gg a,(T-t)\gg a]{} \frac{G_P^{(0)}}{2M_P^{(0)}} \sum_{j=0}^{4} \delta A_P^{\ell,j}\ X_P^{\ell,j} \left[e^{-M_P^{(0)}t} + s_j e^{-M_P^{(0)}(T-t)} \right] , \qquad (4.28)
$$

where $s_0 = -1$, $s_{1,2,3} = 1$ and

$$
X_P^{\ell,j} = \mathrm{Tr}\left[\gamma_j(1-\gamma_5)\ell\bar{\ell}\gamma_0(1-\gamma_5)\nu\overline{\nu} \right] \qquad (4.29)
$$

is the relevant leptonic trace evaluated on the lattice using for the charged lepton the free twisted-mass propagator and for the neutrino the free Wilson propagator in the P-meson rest frame $[p_P^\sigma = (M_P, \vec{0})]$.

Similarly, for the lowest-order correlator one has

$$
C_P^{\ell(0)}(t) \xrightarrow[t\gg a,(T-t)\gg a]{} \frac{G_P^{(0)}}{2M_P^{(0)}} A_P^{(0)}\ X_P^{\ell,0} \left[e^{-M_P^{(0)}t} - e^{-M_P^{(0)}(T-t)} \right] , \qquad (4.30)
$$

where $A_P^{(0)}$ is the renormalized axial amplitude evaluated on the lattice in isosymmetric QCD in the P-meson rest frame, namely

$$Z_A^{(0)} \langle 0|\bar{q}_2 \gamma_j \gamma_5 q_1 |P^{(0)}\rangle = \delta_{j,0} A_P^{(0)} \ . \tag{4.31}$$

The effect of the different signs of the backward-propagating signal in Eq. (4.28) can be removed by introducing the following new correlators:

$$
\begin{aligned}
\delta \overline{C}_P^\ell(t) &\equiv \frac{1}{2}\left\{ \delta C_P^\ell(t) + \frac{\delta C_P^\ell(t-1) - \delta C_P^\ell(t+1)}{e^{M_P^{(0)}} - e^{-M_P^{(0)}}} \right\} \xrightarrow[t\gg a,(T-t)\gg a]{} \delta A_P^\ell \, X_P^{\ell,0} \frac{G_P^{(0)}}{2M_P^{(0)}} e^{-M_P^{(0)}t} \, , \\
\overline{C}_P^{\ell(0)}(t) &\equiv \frac{1}{2}\left\{ C_P^{\ell(0)}(t) + \frac{C_P^{\ell(0)}(t-1) - C_P^{\ell(0)}(t+1)}{e^{M_P^{(0)}} - e^{-M_P^{(0)}}} \right\} \xrightarrow[t\gg a,(T-t)\gg a]{} A_P^{(0)} \, X_P^{\ell,0} \frac{G_P^{(0)}}{2M_P^{(0)}} e^{-M_P^{(0)}t} \, ,
\end{aligned}
\tag{4.32}
$$

where

$$\delta A_P^\ell = \frac{1}{X_P^{\ell,0}} \sum_{j=0}^{4} \delta A_P^{\ell,j} \, X_P^{\ell,j} \ . \tag{4.33}$$

Thus, the quantity $\delta A_P^\ell/A_P^{(0)}$ can be extracted from the plateau of the ratio $\delta \overline{C}_P^\ell(t)/\overline{C}_P^{\ell(0)}(t)$ at large time separations, viz.

$$\frac{\delta \overline{C}_P^\ell(t)}{\overline{C}_P^{\ell(0)}(t)} \xrightarrow[t\gg a,(T-t)\gg a]{} \frac{\delta A_P^\ell}{A_P^{(0)}} \ . \tag{4.34}$$

Note that the diagrams in Fig. 4.2.5(a) - (b) do not contribute to the electromagnetic corrections to the masses of the mesons and therefore the ratio (4.34) has no slope in t in contrast to the ratios (4.24). Moreover, the explicit calculation of $X_P^{\ell,j}$ on the lattice is not required.

In terms of the lattice momenta $a\widetilde{p}_\ell$ and $a\overline{p}_\ell$, defined as

$$a\widetilde{p}_\ell = \sqrt{\sum_{k=1,2,3} \sin^2(ap_{\ell k})} \, , \tag{4.35}$$

$$a\overline{p}_\ell = 2\sqrt{\sum_{k=1,2,3} \sin^2\left(\frac{ap_{\ell k}}{2}\right)} \, , \tag{4.36}$$

the energy-momentum dispersion relations for the charged lepton and the neutrino in the P-meson rest frame are given by

$$a\widetilde{E}_\ell = 2\,\text{arcsinh}\left[\frac{1}{2}\sqrt{\frac{a^2 m_\ell^2 + a^2\widetilde{p}_\ell^2 + a^4\overline{p}_\ell^4/4}{1 + a^2\overline{p}_\ell^2/2}}\right] \, , \tag{4.37}$$

$$a\widetilde{E}_\nu = \text{arcsinh}(a\widetilde{p}_\ell) \, . \tag{4.38}$$

The 3-momentum of the final-state lepton $\vec{p}_\ell$ ($\vec{p}_\nu = -\vec{p}_\ell$) must be chosen to satisfy the equation

$$\widetilde{E}_\ell + \widetilde{E}_\nu = M_P^{(0)} \,. \tag{4.39}$$

Thus, for any given simulated P-meson mass $M_P^{(0)}$, the 3-momentum $\vec{p}_\ell = |\vec{p}_\ell|(1, 1, 1)$, is calculated from Eq. (4.39) and is injected on the lattice using non-periodic boundary conditions [105, 106] for the lepton field. A simple calculation yields

$$X_P^{\ell,0} = \mathrm{Tr}\left[\gamma_0(1 - \gamma_5)\ell\bar{\ell}\gamma_0(1 - \gamma_5)\nu\bar{\nu}\right] = 8a\widetilde{p}_\ell \left[\sinh(a\widetilde{E}_\ell) - a\widetilde{p}_\ell\right] \,. \tag{4.40}$$

In Fig. 4.2.7 we show the correlators $C_\pi^{\mu(0)}(t)$, $\delta C_\pi^\mu(t)$, $\overline{C}_\pi^{\mu(0)}(t)$ and $\delta\overline{C}_\pi^\mu(t)$ for $\pi_{\mu 2}$ decays, multiplied by the ground-state exponential. These were obtained on the gauge ensembles A40.24 and D30.48 of Sec. 2.2. The subtraction of the backward signals, needed for extracting directly the quantity δA_P^ℓ given by Eq. (4.33), is beneficial also for extending the time region from which δA_P^ℓ (as well as the ratio $\delta A_P^\ell / A_P^{(0)}$) can be determined.

The quality of the signal for the ratio $\delta\overline{C}_P^\mu(t)/\overline{C}_P^{\mu(0)}(t)$ is illustrated in Fig. 4.2.8 for charged kaon and pion decays into muons for the case of the ensembles B55.32 and D30.48.

The calculation of the correction due to the diagram 4.2.5(c) is straightforward, since it is obtained by simply multiplying the lowest order amplitude, $A_P^{(0)}$, by the one-loop lepton self-energy evaluated on the lattice.

4.3 RENORMALIZATION OF THE EFFECTIVE HAMILTONIAN

When inserted into the expression for amplitude for the decay $P \to \ell\nu$, the term of order α_{em} of the renormalized operator $O_1^{\mathrm{W\text{-}reg}}(M_W)$ of Eq. (3.27) given in Sec. 3.2.3, namely $\delta O_1^{\mathrm{W\text{-}reg}}(M_W) = O_1^{\mathrm{W\text{-}reg}}(M_W) - O_1^\chi$, provides the contribution denoted as δA_P^W in Eq. (4.14)

$$\delta A_P^W = -\frac{\langle 0| \,\mathrm{Tr}\left\{\delta O_1^{\mathrm{W\text{-}reg}}(M_W)\bar{\ell}\gamma_0(1 - \gamma_5)\nu\right\} |P^{(0)}\rangle}{X_P^{\ell,0}} \,, \tag{4.41}$$

where $X_P^{\ell,0}$ is the leptonic trace defined in Eq. (4.40). We then note that O_1^χ and O_2^χ defined in Eq. (3.25) and entering in Eq. (3.27) give opposite contributions to the tree-level amplitude, i.e.

$$\langle 0|\mathrm{Tr}\left\{O_1^{\mathrm{bare}}\,\bar{\ell}\gamma_0(1 - \gamma_5)\nu\right\} |P^{(0)}\rangle = -\langle 0|\mathrm{Tr}\left\{O_2^{\mathrm{bare}}\,\bar{\ell}\gamma_0(1 - \gamma_5)\nu\right\} |P^{(0)}\rangle = -A_P^{(0)}\,X_P^{\ell,0} \,, \tag{4.42}$$

with $A_P^{(0)}$ given in Eq. (4.31) . Therefore, after averaging the amplitude over the values of the parameter $\bar{r} = \pm 1$, in order to cancel out the contribution of the mixing with O_3 and O_4, one obtains

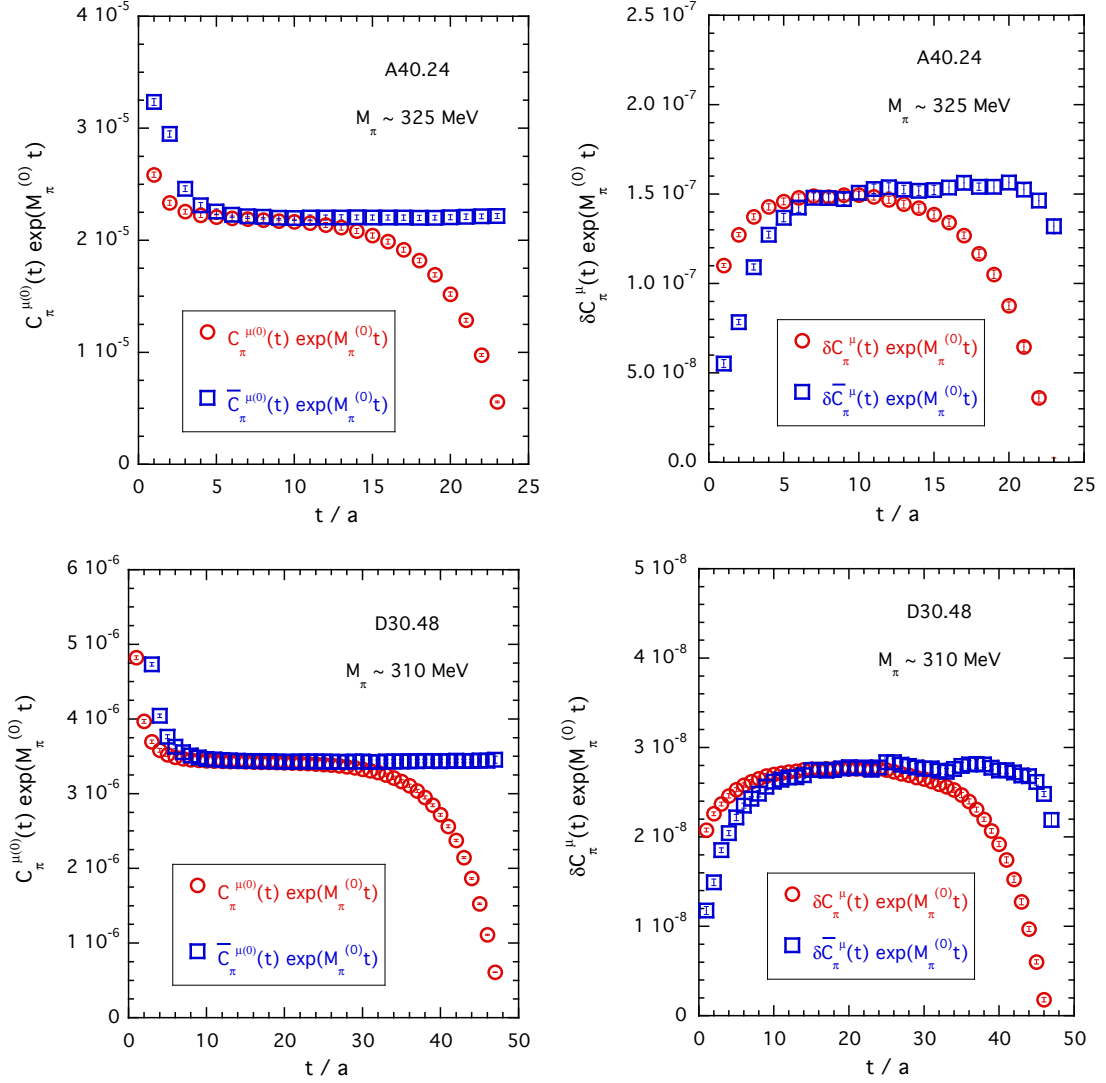$$\delta A_P^W = Z^{\mathrm{W\text{-}reg}} A_P^{(0)} \,, \tag{4.43}$$

Figure 4.2.7: *Time dependence of the correlators $C_\pi^{\mu(0)}(t)$ (left panels) and $\delta C_\pi^\mu(t)$ (right panels) for $\pi_{\mu 2}$ decays. These are given in lattice units and multiplied by the ground-state exponential, and were obtained from gauge ensemble A40.24 (top panels) and D30.48 (bottom panels). The blue squares represent the correlators $\delta \overline{C}_\pi^\mu(t)$ and $\overline{C}_\pi^{\mu(0)}(t)$ given by Eqs. (4.32)-(4.32). Errors are statistical only. For details of the simulations Sec. 2.2.*

with

$$Z^{\text{W-reg}} = \frac{\alpha_{\text{em}}}{4\pi} \left[2 \left(1 - \frac{\alpha_s(1/a)}{4\pi} \right) \log \left(a^2 M_W^2 \right) - 15.0032 + \eta_{11}(\alpha_s(1/a)) - \eta_{12}(\alpha_s(1/a)) \right] . \tag{4.44}$$

As already noted, the contribution δA_P^W of the matching factor at order α_{em} to the decay amplitude, expressed by Eqs. (4.43) and (4.44), is gauge independent. It then follows that also the order α_{em} contribution of the bare diagrams to the amplitude, expressed by the other terms in Eq. (4.14), is by itself gauge independent. Therefore, we can numerically evaluate
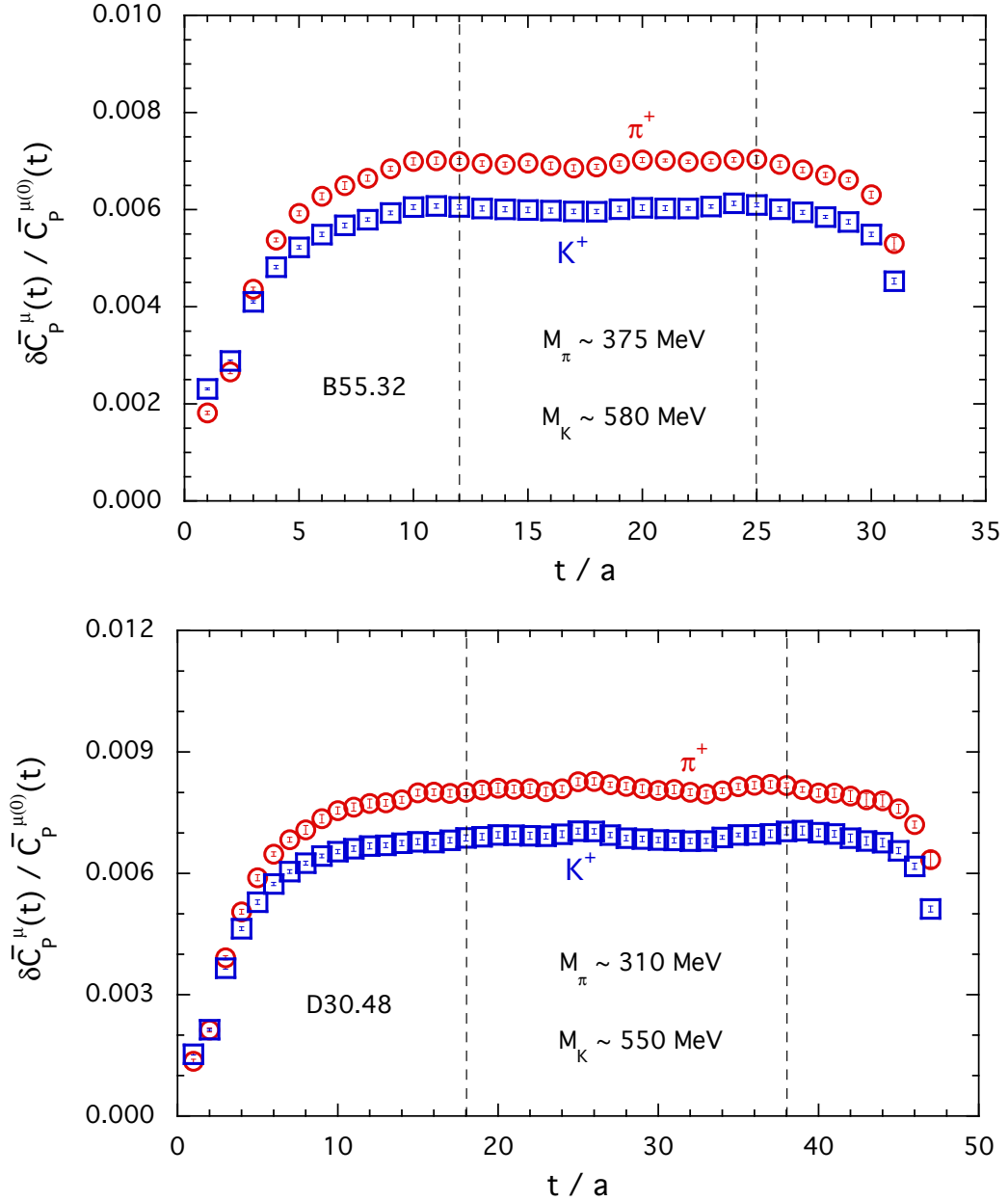
Figure 4.2.8: *Results for the ratio $\delta\overline{C}_P^\mu(t)/\overline{C}_P^{\mu(0)}(t)$, given by Eq. (4.34), for $K_{\mu2}$ and $\pi_{\mu2}$ decays obtained from the gauge ensembles B55.32 (top panel) and D30.48 (bottom panel). The vertical dashed lines indicate the time region used for the extraction of the ratio $\delta A_P^\mu/A_P^{(0)}$. Errors are statistical only.*

the two contributions separately by making different choices for the gluon and the photon gauge in the two cases[3]. In particular, we have chosen to compute the matching factor

---

[3]It should be noted, however, that while $Z^{\text{W-reg}}$ of Eq. (4.44) is gauge independent at any order of perturbation theory, its actual numerical value may display a residual gauge dependence due to higher order

$Z^{\text{W-reg}}$ of Eq. (4.44) in the Landau gauge for both gluons and photons, because this makes RI' equivalent to RI up to higher orders in the perturbative expansions. On the other hand, in the calculation of the physical amplitudes described in Sec. 4.2 we have used a stochastic photon generated in the Feynman gauge, which has been adopted also in the calculation of $\Gamma_0^{\text{pt}}(L)$ in Ref. [88] (see Sec. 3.6).

As already discussed, when we compute the difference $\Gamma_0(L) - \Gamma_0^{\text{pt}}(L)$ in Eq. (4.1) at leading order in α_{em}, the contribution from the lepton wave function RC cancels out provided, of course, it is evaluated in $\Gamma_0(L)$ and $\Gamma_0^{\text{pt}}(L)$ in the same W-regularization scheme and in the same photon gauge. Since $\Gamma_0^{\text{pt}}(L)$ has been computed in Ref. [88] by omitting the lepton wave function RC contribution in the Feynman gauge, we have to subtract the analogous contribution from Eq. (4.44) in the Feynman gauge. The QCD and QED corrections to the the lepton wave function RC at $O(\alpha_{\text{em}})$ factorize, so that their contribution does not enter into the non-perturbative determination of the matrix η, which only contains, by its definition, non-factorisable QCD+QED contributions. Therefore, as discussed in Sec. 3.3, the subtraction of the lepton wave function RC only requires the replacement of $Z^{\text{W-reg}}$ in Eq. (4.44) by the subtracted matching factor [10]

$$\tilde{Z}^{\text{W-reg}} = Z^{\text{W-reg}} - \frac{1}{2} \delta Z_\ell^{\text{W-reg}} \,, \tag{4.45}$$

where

$$\delta Z_\ell^{\text{W-reg}} = \frac{\alpha_{\text{em}}}{4\pi} \left[-\log\left(a^2 M_W^2\right) - 13.3524 \right] \,. \tag{4.46}$$

We have verified with an explicit calculation that the contribution to the matching given in Eq. (4.46) is the same whether evaluated for an on-shell or an off-shell external lepton. The final expression to be used in Eq. (4.14) is therefore

$$\delta A_P^W = \tilde{Z}^{\text{W-reg}} A_P^{(0)} \,, \tag{4.47}$$

with

$$\tilde{Z}^{\text{W-reg}} = \frac{\alpha_{\text{em}}}{4\pi} \left[\left(\frac{5}{2} - 2\frac{\alpha_s(1/a)}{4\pi} \right) \log\left(a^2 M_W^2\right) - 8.3270 + \eta_{11}(\alpha_s(1/a)) - \eta_{12}(\alpha_s(1/a)) \right] \,. \tag{4.48}$$

To make contact with the factorization approximation introduced in Refs. [7, 37], we rewrite Eq. (4.48) as

$$\tilde{Z}^{\text{W-reg}} \equiv Z^{\text{fact}} \cdot Z_{\eta=0}^{\text{W-reg}} \tag{4.49}$$

where $Z_{\eta=0}^{\text{W-reg}}$ is the result in the factorization approximation (i.e. with $\eta = 0$)

$$Z_{\eta=0}^{\text{W-reg}} = \frac{\alpha_{\text{em}}}{4\pi} \left[\left(\frac{5}{2} - 2\frac{\alpha_s(1/a)}{4\pi} \right) \log\left(a^2 M_W^2\right) - 8.3270 \right] \,, \tag{4.50}$$

terms in the non-perturbative determination of η_{11} which are neglected in the perturbatively evaluated matching coefficient.

and Z^{fact} is the factor correcting the result for $\tilde{Z}^{\text{W-reg}}$ to include the entries of the matrix η

$$Z^{\text{fact}} \equiv 1 + \frac{\alpha_{\text{em}}}{4\pi} \frac{\eta_{11}(\alpha_s(1/a)) - \eta_{12}(\alpha_s(1/a))}{Z^{\text{W-reg}}_{\eta=0}} \,. \tag{4.51}$$

The values of the coefficients $Z^{\text{W-reg}}_{\eta=0}$ and Z^{fact} are collected in Table VI for the three values of the inverse coupling β adopted in this work and for $\mu = 1/a$. The two methods M1 and M2 correspond to different treatments of the $O(a^2\mu^2)$ discretization effects and are described in Ref. [66]. The difference of the results obtained with these two methods enters into the systematic uncertainty labelled as $()_{input}$ in Sec. 4.5 below. The results in Table VI show that the non-factorisable corrections are significant, of $\text{O}(12\text{-}25\%)$ for $Z^{\text{W-reg}}$.

		Z^{fact}	
β	$Z^{\text{W-reg}}_{\eta=0}$	Method M1	Method M2
1.90	0.00542 (11)	1.184 (11)	1.126 (7)
1.95	0.00519 (10)	1.172 (9)	1.123 (5)
2.10	0.00440 (7)	1.160 (6)	1.136 (4)

Table VI: *Values of the coefficients $Z^{W\text{-}reg}_{\eta=0}$ (see Eq. (4.50)) and Z^{fact} (see Eq. (4.51)) calculated for the three values of the inverse coupling β adopted in this work and for $\mu = 1/a$. The evaluation of the RCs in the RI'-MOM scheme has been carried using the methods M1 and M2 of Ref. [66].*

We close this section by noting that Eq. (4.13) implies that the contribution to δR_P from the matching factor in Eq. (4.47) is $2\tilde{Z}^{\text{W-reg}}$. Such a term is mass independent. Thus, all the matching and mixing contributions to the axial amplitude in Eq. (4.14) cancel exactly in the difference between the corrections corresponding to two different channels, e.g. in $\delta R_K - \delta R_\pi$. A similar cancelation also occurs in the difference between the corrections to the amplitudes corresponding to the meson P decaying into two different final-state leptonic channels.

4.4 FINITE VOLUME EFFECTS AT ORDER $O(\alpha_{\text{em}})$

The subtraction $\Gamma_0(L) - \Gamma^{\text{pt}}_0(L)$ in Eq. (4.1) cancels both the IR divergences and the structure-independent FVEs of order $O(1/L)$. As discussed in Sec. 3.6, the point-like decay rate $\Gamma^{\text{pt}}_0(L)$ is given by

$$\Gamma^{\text{pt}}_0(L) = \left(1 + 2\frac{\alpha_{\text{em}}}{4\pi} Y^\ell_P(L)\right) \Gamma^{\text{tree}}_P \,, \tag{4.52}$$

where

$$Y^\ell_P(L) = b_{\text{IR}} \log(M_P L) + b_0 + \frac{b_1}{M_P L} + \frac{b^{\text{pt}}_2}{(M_P L)^2} + \frac{b^{\text{pt}}_3}{(M_P L)^3} + O(e^{-M_P L}) \tag{4.53}$$

with the coefficients b_j ($j = \text{IR}, 0, 1$) and b_j^{pt} ($j = 2, 3$) given explicitly in Eq. (3.63). Eq. (4.14) is therefore replaced by

$$\delta A_P = \delta A_P^W + \delta A_P^{\text{SIB}} + \sum_{i=J,T,P,S} \delta A_P^i + \delta A_P^\ell - Y_P^\ell(L) A_P^{(0)} \,, \tag{4.54}$$
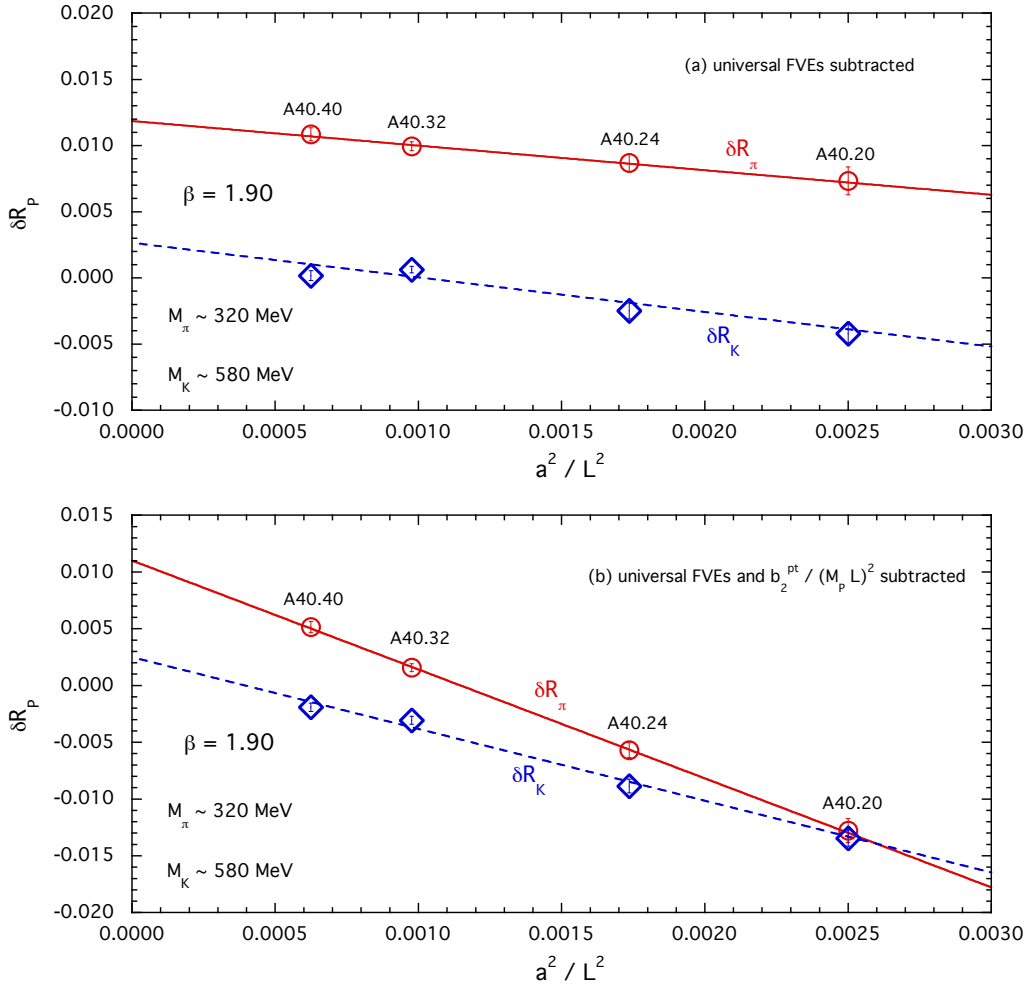
where δA_P^W is given by Eq. (4.47).

Figure 4.4.1: *Results for the corrections δR_π and δR_K for the gauge ensembles A40.20, A40.24, A40.32 and A40.40 sharing the same lattice spacing, pion, kaon and muon masses, but with different lattice sizes (see Table I). Top panel (a): the universal FVEs, i.e. the terms up to order $O(1/M_P L)$ in Eq. (4.53), are subtracted for each quantity. Bottom panel (b): the same as in (a), but in addition to the subtraction of the universal terms, $b_2^{\text{pt}}/(M_P L)^2$, where b_2^{pt} is the pointlike contribution to b_2 in Eq. (4.53), is also removed. The solid and dashed lines are linear fits in $1/L^2$. The maximum photon energy ΔE_γ corresponds to the fully inclusive case $\Delta E_\gamma = \Delta E_\gamma^{max,P} = M_P(1 - m_\mu^2/M_P^2)/2$.*

In order to study the FVEs in detail we consider four ensembles generated at the same values of β and quark masses, but differing in the size of the lattice; these are the ensembles

A40.40, A40.32, A40.24 and A40.20 (see Sec. 2.2). The residual FVEs after the subtraction of the universal terms as in Eq. (4.54) are illustrated in the plots in Fig. 4.4.1 for δR_π and δR_K in the fully inclusive case, i.e. where the energy of the final-state photon is integrated over the full phase space. In this case $\Delta E_\gamma = \Delta E_\gamma^{\max,P} = M_P(1 - m_\mu^2/M_P^2)/2$, which corresponds to $\Delta E_\gamma^{\max,K} \simeq 235$ MeV and $\Delta E_\gamma^{\max,\pi} \simeq 29$ MeV, respectively. With a muon as the final state lepton, the contribution from photons with energy greater than about 20 MeV is negligible and hence the point-like approximation is valid. In the top plot the universal FV corrections have been subtracted and so we would expect the remaining effects to be of order $O(1/(M_P L)^2)$ and this is indeed what we see.

In the bottom plot of Fig. 4.4.1, in addition to subtracting the universal FVEs, we also subtract the contribution to the order $O(1/(M_P L)^2)$ corrections from the point-like contribution to b_2, which can be found in Eq. (3.63). We observe that this additional subtraction does not reduce the $O(1/(M_P L)^2)$ effects, underlining the expectation that these effects are indeed structure dependent.

It can be seen that after subtraction of the universal terms the residual structure-dependent FVEs are almost linear in $1/L^2$, which implies that the FVEs of order $O(1/(M_P L)^3)$ are quite small; indeed they are too small to be resolved with the present statistics.

A more detailed description of the full analysis, including the continuum and chiral extrapolations, is given in the following section. As far as the FVEs are concerned, the central value is obtained by subtracting the universal terms and fitting the residual $O(1/L^2)$ corrections to

$$\frac{K_P}{(M_P L)^2} + \frac{K_P^\ell}{(E_P^\ell L)^2}, \tag{4.55}$$

where K_P and K_P^ℓ are constant fitting parameters and E_P^ℓ is the energy of the charged lepton in the rest frame of the pseudoscalar P (see Eq. (4.56) below). Such an ansatz is introduced to model the unknown dependance of b_2 on the ratio m_ℓ/M_P. For the four points in each of the plots of Fig. 4.4.1 m_ℓ/M_P takes the same value, but this is not true for all the ensembles used in the analysis. We estimate the uncertainty due to the use of the ansatz in Eq. (4.55) by repeating the same analysis, but on the data in which, in addition to subtracting the universal terms in Eq. (4.53), we also subtract the term $b_2^{\mathrm{pt}}/(M_P L)^2$, where b_2^{pt} is contribution to b_2 from a point-like meson [70]. Since b_2^{pt} depends on m_ℓ/M_P, the result obtained with this additional subtraction is a little different from that obtained with only the universal terms removed and we take the difference as an estimate of the residual FV uncertainty.

4.5 RESULTS FOR CHARGED PION AND KAON DECAYS INTO MUONS

We now insert the various ingredients described in the previous sections into the master formula in Eq. (4.13) for the decays $\pi^+ \to \mu^+ \nu[\gamma]$ and $K^+ \to \mu^+ \nu[\gamma]$.

The results for the corrections δR_π and δR_K are shown in Fig. 4.5.1, where the "universal" FVEs up to order $O(1/L)$ have been subtracted from the lattice data (see the empty symbols) and all photon energies (i.e. $\Delta E_\gamma = \Delta E_\gamma^{\max,P} = M_P(1 - m_\mu^2/M_P^2)/2$) are included, since the experimental data on $\pi_{\ell 2}$ and $K_{\ell 2}$ decays are fully inclusive. As already pointed out in Section 4.1, structure dependent contributions to real photon emission should be included. According to the ChPT predictions of Ref. [103], however, these contributions are negligible in for both kaon and pion decays into muons, while the same does not hold as well for decays into final-state electrons (see Sec. 3.7). This important conclusion needs to be explicitly validated by an ongoing dedicated lattice study of the real photon emission amplitudes in light and heavy P-meson leptonic decays (see Sec. 4.6 below).

The combined chiral, continuum and infinite-volume extrapolations are performed using the following SU(2)-inspired fitting function

$$
\begin{aligned}
\delta R_P &= R_P^{(0)} + R_P^{(\chi)} \log(m_{ud}) + R_P^{(1)} m_{ud} + R_P^{(2)} m_{ud}^2 + D_P \, a^2 \\
&+ \frac{K_P}{M_P^2 L^2} + \frac{K_P^\ell}{(E_P^\ell)^2 L^2} + \delta \Gamma^{\text{pt}}(\Delta E_\gamma^{max,P}) ,
\end{aligned}
\tag{4.56}
$$

where $m_{ud} = \mu_{ud}/Z_P$ and μ_{ud} is the bare (twisted) mass (see Table I in Sec. 2.2 below), E_P^ℓ is the lepton energy in the P-meson rest frame, $R_P^{(0),(1),(2)}$, D_P, K_P and K_P^ℓ are free parameters. In Eq. (4.56) the chiral coefficient $R_P^{(\chi)}$ is known for both pion and kaon decays from Ref. [107]; in QED the coefficients are

$$
R_\pi^{(\chi)} = \frac{\alpha_{\text{em}}}{4\pi} (3 - 2X) , \qquad R_K^{(\chi)} = -\frac{\alpha_{\text{em}}}{4\pi} X ,
\tag{4.57}
$$

while in qQED they are

$$
R_\pi^{(\chi)} = \frac{\alpha_{\text{em}}}{4\pi} \left(3 - \frac{10}{9} X \right) , \qquad R_K^{(\chi)} = -\frac{\alpha_{\text{em}}}{4\pi} \frac{8}{9} X ,
\tag{4.58}
$$

where X is obtained from the chiral limit of the $O(\alpha_{\text{em}})$ correction to $M_{\pi^\pm}^2$ (i.e. $\delta M_{\pi^\pm}^2 = 4\pi\alpha_{\text{em}} X f_0^2 + O(m_{ud})$). In Ref. [7] we found $X = 0.658(40)$.

Using Eq. (4.56) we have fitted the data for δR_π and δR_K using a χ^2-minimization procedure with an uncorrelated χ^2, obtaining values of $\chi^2/\text{d.o.f.}$ always around 0.9. The uncertainties on the fitting parameters do not depend on the χ^2-value, because they are obtained using the bootstrap samplings of Ref. [66] (see Sec. 2.2). This guarantees that all the correlations among the data points and among the fitting parameters are properly taken into account.

The quality of our fits is illustrated in Fig. 4.5.1. It can be seen that the residual SD FVEs are still visible in the data and well reproduced by our fitting ansatz in Eq. (4.56). discretization effects on the other hand, only play a minor role.
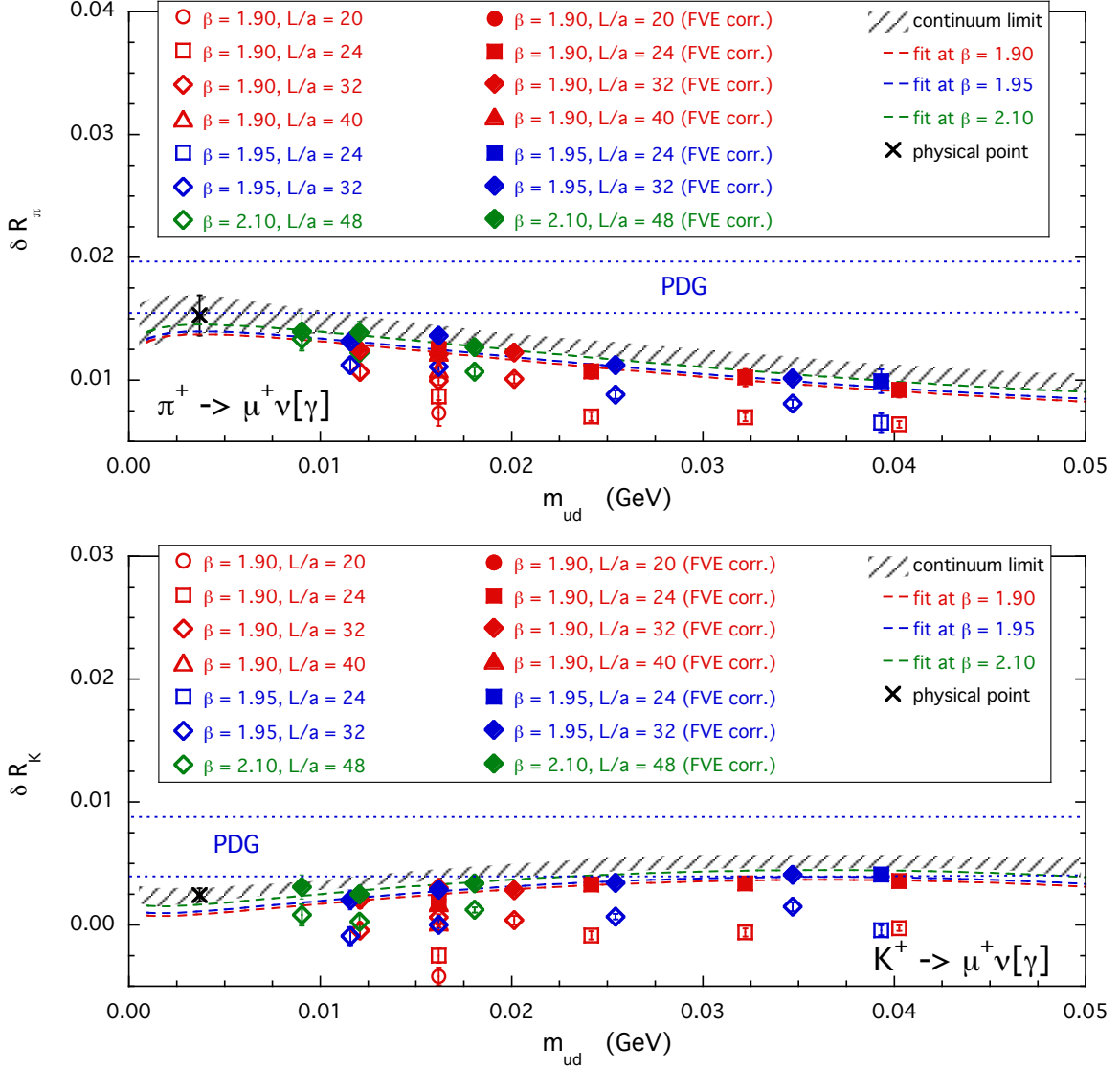
Figure 4.5.1: *Results for the corrections δR_π (top panel) and δR_K (bottom panel) obtained after the subtraction of the "universal" FSE terms up to order $O(1/L)$ in Eq. (4.53) (empty markers). The full markers correspond to the lattice data corrected by the residual FSEs obtained in the case of the fitting function (4.56) including the chiral log. The dashed lines are the (central) results in the infinite volume limit at each value of the lattice spacing, while the shaded areas identify the results in the continuum limit at the level of one standard deviation. The crosses represent the values δR_π^{phys} and δR_K^{phys} extrapolated at the physical point $m_{ud}^{phys}(\overline{\rm MS}, 2\,{\rm GeV}) = 3.70\ (17)$ MeV [66]. The blue dotted lines correspond to the values $\delta R_\pi^{phys} = 0.0176\ (21)$ and $\delta R_K^{phys} = 0.0064\ (24)$, obtained using ChPT [22] and adopted by the PDG [104].*

At the physical pion mass in the continuum and infinite-volume limits we obtain

$$\delta R_\pi^{\rm phys} = +0.0153\,(16)_{stat+fit}\,(4)_{input}\,(3)_{chiral}\,(6)_{FVE}\,(2)_{disc}\,(6)_{qQED}$$
$$= +0.0153\,(19)\,, \tag{4.59}$$
$$\delta R_K^{\rm phys} = +0.0024\,(6)_{stat+fit}\,(3)_{input}\,(1)_{chiral}\,(3)_{FVE}\,(2)_{disc}\,(6)_{qQED}$$
$$= +0.0024\,(10)\,, \tag{4.60}$$

where

- $()_{stat}$ indicates the uncertainty induced by both the statistical errors and the fitting procedure itself;

- $()_{input}$ is the error coming from the uncertainties of the input parameters of the quark-mass analysis of Ref. [66];

- $()_{chir}$ is the difference between including or excluding the chiral logarithm in Eq. (4.56), i.e. taking $R_\chi \neq 0$ or $R_\chi = 0$;

- $()_{FVE}$ is the difference between the analyses of the data corresponding to the FVE subtractions up to the order $O(1/L)$ alone or by also subtracting the term proportional to $b_2^{\mathrm{pt}}/(M_P L)^2$ (see Fig. 4.4.1 and the discussion towards the end of Sec. 4);

- $()_{disc}$ is the uncertainty coming from including ($D \neq 0$) or excluding (setting $D = 0$) the discretization term proportional to a^2 in Eq. (4.56);

- $()_{qQED}$ is our estimate of the uncertainty of the QED quenching. This is obtained using the ansatz (4.56) with the coefficient R_χ of the chiral log fixed either at the value (4.58), which corresponds to the qQED approximation, or at the value (4.57), which includes the effects of the up, down and strange sea-quark charges [107]. The change both in $\delta R_\pi^{\mathrm{phys}}$ and in $\delta R_K^{\mathrm{phys}}$ is $\simeq 0.0003$, which has been already added in the central values given by Eqs. (4.59) and (4.60). To be conservative, we use twice this value for our estimate of the qQED uncertainty.

Our results in Eqs. (4.59)-(4.60) can be compared with the ChPT predictions $\delta R_\pi^{\mathrm{phys}} = 0.0176(21)$ and $\delta R_K^{\mathrm{phys}} = 0.0064(24)$ obtained in Ref. [22] and adopted by the PDG [3, 104]. The difference is within one standard deviation for $\delta R_\pi^{\mathrm{phys}}$, while it is larger for $\delta R_K^{\mathrm{phys}}$. Note that the precision of our determination of $\delta R_\pi^{\mathrm{phys}}$ is comparable to the one obtained in ChPT, while our determination of $\delta R_K^{\mathrm{phys}}$ has a much better accuracy compared to that obtained using ChPT; the improvement in precision is a factor of about 2.4. We stress that the level of precision of our pion and kaon results depends crucially on the non-perturbative determination of the chirality mixing, carried out in Section 3.2.3 by including simultaneously QED at first order and QCD at all orders.

As already stressed, the correction δR_P and the QCD quantity $f_P^{(0)}$ separately depend on the prescription used for the separation between QED and QCD corrections [48]. Only the product $f_P^{(0)}\sqrt{1 + \delta R_P}$ is independent of the prescription and its value, multiplied by the relevant CKM matrix element, yields the P-meson decay rate. We remind the reader that our results (4.59)-(4.60) are given in the GRS prescription (see the dedicated discussion in Sections 1.10.2 and 4.2) in which the renormalized couplings and quark masses in the full theory and in isosymmetric QCD coincide in the $\overline{\mathrm{MS}}$ scheme at a scale of $2\,\mathrm{GeV}$ [46]. We remind the reader that, to the current level of precision, this GRS scheme can be considered equivalent to the FLAG scheme.

Taking the experimental values $\Gamma(\pi^- \to \mu^- \bar{\nu}_\mu[\gamma]) = 3.8408(7) \cdot 10^7 \text{ s}^{-1}$ and $\Gamma(K^- \to \mu^- \bar{\nu}_\mu[\gamma]) = 5.134(11) \cdot 10^7 \text{ s}^{-1}$ from the PDG [3] and using our results (4.59)-(4.60), we obtain

$$f_\pi^{(0)}|V_{ud}| = 127.28\,(2)_{\text{exp}}\,(12)_{\text{th}} \text{ MeV} = 127.28\,(12)\text{ MeV} , \tag{4.61}$$

$$f_K^{(0)}|V_{us}| = 35.23\,(4)_{\text{exp}}\,(2)_{\text{th}} \text{ MeV} = 35.23\,(5)\text{ MeV} , \tag{4.62}$$

where the first error is the experimental uncertainty and the second is that from our theoretical calculations. The result for the pion in Eq. (4.61) agrees within the errors with the updated value $f_\pi^{(0)}|V_{ud}| = 127.12(13)$ MeV [3], obtained by the PDG and based on the model-dependent ChPT estimate of the e.m. corrections from Ref. [22]. Our result for the kaon in Eq. (4.62) however, is larger than the corresponding PDG value $f_K^{(0)}|V_{us}| = 35.09(5)$ MeV [3], based on the ChPT calculation of Ref. [22], by about 2 standard deviations.

As anticipated in the Introduction 4.1 and discussed in detail in Sec. 4.2, we cannot use the result (4.61) to determine the CKM matrix element $|V_{ud}|$, since the pion decay constant was used by ETMC [66] to set the lattice scale in isosymmetric QCD and its value, $f_\pi^{(0)} = 130.41(20)$ MeV, was based on the determination of $|V_{ud}|$ obtained from super-allowed β-decays in Ref. [108]. On the other hand, adopting the best lattice determination of the QCD kaon decay constant, $f_K^{(0)} = 156.11(21)$ MeV [4, 109–111][4], we find that Eq. (4.62) implies

$$|V_{us}| = 0.22567(26)_{\text{exp}}\,(33)_{\text{th}} = 0.22567\,(42) , \tag{4.63}$$

which is a result with the excellent precision of $\simeq 0.2\%$.

In Ref. [16], we have calculated the ratio of the inclusive decay rates of kaons and pions into muons, namely

$$\frac{\Gamma(K_{\mu 2})}{\Gamma(\pi_{\mu 2})} = \left|\frac{V_{us}\,f_K^{(0)}}{V_{ud}\,f_\pi^{(0)}}\right|^2 \frac{M_\pi^3}{M_K^3}\left(\frac{M_K^2 - m_\mu^2}{M_\pi^2 - m_\mu^2}\right)^2 (1 + \delta R_{K\pi}) , \tag{4.64}$$

where $\delta R_{K\pi} \equiv \delta R_K - \delta R_\pi$. Using the same ETMC simulation setup [45, 65], we have calculated $\delta R_{K\pi}$, which, together with a lattice computation of $f_K^{(0)}/f_\pi^{(0)}$, allows us to determine $|V_{us}/V_{ud}|$ from the ratio in Eq. (4.64).

The quantity $\delta R_{K\pi}$ is less sensitive to various uncertainties than the individual terms δR_K and δR_π. Three main features help to reduce the systematic uncertainties in $\delta R_{K\pi}$:

- in $\Gamma_0(L)$ the residual SD FVEs starting at order $O(1/L^2)$ are found to be much milder (≈ 3 smaller) in the case of $\delta R_{K\pi}$ (see Fig. 4.5.2 below);

- the matching of the bare lattice weak operator with the one renormalized using W-regularization and the mixing contributions to the axial amplitude in Eq. (4.14) cancel out in the difference $\delta R_{K\pi}$;

---

[4]The average value of $f_{K^\pm}$ quoted by FLAG [4] includes the strong IB corrections. In order to obtain $f_K^{(0)}$ therefore, we have subtracted this correction which is given explicitly in Refs. [109–111].
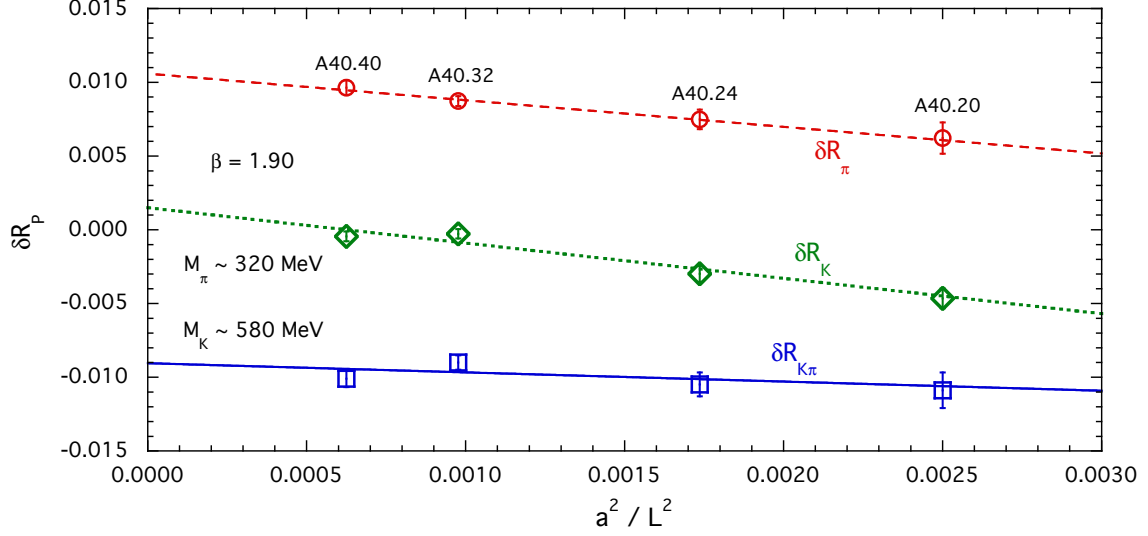
Figure 4.5.2: *Results for the corrections δR_π, δR_K and $\delta R_{K\pi}$ for the gauge ensembles A40.20, A40.24, A40.32 and A40.40 sharing the same lattice spacing, pion and kaon masses, but different lattice sizes (see the supplemental material). The universal FVEs, i.e. the terms up to order $O(1/L)$ in Eq. (4.53), are subtracted for each quantity. The lines are linear fits in $1/L^2$. The maximum photon energy ΔE_γ corresponds to the inclusive case $\Delta E_\gamma = \Delta E_\gamma^{max,P} = M_P(1 - m_\mu^2/M_P^2)/2$.*

- within SU(3) ChPT the effects of the sea-quark electric charges depend on unknown low-energy constants (LECs) starting at next-to-leading-order (NLO) for δR_K and δR_π, but only at NNLO for $\delta R_{K\pi}$ [107]. Thus, the uncertainty due to the qQED approximation, adopted in this work, is expected to be smaller for $\delta R_{K\pi}$.

The inclusive data for $\delta R_{K\pi}$ are shown in Fig. 4.5.3. The "universal" FVEs are subtracted and the combined chiral, continuum and infinite volume extrapolations are performed using the Ansatz in Eq. (4.56) for $\delta R_K - \delta R_\pi$. At the physical pion mass in the continuum and infinite-volume limits we obtain

$$
\begin{aligned}
\delta R_{K\pi}^{phys} &= -0.0126\,(10)_{stat+fit}\,(2)_{input}\,(5)_{chiral}\,(5)_{FVE}\,(4)_{disc}\,(6)_{qQED} \\
&= -0.0126\,(14)\,,
\end{aligned}
\tag{4.65}
$$

where the error budget has been obtained as in the case of Eqs. (4.59) and (4.60). Our result (4.65) can be compared to the value $\delta R_{K\pi}^{phys} = -0.0112\,(21)$ from Refs. [22, 104] adopted by the PDG [3].

Using the pion and kaon experimental decay rates we get

$$
\frac{|V_{us}|}{|V_{ud}|}\frac{f_K^{(0)}}{f_\pi^{(0)}} = 0.27683\,(29)_{exp}\,(20)_{th} = 0.27683\,(35)\,.
\tag{4.66}
$$

Using the best $N_f = 2 + 1 + 1$ lattice determination of the ratio of the QCD kaon and pion decay constants, $f_K^{(0)}/f_\pi^{(0)} = 1.1966\,(18)$ [4, 109–111], we find

$$
\frac{|V_{us}|}{|V_{ud}|} = 0.23135\,(24)_{exp}\,(39)_{th} = 0.23135\,(46)\,.
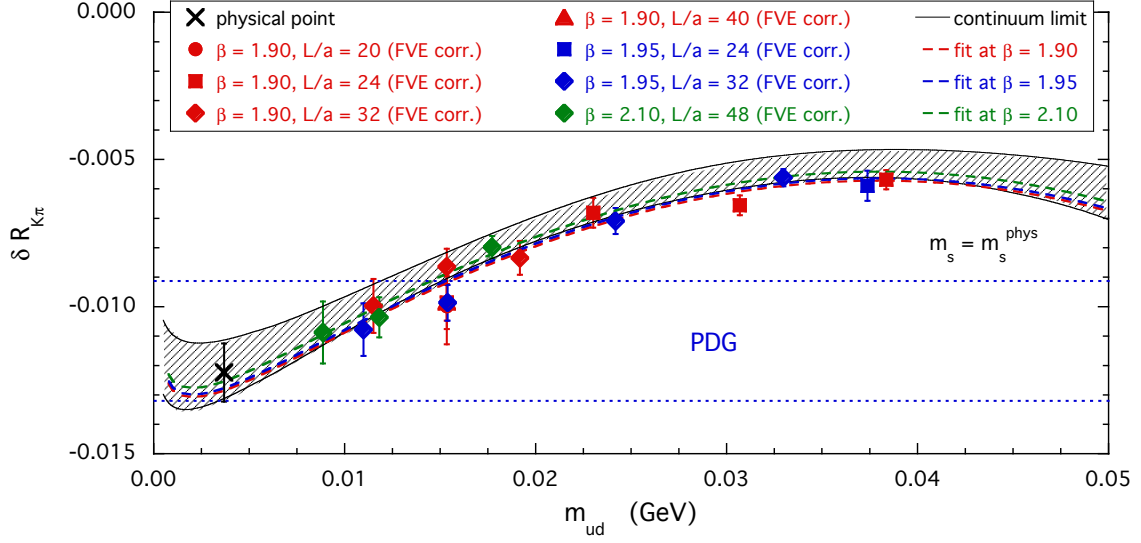\tag{4.67}
$$

Figure 4.5.3: *Results for the correction $\delta R_{K\pi}$ (Eqs. (4.13) and (4.54)) after the subtraction of both the universal FVEs in Eq. (4.53) and the residual FVEs obtained from the fit. The dashed lines are the (central) results at each β, while the shaded area identifies the continuum limit at 1-sigma level. The cross is the extrapolated value at $m_{ud}^{phys}(\overline{\mathrm{MS}}, 2\,GeV) = 3.70(17)\,MeV$ [66]. The blue dotted lines correspond to the value $-0.0112(21)$ from Refs. [22, 104] adopted by the PDG [3]. Errors are statistical only.*

Taking the updated value $|V_{ud}| = 0.97420\,(21)$ from super-allowed nuclear beta decays [15], Eq. (4.67) yields the following value for the CKM element $|V_{us}|$:

$$|V_{us}| = 0.22538\,(24)_{\mathrm{exp}}\,(39)_{\mathrm{th}} = 0.22538\,(46)\,, \tag{4.68}$$

which agrees with our result (4.63) within the errors. Note that our result (4.68) agrees with the latest estimate $|V_{us}| = 0.2253(7)$, recently updated by the PDG [3], but it improves the error by a factor of approximately 1.5.

Taking the values $|V_{ub}| = 0.00413(49)$ [3] and $|V_{ud}| = 0.97420(21)$ [15] our result in Eq. (4.68) implies that the unitarity of the first-row of the CKM matrix is confirmed to better than the per-mille level

$$|V_{ud}|^2 + |V_{us}|^2 + |V_{ub}|^2 = 0.99988\,(46)\,. \tag{4.69}$$

With the same value $|V_{ud}| = 0.97420(21)$ from super-allowed nuclear beta decays [15], our result (4.61) implies for the QCD pion decay constant (in the GRS prescription) the following value

$$f_{\pi}^{(0)} = 130.65\,(12)_{\mathrm{exp+th}}\,(3)_{V_{ud}}\,\mathrm{MeV} = 130.65\,(12)\,\mathrm{MeV}\,, \tag{4.70}$$

which, as anticipated in Sec. 4.2, agrees within the errors with the value $f_{\pi}^{(0)} = 130.41\,(20)\,\mathrm{MeV}$ adopted in Ref. [66] to set the lattice scale in the isosymmetric QCD theory. This demonstrates the equivalence of the GRS and PDG schemes within the precision of our simulation.

In a recent paper [112], the hadronic contribution to the electroweak radiative corrections to neutron and super-allowed nuclear β decays has been analyzed in terms of dispersion relations and neutrino scattering data. With respect to the result $V_{ud} = 0.97420\,(21)$ from Ref. [15], a significant shift in the central value and a reduction of the uncertainty have been obtained, namely $V_{ud} = 0.97370\,(14)$ [112]. The impact of the new value of V_{ud} on our determinations of V_{us} and f_π is $V_{us} = 0.22526\,(46)$ and $f_\pi = 130.72\,(12)$ MeV, i.e., well within the uncertainties shown in Eqs. (4.68) and (4.70), respectively. On the contrary, the first-row CKM unitarity (4.69) will be significantly modified into

$$|V_{ud}|^2 + |V_{us}|^2 + |V_{ub}|^2 = 0.99885\,(34)\,, \tag{4.71}$$

which would imply a $\simeq 3.4\sigma$ tension with unitarity. A confirmation of the new calculation of the radiative corrections made in Ref. [112] is therefore urgently called for.

Before closing this section, we comment briefly about the comparison between our result $\delta R_K^{\text{phys}} = 0.0024(10)$ and the corresponding model-dependent ChPT prediction $\delta R_K^{\text{phys}} = 0.0064(24)$ from Ref. [22]. The latter is obtained by adding a model-dependent QED correction of $0.0107(21)$ and a model-independent NLO strong IB contribution equal to $-0.0043(12)$. Our result on the other hand, obtained in the GRS prescription, stems from a QED correction equal to $0.0088(9)$ and a strong IB term equal to $-0.0064(7)$ (see also Ref. [36]). The difference between our result and the ChPT prediction of Ref. [22] appears to be mainly due to a different strong IB contribution. Thus, in the present $N_f = 2 + 1 + 1$ study, we confirm for the strong IB term a discrepancy at the level of about 2 standard deviations, which was already observed at $N_f = 2$ in Ref. [9].

4.6 REAL PHOTON EMISSION IN LEPTONIC DECAYS: PRELIMINARY RESULTS

In the limit of soft-photon energies, the radiative decay rate $P \to \ell\bar{\nu}_\ell\gamma$ can be reliably calculated perturbatively by treating the meson as a point-like particle. This limit is however an idealization and experimental measurements are inclusive up to photon energies that might be too large to neglect structure-dependent (SD) corrections to the point-like approximation. The region of hard photon energies, which is particularly important for heavy mesons, represents a fundamental probe of the internal structure of the mesons and can only be studied in lattice QCD simulations. On the other hand, even in the case of light mesons, where chiral perturbation theory can be used, the low-energy constants entering at $O(p^6)$ can only be estimated using model-dependent assumptions [94, 95, 113–115].

In Ref. [10] a strategy to compute QED radiative corrections to the $P \to \ell\bar{\nu}_\ell(\gamma)$ decay rates at $O(\alpha_{em})$ on the lattice has been proposed and we have described it in detail in Chapter 3. That strategy has been subsequently applied to provide the first non-perturbative model-independent calculation of the decay rates $\pi^- \to \mu^-\bar{\nu}_\mu(\gamma)$ and $K^- \to \mu^-\bar{\nu}_\mu(\gamma)$ [13, 16]. The real soft-photon contributions has been calculated in the point-like effective theory and the SD corrections were estimated, by relying on the quoted chiral perturbation theory results,

to be negligible (see Sec. 3.7). On the other hand SD corrections might be relevant for the decays of pions and kaons into electrons when the energy of the photon becomes larger than about 20 MeV. Moreover, in the single-pole dominance approximation proposed in Ref. [97], the SD contribution has been estimated to be rather large in the case of heavy flavors. This contribution can be precisely determined only in lattice QCD. Here we present some preliminary results of a non-perturbative, $O(a)$ improved lattice calculation of the form factors entering the radiative decay rate $P \to \ell \bar{\nu}_\ell \gamma$ in the case of pions, kaons, D and D_s mesons. The case of bottom mesons will be studied in a future work on the subject. Results of a lattice calculation of real-photon emission amplitudes have also been presented in Ref. [116]. Making contact with the discussion presented in Sec. 3.7, the non-perturbative hadronic amplitude for the process $P \to \ell \nu_\ell \gamma$ is given by the T-product

$$H_W^{\alpha r}(k,p) = \epsilon_\mu^r(k)\, H_W^{\alpha\mu}(k,p) = \epsilon_\mu^r(k) \int d^4 y\, e^{ik \cdot y}\, \langle 0|\mathrm{T}\{J_W^\alpha(0) J^\mu(y)\}|P(\vec{p})\rangle\,, \qquad (4.72)$$

where $\epsilon_\mu^r(k)$ is the polarization vector of the photon with four-momentum k, J^μ is the electromagnetic current, J_W^α is the hadronic weak current, $J_W^\alpha = V^\alpha - A^\alpha = \bar{q}_1\,(\gamma^\alpha - \gamma^\alpha \gamma_5)\, q_2$, and $\vec{p}$ is the momentum of the meson P with mass M_P. To this amplitude, at $O(\alpha_{em})$, we have to add the diagram in which the photon is emitted from the final-state charged lepton. The latter contribution can however, be computed in perturbation theory using the meson decay constant f_P. The decomposition of $H_W^{\alpha r}(k,p)$ in terms of form-factors has been discussed in Sec. 3.7. By choosing a *physical* basis for the polarization vectors such that $\epsilon_r \cdot k = 0$ and setting the photon on-shell, i.e. by taking $k^2 = 0$, we have [90]

$$H_W^{\alpha r}(k,p) = \epsilon_\mu^r(k)\left\{ -i\frac{F_V(x_\gamma)}{M_P}\varepsilon^{\mu\alpha\gamma\beta}k_\gamma p_\beta + \left[\frac{F_A(x_\gamma)}{M_P} + \frac{f_P}{p \cdot k}\right](p \cdot k\, g^{\mu\alpha} - p^\mu k^\alpha) + \frac{f_P}{p \cdot k}\, p^\mu p^\alpha \right\}.$$
$$(4.73)$$

The terms proportional to f_P correspond to the point-like infrared-divergent contribution and saturate the Ward Identity satisfied by $H_W^{\alpha\mu}(k,p)$, i.e. $k_\mu\, H_W^{\alpha\mu}(k,p) = i\langle 0|J_W^\alpha(0)|P(p)\rangle = f_P\, p^\alpha$. At fixed meson mass the two form-factors $F_{V,A}$ are scalar functions of the Lorentz invariant quantity $p \cdot k$ only. A convenient dimensionless variable is given by $x_\gamma = 2p \cdot k/M_P^2$.

Once the decay constant f_P and the two SD axial and vector form-factors F_A and F_V are known, the decay rate can be calculated by using the formulae given in [90] and in Sec. 3.7.

4.6.1 EXTRACTING THE FORM FACTORS FROM EUCLIDEAN CORRELATORS

The Euclidean correlation function corresponding to Eq. (4.72) is given by

$$C_W^{\alpha r}(t, \vec{p}, \vec{k}) = -i\, \epsilon_\mu^r(\vec{k}) \int d^4 y \int d^3\vec{x}\, \langle 0|\mathrm{T}\{J_W^\alpha(t, \vec{0}) J^\mu(y)\} P(0, \vec{x})|0\rangle\, e^{E_\gamma t_y - i\vec{k}\cdot\vec{y} + i\vec{p}\cdot\vec{x}} \qquad (4.74)$$

where $k = (iE_\gamma, \vec{k})$, with $E_\gamma = |\vec{k}|$, $p = (iE, \vec{p})$ and $\int d^3\vec{x}\, P(0, \vec{x})\, e^{i\vec{p}\cdot\vec{x}}$ is the source of the pseudoscalar meson with momentum $\vec{p}$. The convergence of the integral over t_y is ensured by
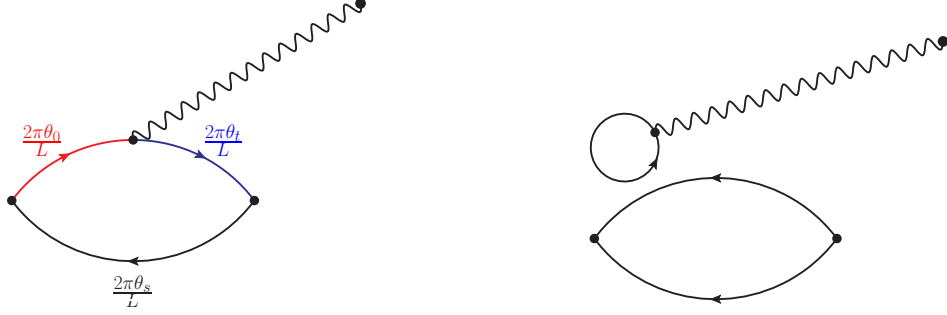
Figure 4.6.1: The *connected* diagram on the left shows our choice of the spatial boundary conditions. By treating the two propagators attached to the electromagnetic current as two different flavors, with the same mass and electric charge but different boundary conditions, we may choose arbitrary values for the meson and photon spatial momenta. The diagram on the right represents the contribution associated with the emission of the photon by the sea-quarks. By neglecting this diagram we have been working in the so-called electro-quenched approximation.

the safe analytic continuation from Minkowski to Euclidean space, because of the absence of intermediate states lighter than the pseudoscalar meson. The physical form factors can be extracted directly from the Euclidean correlation functions

$$R_W^{\alpha r}(t; \vec{p}, \vec{k}) = \frac{2E}{e^{-t(E-E_\gamma)} \langle P(\vec{p})|P|0\rangle} \, C_W^{\alpha r}(t; \vec{p}, \vec{k}) = H_W^{\alpha r}(k, p) + \cdots \qquad (4.75)$$

where $\langle P(\vec{p})|P|0\rangle$ is the matrix element of the operator P between the vacuum and the meson state and the dots represent sub-leading exponentials. It is useful to note that, in order to separate the axial and vector form-factors it is enough to compute separately the ratios $R_{V,A}^{\alpha r}(t; \vec{p}, \vec{k})$ corresponding to the (renormalized) vector and axial component of the weak current, see eq. (4.77) below. For J^μ an exactly conserved lattice vector current is employed. The previous discussion assumed an infinite time extent (T) of the lattice. In our numerical calculations we have employed numerical estimators for the ratios $R_{V,A}^{\alpha r}(t; \vec{p}, \vec{k})$ built in terms of finite–T correlators that properly account for the fact that the simulated quark and gauge fields satisfy respectively anti-periodic and periodic boundary conditions in time.

Within the electro-quenched approximation, i.e. in the absence of the disconnected contribution shown in the right-panel of Fig. 4.6.1, it is possible to choose arbitrary values of the spatial momenta by using different spatial boundary conditions [106, 117] for the quark fields. More precisely, we set the boundary conditions for the "spectactor" quark such that $\psi(x + \vec{k}L) = \exp(2\pi i \vec{k} \cdot \vec{\theta}_s/L)\psi(x)$. Then we treat the two propagators that are connected with the electromagnetic current (the red and blue lines) as the results of the Wick contractions of two different fields having the same mass and electric charge but satisfying different boundary conditions. This is possible at the price of accepting tiny violations of unitarity that are exponentially suppressed in the volume (similar effects are induced in any case by the electro-quenched approximation). By setting the boundary conditions as illustrated in
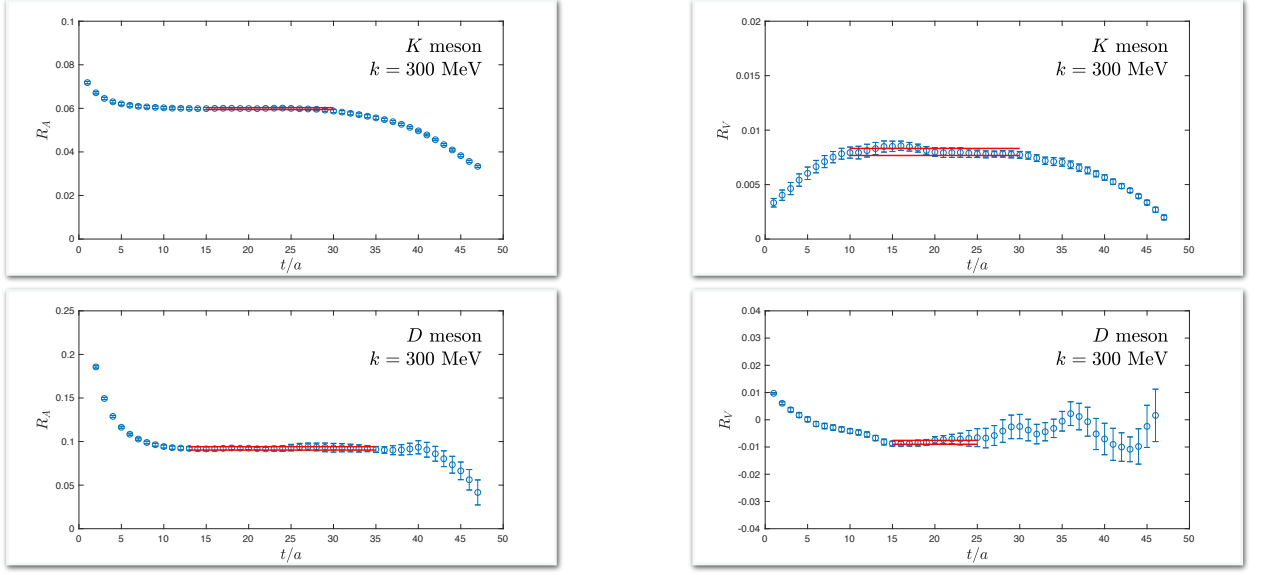
Figure 4.6.2: Examples of plateaux fits for the ratios $R_A(t, T/2)$ (left) and $R_V(t, T/2)$ (right) in the case of the gauge ensemble D20.48 ($M_\pi = 255\,(7)$ MeV, $M_K = 535\,(14)$ MeV, $M_D = 1933\,(50)$ MeV, and $M_{D_s} = 2023\,(52)$ MeV).

the figure, we have thus been able to choose arbitrary values for the meson and photon spatial momenta, $\vec{p} = \frac{2\pi}{L}\left(\vec{\theta}_0 - \vec{\theta}_s\right)$ and $\vec{k} = \frac{2\pi}{L}\left(\vec{\theta}_0 - \vec{\theta}_t\right)$ by tuning the real three-vectors $\vec{\theta}_{0,t,s}$, where the subscript $i = 0, t, s$ in the definition refers to the quark line emerging from the source in the origin, 0; the quark annihilating in the sink given by the hadronic weak current at time t and the *spectator quark* respectively. The numerical results have been obtained by choosing all the non-zero components of the spatial momenta to be along the z-direction, i.e. $\vec{p} = (0, 0, |\vec{p}|)$ and $\vec{k} = (0, 0, E_\gamma)$. With this particular choice a convenient basis for the polarization vectors of the photon is the one in which the *two* physical polarization vectors are given by $\epsilon_{1,2}^\mu = \left(0, \mp\frac{1}{\sqrt{2}}, -\frac{1}{\sqrt{2}}, 0\right)$. In this basis we have $\epsilon_r \cdot p = \epsilon_r \cdot k = 0$ and consequently

$$
\begin{aligned}
H_A^{jr}(k, p) &= \frac{\epsilon_r^j m_P}{2} x_\gamma \left[F_A(x_\gamma) + \frac{2 f_P}{m_P x_\gamma}\right], \\
H_V^{jr}(k, p) &= \frac{i\left(E_\gamma \vec{\epsilon}_r \wedge \vec{p} - E \vec{\epsilon}_r \wedge \vec{k}\right)^j}{m_P} F_V(x_\gamma).
\end{aligned}
\tag{4.76}
$$

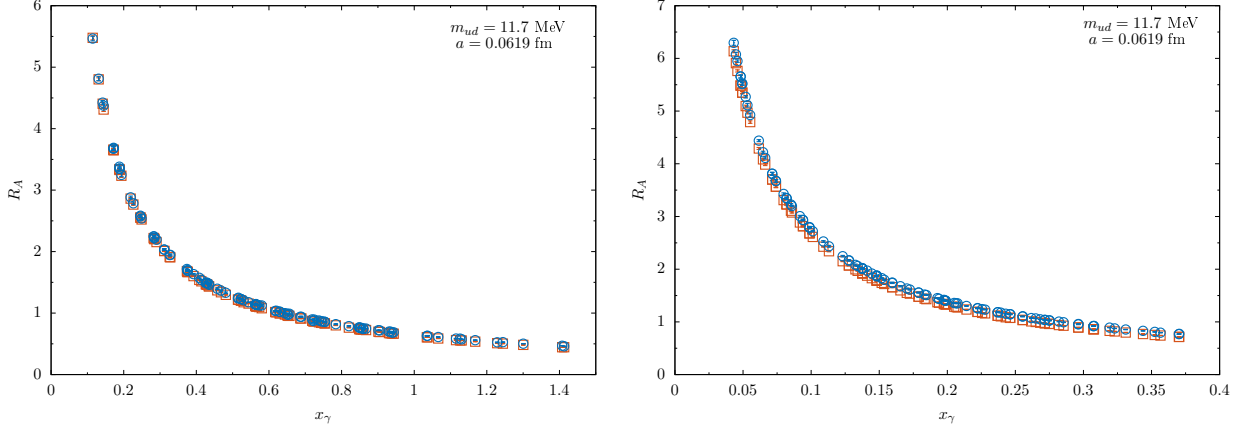For $t \gg 0$ we get the following numerical estimators for the form-factors

Figure 4.6.3: The extracted value of $R_A(x_\gamma)$, Eq. (3.5), as a function of x_γ for the K meson (left) and for the D_s meson (right) in the case of the gauge ensemble D20.48. The (red) squares represent the point-like contribution given by $2f_P/(m_P x_\gamma)$.

$$R_A(t) = \frac{m_P}{4p \cdot k} \sum_{r=1,2} \sum_{j=1,2} \frac{R_A^{jr}(t; \vec{p}, \vec{k})}{\epsilon_r^j} \rightarrow \left[F_A(x_\gamma) + \frac{2f_P}{m_P x_\gamma} \right] ,$$

$$R_V(t) = \frac{m_P}{4} \sum_{r=1,2} \sum_{j=1,2} \frac{R_V^{jr}(t; \vec{p}, \vec{k})}{i \left(E_\gamma \, \vec{\epsilon}_r \wedge \vec{p} - E \, \vec{\epsilon}_r \wedge \vec{k} \right)^j} \rightarrow F_V(x_\gamma) . \qquad (4.77)$$

At finite T, by using the formulae above which are valid for $t > 0$, we fit the ratios $R_{A,V}(t)$ by searching a plateau in the region $0 \ll t \ll T/2$. We also exploit time-reversal symmetries to include the plateaus of $R_{A,V}(t)$ obtained at $t > T/2$. The values of the meson energies and of the matrix element $\langle P(\vec{p})|P|0\rangle$ needed to build these estimators are obtained from standard effective-mass/residue analyses of pseudoscalar-pseudoscalar two-point functions. The pseudoscalar-axial two-point function is used to extract the decay constants f_P in order to separate F_A from the point-like contribution $2f_P/(m_P x_\gamma)$.

4.6.2 NUMERICAL RESULTS

All the results presented in this section are preliminary. We have used the gauge configu-rations given in Sec. 3.2, produced with $2 + 1 + 1$ twisted mass fermions at three different values of the lattice spacing, $a[\text{fm}] = 0.0085(36), 0.00815(30), 0.0619(18)$, with meson masses in the range 250-2110 MeV. In total we have included 125 different combinations of mo-menta obtained by assigning to each of the $\theta_{i=0,t,s}$ five different values; making the same assignments for all choices of the quark masses. All the plots below correspond to the case of π, K and $D_{(s)}$ mesons at unphysical values of the $\overline{\text{MS}}$ renormalized light-quark mass, $m_{ud}(2\,\text{GeV}) = \{11.7,\ 17.5\}$ MeV, and have been obtained from a simulation at $a = 0.0619$ fm (ensembles D20.48 and D30.48, respectively). The reference meson masses are collected in
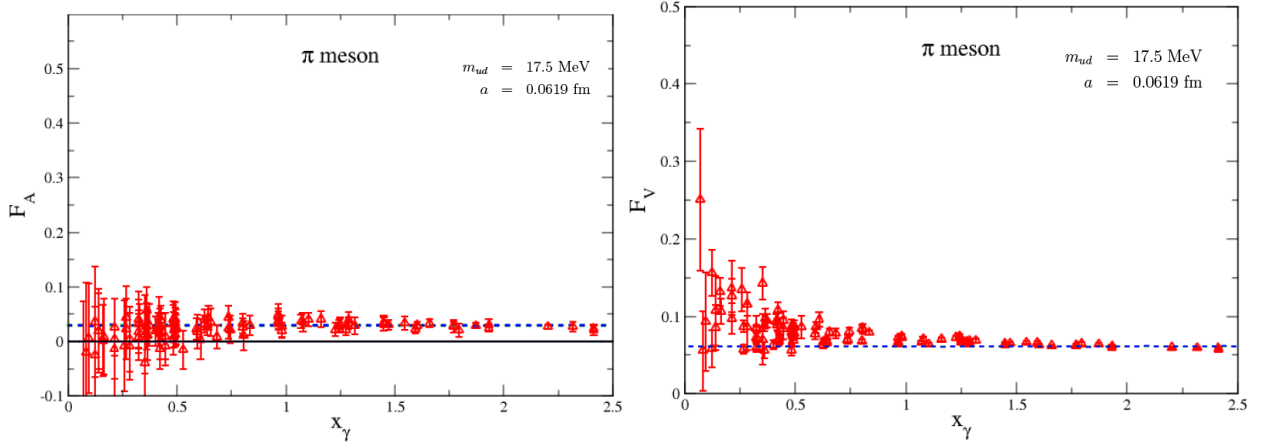
Figure 4.6.4: The extracted value of the pion form factors $F_A(x_\gamma)$ (left) and $F_V(x_\gamma)$ (right) as a function of x_γ in the case of the gauge ensemble D30.48 ($M_\pi = 312\,(8)$ MeV, $M_K = 550\,(14)$ MeV, $M_D = 1937\,(49)$ MeV, and $M_{D_s} = 2025\,(52)$ MeV). The blue dashed lines correspond to the ChPT predictions obtained by using the formulae discussed in the text.
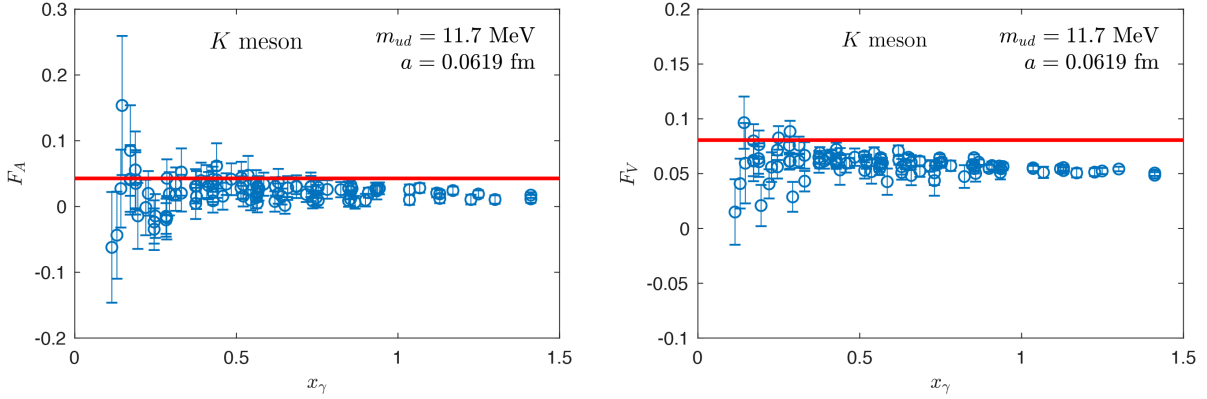

Figure 4.6.5: The extracted value of the kaon form factors $F_A(x_\gamma)$ (left) and $F_V(x_\gamma)$ (right) as a function of x_γ in the case of the gauge ensemble D20.48. The (red) lines correspond to the ChPT predictions.

Table IV. Similar plots can be shown for other values of the simulated parameters. In Fig. 4.6.2 we show examples of plateaux for the ratios $R_{A,V}(t)$ for the K and D mesons. This figure is representative of the signal quality, also for other values of masses and momenta. In Fig. 4.6.3 we show the extracted value of $R_A(x_\gamma)$, Eq. (4.77), for the K meson and for the D_s meson. In both cases the point-like contribution, corresponding to the term $2f_P/(M_P x_\gamma)$ dominates the form factor. From the measured decay constant and mass, we can subtract the point-like term and extract $F_A(x_\gamma)$. In the left-hand plots of Figs. 4.6.4 and 4.6.5 we show $F_A(x_\gamma)$ as a function of x_γ for the π and K mesons and compare it to the lowest non-trivial order in ChPT, given by $F_A(x_\gamma) = \text{const.} = 8M_P(L_9^r + L_{10}^r)/f_P$, with
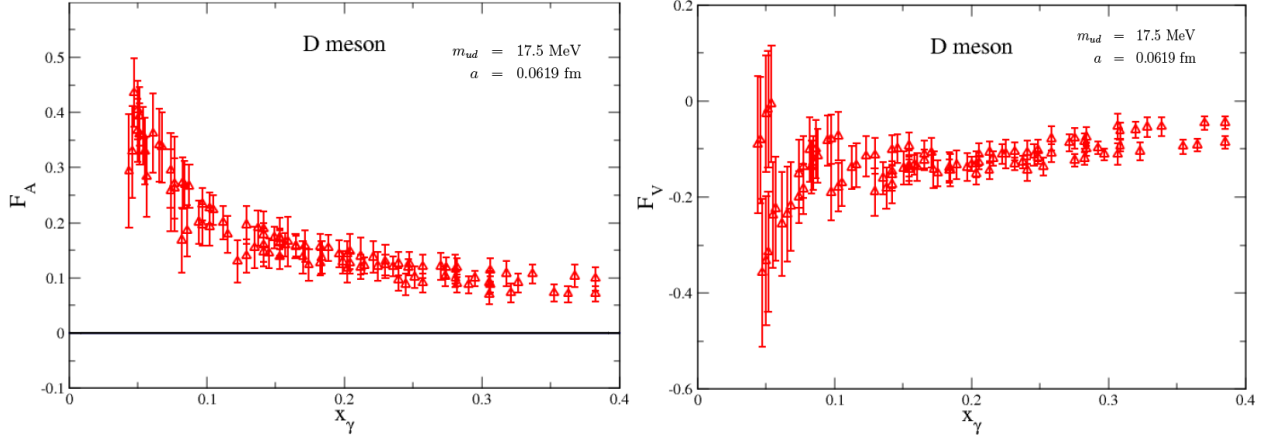
Figure 4.6.6: The extracted value of the D meson form factors $F_A(x_\gamma)$ (left) and $F_V(x_\gamma)$ (right) as a function of x_γ in the case of the gauge ensemble D30.48.
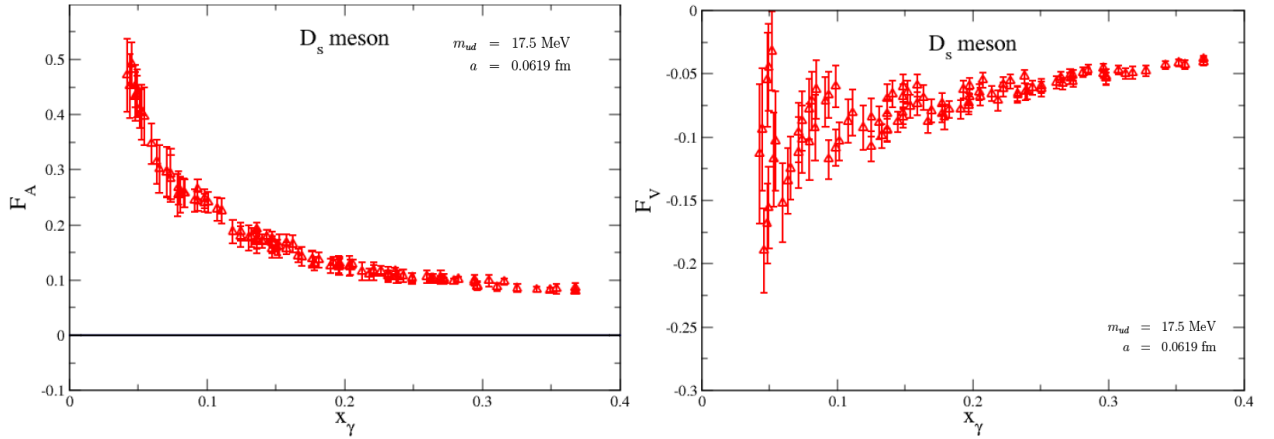

Figure 4.6.7: The extracted value of the D_s meson form factors $F_A(x_\gamma)$ (left) and $F_V(x_\gamma)$ (right) as a function of x_γ in the case of the gauge ensemble D30.48.

$L_9^r + L_{10}^r \simeq 0.0017$ [118]. On the right hand plots of Figs. 4.6.4 and 4.6.5 we can compare the directly computed values of F_V to their ChPT predictions, $F_V(x_\gamma) = \text{const.} = M_P/(4\pi^2 f_P)$. Finally, in Figs. 4.6.6 and 4.6.7 we show preliminary results for $F_A(x_\gamma)$ and $F_V(x_\gamma)$ in the case of the D and D_s mesons. In that first exploratory study we covered the full physical range of x_γ in the pion and kaon cases (indeed we even have data for unphysical values corresponding to $x_\gamma > 1$) and for $0 \leq x_\gamma \leq 0.4$, corresponding to $E_\gamma \lesssim 400$ MeV, for the D_s meson. We are currently improving our lattice data and, after a detailed analysis of all the systematics, we shall provide first-principles phenomenologically relevant results for the form factors in the full kinematical range for both light and heavy mesons. The form factors for heavy mesons will represent in this respect a totally unexplored field of investigation while, in the case of light mesons, our first-principle results will make it possible to avoid ChPT in

phenomenological analyses.

In conclusion we have shown that, with moderate statistics, it is possible to extract with good precision the form factors relevant for $P \to \ell \bar{\nu}_\ell \gamma$ decays for both light and heavy mesons and that it is possible to study their momentum dependence.

CONCLUSIONS

In this work we calculated the isospin breaking corrections to pion, kaon and charmed-meson masses. We performed LQCD numerical simulations with $N_f = 2 + 1 + 1$ sea quarks at three values of the lattice spacing, using gauge configurations produced by the ETM Collaboration and computed pseudoscalar meson two-point correlation functions to determine physical quantities in the continuum and infinite volume limits and at the physical values of quark masses. The RM123 method [9] here adopted is based on a perturbative expansion in $(\widehat{m}_d - \widehat{m}_u)/\Lambda_{\rm QCD}$ and $\widehat{\alpha}_{em}$ in order to evaluate isospin breaking corrections by starting from simulations in the isospin-symmetric QCD theory.

The main sources of systematic uncertainties in our calculation are the one associated with the chiral extrapolations, required because our up and down quark masses are heavier than the physical ones, and the one related to the neglect of quark-disconnected diagrams and to the use of the electro-quenched approximation. Another important source of systematics errors comes from finite volume effects, which are only power suppressed because QED is a long-ranged interaction.

One of our main result is the pion mass splitting, that receives at the leading order only the QED contribution. Considering that the fine structure constant does not renormalize at this order, this splitting is a very clean observable. However, it receives a disconnected contribution coming from the neutral pion that is numerically very expensive to evaluate and presumably very small (being of $O(\alpha_{em}m_{ud})$) and that we neglected in the calculation. We found

$$M_{\pi^+} - M_{\pi^0} = 4.21\ (26)\ {\rm MeV}\ \ [4.5936\ (5)\ {\rm MeV}]_{exp}\ .$$

Kaon and charmed-meson masses receive both electromagnetic and strong isospin breaking contributions. In order to separate the IB effects into such components we implemented the Gasser-Rusetsky-Scimemi (GRS) prescription, in which the renormalized couplings and quark masses in the full QCD+QED theory and in isosymmetric QCD coincide in the $\overline{\rm MS}$ scheme at a scale of 2 GeV [46]. This allows to determine the QED contributions to the pseudoscalar meson masses and the associated values of the Dashen's theorem breaking parameters ε_{π^0}, ε_{γ} and ε_{K^0}. In this case we used the electro-qenched approximation which consists in neglecting the charges of the sea quarks. Our result for $M_{K^+} - M_{K^0}$ is

$$[M_{K^+} - M_{K^0}]^{QED}\ (\overline{MS}, 2\ {\rm GeV}) \;=\; 2.07\ (15)\ {\rm MeV}\ ,$$

$$[M_{K^+} - M_{K^0}]^{SIB}\ (\overline{MS}, 2\ {\rm GeV}) \;=\; -6.00\ (15)\ {\rm MeV}\ ,$$

from which we also obtained

$$(\widehat{m}_d - \widehat{m}_u)(\overline{MS}, 2 \text{ GeV}) = 2.38 \text{ (18) MeV} .$$

Analogously, for the charmed-meson we found

$$
\begin{aligned}
[M_{D^+} - M_{D^0}]^{QED} (\overline{MS}, 2 \text{ GeV}) &= 2.42 \text{ (51) MeV} , \\
[M_{D^+} - M_{D^0}]^{SIB} (\overline{MS}, 2 \text{ GeV}) &= 3.06 \text{ (27) MeV} , \\
M_{D^+} - M_{D^0} &= 5.47 \text{ (53) MeV} \; [4.75 \text{ (8) MeV}]_{exp} , \\
\delta M_{D_s^+} &= 2.3 \text{ (4) MeV} .
\end{aligned}
$$

The uncertainties of the above results contain also an estimation of the error due to the electro-quenched approximation.

Besides the hadronic spectrum, we performed for the first time the *ab initio* calculation of the leading electromagnetic and strong isospin breaking corrections to the $\pi^+ \to \mu^+ \nu_\mu(\gamma)$ and $K^+ \to \mu^+ \nu_\mu(\gamma)$ leptonic decay rates by implementing the method proposed in [10] and described in Chapter 3. For these quantities the presence of infrared divergences in intermediate stages of the calculation makes the procedure much more complicated than is the case for the hadronic spectrum. In order to compute the physical widths, diagrams with virtual photons must be combined with those corresponding to the emission of real photons. After extrapolation of the data to the physical pion mass, and to the continuum and infinite-volume limits, the isospin-breaking corrections to the $\pi_{\mu2}$ and $K_{\mu2}$ decay rates were found to be [13]:

$$
\begin{aligned}
\Gamma(\pi^\pm \to \mu^\pm \nu_\mu[\gamma]) &\equiv (1 + \delta R_\pi^{\text{phys}}) \, \Gamma^{(0)}(\pi^\pm \to \mu^\pm \nu_\mu) \\
&= (1.0153 \pm 0.0019) \, \Gamma^{(0)}(\pi^\pm \to \mu^\pm \nu_\mu), \\
\Gamma(K^\pm \to \mu^\pm \nu_\mu[\gamma]) &\equiv (1 + \delta R_K^{\text{phys}}) \, \Gamma^{(0)}(\pi^\pm \to \mu^\pm \nu_\mu) \\
&= (1.0024 \pm 0.0010) \, \Gamma^{(0)}(K^\pm \to \mu^\pm \nu_\mu) ,
\end{aligned}
$$

where $\Gamma^{(0)}$ is the leptonic decay rate at tree level in the GRS scheme. These results can be compared with the ChPT predictions $\delta R_\pi^{\text{phys}} = 0.0176(21)$ and $\delta R_K^{\text{phys}} = 0.0064(24)$ obtained in Ref. [22] and adopted by the PDG [3, 104]. The difference is within one standard deviation for $\delta R_\pi^{\text{phys}}$, while it is larger for δR_K^{phys}. We also underline that our result $|V_{us}| = 0.22538(46)$ in Eq. (4.68), together with the value of V_{ud} determined in Ref. [15] and $|V_{ub}|$ from the PDG [3], implies that the unitarity of the first row of the CKM matrix is satisfied at the per-mille level (see Eq. (4.69)).

The work presented in this thesis has allowed to determine some isospin breaking effects with unprecedented precision. Still further important improvements and developments are possible:

- In our calculation contributions from disconnected diagrams and from the ones present in unquenched QED have been neglected (the latter because we used the electro-quenched approximation). The only way to quantify precisely the associated systematic error is to actually compute them. We note, however, that, within the quoted

uncertainties, our results are compatible with the experimental ones (when present) and with previous lattice determinations. It is currently underway a theoretical study that discusses how twisted mass lattice QCD can be conveniently combined with the RM123 approach beyond the quenched-QED approximation [119]; numerical simulations are in progress.

- Another source of systematic uncertainty is associated to the chiral extrapolation. Only recently, thanks to the increased computational power, the first lattice computations at physical light quark mass have been presented. An important improvement of the present work would consist in performing the same calculation with simulations at the physical point. In this respect new ETMC gauge ensembles at the physical pion mass will soon become available.

- Till now the experimental data on the decay $P \to \ell \nu_\ell(\gamma)$ are inclusive, i.e. all photon energies are included. In the case of pion and kaon decays the maximum value of the photon energy is $\Delta E \simeq 29$ MeV and 235 MeV, respectively. This means that in principle structure dependent (SD) contributions to the real photon emission might be relevant, especially for kaon decays. Present estimates based on chiral perturbation theory (ChPT) up to order $O(p^4)$ [90, 103] indicate, however, a negligible contribution of the SD terms for the inclusive pion and kaon decays into muons studied in the present work. In the case of heavy meson decays the maximum photon energy is much larger than the QCD scale, $\Lambda_{\text{QCD}} \approx 300$ MeV. In this case real photons can be emitted with a momentum much larger than ≈ 300 MeV, so that they can probe distances definitely lower than ≈ 0.5 fm, becoming in this way very sensitive to the internal electromagnetic structure of the decaying meson. Thus, a non-perturbative determination of the real emission amplitudes is essential for the decays of heavy mesons and it is certainly very important also for light and strange mesons in order to check the possible relevance of higher-order ChPT contributions. In Sec. 4.6 we presented a preliminary lattice calculation of the form factors entering the radiative decay rate $P \to \ell \nu_\ell \gamma$ in the case of pions, kaons, D and D_s mesons. We are currently improving our lattice data and, in the near future, we will be able to compare precise theoretical predictions with experimental measurements for both light and heavy mesons.

- In the heavy flavor sector ChPT is not applicable and the method presented in this thesis could be applied to provide model independent theoretical estimates (not available so far in the literature) of the radiative QED corrections to these hadronic decays. We stress that in the limit of large heavy quark masses an enhancement of the radiative corrections may be expected due to the presence of nearby resonances [97]. Thus, a direct lattice computation of the leptonic decay rate of mesons with charm and beauty is important both in itself and for our understanding of the QCD dynamics.

- For the present study of the pion and kaon leptonic decay rates the choice of using the quantity $\mathcal{F}_\pi$ defined in Eq. (4.11) to calibrate our simulations prevented us from being able to predict the value of $|V_{ud}|$. The physical value $\mathcal{F}_\pi^{phys}$ can be indeed obtained by

taking the experimental pion decay rate and the result for $|V_{ud}|$ determined accurately from super-allowed β-decay (see discussion in Sec. 4.2). Since we are currently producing the Ω baryon correlators, we will soon be able to alternatively use M_Ω to set the lattice scale. In this way, by repeating the calculation described in Chapter 4 we could use the result for $\delta R_\pi^{\text{phys}}$ to determine the CKM matrix element $|V_{ud}|$. This is one of the reasons supporting the use of hadronic schemes, as extensively proposed in Sec. 1.10, with hadron masses as experimental inputs for future lattice calculations.

- In Chapter 4 we have discussed in detail a specific case, namely the first lattice calculation of the $\mathcal{O}(\alpha_{em})$ corrections to the pion and kaon decays into muons. The adopted strategy can however, be extended to many other processes, for example to the case of final electrons and to the hadronic tau decays $\tau \to \pi\nu_\tau, K\nu_\tau$. Those investigations could provide powerful tests of CKM unitarity and of lepton flavor universality of electroweak interactions.

- In Sec. 3.8 we discussed the theoretical framework required for the computation of radiative corrections to semileptonic decay rates in lattice simulations, and in particular to those for $K_{\ell3}$ decays. This is an extension of the framework we have developed and successfully implemented for leptonic decays. New issues which arise for semileptonic decays, include the presence of unphysical terms which grow exponentially with the time separation between the insertion of the weak Hamiltonian and the sink for the final-state meson-lepton pair. Such terms must be identified and subtracted. The method needs to be implemented and tested numerically and could lead to improved precision in the determination of the corresponding CKM matrix elements and other tests of the Standard Model.

Matching in the Twisted Mass Regularization

<div style="text-align: right">A</div>

In the main text we have described the renormalization of the relevant operators in the *physical basis*. This discussion is valid for a generic Wilson-like fermion regularization. In this appendix we address instead some important aspects peculiar to the twisted mass fermions used in our numerical calculation. We derive, in particular, the relations between RCs in the so-called physical and twisted basis, for the bilinear and four-fermion operators considered in this work.

The relevant observation is that the lattice action for twisted mass fermions at maximal twist in the twisted basis only differs from the standard Wilson fermion lattice action for the twisted rotation of the fermion mass term. The two actions become identical in the chiral limit. It then follows that, in any mass-independent renormalization scheme, the RCs for twisted mass operators in the twisted basis are the same as those of the corresponding operators with standard Wilson fermions. It is customary to denote these RCs, for a generic operator O, as Z_O. They are valid for both standard Wilson and twisted mass operators in the twisted basis and differ, in general, from the RCs for twisted mass operators in the physical basis, that we denote here as $Z_O^{(0)}$.

At maximal twist the rotation from the twisted to the physical basis for both quark and lepton fields is given by

$$q_{\text{twisted}} = \frac{1}{\sqrt{2}} \left(1 + i\gamma_5 r_q\right) q \, , \qquad \ell_{\text{twisted}} = \frac{1}{\sqrt{2}} \left(1 + i\gamma_5 r_\ell\right) \ell \, , \tag{4.78}$$

where q and ℓ are the quark and lepton fields in the physical basis and r_q and r_ℓ are the corresponding r-parameters. In our simulations we use opposite values of the r-parameter for the two valence quarks, $r_2 = -r_1$ ($r_i = \pm 1$). The quark and lepton bilinears then transform

as

$$
\begin{aligned}
\left[\overline{q}_2\gamma_\mu(1\pm\gamma_5)q_1\right]_{\text{twisted}} &= \pm ir_1\left[\overline{q}_2\gamma_\mu(1\pm\gamma_5)q_1\right] \ , \\
\left[\overline{q}_2(1\pm\gamma_5)q_1\right]_{\text{twisted}} &= \left[\overline{q}_2(1\pm\gamma_5)q_1\right] \ , \\
\left[\overline{q}_2\sigma_{\mu\nu}(1+\gamma_5)q_1\right]_{\text{twisted}} &= \left[\overline{q}_2\sigma_{\mu\nu}(1+\gamma_5)q_1\right] \\
\left[\overline{\nu}\gamma_\mu(1-\gamma_5)\ell\right]_{\text{twisted}} &= \frac{1}{\sqrt{2}}\left(1-ir_\ell\right)\left[\overline{\nu}\gamma_\mu(1-\gamma_5)\ell\right] \ , \\
\left[\overline{\nu}(1+\gamma_5)\ell\right]_{\text{twisted}} &= \frac{1}{\sqrt{2}}\left(1+ir_\ell\right)\left[\overline{\nu}(1+\gamma_5)\ell\right] \\
\left[\overline{\nu}\sigma_{\mu\nu}(1+\gamma_5)\ell\right]_{\text{twisted}} &= \frac{1}{\sqrt{2}}\left(1+ir_\ell\right)\left[\overline{\nu}\sigma_{\mu\nu}(1+\gamma_5)\ell\right] \ .
\end{aligned}
\tag{4.79}
$$

From Eqs. (4.79) one readily derives the relations between the quark vector and axial vector current in the two basis,

$$
\begin{aligned}
(V_\mu)_{\text{twisted}} &= \left[\overline{q}_2\gamma_\mu q_1\right]_{\text{twisted}} = i\,r_1\left[\overline{q}_2\gamma_\mu\gamma_5 q_1\right] = i\,r_1\,A_\mu \ , \\
(A_\mu)_{\text{twisted}} &= \left[\overline{q}_2\gamma_\mu\gamma_5 q_1\right]_{\text{twisted}} = i\,r_1\left[\overline{q}_2\gamma_\mu q_1\right] = i\,r_1\,V_\mu \ ,
\end{aligned}
\tag{4.80}
$$

which, in turn, determine the relation between the RCs in the two basis

$$
\begin{aligned}
\widehat{V}_\mu &= Z_V^{(0)}\,V_\mu = -i\,r_1\,(\widehat{A}_\mu)_{\text{twisted}} = -i\,r_1\,Z_A\,(A_\mu)_{\text{twisted}} = Z_A\,V_\mu \ , \\
\widehat{A}_\mu &= Z_A^{(0)}\,A_\mu = -i\,r_1\,(\widehat{V}_\mu)_{\text{twisted}} = -i\,r_1\,Z_V\,(V_\mu)_{\text{twisted}} = Z_V\,A_\mu \ ,
\end{aligned}
\tag{4.81}
$$

where $\widehat{O}$ denotes the generic renormalized operator. One then sees from Eq. (4.81) that the RC $Z_V^{(0)}$ of the vector current in the physical basis, with $r_1 = -r_2$, is simply the RC of the axial current in the twisted basis, which in turn is just Z_A computed with Wilson fermions in the chiral limit. Analogously, $Z_A^{(0)}$ in the physical basis, with $r_1 = -r_2$, corresponds to Z_V computed with Wilson fermions in the chiral limit.

From the transformations (4.79) one can also derive the relations between the four-fermion operators $O_1 - O_5$ of Eq. (3.20) in the physical and twisted basis

$$
\begin{aligned}
(O_1)_{\text{twisted}} &= -\frac{i}{\sqrt{2}}\,r_1\,(1-ir_\ell)\,O_1 \ , & O_1 &= +\frac{i}{\sqrt{2}}\,r_1\,(1+ir_\ell)\,(O_1)_{\text{twisted}} \ , \\
(O_2)_{\text{twisted}} &= +\frac{i}{\sqrt{2}}\,r_1\,(1-ir_\ell)\,O_2 \ , & O_2 &= -\frac{i}{\sqrt{2}}\,r_1\,(1+ir_\ell)\,(O_2)_{\text{twisted}} \ , \\
(O_3)_{\text{twisted}} &= \frac{1}{\sqrt{2}}\,(1+ir_\ell)\,O_3 \ , & O_3 &= \frac{1}{\sqrt{2}}\,(1-ir_\ell)\,(O_3)_{\text{twisted}} \ , \\
(O_4)_{\text{twisted}} &= \frac{1}{\sqrt{2}}\,(1+ir_\ell)\,O_4 \ , & O_4 &= \frac{1}{\sqrt{2}}\,(1-ir_\ell)\,(O_4)_{\text{twisted}} \ , \\
(O_5)_{\text{twisted}} &= \frac{1}{\sqrt{2}}\,(1+ir_\ell)\,O_5 \ , & O_5 &= \frac{1}{\sqrt{2}}\,(1-ir_\ell)\,(O_5)_{\text{twisted}} \ .
\end{aligned}
\tag{4.82}
$$

We can then obtain the relation between the renormalization matrix in the physical basis, $Z^{(0)}$, and the corresponding matrix Z for standard Wilson fermions. In particular, for the weak operator O_1 one finds

$$
\begin{aligned}
\widehat{O}_1 &= \sum_{j=1,\ldots,5} Z^{(0)}_{1j} O_j = \frac{i}{\sqrt{2}} r_1 \left(1 + ir_\ell\right) (\widehat{O}_1)_{\text{twisted}} = \frac{i}{\sqrt{2}} r_1 \left(1 + ir_\ell\right) \sum_{j=1,\ldots,5} Z_{1j} (O_j)_{\text{twisted}} = \\
&= \frac{i}{\sqrt{2}} r_1 \left(1 + ir_\ell\right) \left[-\frac{i}{\sqrt{2}} r_1 \left(1 - ir_\ell\right) \left(Z_{11} O_1 - Z_{12} O_2\right) + \frac{1}{\sqrt{2}} \left(1 + ir_\ell\right) \sum_{j=3,4,5} Z_{1j} O_j \right] = \\
&= Z_{11} O_1 - Z_{12} O_2 - \overline{r} \sum_{j=3,4,5} Z_{1j} O_j \, ,
\end{aligned}
\tag{4.83}
$$

with $\overline{r} \equiv r_1 r_\ell$. Therefore

$$
Z^{(0)}_{11} = Z_{11} \, , \quad Z^{(0)}_{12} = -Z_{12} \, , \quad Z^{(0)}_{13} = -\overline{r} \, Z_{13} \, , \quad Z^{(0)}_{14} = -\overline{r} \, Z_{14} \, , \quad Z^{(0)}_{15} = -\overline{r} \, Z_{15} \, . \tag{4.84}
$$

Eq. (4.84) shows in particular that the mixing coefficients $Z_{13,14,15}$ for the operators $O_{3,4,5}$ are proportional to $\overline{r} \equiv r_1 r_\ell$. Thus, we can eliminate the mixing with these operators by simply averaging the numerical results over the two possible values $\overline{r} = \pm 1$.

In order to illustrate the above point, we mention the results of Ref. [10] obtained in perturbation theory at order $O(\alpha_s^0)$, for the coefficients $\delta Z^{QED}_{1j} = Z^{(0)}_{1j}/(\alpha_{\text{em}}/4\pi)$. The evaluation of the matrix δZ^{QED}_{ij} which relates the operators $O_1 - O_5$ in the lattice and W regularizations requires the computation of the Feynman diagrams shown in Fig. 4.6.8 in the two regularization schemes. All the external momenta are chosen to be equal to p and all external particles
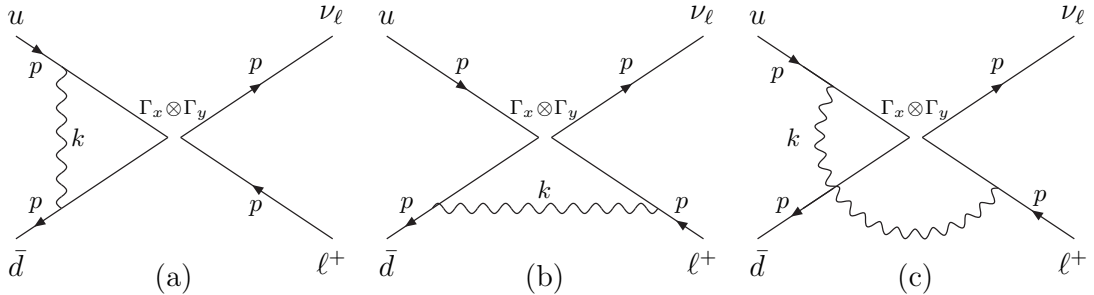

Figure 4.6.8: One-loop Feynman diagrams computed for the renormalization of the four-fermion operators $O_{XY} = (\bar{d}\,\Gamma_X\,u)\,(\bar{\nu}_\ell\,\Gamma_Y\,\ell) \equiv \Gamma_X \otimes \Gamma_Y$.

are taken to be massless. In Ref. [10] the main ingredients for the calculation in the lattice regularization are deduced from the results of the corresponding QCD calculation performed in [120]. The expression for the lattice wave function renormalization can be obtained from [121].

We now present results for twisted mass fermions and "naive" QED gauge action, for which the tree-level lattice photon propagator in the Feynman gauge is given in Eq. (3.37). In infinite volume the sum over momenta in Eq. (3.37) is replaced by the corresponding integral.

The $O(\alpha_{em})$ matching matrix δZ^{QED}_{ij} including the lepton wave function renormalization is explicitly given in the physical basis by:

$$\delta Z^{QED} = \begin{pmatrix} 2L_W - 15.5389 & -0.5357 & -1.6072\,\bar{r} & 3.2143\,\bar{r} & 0.8036\,\bar{r} \\ -0.5357 & L_W - 14.850 & -3.2143\,\bar{r} & 1.6072\,\bar{r} & -0.4018\,\bar{r} \\ -0.4018\,\frac{r_\ell}{r_1} & -0.8036\,\frac{r_\ell}{r_1} & -\frac{2}{3}L_W - 13.7017 & -1.0715 & 0 \\ 0.8036\,\frac{r_\ell}{r_1} & 0.4018\,\frac{r_\ell}{r_1} & -1.0715 & -\frac{2}{3}L_W - 13.7017 & \frac{1}{12}L_W - 0.0574 \\ 9.6430\,\frac{r_\ell}{r_1} & -4.8215\,\frac{r_\ell}{r_1} & 0 & 4L_W - 2.7559 & \frac{20}{9}L_W - 15.6920 \end{pmatrix},$$

$$(4.85)$$

where $L_W = \log(a^2 M_W^2)$.

Bibliography

[1] N. Cabibbo, *Meeting of the Italian School of Physics and Weak Interactions Bologna, Italy, April 26-28, 1984*, Phys. Rev. Lett. **10**, 531 (1963), [,648(1963)].

[2] M. Kobayashi and T. Maskawa, Prog. Theor. Phys. **49**, 652 (1973).

[3] M. Tanabashi *et al.* (Particle Data Group), Phys. Rev. **D98**, 030001 (2018).

[4] S. Aoki *et al.* (Flavour Lattice Averaging Group), (2019), arXiv:1902.08191 [hep-lat] .

[5] A. Portelli, *Proceedings, 32nd International Symposium on Lattice Field Theory (Lattice 2014): Brookhaven, NY, USA, June 23-28, 2014*, PoS **LATTICE2014**, 013 (2015), arXiv:1505.07057 [hep-lat] .

[6] R. F. Dashen, Phys. Rev. **183**, 1245 (1969).

[7] D. Giusti, V. Lubicz, C. Tarantino, G. Martinelli, S. Sanfilippo, S. Simula, and N. Tantalo, Phys. Rev. **D95**, 114504 (2017), arXiv:1704.06561 [hep-lat] .

[8] G. M. de Divitiis *et al.*, JHEP **04**, 124 (2012), arXiv:1110.6294 [hep-lat] .

[9] G. M. de Divitiis, R. Frezzotti, V. Lubicz, G. Martinelli, R. Petronzio, G. C. Rossi, F. Sanfilippo, S. Simula, and N. Tantalo (RM123), Phys. Rev. **D87**, 114505 (2013), arXiv:1303.4896 [hep-lat] .

[10] N. Carrasco, V. Lubicz, G. Martinelli, C. T. Sachrajda, N. Tantalo, C. Tarantino, and M. Testa, Phys. Rev. **D91**, 074506 (2015), arXiv:1502.00257 [hep-lat] .

[11] F. Bloch and A. Nordsieck, Phys. Rev. **52**, 54 (1937).

[12] A. Sirlin, Nucl. Phys. **B196**, 83 (1982).

[13] M. Di Carlo, D. Giusti, V. Lubicz, G. Martinelli, C. T. Sachrajda, F. Sanfilippo, S. Simula, and N. Tantalo, Phys. Rev. **D100**, 034514 (2019), arXiv:1904.08731 [hep-lat] .

[14] G. Martinelli, C. Pittori, C. T. Sachrajda, M. Testa, and A. Vladikas, Nucl. Phys. **B445**, 81 (1995), arXiv:hep-lat/9411010 [hep-lat] .

[15] J. Hardy and I. S. Towner, *Proceedings, 9th International Workshop on the CKM Unitarity Triangle (CKM2016): Mumbai, India, November 28-December 3, 2016*, PoS **CKM2016**, 028 (2016).

[16] D. Giusti, V. Lubicz, G. Martinelli, C. T. Sachrajda, F. Sanfilippo, S. Simula, N. Tantalo, and C. Tarantino, Phys. Rev. Lett. **120**, 072001 (2018), arXiv:1711.06537 [hep-lat] .

[17] S. Borsanyi *et al.*, Science **347**, 1452 (2015), arXiv:1406.4088 [hep-lat] .

[18] M. Antonelli *et al.* (FlaviaNet Working Group on Kaon Decays), Eur. Phys. J. **C69**, 399 (2010), arXiv:1005.2323 [hep-ph] .

[19] G. Amoros, J. Bijnens, and P. Talavera, Nucl. Phys. **B602**, 87 (2001), arXiv:hep-ph/0101127 [hep-ph] .

[20] J. Bijnens and K. Ghorbani, (2007), arXiv:0711.0148 [hep-ph] .

[21] A. Kastner and H. Neufeld, Eur. Phys. J. **C57**, 541 (2008), arXiv:0805.2222 [hep-ph] .

[22] V. Cirigliano and H. Neufeld, Phys. Lett. **B700**, 7 (2011), arXiv:1102.0563 [hep-ph] .

[23] A. Duncan, E. Eichten, and H. Thacker, Phys. Rev. Lett. **76**, 3894 (1996), arXiv:hep-lat/9602005 [hep-lat] .

[24] S. Basak *et al.* (MILC), *Proceedings, 26th International Symposium on Lattice field theory (Lattice 2008): Williamsburg, USA, July 14-19, 2008*, PoS **LATTICE2008**, 127 (2008), arXiv:0812.4486 [hep-lat] .

[25] T. Blum, R. Zhou, T. Doi, M. Hayakawa, T. Izubuchi, S. Uno, and N. Yamada, Phys. Rev. **D82**, 094508 (2010), arXiv:1006.1311 [hep-lat] .

[26] A. Portelli *et al.* (Budapest-Marseille-Wuppertal), *Proceedings, 28th International Symposium on Lattice field theory (Lattice 2010): Villasimius, Italy, June 14-19, 2010*, PoS **LATTICE2010**, 121 (2010), arXiv:1011.4189 [hep-lat] .

[27] B. C. Tiburzi and A. Walker-Loud, Nucl. Phys. **A764**, 274 (2006), arXiv:hep-lat/0501018 [hep-lat] .

[28] S. R. Beane, K. Orginos, and M. J. Savage, Nucl. Phys. **B768**, 38 (2007), arXiv:hep-lat/0605014 [hep-lat] .

[29] C. McNeile, C. Michael, and C. Urbach (ETM), Phys. Lett. **B674**, 286 (2009), arXiv:0902.3897 [hep-lat] .

[30] A. Walker-Loud, (2009), arXiv:0904.2404 [hep-lat] .

[31] A. Walker-Loud, *Proceedings, 28th International Symposium on Lattice field theory (Lattice 2010): Villasimius, Italy, June 14-19, 2010*, PoS **LATTICE2010**, 243 (2010), arXiv:1011.4015 [hep-lat] .

[32] T. Ishikawa, T. Blum, M. Hayakawa, T. Izubuchi, C. Jung, and R. Zhou, Phys. Rev. Lett. **109**, 072002 (2012), arXiv:1202.6018 [hep-lat] .

[33] A. Portelli *et al.*, *Proceedings, 29th International Symposium on Lattice field theory (Lattice 2011): Squaw Valley, Lake Tahoe, USA, July 10-16, 2011*, PoS **LATTICE2011**, 136 (2011), arXiv:1201.2787 [hep-lat] .

[34] S. Basak *et al.* (MILC), *Proceedings, 7th International Workshop on Chiral Dynamics (CD12): Newport News, Virginia, USA, August 6-10, 2012*, PoS **CD12**, 030 (2013), arXiv:1301.7137 [hep-lat] .

[35] D. Giusti, `http://www.infn.it/thesis/thesis_dettaglio.php?tid=10863` (2016).

[36] D. Giusti, V. Lubicz, G. Martinelli, F. Sanfilippo, S. Simula, N. Tantalo, and C. Tarantino, *Proceedings, 35th International Symposium on Lattice Field Theory (Lattice 2017): Granada, Spain, June 18-24, 2017*, EPJ Web Conf. **175**, 06002 (2018), arXiv:1710.06633 [hep-lat] .

[37] D. Giusti, V. Lubicz, G. Martinelli, F. Sanfilippo, and S. Simula, JHEP **10**, 157 (2017), arXiv:1707.03019 [hep-lat] .

[38] D. Giusti, V. Lubicz, G. Martinelli, F. Sanfilippo, and S. Simula, Phys. Rev. **D99**, 114502 (2019), arXiv:1901.10462 [hep-lat] .

[39] A. Patella, *Proceedings, 34th International Symposium on Lattice Field Theory (Lattice 2016): Southampton, UK, July 24-30, 2016*, PoS **LATTICE2016**, 020 (2017), arXiv:1702.03857 [hep-lat] .

[40] R. Frezzotti, P. A. Grassi, S. Sint, and P. Weisz (Alpha), JHEP **08**, 058 (2001), arXiv:hep-lat/0101001 [hep-lat] .

[41] R. Frezzotti and G. C. Rossi, JHEP **08**, 007 (2004), arXiv:hep-lat/0306014 [hep-lat] .

[42] R. Frezzotti and G. C. Rossi, JHEP **10**, 070 (2004), arXiv:hep-lat/0407002 [hep-lat] .

[43] M. Constantinou *et al.* (ETM), Phys. Rev. **D83**, 014505 (2011), arXiv:1009.5606 [hep-lat] .

[44] R. Frezzotti and G. C. Rossi, *Lattice hadron physics. Proceedings, 2nd Topical Workshop, LHP 2003, Cairns, Australia, July 22-30, 2003*, Nucl. Phys. Proc. Suppl. **128**, 193 (2004), [,193(2003)], arXiv:hep-lat/0311008 [hep-lat] .

[45] R. Baron *et al.*, JHEP **06**, 111 (2010), arXiv:1004.5284 [hep-lat] .

[46] J. Gasser, A. Rusetsky, and I. Scimemi, Eur. Phys. J. **C32**, 97 (2003), arXiv:hep-ph/0305260 [hep-ph] .

[47] R. Baron *et al.* (ETM), JHEP **08**, 097 (2010), arXiv:0911.5061 [hep-lat] .

[48] J. Gasser and G. R. S. Zarnauskas, Phys. Lett. **B693**, 122 (2010), arXiv:1008.3479 [hep-ph] .

[49] M. Luscher, Commun. Math. Phys. **105**, 153 (1986).

[50] Z. Davoudi and M. J. Savage, Phys. Rev. **D90**, 054503 (2014), arXiv:1402.6741 [hep-lat] .

[51] M. Luscher, Commun. Math. Phys. **104**, 177 (1986).

[52] D. Giusti, V. Lubicz, G. Martinelli, C. Sachrajda, F. Sanfilippo, S. Simula, and N. Tantalo, *Proceedings, 36th International Symposium on Lattice Field Theory (Lattice 2018): East Lansing, MI, United States, July 22-28, 2018*, PoS **LATTICE2018**, 266 (2019), arXiv:1811.06364 [hep-lat] .

[53] M. Bochicchio, L. Maiani, G. Martinelli, G. C. Rossi, and M. Testa, *Asia Pacific Conf.1987:439, Trieste Electroweak 1985:25*, Nucl. Phys. **B262**, 331 (1985).

[54] M. Hayakawa and S. Uno, Prog. Theor. Phys. **120**, 413 (2008), arXiv:0804.2044 [hep-ph] .

[55] B. Lucini, A. Patella, A. Ramos, and N. Tantalo, JHEP **02**, 076 (2016), arXiv:1509.01636 [hep-th] .

[56] C. Sturm, Y. Aoki, N. H. Christ, T. Izubuchi, C. T. C. Sachrajda, and A. Soni, Phys. Rev. **D80**, 014501 (2009), arXiv:0901.2599 [hep-ph] .

[57] S. Aoki *et al.*, Phys. Rev. **D86**, 034507 (2012), arXiv:1205.2961 [hep-lat] .

[58] S. Basak *et al.* (MILC), *Proceedings, 32nd International Symposium on Lattice Field Theory (Lattice 2014): Brookhaven, NY, USA, June 23-28, 2014*, PoS **LATTICE2014**, 116 (2014), arXiv:1409.7139 [hep-lat] .

[59] M. G. Endres, A. Shindler, B. C. Tiburzi, and A. Walker-Loud, Phys. Rev. Lett. **117**, 072002 (2016), arXiv:1507.08916 [hep-lat] .

[60] Z. Fodor, C. Hoelbling, S. D. Katz, L. Lellouch, A. Portelli, K. K. Szabo, and B. C. Toth, Phys. Lett. **B755**, 245 (2016), arXiv:1502.06921 [hep-lat] .

[61] R. Horsley *et al.*, J. Phys. **G43**, 10LT02 (2016), arXiv:1508.06401 [hep-lat] .

[62] Z. Fodor, C. Hoelbling, S. Krieg, L. Lellouch, T. Lippert, A. Portelli, A. Sastre, K. K. Szabo, and L. Varnhorst, Phys. Rev. Lett. **117**, 082001 (2016), arXiv:1604.07112 [hep-lat] .

[63] P. Boyle, V. Gülpers, J. Harrison, A. Jüttner, A. Portelli, and C. Sachrajda, *Proceedings, 34th International Symposium on Lattice Field Theory (Lattice 2016): Southampton, UK, July 24-30, 2016*, PoS **LATTICE2016**, 172 (2016), arXiv:1612.05962 [hep-lat] .

[64] N. Tantalo, *Proceedings, 31st International Symposium on Lattice Field Theory (Lattice 2013): Mainz, Germany, July 29-August 3, 2013*, PoS **LATTICE2013**, 007 (2014), arXiv:1311.2797 [hep-lat] .

[65] R. Baron *et al.* (ETM), *Proceedings, 28th International Symposium on Lattice field theory (Lattice 2010): Villasimius, Italy, June 14-19, 2010*, PoS **LATTICE2010**, 123 (2010), arXiv:1101.0518 [hep-lat] .

[66] N. Carrasco *et al.* (European Twisted Mass), Nucl. Phys. **B887**, 19 (2014), arXiv:1403.4504 [hep-lat] .

[67] J. Bijnens, Phys. Lett. **B306**, 343 (1993), arXiv:hep-ph/9302217 [hep-ph] .

[68] C. McNeile and C. Michael (UKQCD), Phys. Rev. **D73**, 074506 (2006), arXiv:hep-lat/0603007 [hep-lat] .

[69] S. Aoki, K.-i. Nagai, Y. Taniguchi, and A. Ukawa, Phys. Rev. **D58**, 074505 (1998), arXiv:hep-lat/9802034 [hep-lat] .

[70] N. Tantalo, V. Lubicz, G. Martinelli, C. T. Sachrajda, F. Sanfilippo, and S. Simula, (2016), arXiv:1612.00199 [hep-lat] .

[71] R. Horsley *et al.*, JHEP **04**, 093 (2016), arXiv:1509.00799 [hep-lat] .

[72] G. Colangelo, S. Lanz, H. Leutwyler, and E. Passemar, Phys. Rev. Lett. **118**, 022001 (2017), arXiv:1610.03494 [hep-ph] .

[73] S. Basak *et al.* (MILC), Phys. Rev. **D99**, 034503 (2019), arXiv:1807.05556 [hep-lat] .

[74] J. Gasser and H. Leutwyler, Nucl. Phys. **B250**, 465 (1985).

[75] J. Gasser and H. Leutwyler, Phys. Lett. **B184**, 83 (1987).

[76] J. Bijnens and K. Ghorbani, JHEP **11**, 030 (2007), arXiv:0709.0230 [hep-ph] .

[77] G. M. de Divitiis *et al.*, (2019), arXiv:1908.10160 [hep-lat] .

[78] F. Ambrosino *et al.* (KLOE), Phys. Lett. **B632**, 76 (2006), arXiv:hep-ex/0509045 [hep-ex] .

[79] F. Ambrosino *et al.* (KLOE), Eur. Phys. J. **C64**, 627 (2009), [Erratum: Eur. Phys. J.65,703(2010)], arXiv:0907.3594 [hep-ex] .

[80] S. M. Berman, Phys. Rev. **112**, 267 (1958).

[81] T. Kinoshita and A. Sirlin, Phys. Rev. **113**, 1652 (1959).

[82] A. Sirlin, Phys. Rev. **D22**, 971 (1980).

[83] E. Braaten and C.-S. Li, Phys. Rev. **D42**, 3888 (1990).

[84] A. J. Buras, M. Jamin, and M. E. Lautenbacher, Nucl. Phys. **B408**, 209 (1993), arXiv:hep-ph/9303284 [hep-ph] .

[85] M. Ciuchini, E. Franco, G. Martinelli, and L. Reina, Nucl. Phys. **B415**, 403 (1994), arXiv:hep-ph/9304257 [hep-ph] .

[86] J. Brod and M. Gorbahn, Phys. Rev. **D78**, 034006 (2008), arXiv:0805.4119 [hep-ph] .

[87] T. Kinoshita, Phys. Rev. Lett. **2**, 477 (1959).

[88] V. Lubicz, G. Martinelli, C. T. Sachrajda, F. Sanfilippo, S. Simula, and N. Tantalo, Phys. Rev. **D95**, 034504 (2017), arXiv:1611.08497 [hep-lat] .

[89] P. Hasenfratz and H. Leutwyler, Nucl. Phys. **B343**, 241 (1990).

[90] J. Bijnens, G. Ecker, and J. Gasser, Nucl. Phys. **B396**, 81 (1993), arXiv:hep-ph/9209261 [hep-ph] .

[91] J. Bijnens, G. Colangelo, G. Ecker, and J. Gasser, in *2nd DAPHNE Physics Handbook:315-389* (1994) pp. 315–389, arXiv:hep-ph/9411311 [hep-ph] .

[92] V. Cirigliano and I. Rosell, Phys. Rev. Lett. **99**, 231801 (2007), arXiv:0707.3439 [hep-ph] .

[93] L. Ametller, J. Bijnens, A. Bramon, and F. Cornet, Phys. Lett. **B303**, 140 (1993), arXiv:hep-ph/9302219 [hep-ph] .

[94] C. Q. Geng, I.-L. Ho, and T. H. Wu, Nucl. Phys. **B684**, 281 (2004), arXiv:hep-ph/0306165 [hep-ph] .

[95] V. Cirigliano, G. Ecker, H. Neufeld, A. Pich, and J. Portoles, Rev. Mod. Phys. **84**, 399 (2012), arXiv:1107.6001 [hep-ph] .

[96] `http://pdg8.lbl.gov/rpp2014v1/pdgLive/Particle.action?node=S008` .

[97] D. Becirevic, B. Haas, and E. Kou, Phys. Lett. **B681**, 257 (2009), arXiv:0907.1845 [hep-ph] .

[98] G. Isidori, Eur. Phys. J. **C53**, 567 (2008), arXiv:0709.2439 [hep-ph] .

[99] S. de Boer, T. Kitahara, and I. Nisandzic, Phys. Rev. Lett. **120**, 261804 (2018), arXiv:1803.05881 [hep-ph] .

[100] L. Maiani and M. Testa, Phys. Lett. **B245**, 585 (1990).

[101] P. Boyle, V. Gülpers, J. Harrison, A. Jüttner, C. Lehner, A. Portelli, and C. T. Sachrajda, JHEP **09**, 153 (2017), arXiv:1706.05293 [hep-lat] .

[102] M. Hansen, B. Lucini, A. Patella, and N. Tantalo, JHEP **05**, 146 (2018), arXiv:1802.05474 [hep-lat] .

[103] V. Cirigliano and I. Rosell, JHEP **10**, 005 (2007), arXiv:0707.4464 [hep-ph] .

[104] J. L. Rosner, S. Stone, and R. S. Van de Water, Submitted to: Particle Data Book (2015), arXiv:1509.02220 [hep-ph] .

[105] P. F. Bedaque, Phys. Lett. **B593**, 82 (2004), arXiv:nucl-th/0402051 [nucl-th] .

[106] G. M. de Divitiis, R. Petronzio, and N. Tantalo, Phys. Lett. **B595**, 408 (2004), arXiv:hep-lat/0405002 [hep-lat] .

[107] J. Bijnens and N. Danielsson, Phys. Rev. **D75**, 014505 (2007), arXiv:hep-lat/0610127 [hep-lat] .

[108] J. C. Hardy and I. S. Towner, Phys. Rev. **C91**, 025501 (2015), arXiv:1411.5987 [nucl-ex] .

[109] R. J. Dowdall, C. T. H. Davies, G. P. Lepage, and C. McNeile, Phys. Rev. **D88**, 074504 (2013), arXiv:1303.1670 [hep-lat] .

[110] N. Carrasco *et al.*, Phys. Rev. **D91**, 054507 (2015), arXiv:1411.7908 [hep-lat] .

[111] A. Bazavov *et al.*, Phys. Rev. **D98**, 074512 (2018), arXiv:1712.09262 [hep-lat] .

[112] C.-Y. Seng, M. Gorchtein, H. H. Patel, and M. J. Ramsey-Musolf, Phys. Rev. Lett. **121**, 241804 (2018), arXiv:1807.10197 [hep-ph] .

[113] J. Bijnens and P. Talavera, Nucl. Phys. **B489**, 387 (1997), arXiv:hep-ph/9610269 [hep-ph] .

[114] V. Mateu and J. Portoles, Eur. Phys. J. **C52**, 325 (2007), arXiv:0706.1039 [hep-ph] .

[115] R. Unterdorfer and H. Pichl, Eur. Phys. J. **C55**, 273 (2008), arXiv:0801.2482 [hep-ph] .

[116] C. Kane, C. Lehner, S. Meinel, and A. Soni, in *37th International Symposium on Lattice Field Theory (Lattice 2019) Wuhan, Hubei, China, June 16-22, 2019* (2019) arXiv:1907.00279 [hep-lat] .

[117] C. T. Sachrajda and G. Villadoro, Phys. Lett. **B609**, 73 (2005), arXiv:hep-lat/0411033 [hep-lat] .

[118] J. Bijnens and G. Ecker, Ann. Rev. Nucl. Part. Sci. **64**, 149 (2014), arXiv:1405.6488 [hep-ph] .

[119] R. Frezzotti, G. C. Rossi, and N. Tantalo, *Proceedings, 34th International Symposium on Lattice Field Theory (Lattice 2016): Southampton, UK, July 24-30, 2016*, PoS **LATTICE2016**, 320 (2016), arXiv:1612.02265 [hep-lat] .

[120] M. Constantinou, P. Dimopoulos, R. Frezzotti, V. Lubicz, H. Panagopoulos, A. Skouroupathis, and F. Stylianou, Phys. Rev. **D83**, 074503 (2011), arXiv:1011.6059 [hep-lat] .

[121] M. Constantinou, V. Lubicz, H. Panagopoulos, and F. Stylianou, JHEP **10**, 064 (2009), arXiv:0907.0381 [hep-lat] .